PATTERN-BASED DISCRIMINATION OF CARBOXYLATE ANIONS IN AQUEOUS MEDIA AND ON SOLID SUPPORTS

by

YIFEI XU

MARCO BONIZZONI, COMMITTEE CHAIR
JARED M. ALLRED
CAROLYN J. CASSADY
SHANLIN PAN
KARL J. WALLACE

A DISSERTATION

Submitted in partial fulfillment of the requirements
for the degree of Doctor of Philosophy
in the Department of Chemistry and Biochemistry
in the Graduate School of
The University of Alabama

TUSCALOOSA, ALABAMA

2021

ABSTRACT

Carboxylate-containing species play important roles in biosynthesis, energy generation and biological signaling; they are also common functional groups in pharmaceuticals, and potential pollutants in aqueous media. Sensing and discrimination of carboxylates was achieved using non-covalent interactions mediated by poly(amidoamine) (PAMAM) dendrimers, a family of macromolecular polyelectrolytes.

Our focus was on fast, sensitive, and inexpensive detection methods based on optical spectroscopy. However, neither the dendrimers nor the analytes have spectroscopic signals in the visible region, so we first designed and tested an indicator displacement assay (IDA), built from PAMAM dendrimers and common organic dyes, whose response was monitored through absorbance, fluorescence emission and fluorescence anisotropy (Chapter 2).

We achieved qualitative and quantitative discrimination among structurally similar carboxylates using pattern-based clustering methods applied to the output of the IDA sensing system (Chapter 3). It is noteworthy that we obtained not only qualitative discrimination (where pattern recognition commonly excels) but also *quantitative* measurements, a much rarer accomplishment.

In Chapter 4, the scope was extended to the discrimination of β-lactam antibiotics, a family of environmentally and biologically relevant analytes that contain carboxylate groups and comprise more than half of the world market for antibiotics. A novel partial hydrolysis method, introduced here, significantly increased the affinity of these compounds for the PAMAM hosts;

this in turn allowed us to successfully differentiate samples drawn from an analyte panel comprising two penicillins, five cephalosporins, and two references.

In Chapter 5 we move these carboxylate sensing methods to solid supports with lower cost and higher stability, on a path towards the construction of a portable, deployable device. Studied support media included cellulose acetate, SiO_2 dispersions, regular printing paper, filter paper, and chromatography paper. Chromatography paper, the best performer, yielded excellent differentiation and repeatability, and improved long-term stability over the same system in water.

Finally, Chapter 6 describes our efforts to improve the determination of the concentration of chloroform, a halogenated byproduct of water chlorination and a dangerous water pollutant. We attempted to improve upon the common colorimetric Fujiwara test, using the intensely colored Fujiwara product as an optical filter to modulate the fluorescence emission of organic fluorophores.

LIST OF ABBREVIATIONS AND SYMBOLS

ANSI	American National Standards Institute
BsDA	*Bacillus stearothermophilus* disc assay
CB	Calcein Blue
Em	Emission
Ex	Excitation
EU4pt	European Union four-plate test
G5	5^{th} Generation
GPR91	G protein coupled receptor
HEPES	4-(2-Hydroxyethyl)-1-piperazineethanesulfonic acid
IDA	Indicator displacement assay
LDA	Linear discriminant analysis
LED	Light-emitting diode
LOD	Limit of discrimination
MC	7-Diethylamino-4-methylcoumarin
ML	4-Methylesculetin
NAT	Nouws antibiotic test
PAMAM	Poly(amidoamine)
PC	Principle component
PCA	Principal component analysis
PMT	Photomultiplier tube
RET	Resonance energy transfer

SLAS	Society for Laboratory Automation and Screening
TLC	Thin layer chromatography
UV-Vis	Ultraviolet-visible spectroscopy
VOC	Volatile organic compounds
ZIP1	Zinc transporter

ACKNOWLEDGEMENTS

I would like to acknowledge my research advisor, Prof. Marco Bonizzoni: this dissertation could not have been finished without his continuous support and guidance throughout the past five years of my graduate study. I appreciate his encouragement and suggestions not only for the advice on experiments, but also how to see the bigger picture as a scientist, and how to present my research properly.

I would also like to thank my dissertation committee members, Prof. Jared M. Allred, Prof. Carolyn J. Cassady, Prof. Shanlin Pan, and Prof. Karl J. Wallace for their precious suggestions on my research projects. I would like to thank my group members: Dr. Nicholas White, Dr. Xiaoli Liang, Dr. Michael Ihde, Xiyuan Yao, Flor Lozada and Yichun Yuan, who I met in the past 5 years and gave me a lot of help. I would like to show my appreciation to the University of Alabama, the Alabama Water Institute, and the National Science Foundation for their financial support of my research.

I would like to acknowledge all my family members and friends, for their love and emotional support online and offline throughout the past years. Finally, I would like to dedicate my dissertation to my parents, Xiaoliang Xu and Meiying Zhang, as well as my cats, Yishou Xu and Tiezhu Li, for their unconditional love and trust.

CONTENTS

LIST OF TABLES

LIST OF FIGURES

LIST OF SCHEMES

CHAPTER 1
INTRODUCTION

1.1 Supramolecular analytical chemistry

Supramolecular chemistry studies mostly non-covalent intermolecular interactions in artificial systems.[1-2] In 1987, Jean-Marie Lehn, Donald Cram, and Charles Pedersen won the Nobel Prize in chemistry for their contribution to the development in supramolecular chemistry; and after 30 years, in 2016, Jean-Pierre Sauvage, Sir J. Fraser Stoddart and Bernard L. Feringa won the Nobel Prize in chemistry for their contribution in the same field. Areas of supramolecular chemistry include molecular recognition,[3-4] host-guest chemistry,[5-7] intramolecular self-assembly or molecular folding,[8-10] intermolecular self-assembly,[11-13] and dynamic covalent chemistry.[14-16]

The combination of analytical chemistry and supramolecular chemistry generated a new area called “supramolecular analytical chemistry”. This term was first defined by Prof. Eric Anslyn in 2007 as he discussed the analytical applications of supramolecular chemistry involving molecular recognition and molecular self-assembly. Molecular sensing and discrimination, the most important concept in this area, take advantage of weak and reversible interactions among molecules, such as electrostatic interactions, hydrophobic interactions, and π-interactions.[17-19] Often a sensing or differentiation system involves multiple intermolecular interactions. Some of those will be discussed below.

1.1.1 Electrostatic interactions

Electrostatic interactions involve the attractive forces between species with opposite charges, including ionic bonding, weaker hydrogen bonding, and halogen bonding. They are the strongest non-covalent interactions at up to 240 kJ/mol, but they are easily weakened in highly polar solvents, and can also be as low as 5 kJ/mol.[20] Ionic interactions involve species with full charges. Hydrogen bonding involves dipole-dipole interaction between partially charged species, and it is a strong non-covalent interaction.

1.1.2 Hydrophobic effect

The hydrophobic effect drives the aggregation among non-polar molecules in polar solutions, mostly water. It is the desire of minimizing the contact among water molecules and non-polar molecules therefore lowering the overall free energy of the entire system. The source of the hydrophobic effect is still hotly debated, but a reasonable explanation is mostly ascribed to the high cohesive energy of water (and other polar protic solvents). The oligomerization of non-interacting apolar solutes in water is mostly driven by the fact that it minimizes the number of water molecules that are forced to assume a more ordered structure when in contact with a hydrophobic surface, which is entropically disadvantageous. Forcing multiple molecules of hydrophobic compound into a single apolar "bubble" requires fewer molecules of water to solvate the bubble. This frees up some of the solvent molecules that had been previously involved in solvation back into the solvent bulk, leading to an advantageous net entropy increase. Therefore, hydrophobic association is for the most part entropy-driven. This effect can also be characterized as an instance of entropy enthalpy compensation, instead of a non-covalent interaction, because it can happen between molecules that otherwise lack significant interaction points for intermolecular interactions.[21-22]

1.1.3 π interactions

The π system of conjugated molecules, and particularly those of aromatic moieties (using benzene here as an example), has high electron density on the top and bottom of its plane. The π orbitals can interact with cations, permanent dipoles, and other π orbitals as shown in Scheme 1-1:these interactions can have strength between 5-20 kJ/mol.[20] Cation-π interaction usually involves cations being at the top center of the π orbital, where the electron density is largest, and can be used in sensing systems.[23] Polar-π interaction are established between the quadrupole moment induced by the π orbital and molecules with permanent dipoles, for example water molecules. π-π interactions are the interactions between two π systems, which typically take place in the displaced and edge-to-face configurations, whereas "sandwich" configurations are less stable. The π-π interactions play an important role in the secondary and tertiary interactions among nucleobases.[24]

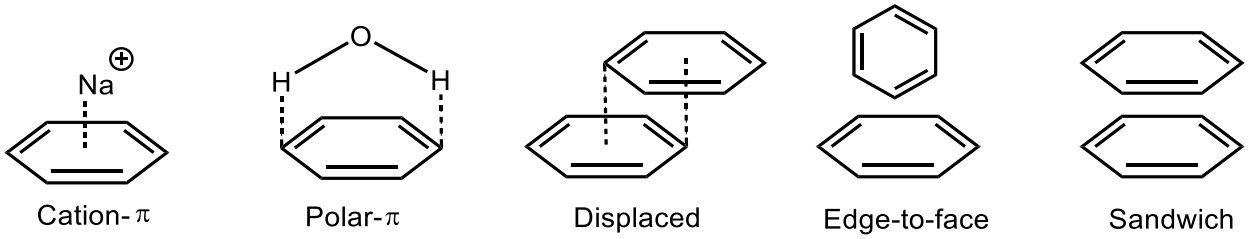

Scheme 1-1 Different types of π interactions including cation-π interaction, polar-π interaction, and displaced, edge-to-face, and sandwich π-π interactions, respectively from left to right.

1.2 Optical sensing methods

Using molecular recognition for analyte sensing usually requires detectable signal changes, which can be optical, electronic, and mechanical.[17] In supramolecular analytical chemistry, the sensor is often referred to as the "host" molecule, while the analyte is often called a "guest". Among all sensing techniques, sensing using optical spectroscopic signals is

particularly interesting because it is easy, fast, and sensitive, and it takes advantage of common and portable instruments. Based on the sensing principles, sensors can take advantage of direct sensing or of an indicator displacement assay (IDA) approach; and based on the number of analytes in their scope, supramolecular sensing systems are single analyte sensing and discrimination sensing among analytes.

1.2.1 Direct sensing and indicator displacement assays (IDA)

In direct sensing, the signaling unit and recognition unit are covalently bonded, and upon the binding of analyte onto the recognition unit, the signaling unit shows a detectable signal change (see Figure 1-1). Optical signals often used in this context include changes in absorption intensity or position, fluorescence emission and anisotropy, phosphorescence emission, etc. Such sensors are often designed by covalently binding a well-known dye molecule to the recognition unit, or by covalently adding a specific receptor subunit to a dye.[25-29]

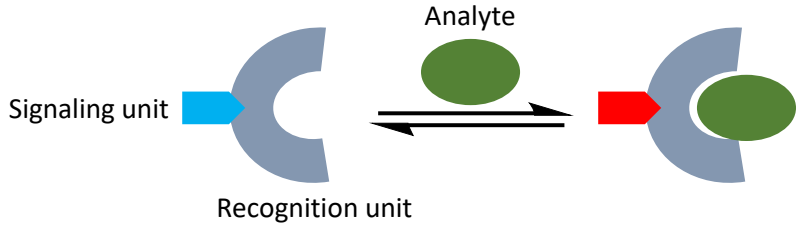

Figure 1-1. Example of direct sensing: signaling unit is covalently bounded with recognition unit, and signal changes upon analyte binding.

An indicator displacement assay (IDA) starts with the indicator (dye) bound with the recognition unit forming a complex; in most cases the indicator is bound to the receptor through non-covalent interactions,[30-31] although examples of covalently bound indicators have also been reported.[32-33] The function of an IDA depends on the indicator's optical signal being different between its free and bound forms. Upon introduction of an analyte to this sensing complex, the

analyte can displace the indicator from its complex, reforming its free form (shown in Figure 1-2). Analyte sensing is achieved through monitoring the behavior of the indicator. This method became popular because it has great advantages.[34-38] The non-covalent binding between the indicator and recognition unit can be achieved without covalent synthesis; competitive binding between the analyte and indicator increases the sensing selectivity among different analytes; and different combinations of recognition unit and the indicator are easily available, which creates the possibility of array sensing that will be discussed below.

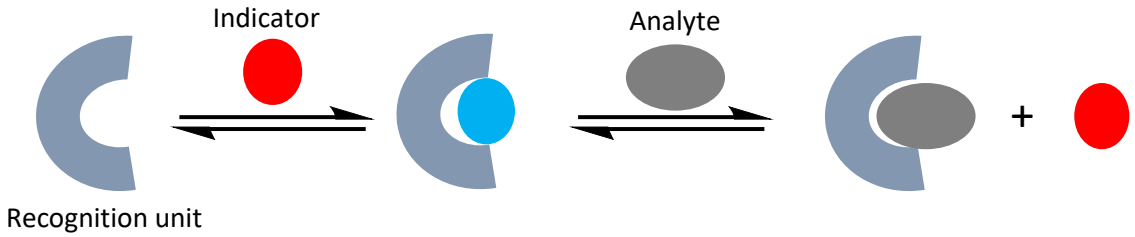

Figure 1-2 Example of a non-covalently assembled indicator displacement assay (IDA): a recognition unit and the indicator form a complex, changing the optical behavior of the indicator. Then, a spectroscopically silent analytedisplaces the indicator from the recognition unit, which causes the indicator to display its original optical signature. Signal changes in both steps report on the binding state of the indicator and, indirectly, on the binding of the analyte.

1.2.2 Single analyte sensing and array-based sensing

Single analyte sensors are developed for a specific target; the sensor designer attempts to achieve a system in which the sensor only responds upon the introduction of the target analyte, but not other interferents (Figure 1-3).[39-41] This is a traditional way of molecule sensing. In practice, however, interferents can be structurally very similar to the target analyte, therefore this approach requires careful sensor design. An alternative method is using array sensing for discrimination among different analytes.

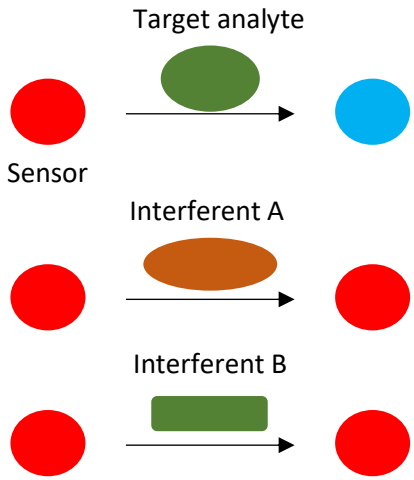

Figure 1-3 Example of single analyte sensing: the signal of the sensor only changes upon introduction of a specific analyte target, and does not change with other interferents. In other words, the system responds selectively to the analyte of interest.

Array sensing for discrimination among analytes takes advantage of multiple sources of information, none of which are necessarily selective. These sources of information may come from an array of different sensors, or from the concomitant measurement of multiple instrumental responses on a single system. As shown in Figure 1-4, each dot represents an information source. Commonly, a single information source in these systems cannot discriminate all analytes: for example, the top left source in the scheme can discriminate analyte A and C from B and D, but cannot discriminate between analytes A and C, or analytes B from D; another example is the bottom left source, which can only discriminate analyte D from A, B and C, but cannot distinguish among A, B and C. However, when combining the responses from all sources, a distinctive pattern emerges: this unique pattern is also called a "chemical fingerprint" for each analyte. Thus, this method allows the discrimination of each analyte from the others. This method provides the ability to analyze mixtures and unknown components.[42] This array-based sensing was used to discriminate a wide range of analytes, including amino acids,[43-45] proteins,[46-

[48] glycans,[49-50] bacteria,[51-52] metal ions,[42,53-54] sugars,[55-56] phosphates,[57-58] small organic molecules,[59-62] gases,[63-66] odorants,[67] and wines.[68]

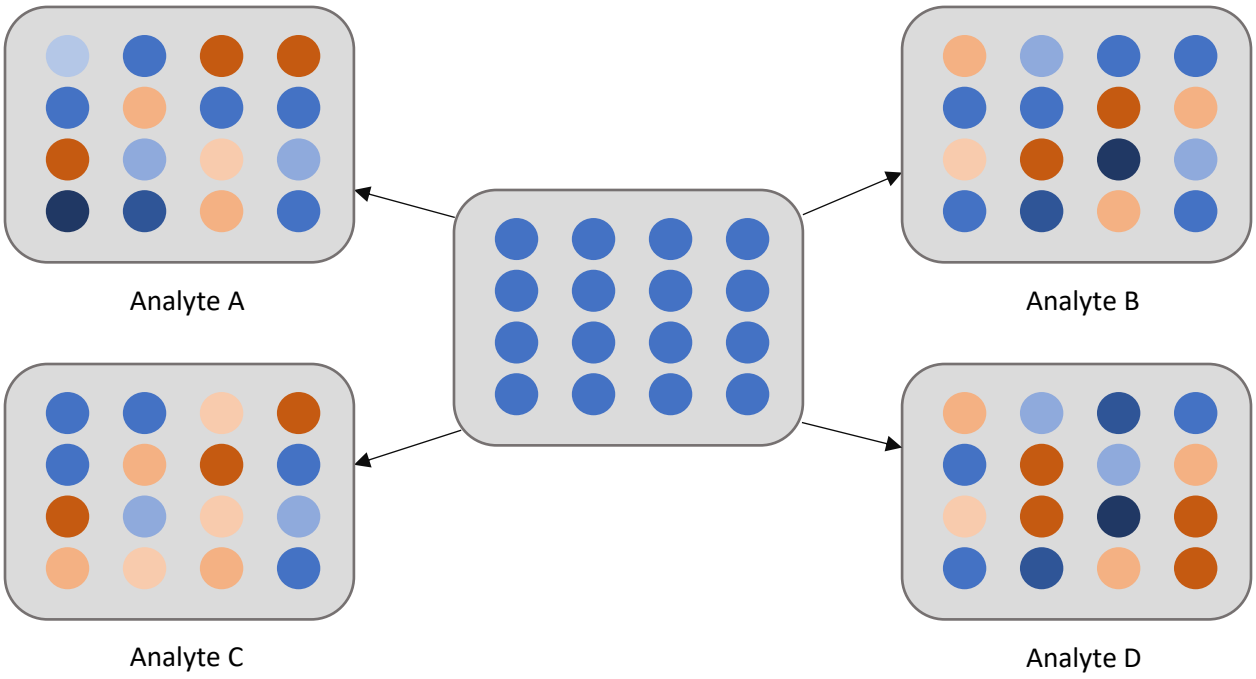

Figure 1-4 Example of pattern-based analytical discrimination: a series of sensors or instrumental measurements that respond differently upon the addition of different analytes generates a unique pattern for each analyte. The system can discriminate among analytes.

1.3 Poly(amidoamine) (PAMAM) dendrimers

Our group has established the use of Poly(amidoamine) (PAMAM) dendrimers as host molecules for supramolecular sensing, in the construction of indicator displacement assays and array-based sensors. Dendrimers are a type of hyperbranched dendritic polymers, with regular, well-defined structures .[69-70] Dendrimers are regularly branched and globular: divalent or multivalent repeat units branch out from a “core” structure in their center. Important structural features also include interior structures and cavities, and surface functional groups. Among many hyperbranched and dendritic polymers available nowadays, PAMAM dendrimers are of particular interest because they are water soluble, they assume a well-defined globular structure

in solution, and they are commercially available in good purity. This has led to many applications in aqueous and biological environments; they also have a large loading capacity, i.e. they can take up large quantity of smaller molecules from solution, either as encapsulated supramolecular guests, or through binding to the large number of surface functional groups. For instance, our group reported that a sixth-generation PAMAM dendrimer can encapsulate up to 16 molecules of 4(5)-carboxyfluorescein dye in aqueous solution at neutral pH.[71] This is often facilitated by the high density of charged species on the solvent-exposed surface of these polymers, which leads to high charge density. In addition to their hydrophilic surface, large PAMAM dendrimers also offer large hydrophobic internal cavities that can also accommodate hydrophobic guest molecules.[72-73]

The first synthesis of PAMAM dendrimers was reported in 1985;[74] since then, this family of hyperbranched polymers has gained a lot of interest and has become one of the most well-studied.[75] It has since become the first commercially available dendrimer family.[76] The most common core is 1,2-diaminoethane (ethylenediamine); each increasing generation of PAMAM dendrimers doubles the number of surface functional group: a sample structure of PAMAM 1st generation (PAMAM G1) is shown in Scheme 1-2. Applications of PAMAM dendrimers so far have included drug delivery,[77-78] gene therapy,[79-80] and nanoreactor systems.[81-82] The most common terminal groups in these polymers are primary amines. Amine terminated PAMAM dendrimers are polycations at neutral pH in aqueous environment, and about half of the amine functional groups carry a positive charge.[83] The high positive charge density allows them to interact non-covalently with negatively charged molecules and act as supramolecular ligands for such molecules, with interesting applications to array-based chemical sensing for various analytes.[84-86]

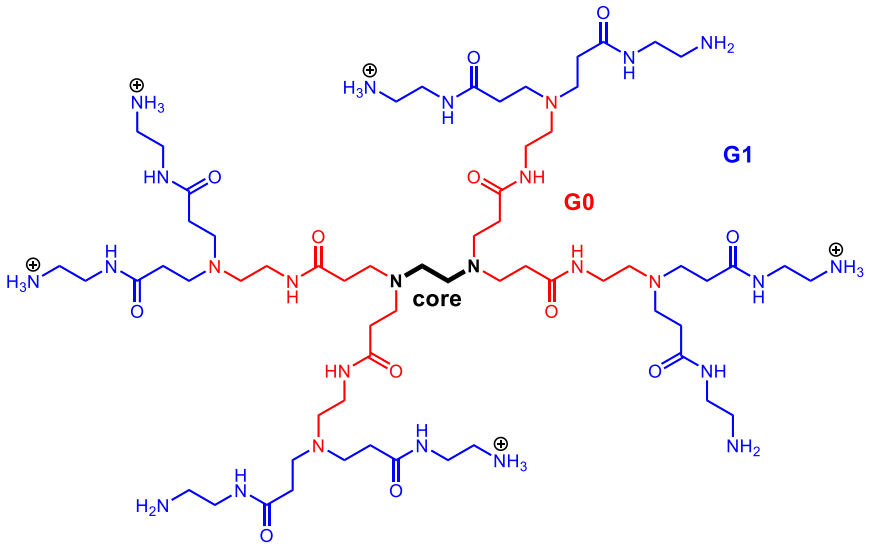

Scheme 1-2 First generation amine-terminated PAMAM dendrimer (G1) with ethylenediamine core. Each generation ends with an amine group, and two new branches are present at each amine point in the structure. Black: ethylenediamine core; red: generation 0; blue: generation 1.

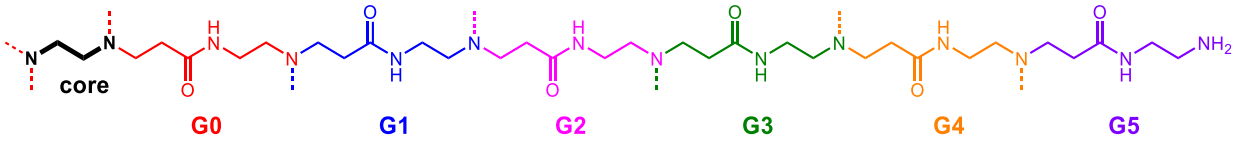

Scheme 1-3 One branch of an amine-terminated fifth generation poly(amidoamine) (PAMAM G5) dendrimer with ethylenediamine core. Each generation ends with a primary amine group, from which two branches originate: one branch is shown in the scheme, and the other branch is represented by the dashed line.

A common synthesis pathway for amine terminated PAMAM dendrimer is shown in Scheme 1-4. Starting with 1,2-diaminoethane (ethylenediamine) as a core molecule, two methyl acrylate groups are attached to each amine through a Michael addition, creating ester terminal groups. Then, each ester group is coupled with an ethylenediamine molecule through a transamidation reaction to create new primary amine terminal groups. Once these two steps are completed, a new generation of PAMAM dendrimer is achieved, referred to as generation *n*, or

G*n* (*n* is an integer "generation number", starting at 0). Therefore, molar mass and the number of surface groups essentially double for each increasing generation as shown in Table 1-1. It is crucial for the synthesis process to complete before the following reaction, and any products of incomplete reactions need to be removed at each step. As a result, the synthetic yield of pure homogeneous product decreases with increasing generation number. Therefore, higher-generation dendrimers need large amount of raw materials and extensive workup procedures to eliminate byproducts with incomplete substitution ("dead branches"), and can take months to synthesize, resulting in their high price.

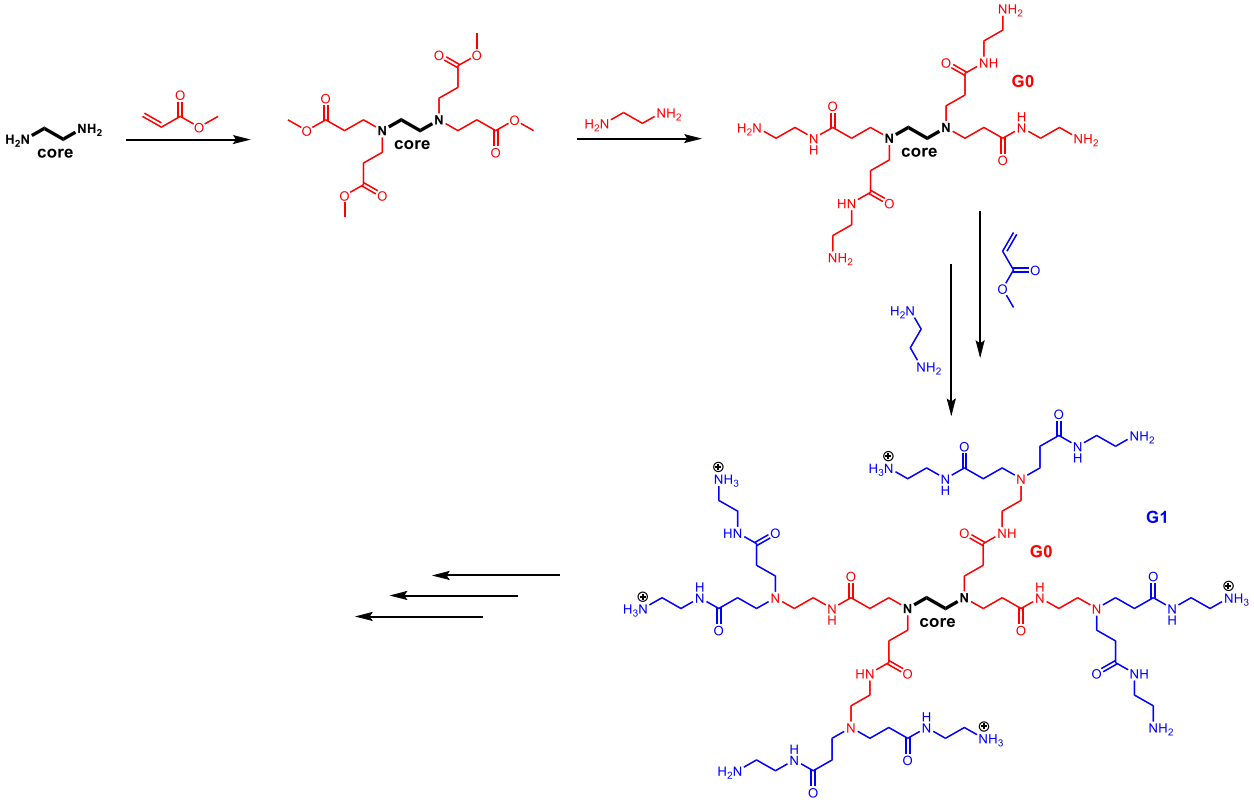

Scheme 1-4 A common synthesis of PAMAM G5 dendrimers with ethylene diamine core. Black: ethylene diamine core; red: generation 0; blue: generation 1.

Table 1-1 Structural parameters of different generations of PAMAM dendrimers.

Generation	Molar mass	Diameter	Surface groups	Price ($/g)
G3	6.9 k	36 Å	32	166
G4	14.2 k	45 Å	64	231
G5	28.8 k	54 Å	128	346
G6	58.0 k	67 Å	256	1020

In addition to amine termination, PAMAM dendrimers with other surface functional groups are also commercially available (see Scheme 1-5). The amine terminated PAMAM dendrimers can also be further modified for different purposes.[55,87-89]

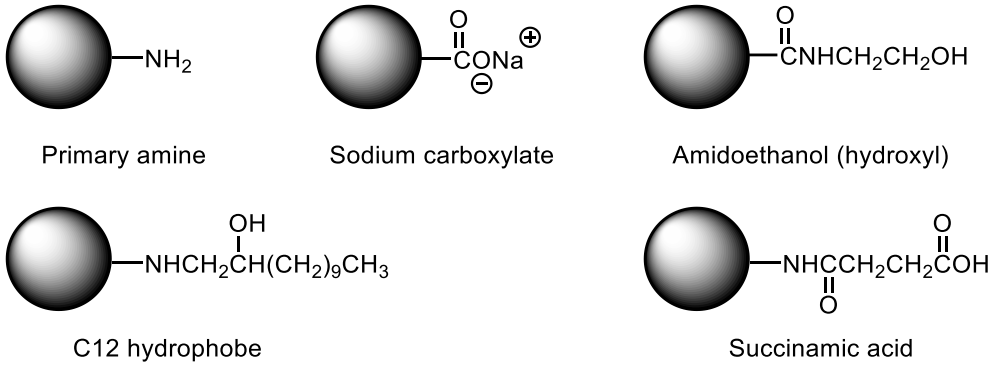

Scheme 1-5 Different terminal groups of PAMAM dendrimers that are commercially available.

Our group has done extensive work on PAMAM dendrimers, both from a fundamental standpoint studying the nature of the interactions they establish with smaller molecular in solution, and on their analytical applications. In a previous study on the interactions of guest molecule with PAMAM dendrimers, electrostatics were shown to be the major driving force of interactions; PAMAM dendrimers are good hydrogen bonding acceptor through their amide carbonyl group, but a negligible hydrogen bonding donor; they also establish stabilizing interactions with guest molecules containing π systems; due to their great flexibility, the shape and size of guest molecule are irrelevant for the interactions.[90] Previously in the group, PAMAM

dendrimers have been used for the sensing and discrimination of carbohydrates,[55] and phosphates.[57-58] In this study, we will discuss using PAMAM G5 dendrimers (shown in Scheme 1-3) as supramolecular hosts for sensing and discrimination of carboxylates and β-lactam antibiotic in neutral buffered water, as well as sensing and discrimination of carboxylates on solid supports.

1.4 Pattern-based recognition

As discussed above, array-based sensing generally involves multiple sensors, or multiple instrumental channels on the same sensing system. Therefore, each measured sample point is associated with multiple instrumental measurements, generating a multidimensional dataset that is hard to interpret. Pattern-based recognition algorithms are often used for data interpretation and dimensionality reduction. Such algorithms include Principal Component Analysis (PCA) and Linear Discriminant Analysis (LDA).[91] Both PCA and LDA algorithms are clustering techniques that can be used to reduce the data complexity and generates two- or three-dimensional scores plot that can be visualized.[92-93] Both algorithms transform the raw dataset resulting from instrumental measurements into a new matrix with the same dimensions; the original measurements are combined into principal components (PC) for PCA, and factors for LDA. An important feature of these algorithms is the fact that these new descriptors (principal components or factors) are returned sorted by decreasing total variance (i.e. information content). The results contain the same information and have the same dimensions as the original data matrix, but the information density is concentrated in the first few PCs or factors. Thus, retaining the first two or three PCs or factors would retain the maximum amount of information while at the same time greatly simplifying the data set, and could become the new “axes” of a two or three-dimensional interpretation of the data.

The two- or three-dimensional result of analyte discrimination are typically presented as 2D or 3D scatter plots called “scores plot” for both PCA and LDA: in these plots, the multiple replicates of each analyte sample appear as a cluster of points. To each scores plot corresponds a “loadings plot”, providing the relative contribution of each original measurement to the new PCs or factors. This information allows us to link the discrimination results to the original measurements, as well as to the structural and chemical features of the analytes. Through the position of sample cluster on the scores plots, scientists are also able to summarize the chemical relationship between different analytes, such as the chemical structures and the type of interactions, and predict the chemical feature of unknown samples.

PCA is an *unsupervised* clustering technique, meaning that the identity of analytes is not provided to the algorithm before data transformation; it simply finds the linear combinations of original measurements that brings about the best separation of the full dataset; clustering and classification naturally emerge from these results.[94] In an analytical chemistry context, PCA has been used for the discrimination of drugs,[95-96] metal ions,[97-98] proteins,[99] phosphates,[58] and volatiles.[100].

LDA is a *supervised* clustering technique, in which the identity of the samples is provided to the algorithm at the beginning. LDA finds the linear combinations of the raw instrumental variables that minimize the cluster size (intracluster distances) while maximizing the distances among clusters (intercluster distances), providing optimal separation among each analyte clusters.[101-102] It has been used for the discrimination of various analytes including bacteria,[103] proteins,[104] wines,[105] sugars,[55-56] metal ions,[42,54] food additives,[106] and drugs.[107]. Due to the additional information provided, LDA normally leads to a better separation of clusters than PCA.

CHAPTER 2
CARBOXYLATE SENSING IN NEUTRAL AQUEOUS SOLUTION – BINDING TO [DYE•PAMAM] COMPLEXES

2.1 Introduction

2.1.1 Citric acid cycle intermediates and their relevance to human health

The citric acid cycle plays a major role in metabolism, since it generates energy in aerobic organisms, and anabolism. The polycarboxylic acid intermediates in the cycle contribute as biosynthetic precursors for glucose, non-essential amino acids, fatty acids, and carbohydrate synthesis.[108-111] However, recent studies show that the citric acid cycle intermediates also act as biological signaling molecules in bacteria, animals, plants, and humans.[112-115] Diseases caused by mutations of enzymes involved in the citric acid cycle have been reported.[116] In particular, citrate can be used as a reliable screening method for prostate cancer:[117] normal prostatic fluid contains high levels of citrate, which can be 400-1500 times higher than in blood plasma. However, in premalignant cells and malignant cells, because of mis-regulation of the ZIP1 zinc transporter, most of the citrate is convert to isocitrate. In this case, the citrate level will be ~10 times lower than normal.[118] Sensors have been developed for citrate,[119-121] but none has displayed good selectivity between citrate and isocitrate.

Another example is succinate, whose level in blood influences blood pressure, and its receptor protein, G protein coupled receptor GPR91, plays a role in renovascular hypertension,[114] which is closely linked to diabetes, renal failure, and atherosclerosis.[122-123]

The third example in which structural differentiation among isomers is important is that of fumarate, a citric acid cycle intermediate whose isomer maleate works as an inhibitor of this cycle, also known for causing kidney diseases (e.g. Fanconi syndrome).[124-125] Selective sensing of fumarate over maleate[126] or maleate over fumarate[127] has been reported. However, there is still a need to develop a sensor recognizing all carboxylates involved in the citric acid cycle. Thus, it is necessary to develop a simple, fast and chemoselective method to detect the presence and the concentration of multiple carboxylates in neutral aqueous media. We describe here a system that can discriminate among multiple relevant dicarboxylates anions in aqueous media of neutral pH, using supramolecular interactions and chemical fingerprinting approaches.

As discussed in the introductory chapter, supramolecular analytical chemistry has been gaining attention for anion sensing. Previously, carboxylates have been commonly recognized and discriminated using enzyme or protein as sensors.[128-129] However, in recent years, using fluorophores or chromophores as chemosensors for chemical discrimination has been brought into focus due to their high sensitivity, easier and faster operation, and their use of common and relatively inexpensive instrumentation such as UV-vis spectrometers, fluorometers, and microwell plate readers.[130-132] When applying optical chemosensors for discriminating common carboxylates, there are several existing problems: first, most existing carboxylate sensors only function in aprotic solutions,[133-135] which are not convenient for physiological or biochemical applications; additionally, most reported synthetic sensors carry a heavy synthetic burden;[136-137] finally, some target a set of carboxylate analytes that are already significantly different,[138-139] and not directly relevant to biosensing applications. A sensing system working in water at pH 7.4 would be ideal, but this is also quite challenging because these anions are good hydrogen bond acceptors and typically interact strongly with water molecules. This in turn leads to their strong

solvation in H_2O; therefore there in a strong energetic penalty arising from the cost of desolvation upon binding. Here, we selected 7 carboxylates from the citric acid cycle (shown in red in Scheme 2-1), as well as 3 more structurally similar carboxylates (shown in blue) that may also be found in physiological media and act as interferents (Scheme 2-1). According to their pK_a values shown in Table 2-1, at pH 7.40 these structures carry 2 or 3 negative charges.

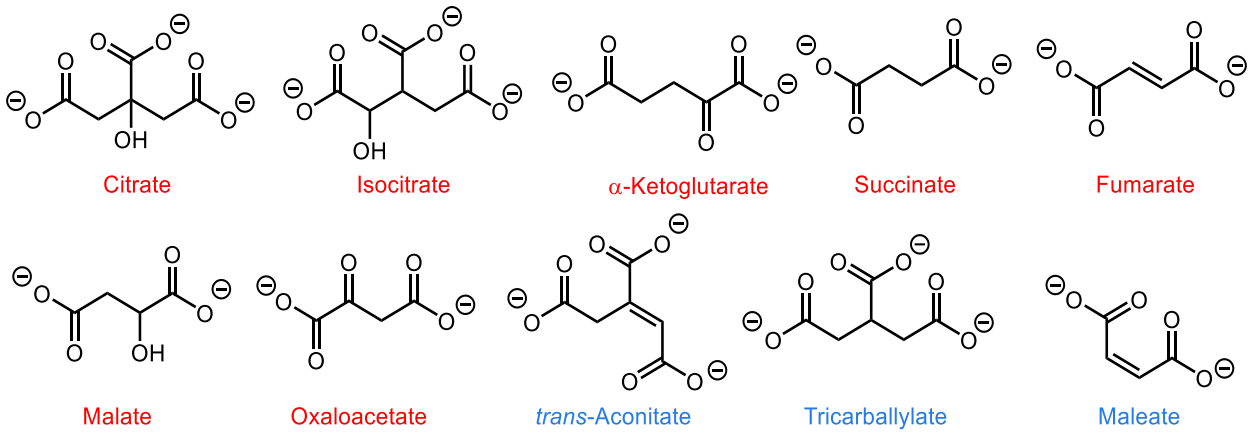

Scheme 2-1 Structures of the carboxylates of interest (red: citric acid cycle intermediate, blue: involved in citric acid cycle as inhibitors), shown in their protonation state in water at pH 7.4; see Table 2-1 for relevant pK_a values.

Table 2-1 pK_a of carboxylic acids and dyes.

Name	pK_a1	pK_a2	pK_a3	pK_a4	pK_a5	pK_a6
Citric acid[140]	3.13	4.76	6.40			
Isocitric acid[140]	3.29	4.71	6.40			
Tricarballylic[141]	3.49	4.58	5.83			
trans-Aconitic acid[142]	2.91	4.33	6.16			
α-Ketoglutaric acid[143]	2.35	4.85				
Succinic acid[140]	4.21	5.64				
Fumaric acid[140]	3.02	4.38				
Malic acid[140]	3.40	5.11				
Oxaloacetic acid[140]	2.55	4.37				
Maleic acid[140]	1.92	6.23				
Calcein blue[144]	3.07	6.8	11.3			

Pyranine[145]	7.2					
Calcein[146]	2.1	2.9	4.2	5.5	10.8	11.7

2.1.2 Dye-displacement experimental design

In our group's previous study, amine-terminated poly(amidoamine) (PAMAM) dendrimers can be used as supramolecular hosts for anionic organic compounds in array sensing applications, and for each sensor, the requirement for selectivity is greatly diminished with simple conditions and simple instrumentation.[90] PAMAM dendrimers are commercially available and water-soluble, and they are also globular hyperbranched polymers which display primary ammonium surface functional group homogeneously. These high-density surface functional groups provide high capacity to bind smaller molecules in solution through non-covalent interactions.[147-148] Such hosts carry positive charges at neutral pH by protonation of half of the amine groups,[83] so they can establish H-bonding and electrostatic interactions with a variety of anionic species. We were interested in using these interactions for sensing and discrimination of carboxylate analytes in water. In our experiment, fifth generation (G5) PAMAM dendrimers (shown in Scheme 2-2) were used, and about half of the 128 surface amine groups was protonated and carries positive charges at pH 7.40, which would bond with the carboxylate anions through electrostatic interaction.

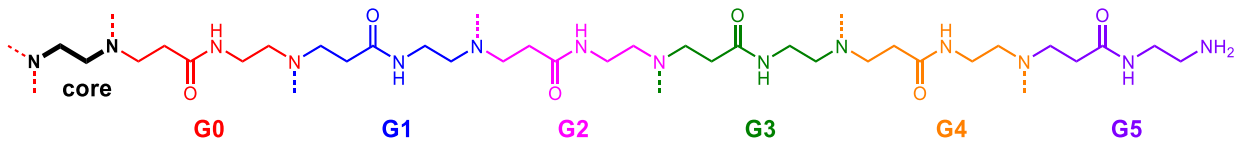

Scheme 2-2 One branch of an amine-terminated fifth generation poly(amidoamine) (PAMAM G5) dendrimer with ethylene diamine core. Each generation ends with an amine group, and branches out twice: one branch is shown in the scheme, and the other branch is represented by the dashed line.

However, because both the selected PAMAM receptors and the carboxylates are spectroscopically silent in the visible region of the spectrum, those interactions are hard to monitor. In this study, this problem has been circumvented by building an indicator displacement assay (IDA), which is a dye displacement assay based on [dye•PAMAM] complexes to transform these silent receptors into full-fledged chemical sensors. In aqueous HEPES (2-[4-(2-hydroxyethyl)piperazin-1-yl]ethanesulfonic acid) buffer under neutral condition, the complex between an anionic organic dye and a PAMAM G5 dendrimer was first formed. Then, with the introduction of the analyte, a carboxylate, the analyte formed its complex with PAMAM and caused dye displacement, and the binding between dendrimer and analyte could therefore be monitored through the spectroscopic behavior of the dye. Dye candidates for this study had to be soluble and stable in water, they had to be themselves anionic, excellent fluorophores with high quantum yields, and commercially available in good purity, as those shown in Scheme 2-3 and Scheme 2-4. Among those dyes, calcein blue, pyranine, and calcein (structure shown in Scheme 2-3) gave the best [dye•PAMAM] complexes, which had excellent sensitivity, optical signal dynamic range, and good selectivity among different carboxylate analytes; and their benchtop study will be discussed in this chapter.

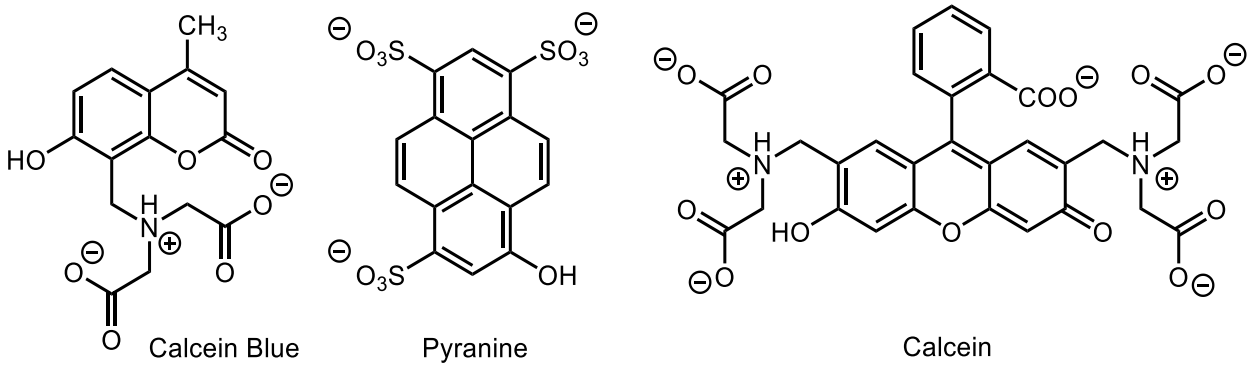

Scheme 2-3 Structures of calcein and pyranine in their most likely protonation state in water at pH 7.4; see Table 2-1 for pK_a values.

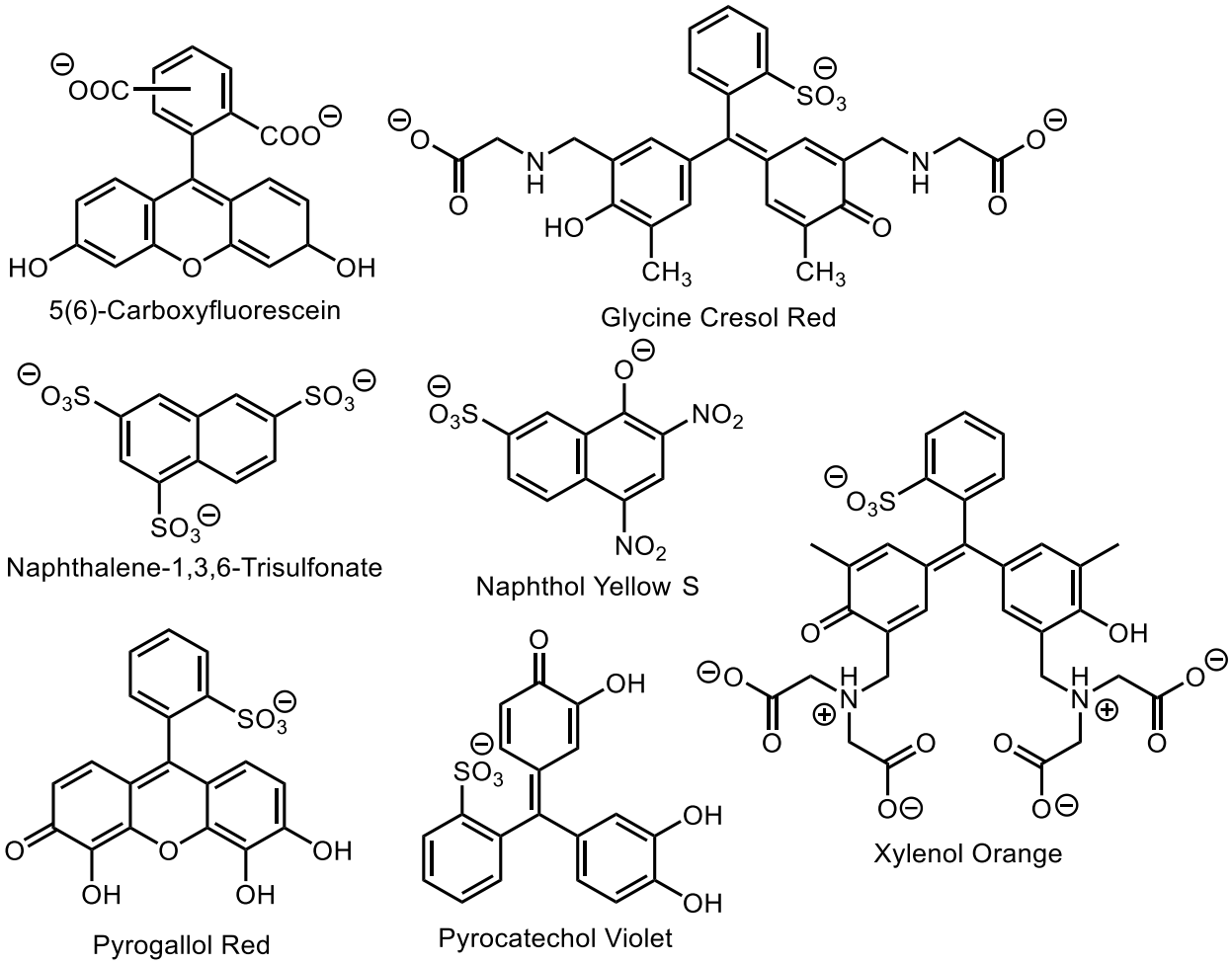

Scheme 2-4 Organic dyes that were investigated and rejected as candidate indicators in [dye•PAMAM G5] sensing complex, in their most likely protonation state in water at pH 7.4.

2.2 Dye complexation

2.2.1 Dye selection

After binding experiments trying to build different [dye•PAMAM] sensing complexes, the dyes shown in Scheme 2-4 were ultimately eliminated from consideration. Among those dyes, alizarin red S, naphthol yellow S, pyrogallol red, and pyrocatechol violet did bind with PAMAM G5 forming a complex, however, the dynamic change in spectroscopic signal between the bound and the free state was too small for further use (see Figure 2-1a). Additionally, even

though naphthalene-1,3,6-trisulfonate bound with PAMAM G5 and displayed significant enough change, its absorption lay within the UV range, which is incompatible with planned studies to take place in polystyrene microwell plates, which are not transparent in the UV region (see Figure 2-1b); glycine cresol red and 5(6)-carboxyfluorescein, absorb in the visible range, did bind with PAMAM G5 and provided a good dynamic range, but unfortunately they were found to be relatively indiscriminate among different carboxylate analytes (see Figure 2-1c). Thus, these dyes were not studied further.

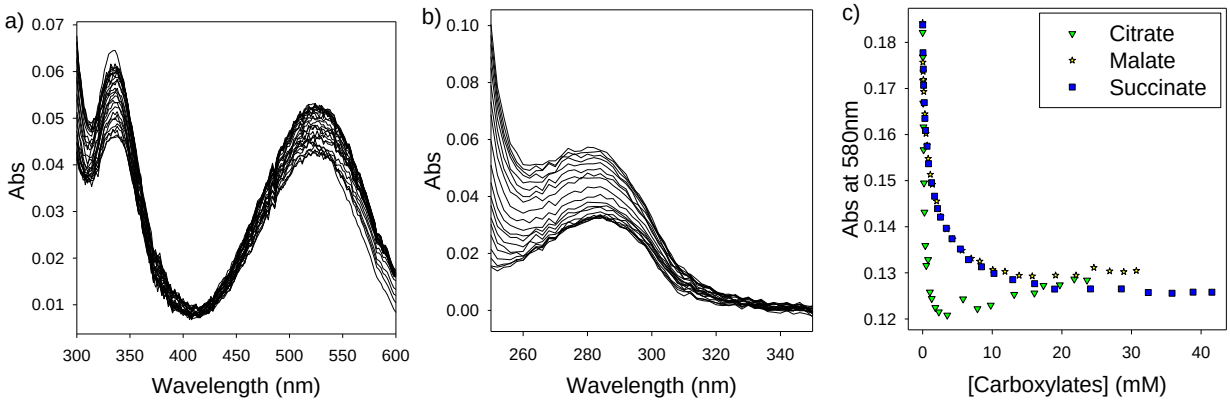

Figure 2-1 a) Absorbance spectra obtained from the titration of PAMAM G5 into alizarin red S solution; b) absorbance spectra obtained from the titration of PAMAM G5 into naphthalene-1,3,6-trisulfonate solution; c) absorbance profile at 500 nm, obtained from the titration of carboxylates into a [glycine cresol red•PAMAM] complex. Performed in 50 mM aqueous HEPES buffer at pH 7.4, T = 25 °C.

2.2.2 Formation of [calcein blue•PAMAM] complex

We first studied the interaction of calcein blue with PAMAM G5 in HEPES buffer at pH 7.4. Upon the addition of PAMAM G5 into calcein blue solution, the absorption band of calcein blue shifted to a lower energy absorbance band, with a clear isosbestic point at 338 nm (Figure 2-2a), indicating the formation of [calcein blue•PAMAM] complex. Figure 2-2b is the profile of the new absorbance peak at 364 nm, which reached a plateau at PAMAM

concentration around 40 μM. The concentration of calcein blue in these experiments was 10.2 μM.

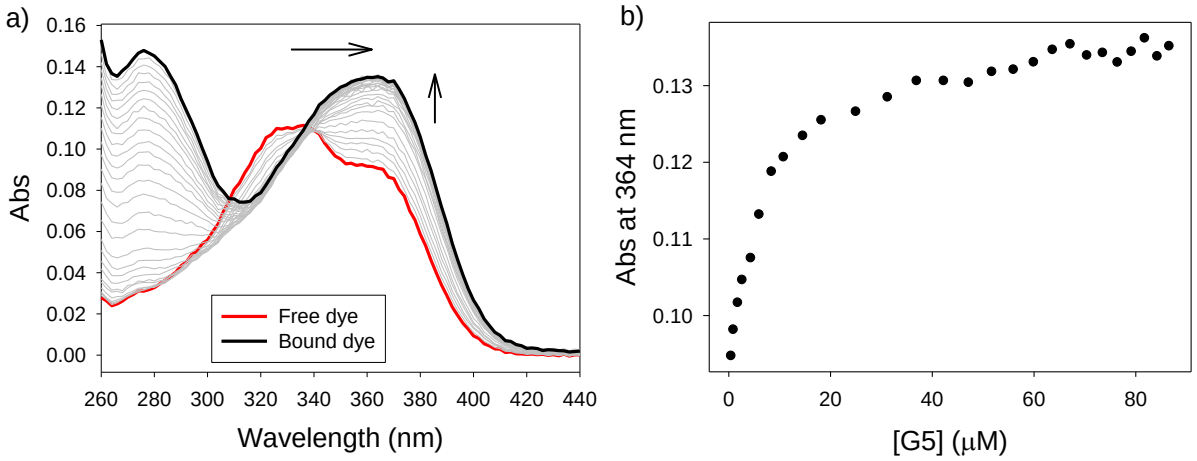

Figure 2-2 Binding of calcein blue to PAMAM G5 dendrimer. a) Absorbance spectra; b) Absorbance profile at 364 nm. [calcein blue] = 10.2 μM. Performed in 50 mM aqueous HEPES buffer at pH 7.4, T = 25 °C.

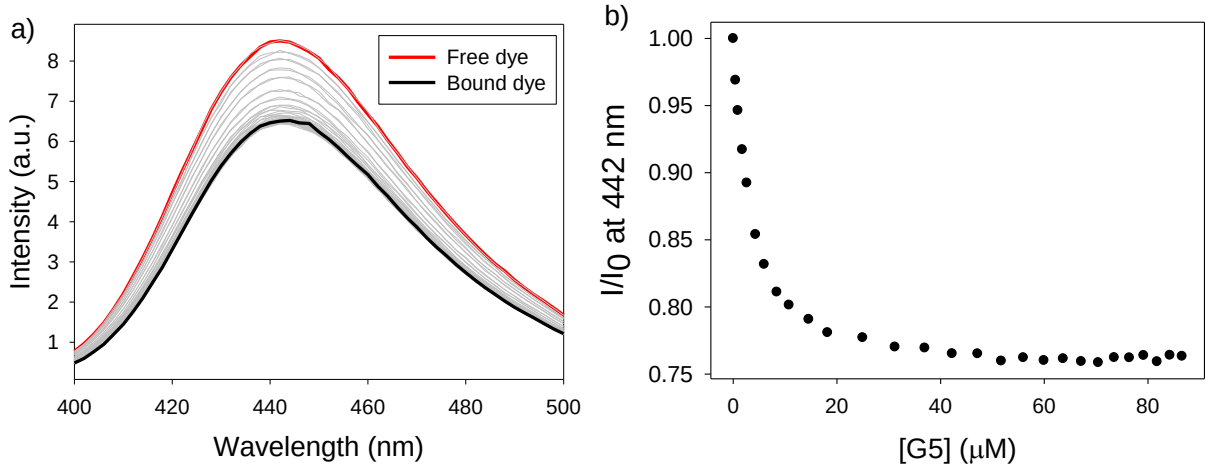

Figure 2-3 Binding of calcein blue to PAMAM G5 dendrimer. a) Fluorescence emission spectra; b) emission intensity profile at 442 nm. [calcein blue] = 10.2 μM. Performed in 50 mM aqueous HEPES buffer at pH 7.4, T = 25 °C, excitation: 338 nm.

The binding titration was also monitored through fluorescence intensity measurements were performed in the same conditions and shown in Figure 2-3a; the profile of the emission

peak at 442 nm (Figure 2-3b) shows that the fluorescence emission decreases upon the addition of PAMAM.

Fluorescence anisotropy (Figure 2-4) measurements were also conducted. Fluorescence anisotropy, i.e., the directional dependence of the polarization of the fluorescence emission when excited with plane-polarized light, is a direct reporter of the binding and unbinding of the dye and dendrimer. In particular, a significant increase in the fluorescence anisotropy signal is linked with the binding of a small fluorophore to a macromolecule. Specifically, in this experiment, it is associated with the binding between the small fluorophore (dye) and a large non-fluorescent molecule (PAMAM G5). The rotational correlation time of a small organic dye typically in hundreds of picoseconds due to its small size, whereas its fluorescence lifetime is several nanoseconds. In this case, when calcein blue was excited by a polarized light, by the time it emitted, the dipole of calcein blue had rotated randomly and scrambled the polarization, resulting in low anisotropy reading. However, when calcein blue was bound to the bulky dendrimer whose rotational correlation time was around 120 nanoseconds, by the time calcein blue emitted, its dipole still remained at a very similar position, resulting in high polarization in the emission. This was very helpful for us because the changes in absorbance and fluorescence emission behavior of the dye shown so far did clearly indicate that there was an interaction between the dye and the PAMAM dendrimer, but on the other hand did not prove the formation of a complex between the two. However, an increase in fluorescence anisotropy could only be ascribed to the formation of a complex in which the small fluorophore's rate of tumbling in solution is greatly reduced; this is strongly indicative of the formation of a complex of significant stability between this fluorophore and a much larger host molecule, i.e. the postulated [dye•PAMAM] complex.

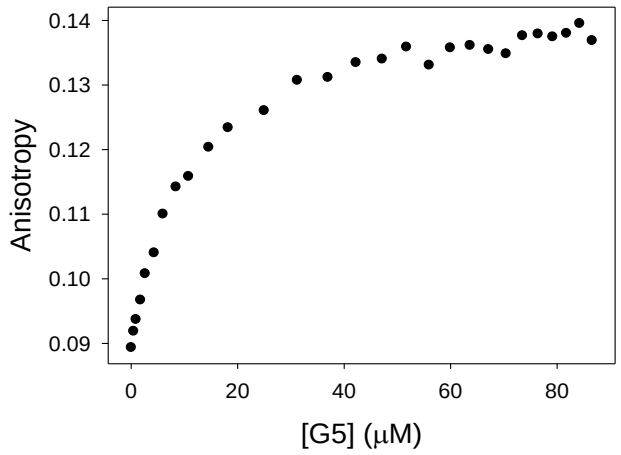

Figure 2-4 Fluorescence anisotropy profile for the binding of calcein blue to PAMAM G5 dendrimer. Excitation: 338 nm; emission: 442 nm. [calcein blue] = 10.2 μM. Performed in 50 mM aqueous HEPES buffer at pH 7.4, T = 25 °C.

2.2.3 Formation of [pyranine•PAMAM] complex

Another dye that showed great affinity to PAMAM dendrimer was pyranine, which carries 3 negative charges and has a lower solubility than calcein blue in water. Titration spectra are shown in Figure 2-5a: with the addition of PAMAM G5 into pyranine solution, the absorbance peak of pyranine shifted towards lower energy, with an isosbestic point at 417 nm, indicating that there was interaction between pyranine and PAMAM G5. Taking the absorbance profile of the new band at 460 nm (Figure 2-5b), absorbance increased and reached a plateau when G5 reached concentration at around 1 μM.

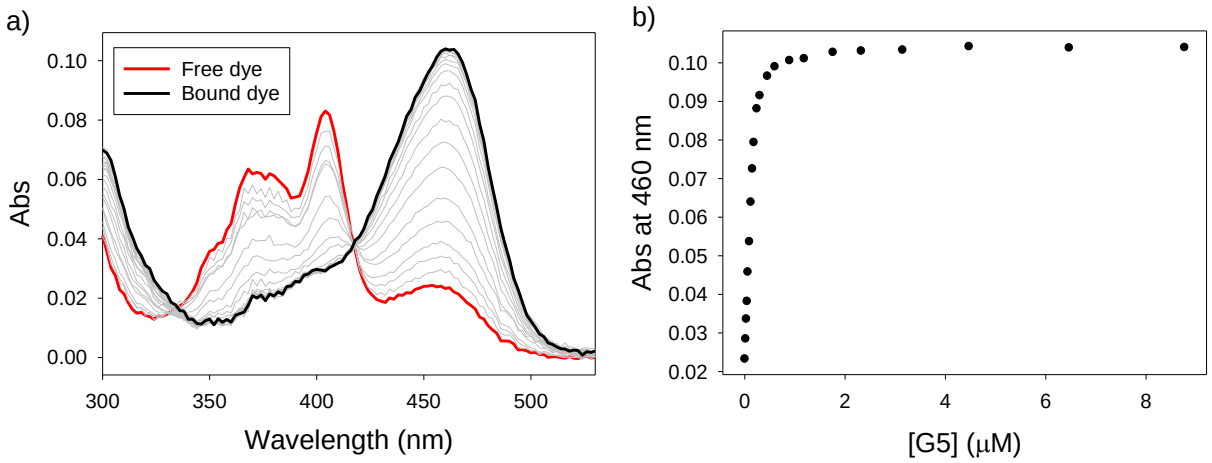

Figure 2-5 Binding of pyranine to PAMAM G5 dendrimer. a) Absorbance spectra; b) Absorbance profile at 460 nm. [pyranine] = 6.04 μM. Performed in 50 mM aqueous HEPES buffer at pH 7.4, T = 25 °C.

Fluorescence binding measurements were performed in the same conditions as the absorbance measurements. As shown in Figure 2-6a, the fluorescence intensity decreased in the beginning, followed by an increase to plateau. This sharp decrease was hard to see in a normal scale (see Figure 2-6b), thus, it was best visualized on a logarithmic scale (see Figure 2-6c). We assume that at first, when only a small amount of PAMAM G5 was added, the ratio of pyranine/G5 was high, so a complex combining multiple pyranine molecules per G5 dendrimer was formed, thus, the distance between two dye molecules in the same complex was very small. Fluorescence intensity decreased due to resonance energy transfer (RET) that resulted in self-quenching between dye molecules held in close proximity to each other by the G5 dendrimer. Then, with further additions of dendrimer the pyranine/G5 ratio decreased, favoring the formation of 1 to 1 [pyranine•PAMAM] complexes in solution, and removing the opportunity for pyranine to self-quench, which led to a gradual increase in intensity. Finally, the fully bound dye was found to be more fluorescent than the free dye, probably because binding to the dendrimer rendered it more rigid and removed chances of non-radiative decay.

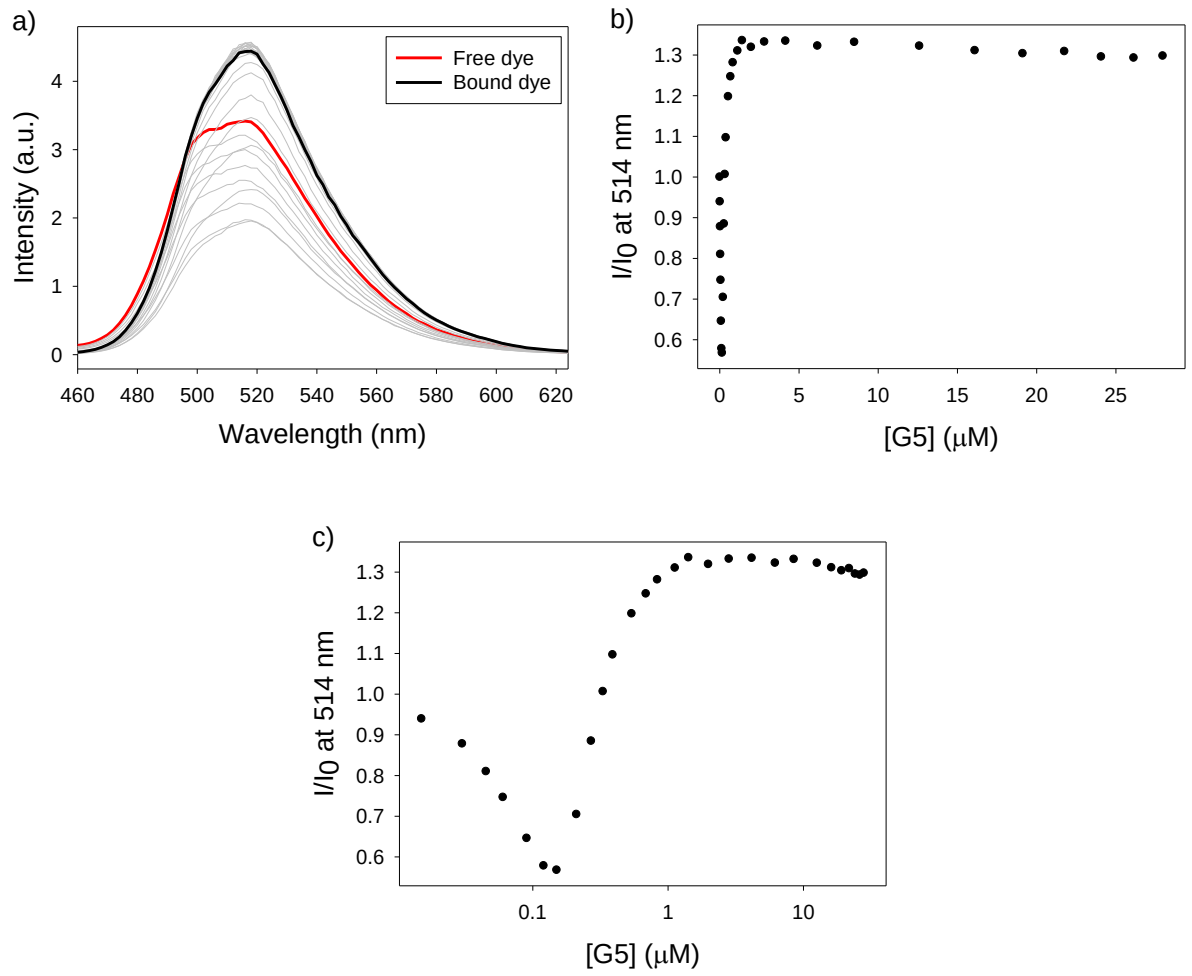

Figure 2-6 Binding of pyranine to PAMAM G5 dendrimer. a) Fluorescence emission spectra; b) emission intensity profile at 514 nm (linear scale); emission intensity profile at 514 nm (logarithmic scale). [pyranine] = 6.04 μM. Performed in 50 mM aqueous HEPES buffer at pH 7.4, T = 25 °C, excitation: 418 nm.

Looking at the fluorescence anisotropy profile obtained for the same titration, shown in Figure 2-7, we found that it took more dendrimer to reach a plateau than it took for absorbance and fluorescence emission titration experiments with the same binding pair. We believe that this was due to RET scrambling of the anisotropy, a known side effect of RET quenching: a bound dye in its excited state relaxes by passing energy to another dye nearby with some different transition dipole orientations; when this second dye emits, the polarization of emitted light is

scrambled with respect to the excitation light, even though no rotation has occurred.[149-150] Unfortunately, this less sensitive response would not be informative for analyte binding study, due to the fact that the signal was very low at the desired G5 concentration. Study of absorbance, fluorescence emission and anisotropy all gave evidence of the formation of a complex between the dye pyranine and the dendrimer PAMAM G5, which would be viable to give optical signal of binding between carboxylate and PAMAM G5.

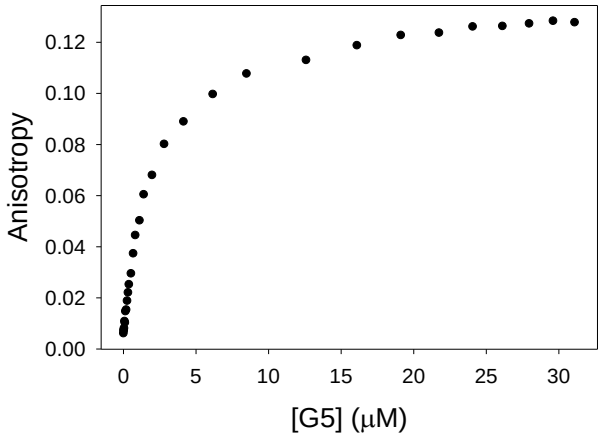

Figure 2-7 Fluorescence anisotropy profile for the binding of pyranine to PAMAM G5. Excitation: 418 nm; emission: 514 nm. [pyranine] = 6.04 μM. Performed in 50 mM aqueous HEPES buffer at pH 7.4, T = 25 °C.

2.2.4 Formation of [calcein•PAMAM] complex

Calcein was the last dye that showed a good binding affinity to PAMAM dendrimer. It carries 3 negative charges and is very soluble in water. Binding of calcein to the dendrimer caused a red shift in the absorbance (see Figure 2-8), as seen before for other dyes. Fluorescence emission had a similar trend as pyranine (see Figure 2-9), however, the bound dye had a lower fluorescence emission than its free form. Calcein is a xanthene dye, like fluorescein and carboxyfluorescein, which were both reported previously in our group to have this fluorescence behavior when binding with PAMAM dendrimer.[71,84] Measurements reached a plateau at 5 μM

of PAMAM dendrimer, which was near 2 equivalents of calcein. This was expected because compare with calcein blue which is also hydrophilic, calcein carries 2 more charges so its hydrogen bonding and electrostatic interaction with PAMAM dendrimer is stronger; compared with pyranine who carries the same charge, calcein is more hydrophilic, therefore, hydrophobic interaction is weaker. Fluorescence anisotropy response (see Figure 2-10) was also slower due to RET quenching but still sensitive enough to be informative compare with pyranine.

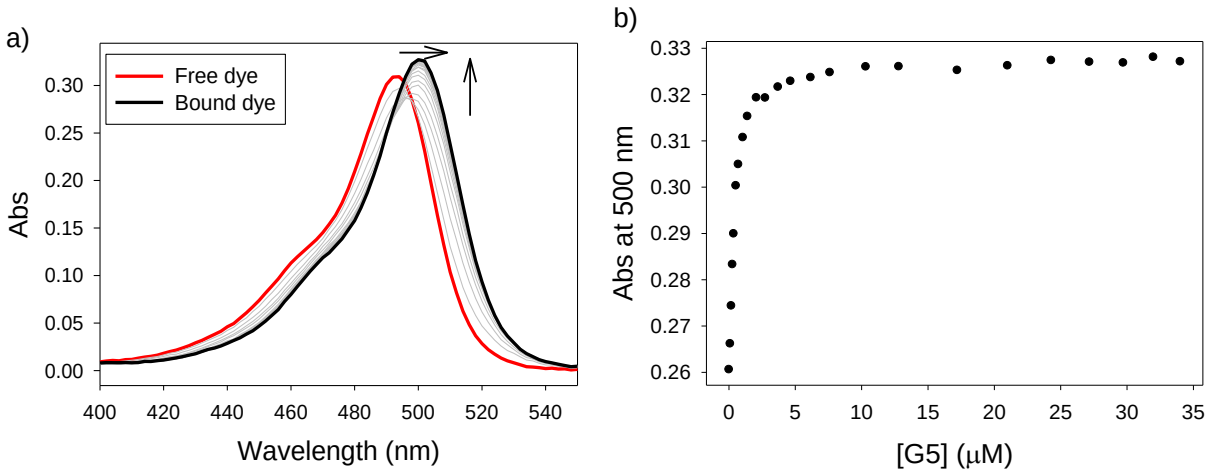

Figure 2-8 Binding of calcein to PAMAM G5 dendrimer. a) Absorbance spectra; b) Absorbance profile at 500 nm. [calcein] = 6.36 μM. Performed in 50 mM HEPES buffer at pH 7.4, T = 25 C.

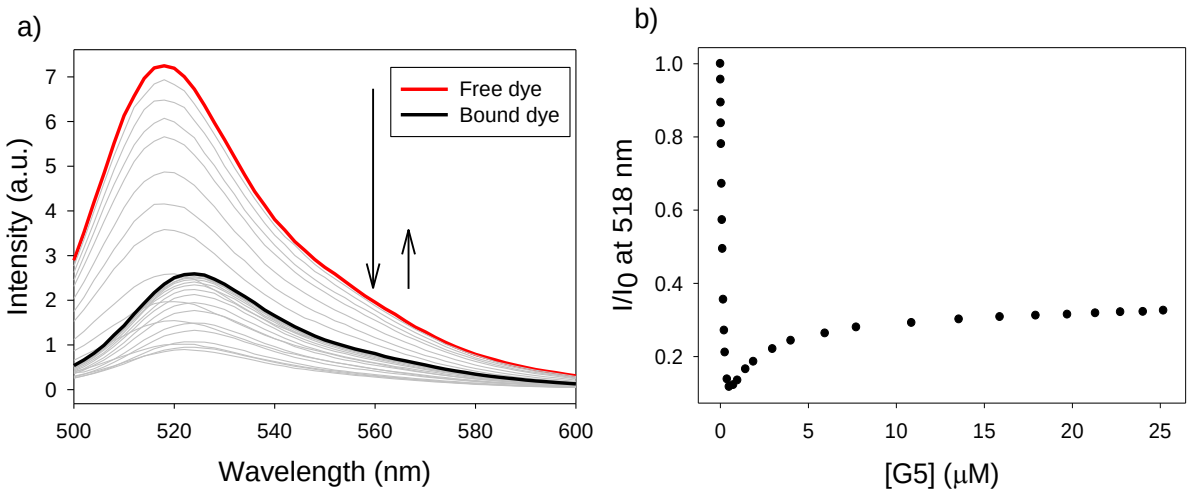

Figure 2-9 Binding of calcein to PAMAM G5 dendrimer. a) Fluorescence emission spectra; b) emission intensity profile at 518 nm. [calcein] = 6.36 μM. Performed in 50 mM aqueous HEPES buffer at pH 7.4, T = 25 °C, excitation: 494 nm.

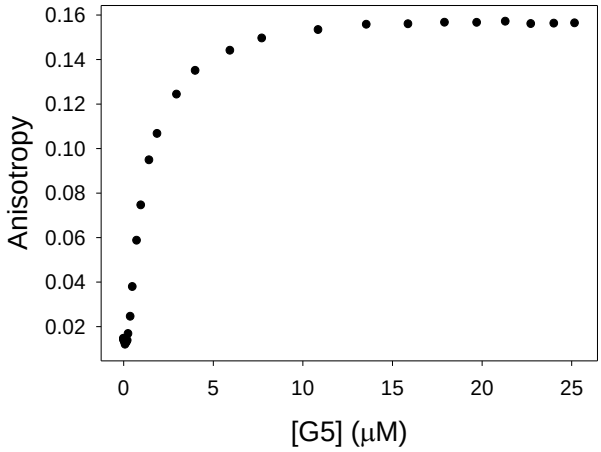

Figure 2-10 Fluorescence anisotropy profile for the binding of calcein to PAMAM G5. Excitation: 494 nm; emission: 514 nm. [pyranine] = 6.04 μM. Performed in 50 mM aqueous HEPES buffer at pH 7.4, T = 25 °C.

2.3 Carboxylate binding

Once the previously discussed three dyes had been proved to have a good binding affinity to G5 PAMAM, and large optical signal changes during binding, we moved on to setting up the IDA, to determine if the carboxylate analytes were able to bind G5 and cause the displacement of

the dye. From our group's previous experience, the best compromise between sensitivity and dynamic range of a displacement assay can be achieved when around 85% of the dye guest is bound to the dendrimer host.[151] In particular, at this relative concentration of G5, the corresponding signal on any of the dye-binding profiles (absorbance, fluorescence emission and anisotropy) was almost the same as the final value at the plateau. This provided maximum dynamic range, i.e. nearly the full range of signal change to be obtained when transitioning from free to bound dye, thereby providing maximum signal to noise ratio. On the other hand, at this relative concentration of titrant the system was not yet saturated, i.e. even a small change in concentration of titrant would still cause a relatively significant change in the system's optical response.

In this case, the concentrations of dyes and PAMAM G5 for carboxylates binding study were the following: for [calcein blue•PAMAM] sensor, [calcein blue] = 10.2 μM, and [G5] = 12.7 μM; for [pyranine•PAMAM]sensor, [pyranine] = 6.04 μM and [G5] = 0.213 μM; for [calcein •PAMAM] sensor, [calcein] = 6.36 μM and [G5] = 2.13 μM.

2.3.1 Monitoring anion binding using the [calcein blue•PAMAM] sensor

The titration spectra of carboxylates into [calcein blue•PAMAM] complexes shown in Figure 2-11, indicated that they have different behavior upon binding to the PAMAM dendrimer. Some carboxylates, such as oxaloacetate and α-ketoglutarate, displayed significant absorption in the UV range, which led to an overwhelming contribution to the profile due exclusively to the increasing concentration of anion during the course of the titration. This effect made the binding profiles for these anions difficult to interpret as such. In order to isolate the portion of the absorbance change signal due to the binding process, the absorbance signal at 360 nm was corrected by subtracting from the original raw profile the calculated absorbance due to the

carboxylate alone; thus corrected, the absorbance profiles for these anions could be evaluated alongside the others as shown in Figure 2-12.

In fact, all carboxylates showed similar trends, albeit with key differences. As the displacement proceeded, we expected the fluorescence emission intensity to increase as carboxylates were added in, because more calcein blue was displaced (free calcein has higher emission than the bound species, see Figure 2-3). However, the addition of some carboxylates such as oxaloacetate and *trans*-aconitate resulted in further quenching of the dye's emission. The quenching showed a linear behavior after displacement (~after 2.5 mM of carboxylates were added in). This might be due to inner filter effect: with an increasing concentration of these carboxylates over the course of the titration, a portion of the incoming excitation light was absorbed by the carboxylates instead of calcein blue, therefore causing an apparent quenching of its emission. Nevertheless, the fluorescence anisotropy signal showed different ability among carboxylates in displacing the dye: for example, citrate had the best affinity to the dendrimer. There was also an obvious difference between the tricarboxylate profiles and the dicarboxylate profiles, which agreed with the group's previous study: tricarboxylates had higher binding affinity to PAMAM dendrimers than dicarboxylates.[152]

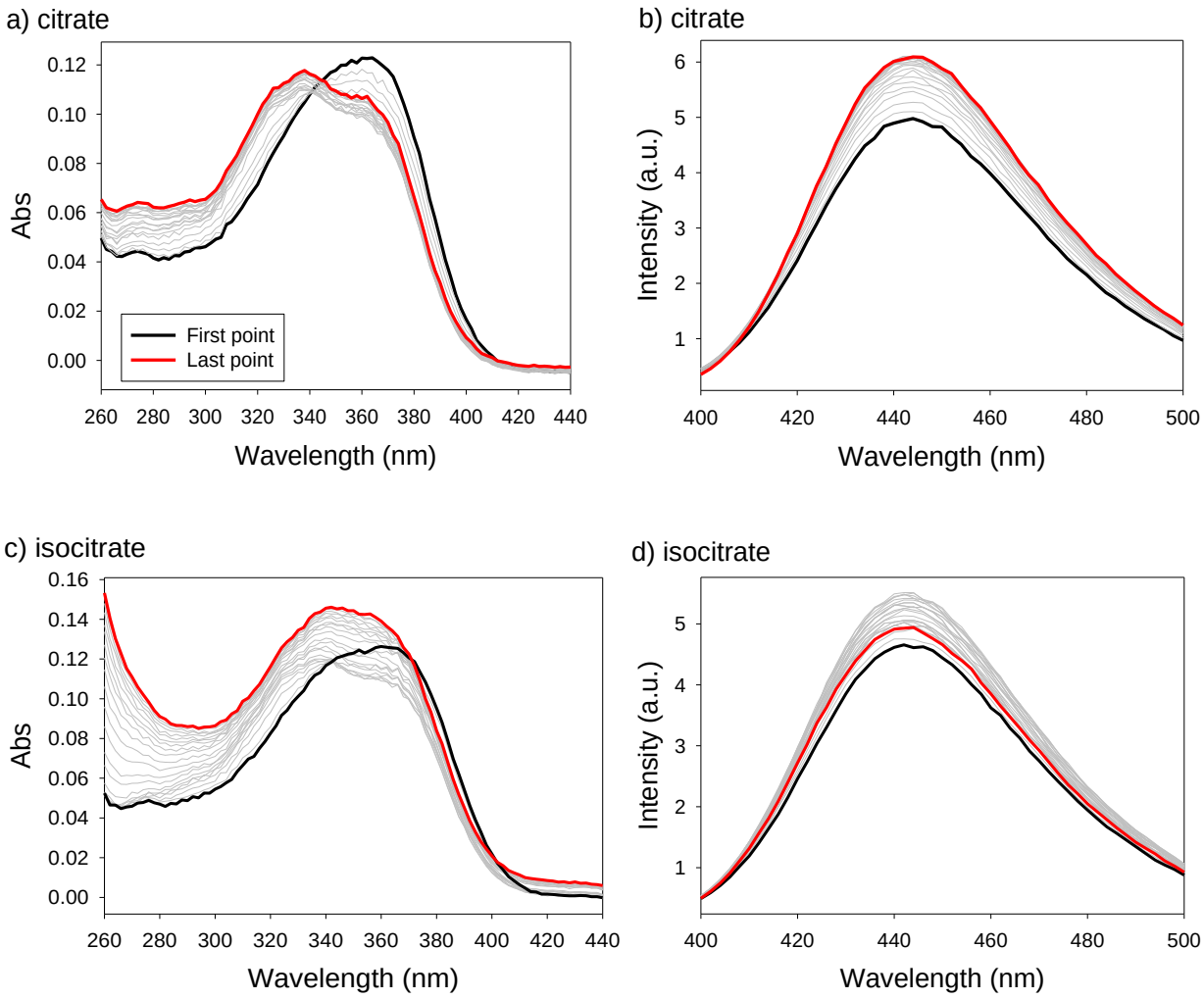

Continued on the next page.

e) α-ketoglutarate

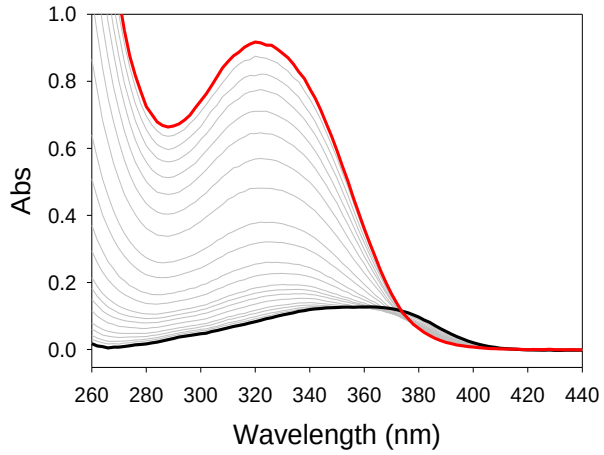

f) α-ketoglutarate

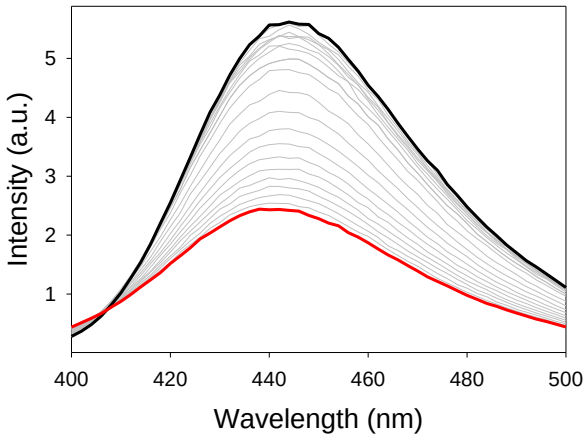

g) succinate

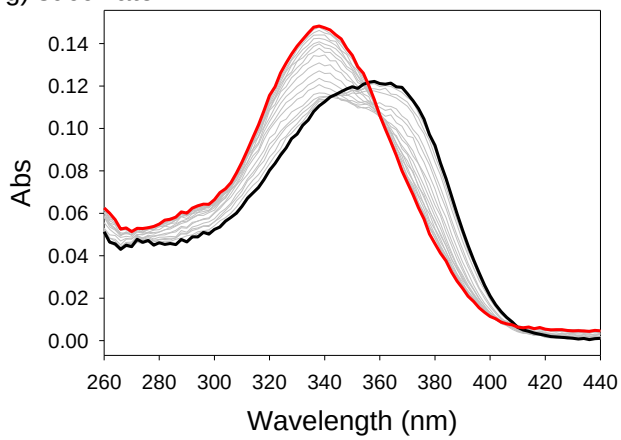

h) succinate

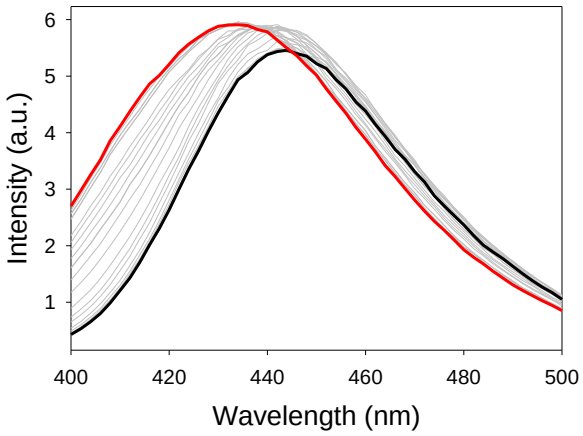

i) fumarate

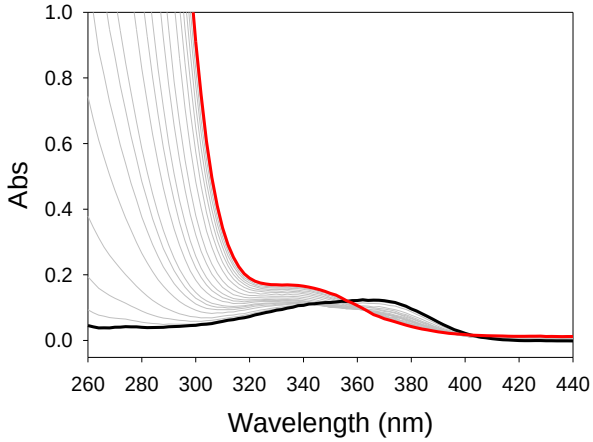

j) fumarate

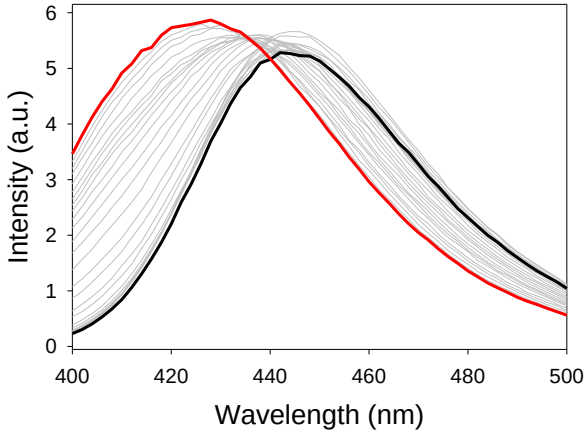

Continued on the next page.

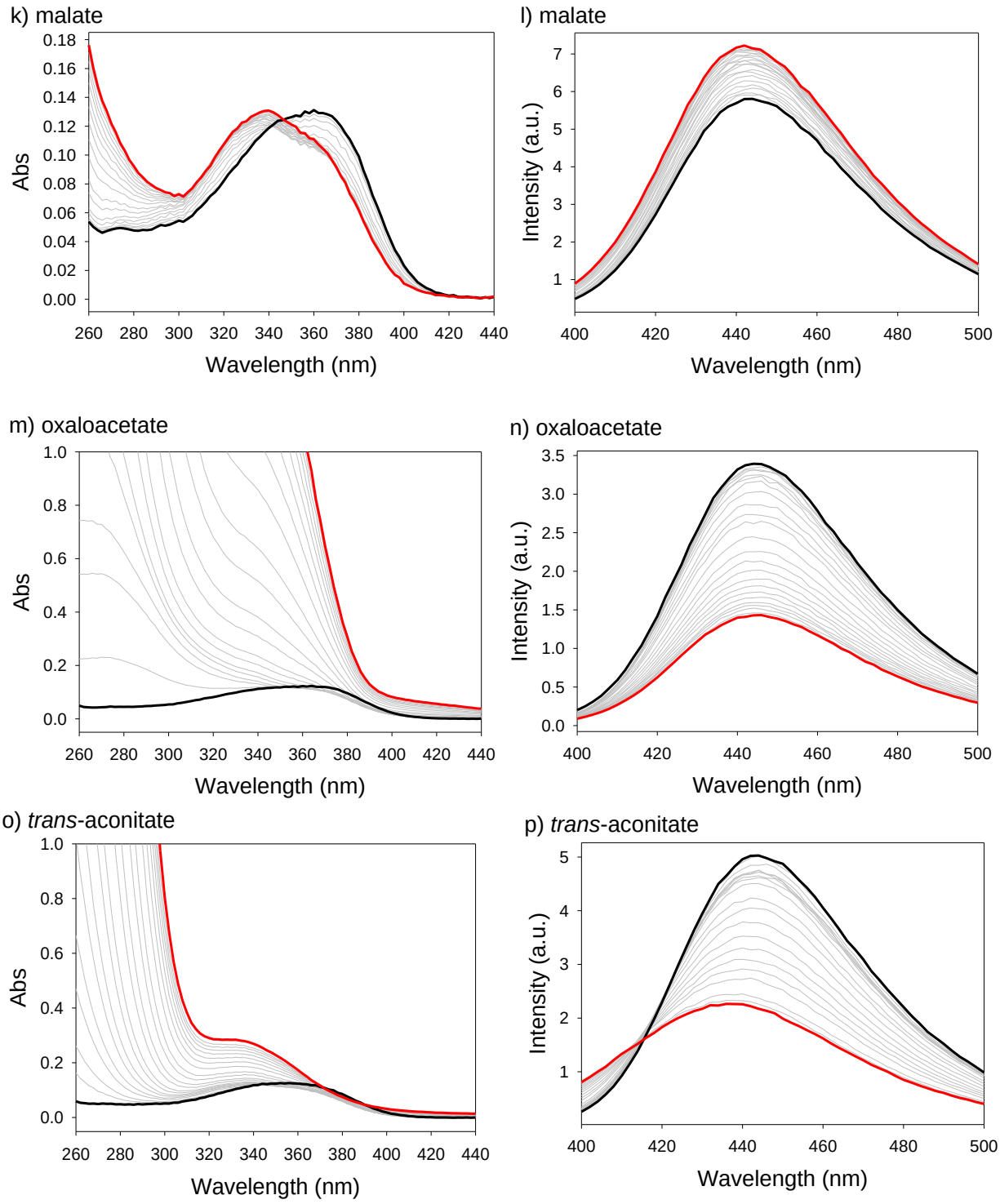

Continued on the next page.

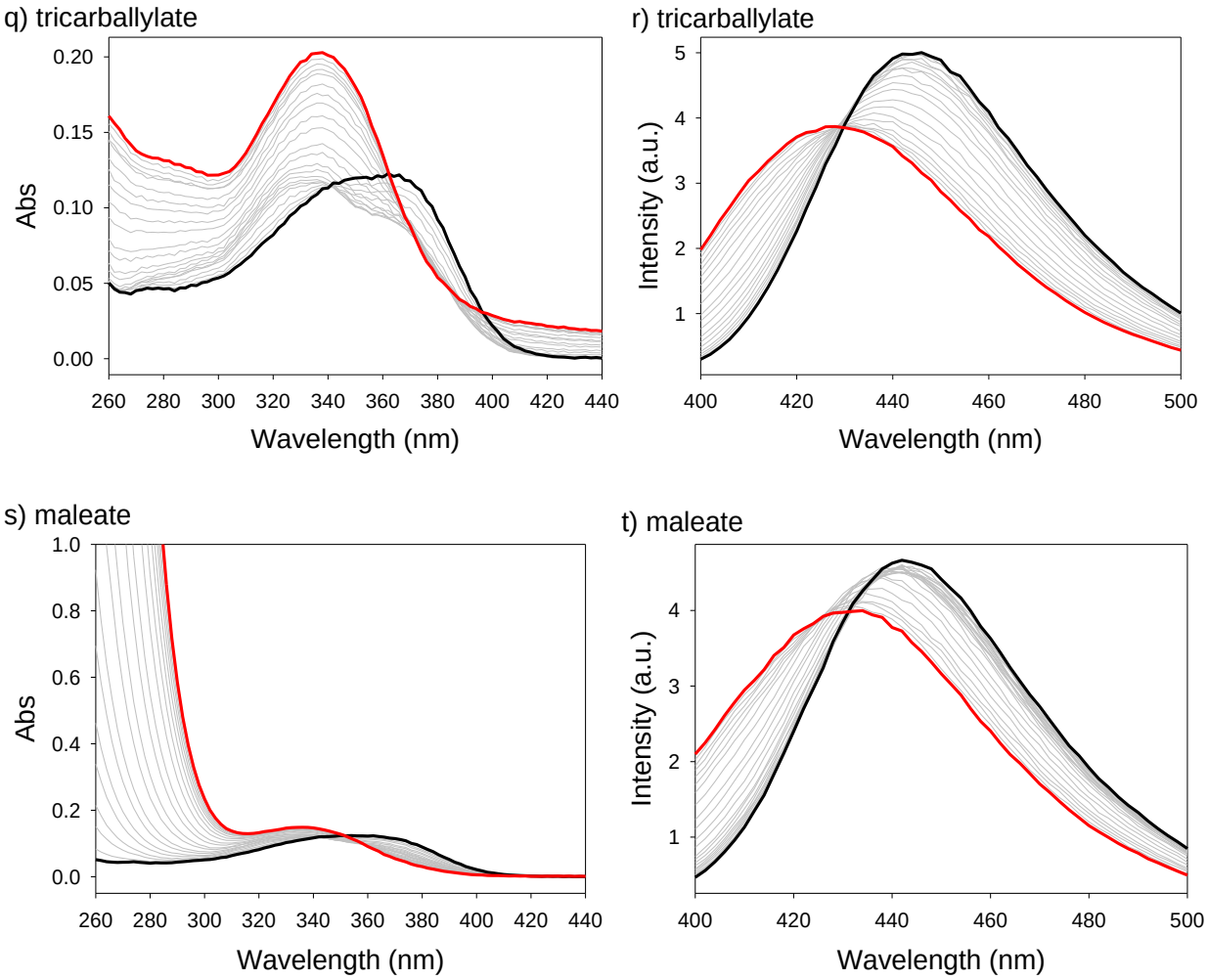

Figure 2-11 The binding of citrate (a, b), isocitrate (c, d), α-ketoglutarate (e, f), succinate (g, h), fumarate (i, j), malate (k, l), oxaloacetate (m, n), *trans*-aconitate (o, p), tricarballylate (q, r), and maleate (s, t) to PAMAM G5 is indicated by the displacement of the calcein blue dye from its complex with PAMAM G5. left: Absorbance spectra; right: Fluorescence emission spectra. Spectrum in black: first titration point; spectrum in red: the last titration point; spectra in gray: titration points in between. Performed in 50 mM aqueous HEPES buffer at pH 7.4, T = 25 °C. [calcein blue] = 10.2 μM, [PAMAM G5] = 12.7 μM, excitation: at the isosbestic point of the absorbance spectra from the corresponding titration study, so that any changes in fluorescence during the titration process could be ascribed to chemical interactions rather than to changes in absorbance (i.e. excitation efficiency).

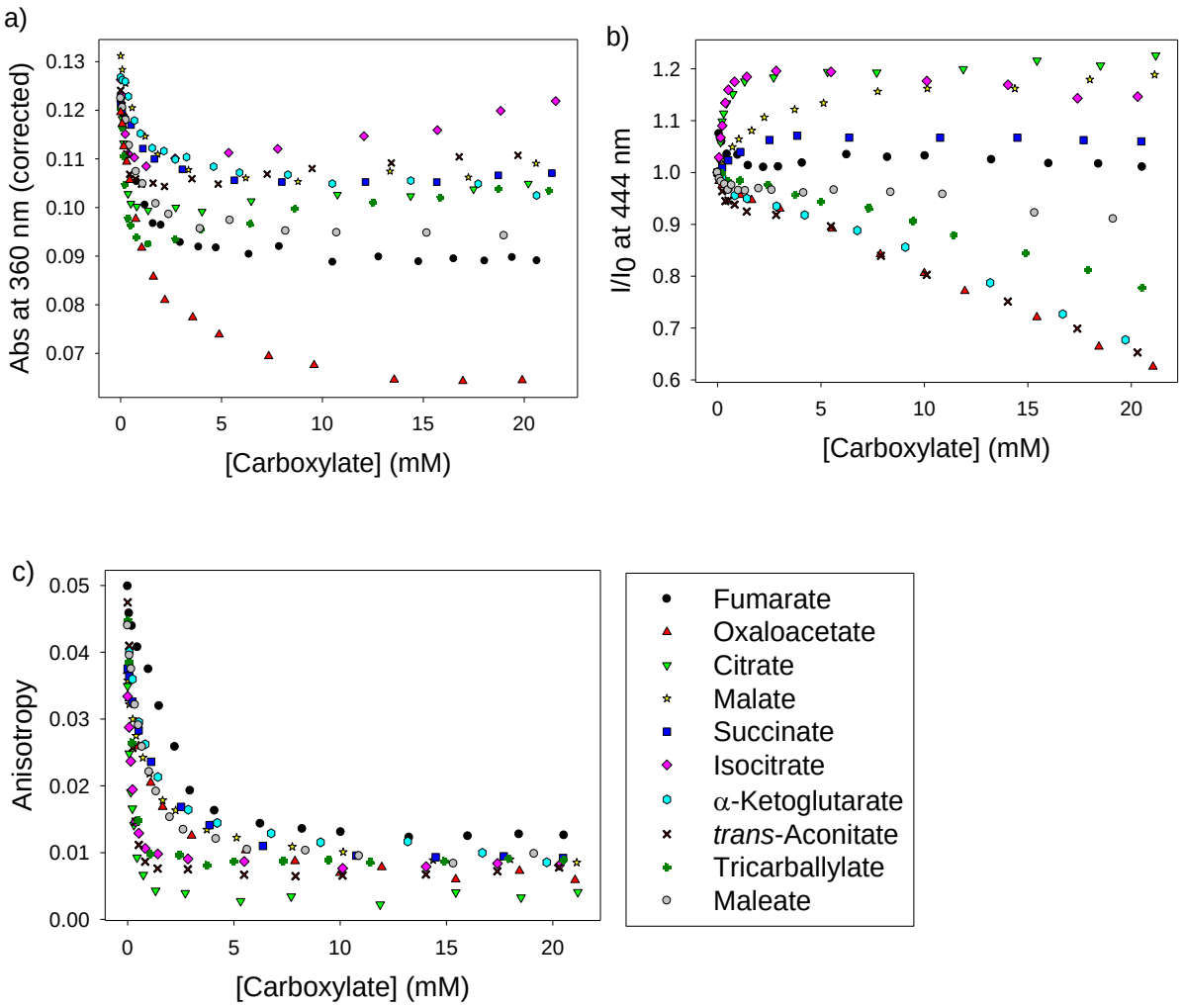

Figure 2-12 Binding of carboxylates to PAMAM G5 using calcein blue as indicator. Titration profiles of all carboxylates of interest into [calcein blue•PAMAM G5] complex: a) corrected absorbance; b) fluorescence emission; c) fluorescence anisotropy. Excitation: isosbestic point from absorbance spectra of each carboxylate in Figure 2-11, emission: 444 nm. [calcein blue] = 10.2 μM, [PAMAM G5] = 12.7 μM. Performed in 50 mM aqueous HEPES buffer at pH 7.4, T = 25 °C.

2.3.2 Monitoring anion binding using the [pyranine•PAMAM] sensor

The binding of citrate and α-ketoglutarate was also studied using the [pyranine•PAMAM] sensor in an indicator displacement assay to evaluate the performance of this dye as an indicator. These two anions were particularly chosen because they had been among the most successful in the anion binding studies described above. The absorbance and fluorescence emission spectra

obtained when introducing citrate or α-ketoglutarate to the [pyranine•PAMAM] complex, which caused the displacement of pyranine from PAMAM G5, are shown in Figure 2-13. From absorbance spectra, the rise of a free pyranine peak around 400 nm and the decrease of the complex peak around 460 nm indicated that the addition of citrate displaces pyranine from the complex, leaving most of the pyranine dye in its free form. On the other hand, even a large excess of α-ketoglutarate was not enough to completely displace pyranine from its PAMAM complex (at the last titration point, the optical behavior of pyranine dye was still not its "free form", which should look like the last point of titration of citrate), which was possibly due to some of the pyranine being buried in the cavity of PAMAM G5 driven by the hydrophobic effect. The latter dye fraction cannot be displaced by α-ketoglutarate, whom as a dicarboxylate, had a much lower binding affinity to dendrimer than citrate (a tricarboxylate).

In the course of citrate binding, fluorescence emission decreased first, then increased. This was consistent with the behavior that we observed in the study of binding between pyranine and G5: with small amount of citrate addition, the pyranine was not fully displaced, but instead it "re-bound" to a new binding site on the dendrimer. The resulting decreased distance between bound pyranine molecules led to self-quench and gave a low fluorescence emission. When more citrate was introduced, it saturated all binding sites on the dendrimer, displacing the pyranine dye from dendrimer; the increasing amount of more fluorescent free pyranine dye caused the observed increase in fluorescence emission.

Figure 2-14 showed the absorbance and fluorescence emission profiles for citrate and α-ketoglutarate when interacting with the [pyranine•PAMAM] complex. The two anions showed similar trends with noticeable differences, which will be beneficial in the differentiation. Finally,

the fluorescence anisotropy profile was unfortunately not informative at this PAMAM G5 concentration, due to the RET scrambling discussed above.

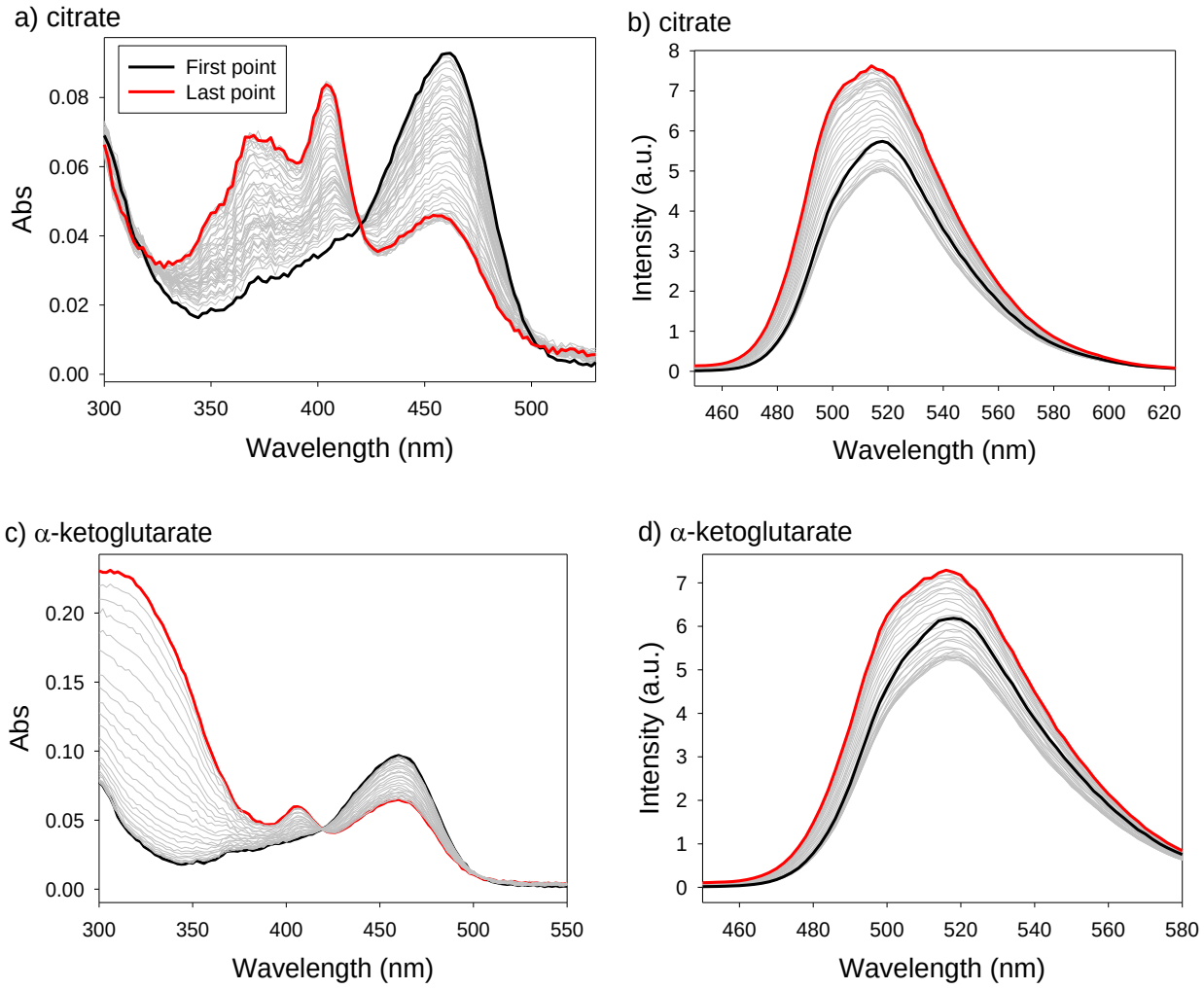

Figure 2-13 The binding of citrate (a, b), and α-ketoglutarate (c, d) to PAMAM G5 is indicated by the displacement of the pyranine dye from its complex with PAMAM G5. left: Absorbance spectra acquired during a titration of anion into the [pyranine•PAMAM] complex; right: Fluorescence emission spectra. Spectrum in black: first titration point; spectrum in red: the last titration point; spectra in gray: titration points in between. Performed in 50 mM aqueous HEPES buffer at pH 7.4, T = 25 °C. [pyranine] = 6.04 μM, [PAMAM G5] = 0.213 μM, excitation: 418 nm.

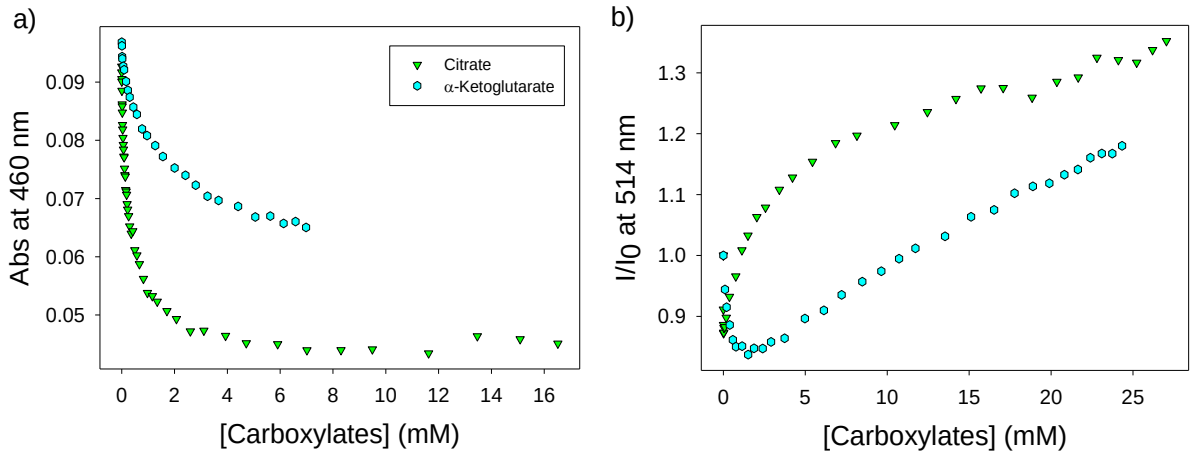

Figure 2-14 Binding of carboxylates to PAMAM G5 using pyranine as indicator. Titration profiles for binding citrate and α-ketoglutarate to PAMAM G5: b) absorbance; d) fluorescence emission. Excitation: 420 nm, emission: 514 nm. [pyranine] = 6.04 μM, [G5] = 0.213 μM. Performed in 50 mM aqueous HEPES buffer at pH 7.4, T = 25 °C.

2.3.3 Monitoring anion binding using the [calcein•PAMAM] sensor

The absorbance and fluorescence emission spectra obtained upon addition of carboxylates to the [calcein•PAMAM] sensor and the corresponding profiles are shown in Figure 2-15 and Figure 2-16, respectively. The absorbance spectrum shifted back to the dye's free form with the addition of carboxylates, indicating that the carboxylates displaced calcein from its complex. Unlike pyranine, fluorescence of calcein steadily increased during titration. This was due to the different concentration ratios of calcein and pyranine vs. G5. In fact, calcein : G5 was roughly 3:1, compared to the ratio between pyranine and G5 which was roughly 30:1. Therefore, the displaced calcein would not be able to concentrate at the surface of PAMAM G5 to cause RET quenching. In both cases, fluorescence anisotropy decreased and reached a plateau, which proved the displacement of calcein dye from PAMAM G5. The slopes of the anisotropy profiles reflect the relative affinities of the two anions (a steeper slope pointing to a stronger interaction). As discussed previously, tricarboxylates have higher affinity to PAMAM G5.

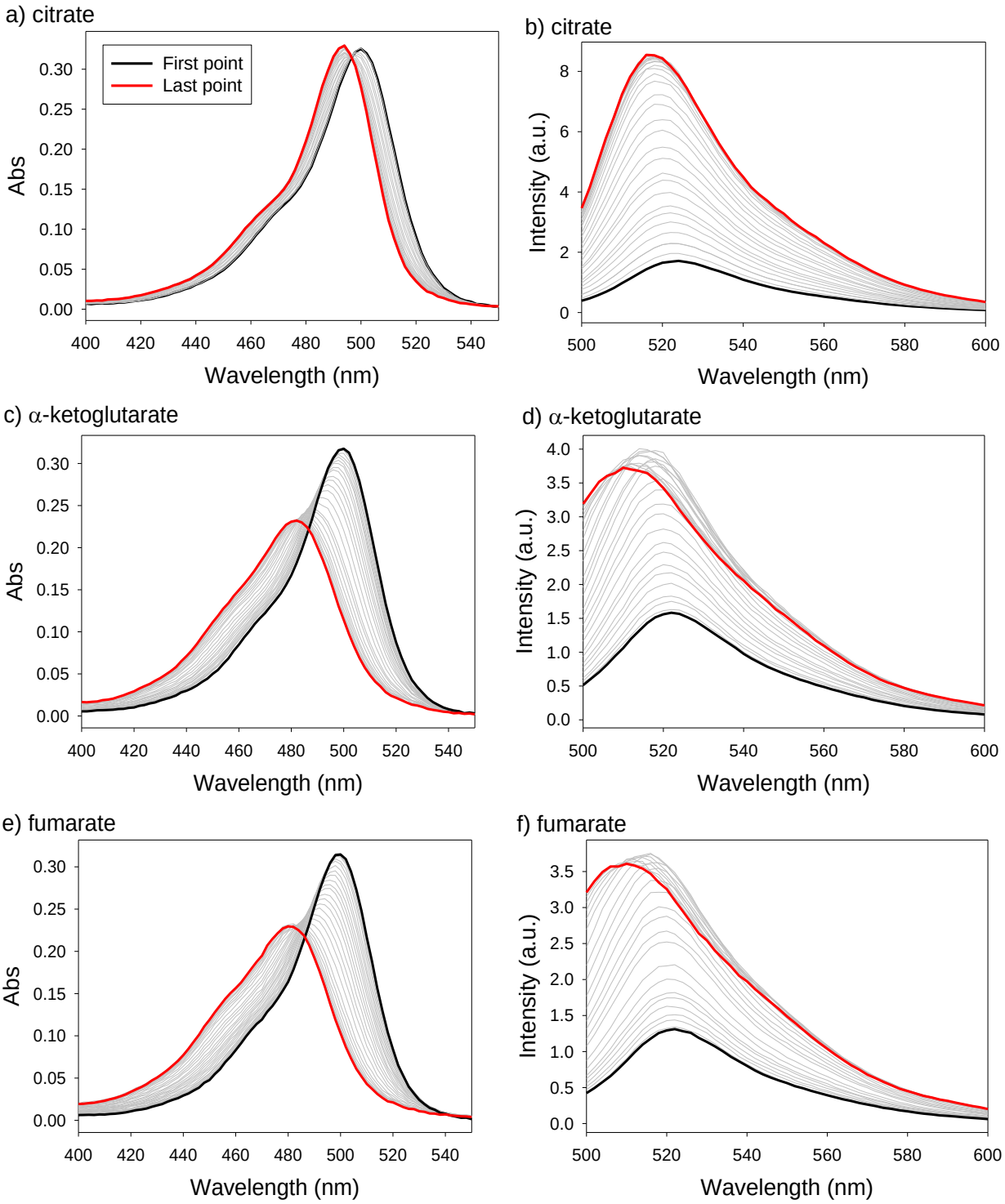

Continued on the next page.

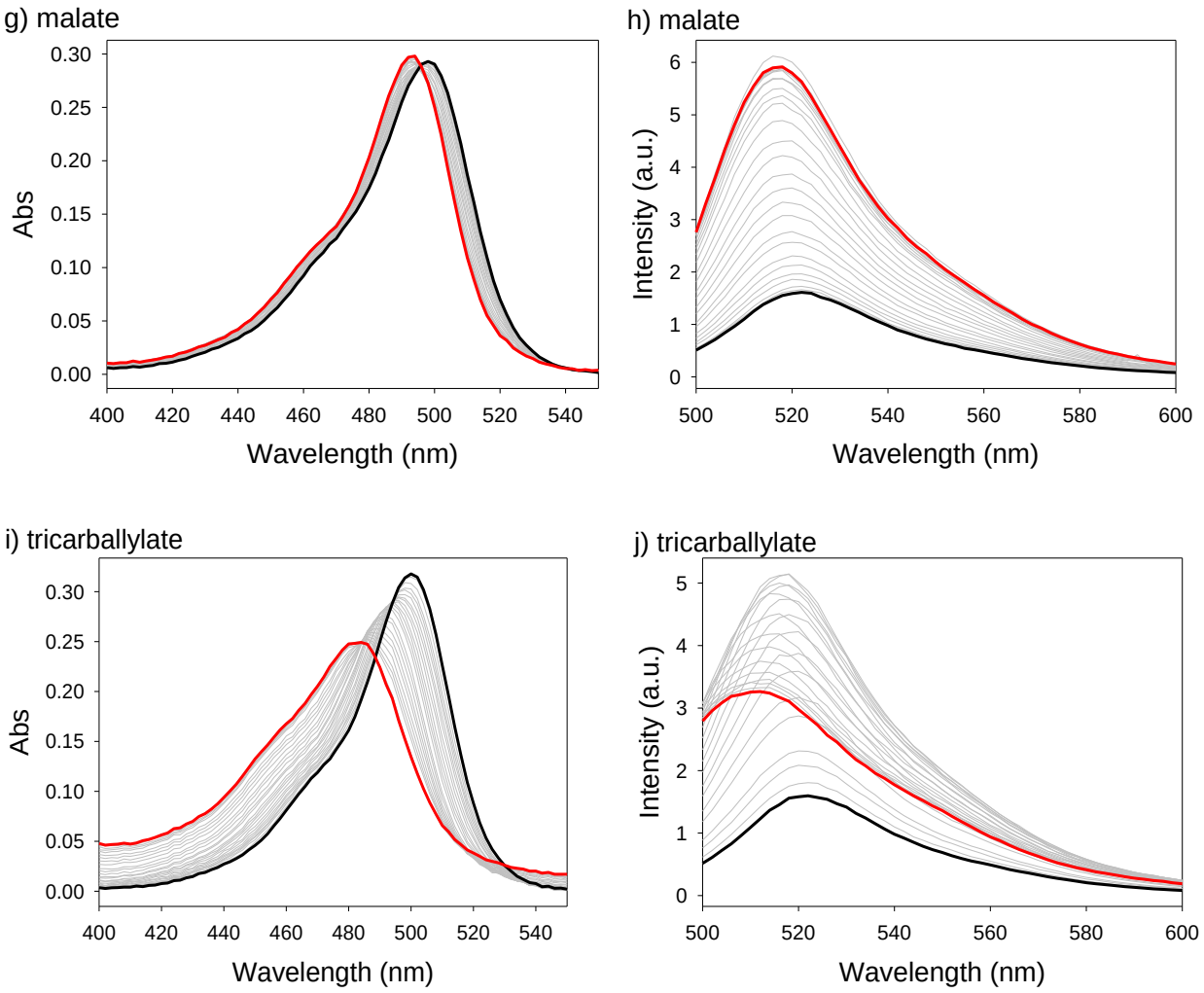

Figure 2-15 The binding of citrate (a, b), α-ketoglutarate (c, d), fumarate (e, f), malate (g, h), and tricarballylate (i, j) to PAMAM G5 is indicated by the displacement of the calcein dye from its complex with PAMAM G5. left: Absorbance spectra; right: Fluorescence emission spectra. Spectrum in black: first titration point; spectrum in red: the last titration point; spectrum in gray: titration points in between. Performed in 50 mM aqueous HEPES buffer at pH 7.4, T = 25 °C. [calcein] = 6.36 μM, [PAMAM G5] = 2.13 μM, excitation: at the isosbestic point from the absorbance spectra obtained from the corresponding carboxylate titration study.

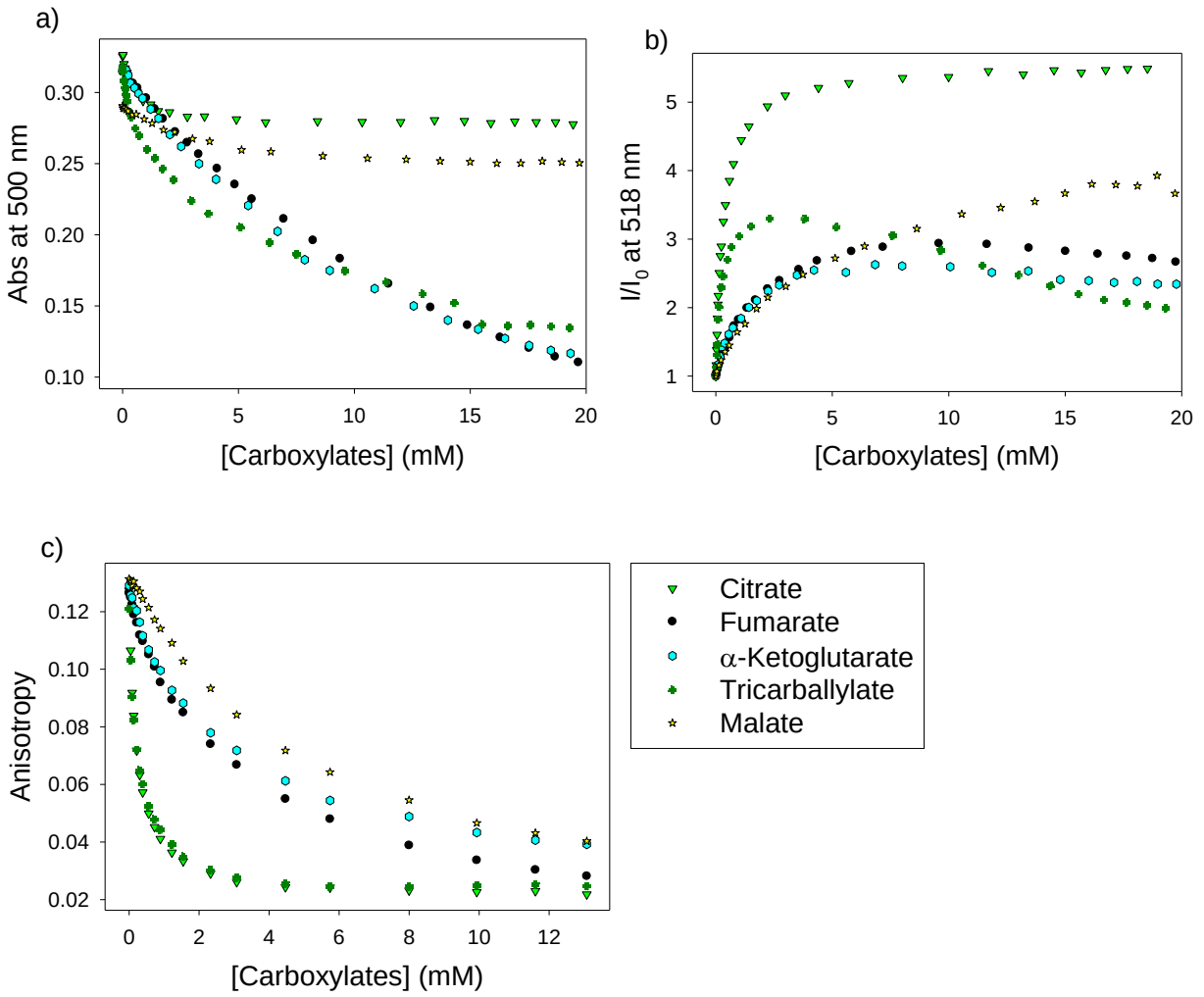

Figure 2-16 Binding of carboxylates to PAMAM G5 using calcein blue as indicator. Titration profiles 5 carboxylates into [calcein blue•PAMAM G5] complex: a) absorbance; b) fluorescence emission; c) fluorescence anisotropy. Excitation: isosbestic point from absorbance spectra of each carboxylate in Figure 2-15, emission: 518 nm. [calcein] = 6.36 μM, [PAMAM G5] = 2.13 μM. Performed in 50 mM aqueous HEPES buffer at pH 7.4, T = 25 °C.

Looking at the profiles shown in Figure 2-16, it is obvious that for some carboxylates such as tricarballylate and fumarate, even a large excess of carboxylates would not bring the titration to a plateau; instead, after ~4 mM, the absorbance and fluorescence of calcein continued to decrease linearly. We suspected that this was due to an additional interaction between the excess free carboxylate and the free dye in solution, not involving the dendrimer. Thus, titrations

of these two carboxylates into calcein in the absence of PAMAM were performed; the comparison of these titration and the corresponding anion binding titration is shown in Figure 2-17.

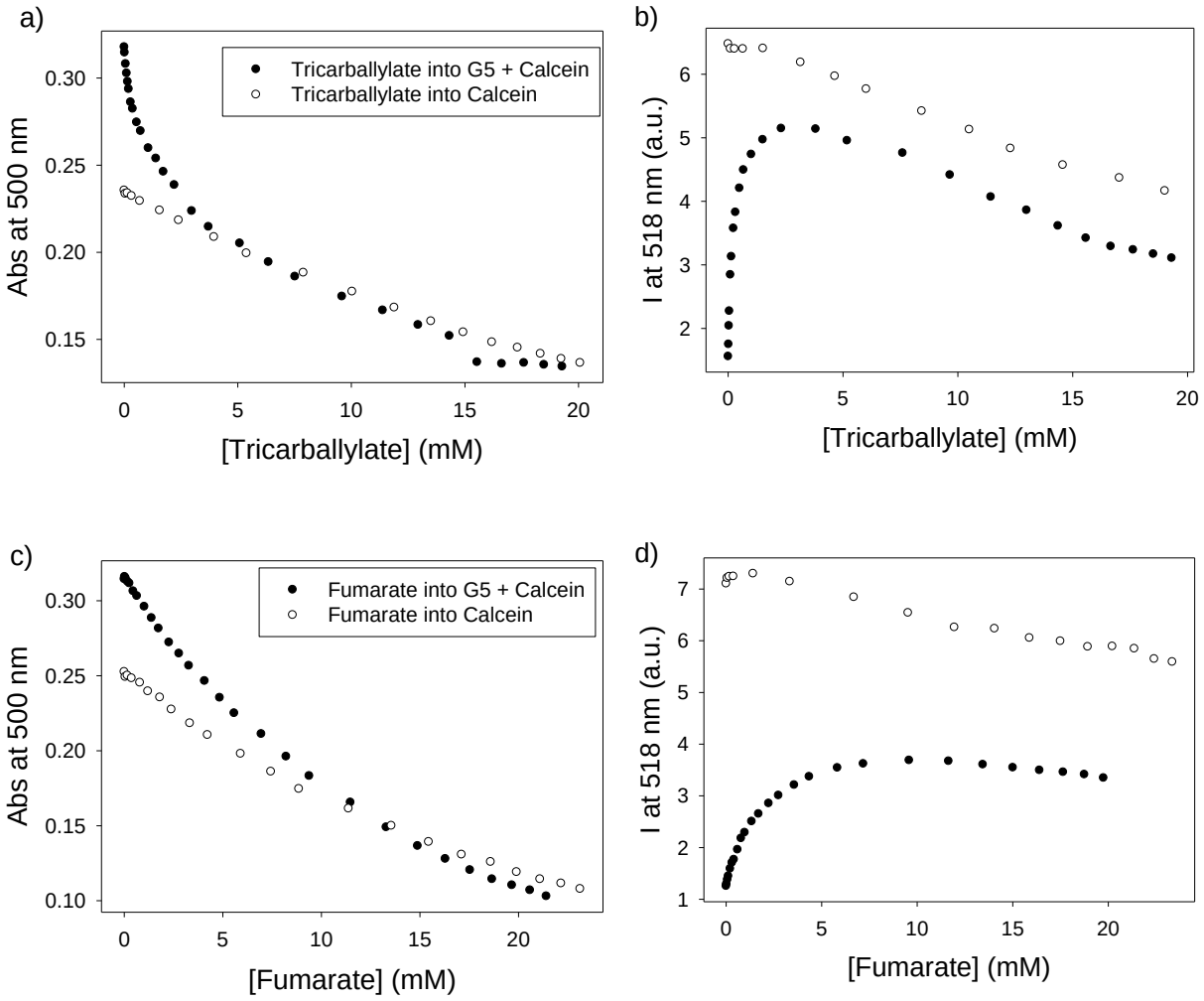

Figure 2-17 Comparison of the interaction of carboxylates with [calcein•PAMAM G5] complex (black dots) with the interaction of carboxylates and calcein alone (hollow dots). left: absorbance; right: fluorescence. Performed in 50 mM HEPES buffer at pH 7.4, T = 25 °C. [calcein] = 6.36 μM, [G5] = 2.13 μM, excitation: 486 nm, emission: 518 nm.

When the two carboxylates were titrated into calcein solution separately, they both reduced the absorbance and fluorescence emission of calcein, with a slope matching the one observed at the end of the displacement titration. The interaction among analytes to calcein still

needs further explanation, however, we believe that such interaction would provide a further beneficial source of diversity for our ultimate goal, i.e., the differentiation of carboxylate analytes.

2.4 Conclusions

All three dyes, calcein blue, pyranine, and calcein, showed a great binding affinity to PAMAM G5 and provided a large spectroscopic dynamic range. The building of [dye•PAMAM] complexes were formed using non-covalent interaction including electrostatic, hydrogen bonding, and hydrophobic interactions. Among the three dyes, pyranine had the highest affinity towards PAMAM dendrimer, due to its 3 negative charges, and hydrophobic nature; calcein, a trianion overall, but less hydrophobic than pyranine, had intermediate affinity; and finally calcein blue, an overall monoanion, had the lowest affinity for polycationic PAMAM. Upon addition of carboxylate solutions to [dye•PAMAM] complexes, there was dissociation of these three dyes, indicating the binding between carboxylates and PAMAM dendrimers. Due to the complexity of the binding process, explicit binding constant could not be calculated. Nevertheless, the large dynamic range allowed the amplification of the different behaviours among the carboxylates when interacting with PAMAM dendrimers. Overall, a supramolecular sensing system was successfully built for detection of carboxylates.

2.5 Experimental details

2.5.1 Materials

Fifth generation, amine-terminated poly(amidoamine) (PAMAM) dendrimer with a 1,2-diaminoethane core was manufactured by Dendritech, Inc., and purchased as a solution in methanol with exact concentration of 1.419 mM depending on the specific lot. The final solution used for all experiment was obtained by dilution with buffer and contained negligible amount of

methanol (< 0.8%). Dye solution were prepared from 5(6) -carboxyfluorescein, glycine cresol red sodium salt, calcein disodium salt, xylenol orange tetrasodium salt, pyrogallol red, pyrocatechol violet, calcein blue, and naphthol yellow S purchased from Sigma Aldrich; pyranine, and naphthalene-1,3,6-trisulfonic acid trisodium salt hydrate purchased from Alfa Aesar; alizarin red S was purchased Acros. Carboxylate solutions were prepared from DL-isocitric acid trisodium salt hydrate purchased from Acros; fumaric acid, α-ketoglutaric acid, *trans*-aconitic acid, succinic acid, DL-malic acid, and oxaloacetic acid purchased from Sigma Aldrich; tricarballylic acid, and maleic acid purchased from Alfa Aesar; anhydrous citric acid purchased from EMD Millipore. 50 mM 4-(2-hydroxyethyl) piperazine-1-ethanesulfonic acid (HEPES) buffer was prepared from HEPES purchased from IBI Scientific. All prepared solutions were adjusted to pH 7.4 using solutions of NaOH, prepared from NaOH purchased from Fisher Scientific, and HCl, prepared from HCl purchased from BDH Aristar. All materials were used as received.

2.5.2 Instrumentation

Absorbance titrations were carried out by HP 8452A diode array spectrophotometer, with the measuring range from 230 nm to 800 nm and a 2 nm resolution. Fluorescence emission and fluorescence anisotropy titration were carried out on an ISS PC1 spectrofluorometer, with an excitation light source as a broad-spectrum high-pressure xenon lamp (CERMAX, 300W); manual calibrated slits; excitation correction by a rhodamine B quantum counter with a dedicated detector; and emission light detector was a Hamamatsu red-sensitive PMT operating in photon-counting mode. High aperture Glan Thompson calcite polarizers were used for fluorescence anisotropy measurement. For all titration experiments, an external circulating water bath was used to control the cuvette temperature as 25 °C.

2.5.3 Titration conditions

All experiments were performed in 50 mM HEPES buffer at pH 7.4. pH was adjusted by NaOH or HCl solutions. Concentrations for dye binding titrations: [calcein blue] = 10.2 μM; [pyranine] = 6.04 μM; or [calcein] = 6.36 μM. Concentrations for carboxylates binding titrations: [calcein blue] = 10.2 μM with [G5] = 12.7 μM; [pyranine] = 6.04 μM with [G5] = 0.213 μM; or [calcein] = 6.36 μM with [G5] = 2.13 μM.

2.5.4 General dye binding and anion binding titration protocol

Dye binding experiments were studied by titrating a "titrant" solution with dye (concentration listed above) and a concentrated PAMAM G5, into a 2 mL "cuvette" solution of the dye with corresponding concentration. Therefore, concentration of the dye was maintained the same during titration. For anion binding experiment, the new "cuvette" solution contained [dye•PAMAM] complex with the concentration stated above; and the "titrant" solution contained the same concentration of [dye•PAMAM] complex as well as a carboxylate at a concentration about 5000 times higher than the dye. During the anion binding titration, the concentration of [dye•PAMAM] complex was kept constant. All titrations were performed in a 1 cm quartz cuvette.

CHAPTER 3
CARBOXYLATE SENSING IN NEUTRAL AQUEOUS SOLUTION – DISCRIMINATION

3.1 Introduction

3.1.1 Pattern-based recognition

Pattern recognition is regularly used for the differentiation of a series of structurally similar compounds, by taking advantage of the combination of diverse chemical responses of an array of non-selective probes to different analytes.[153-154] Multiple measurable properties of the probe molecule change upon interaction with guest molecule, through supramolecular interactions such as electrostatics, hydrogen bonding, π-π interactions, and hydrophobic interactions.[49,155] Many pattern-based recognition systems have been developed for the discrimination of analytes, including amino acids,[43] neucleotides,[156] gases,[65] odorants,[67] glycans,[49] metal ions,[53] bacteria,[51] and wines.[68] Multiple measurements often generate large datasets that are too difficult to interpret by simple manual calibration methods, so pattern-based recognition is generally achieved through well-established data interpreting algorithms.

3.1.2 Principal component analysis and linear discriminant analysis

Principal component analysis (PCA) and linear discriminant analysis (LDA) are two commonly used clustering techniques for reducing the complexity of a dataset and discrimination of analytes. PCA is an *unsupervised* clustering technique, meaning that the identity of analytes is not provided to the algorithm before data transformation; it simply finds the linear combinations of original measurements that makes the best separation of the full dataset; clustering and the

result and classification naturally emerge from these results. On the other hand, LDA is a *supervised* clustering technique, in which the identity of analytes is provided to the algorithm before data transformation. It finds the linear combination that maximizes intercluster distances while minimizing intracluster distances at the same time.[101] Due to the additional information provided, LDA normally leads to a better separation of clusters than PCA. However, when two samples are essentially identical, LDA might overemphasize adventitious noise in the data to separate the two clusters. In this study, both PCA and LDA are used.

3.2 Qualitative discrimination of carboxylates

3.2.1 General qualitative discrimination experiment design and data processing

As discussed in the previous chapter, the ten carboxylates of interest (see Scheme 1-1) showed differential behaviors on binding to PAMAM G5 dendrimer using each of the three [dye•PAMAM] sensors (see Scheme 3-2 for the structure of PAMAM G5, Scheme 3-3 for structure of the dyes used). However, the differences are small and need interpretation. Thus, we set up a pattern-based recognition system, with the same [dye•PAMAM] complexes as sensors. Each carboxylate analyte was exposed to one of the sensors. With the advantage of a polystyrene-based, black wall 384-well microplate and a plate reader, we were able to perform fast automated reading of absorbance, fluorescence emission and anisotropy measurements for multiple samples. The 384-well microplate also allowed us to measure multiple replicates for each sample at the same time, with minimum reagent consumption due to the small well volume (100 μL).

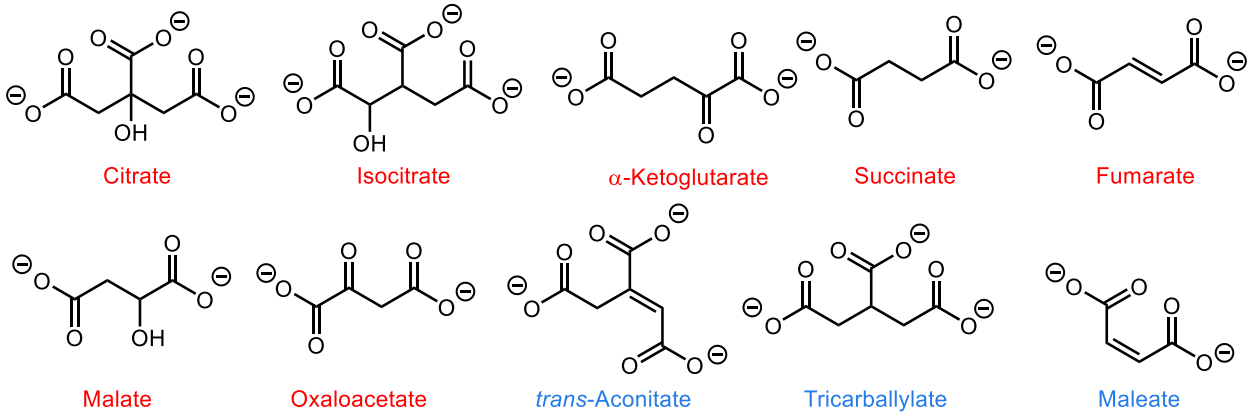

Scheme 3-1 Structures of the carboxylates of interest (red: citric acid cycle intermediate, blue: involved in citric acid cycle as inhibitors), shown in their protonation state in water at pH 7.4.

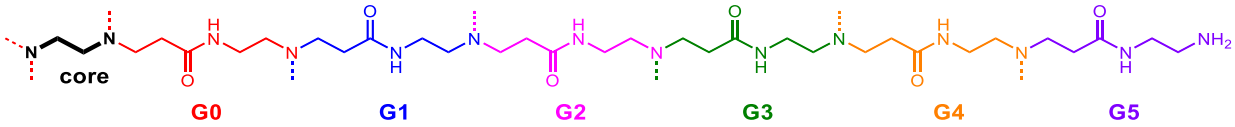

Scheme 3-2 One branch of an amine-terminated fifth generation poly(amidoamine) (PAMAM G5) dendrimer with ethylene diamine core. Each generation ends with an amine group, and branches out twice: one branch is shown in the scheme, and the other branch is represented by the dashed line.

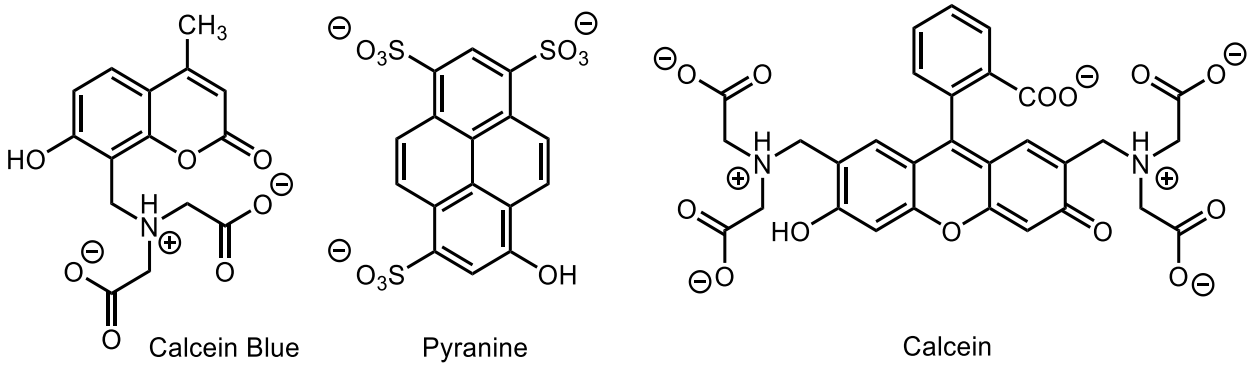

Scheme 3-3 Structures of calcein and pyranine in their most likely protonation state in water at pH 7.4.

A common plate design for quantitative discrimination of carboxylates included 36 replicates of each of the ten carboxylates interacting with each one of the [dye•PAMAM]

complexes, 8 replicates of dye solution (marked as “free dye”), 8 replicates of the same [dye•PAMAM] complex solution (marked as “bound dye”), and 8 replicates of 50 mM HEPES buffer as blank. Carboxylates were deposited at the concentration at which they display the largest pair-wise difference between each other in the binding profiles. Absorbance, fluorescence emission and anisotropy were measured by a plate reader for all 384 samples within a 2 to 3 hour period. Multiple optical measurements collected for each sample generated a multidimensional dataset. Finally, in order to pinpoint the most useful information among these measurements for carboxylate discrimination, principal component analysis (PCA) and linear discriminant analysis (LDA) were used to further process the data.

In the first step, the averaged value of the corresponding blank readings was subtracted from all optical measurements. Then, each measurement was evaluated individually. Those that responded similarly to each analyte were eliminated because they would not contribute to the discrimination, but would only increase experimental noise. For example, in Figure 3-1, measurements for fluorescence emission at $\lambda_{ex}/\lambda_{em}$ of 485/516 nm, and the absorbance at 530 nm, were separately plotted as a function of the well number on the 384-well plate. For fluorescence emission measurements, it is clear that for most analytes, the measurements within the 36 replicates of the same analyte were very similar, and the measurements among different analytes were clearly different. This was considered an informative measurement, so it was kept for further data processing. However, for absorbance at 530 nm, the signal to noise ratio was too low, which would introduce noise to the system instead of contributing to the discriminatory power. This low signal was expected because calcein had very low absorption at this wavelength. Thus, this measurement as well as other similar ones were removed from the dataset and no longer used in further data processing.

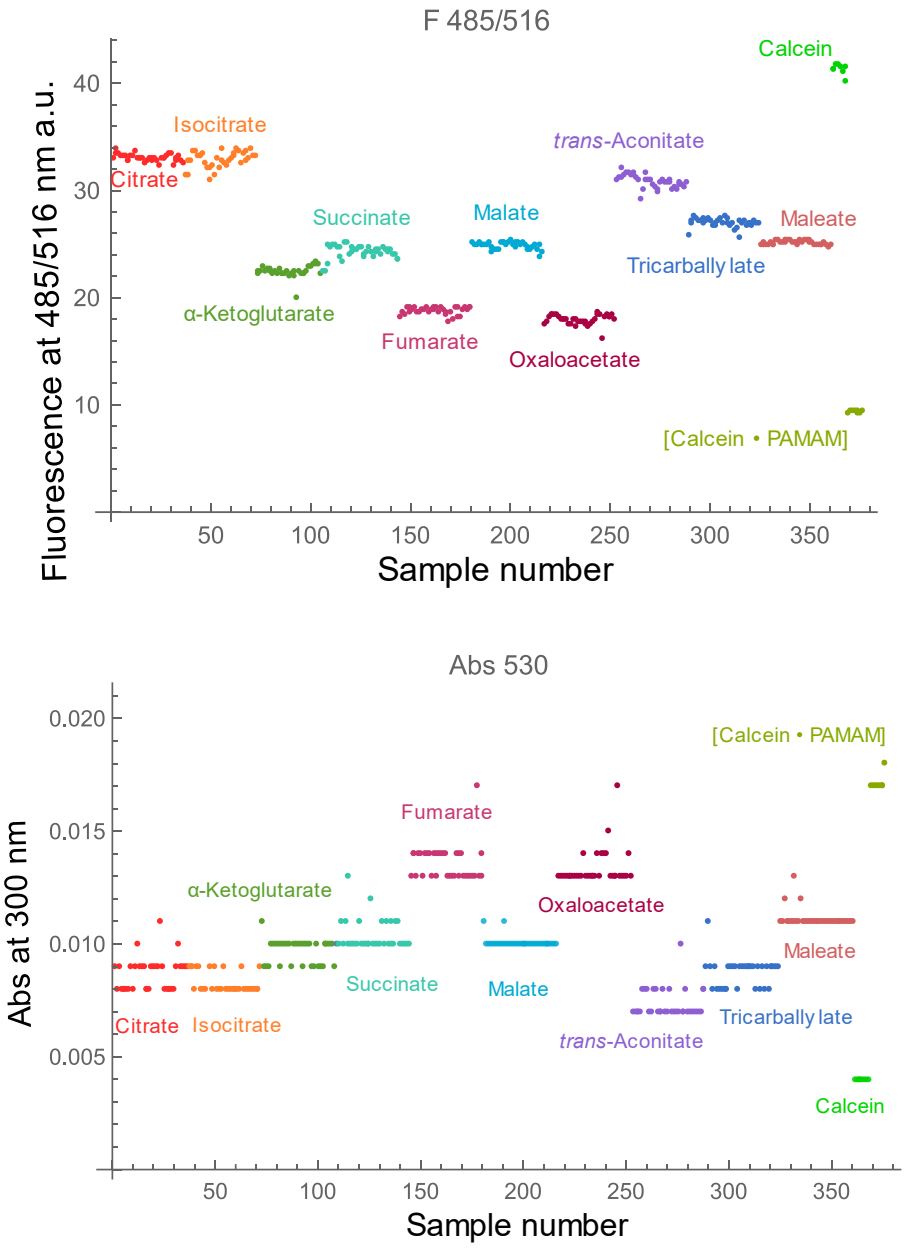

Figure 3-1 Responses of the [calcein•PAMAM]sensor as a function of the sample number, which are 10 different carboxylate analytes with 36 replicates each, on a 384-well plate for qualitative carboxylate discrimination. Top: fluorescence emission intensity at $\lambda_{ex}/\lambda_{em}$: 485 nm/516 nm: different analytes showed clear difference. This was retained in the following discrimination analysis. Bottom: absorbance at 530 nm; all carboxylates showed minimal difference; discarded. Performed in 50 mM HEPES buffer at pH 7.4, T = 25 °C. [calcein] = 6.36 μM, [G5] = 2.13 μM, [carboxylates] = 2.30 mM. PCA and LDA results for this data set are shown in Figure 3-10 and Figure 3-11, respectively.

With the reduced measurement dataset, outlier tests were carried out for each group of carboxylate replicates. Figure 3-2 is an example of outlier test: measurements of 36 replicates of *trans*-aconitate were fed to PCA, then the first two principal components were used to generate a 2D scores plot. An ellipsoid was generated as a bivariate confidence interval at a 95% confidence level. From this plot, replicate #7, shown in red, fell out of this 95% confidence interval, so, it was removed from the *trans*-aconitate dataset. In our experience, common causes of such outliers could be mistakes during sample deposition (multichannel pipettes are affected by small volume variation), or the formation of small bubbles in the well that scatters light, or minute scratches causing slight opacity of the clear bottom of the plastic plate.

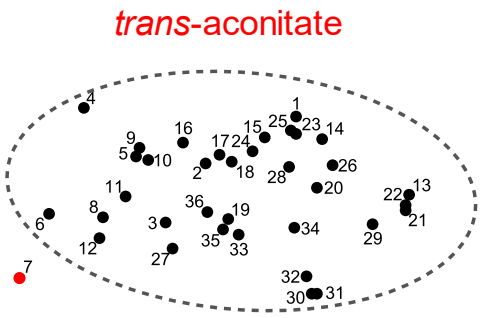

Figure 3-2 Outlier rejection of a group of *trans*-aconitate replicates from the result of the 384-well plate for qualitative carboxylate discrimination, after measurement reduction shown in Figure 3-1. Black dots: replicates that fall within 95% confidence interval and retained for further analysis; red dot: replicate that fell outside in the 95% interval and was rejected. Performed on a 384-well plate in 50 mM HEPES buffer at pH 7.4, T = 25 °C. [calcein] = 6.36 μM, [G5] = 2.13 μM, [*trans*-aconitate] = 2.30 mM. PCA and LDA results for this data set are shown in Figure 3-10 and Figure 3-11, respectively.

After measurement reduction and outlier rejection, the rest of the dataset was then subjected to PCA and LDA algorithms. They both transform the original dataset into a new matrix with the same dimensions as the original; the original measurements then were integrated

into principal components (PC) for PCA, and factors for LDA. These new PCs or factors were then sorted by decreasing total variance. The transformed data matrix had the same amount of information and same dimensions as the original data matrix, only with the information density leaning to the first few PCs or factors. Thus, retaining the first two or three PCs or factors would retain the maximum amount of information while at the same time greatly simplifying the data set, and could become the new "axes" of a two or three-dimensional interpretation of the data. The 2-dimensional result of analyte discrimination was called "scores plot" for both PCA and LDA. There was also a "loadings plot" corresponds to each scores plot, providing the relative contribution of each original measurement to the new PCs or factors. This would allow us to link the discrimination results to the original measurements, as well as the structural and chemical features of the analytes. Ideally, high and balanced information content in the first two factors would be most desirable, but any distribution in which the two factors on PCs both contribute substantially to the discrimination is typically acceptable.

3.2.2 Qualitative discrimination of carboxylates using [calcein blue•PAMAM G5] sensor

Figure 3-3 is the same titration set as Figure 2-11 in Chapter 2; carboxylate analytes showed maximum pair-wise differences at a concentration of 1.28 mM. In this case, a 384-well plate was used to analyze the carboxylate analytes with 36 replicates each, and 24 instrumental measurements were collected for each sample. 16 instrumental measurements were retained for PCA and LDA studies, as shown in Table 3-1.

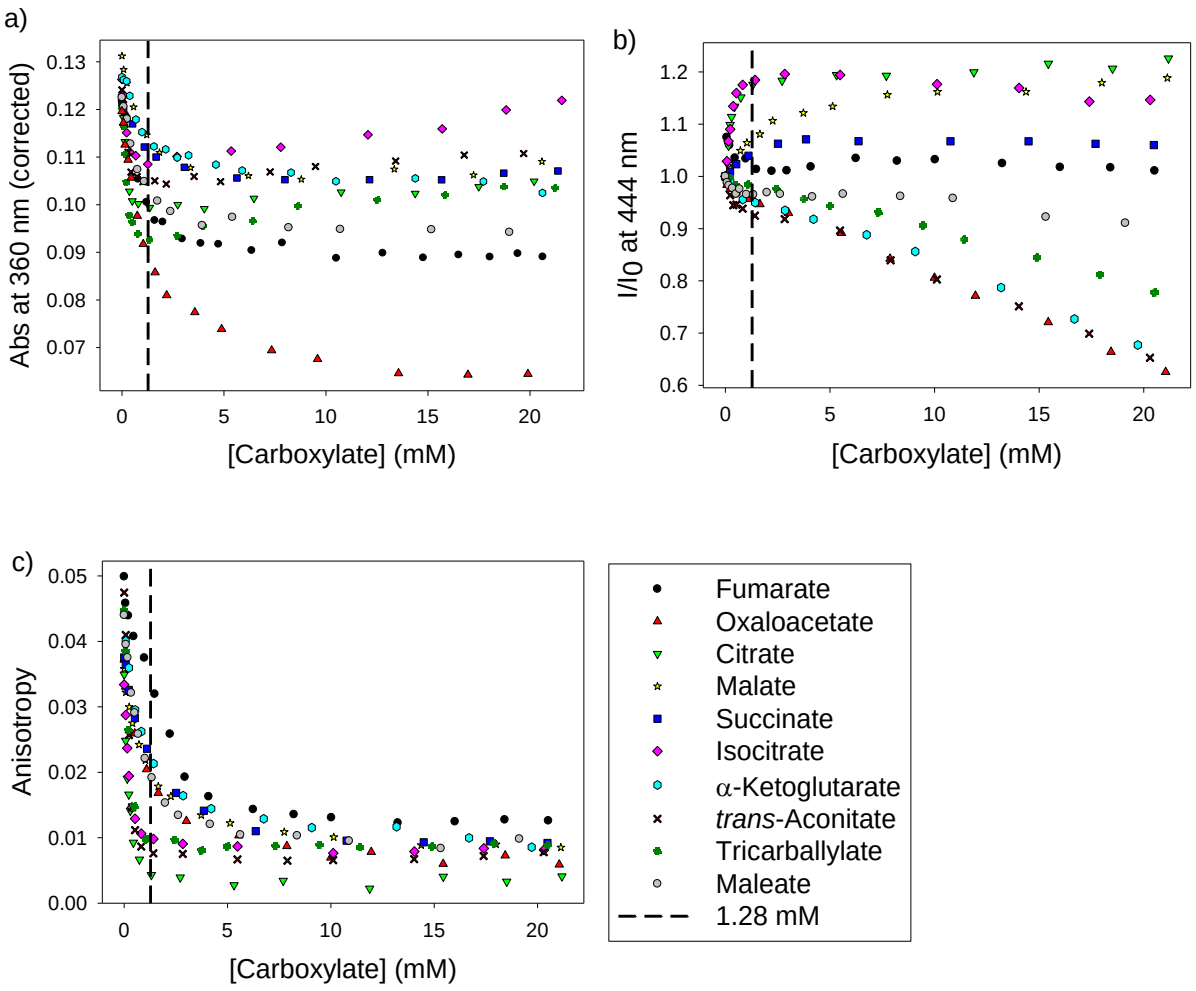

Figure 3-3 Binding of carboxylates to PAMAM G5 using calcein blue as indicator (the same set as shown in Figure 2-11). Titration profiles of all carboxylates of interests into [calcein blue•PAMAM G5] complex: a) corrected absorbance; b) fluorescence emission; c) fluorescence anisotropy; dashed line: at 1.28 mM, the maximum pair-wise difference. Excitation: isosbestic point from absorbance spectra of each carboxylate in Figure 2-10, emission: 444 nm. [calcein blue] = 10.2 μM, [PAMAM G5] = 12.7 μM. Performed in 50 mM aqueous HEPES buffer at pH 7.4, T = 25 °C.

After data processing as discussed previously, the PCA scores plot and loadings plot are shown in Figure 3-4. Most of the carboxylates were discriminated, except two sets of carboxylate analytes with similar structures, the first set containing malate and maleate, and the second set tricarballylate and isocitrate. PC1 summarized 66.8% of the information. Most important contributions to the separation along PC1 came from absorbance measurements in the

360-390 nm range, where the [calcein blue•PAMAM] complex absorbs. PC2 summarized 26.7% of the total information content of the dataset. Its most important contributing measurements included many absorbance measurements in the 300 nm region, which correspond to intrinsic absorption features of the carboxylate analytes; the other major contribution was from fluorescence of the sensing complex. A strong reliance on signals typical of the carboxylates themselves would not bode well for the role of the macromolecular sensor and for the extensibility of this method in general. Nevertheless, it was a promising first result.

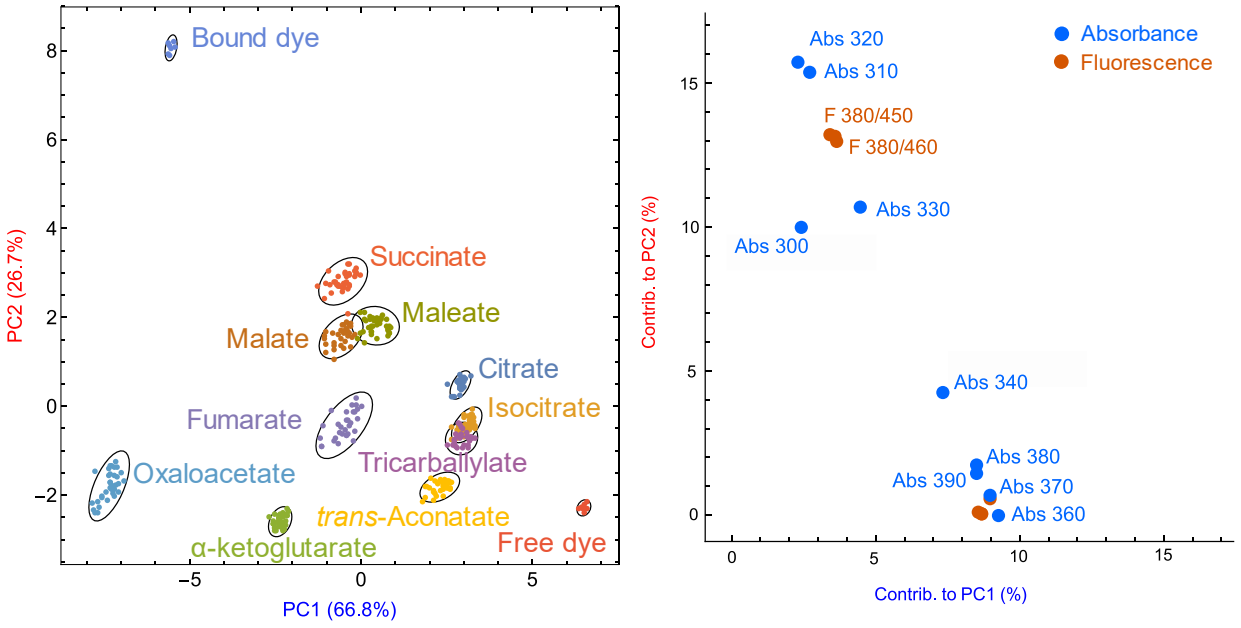

Figure 3-4 PCA results of ten carboxylates for qualitative discrimination using [calcein blue•PAMAM] sensor. Left: scores plot; right: loadings plot (Abs: absorbance, F: fluorescence emission $\lambda_{ex}/\lambda_{em}$, A: fluorescence anisotropy $\lambda_{ex}/\lambda_{em}$). [calcein blue] = 10.2 μM, [PAMAM G5] = 12.7 μM, [carboxylates] = 1.28 mM. Performed in 50 mM aqueous HEPES buffer at pH 7.4, T = 25 °C.

Due to its nature, LDA normally has better discriminatory power. When used for the same set of data, the resulting scores and loadings plot are shown in Figure 3-5. The clusters of carboxylates are smaller and further apart comparing to the PCA scores plot, suggesting a more effective differentiation. The [calcein blue•PAMAM] sensor was able to differentiate most of the

carboxylates. In addition, it is interesting to note that there is a correlation with the expected affinity of these carboxylates for the positively charged G5 dendrimers, and the position of the corresponding clusters in the LDA score plot with respect to the free and bound dye clusters. In fact, all the carboxylate clusters lie between the free dye (calcein blue) and bound dye ([calcein blue•PAMAM] complex) clusters. On the one hand, tricarboxylates are expected to have higher affinity for the polycationic G5 dendrimers thanks to stronger electrostatic interactions, so they should cause a more complete displacement of the dye. As a consequence, their solution contains the dye mostly in its free, unbound state. Indeed, the clusters corresponding to tricarboxylate anions are found closer to the free dye cluster in the scores plot. Conversely, the same concentration of dicarboxylate anions only displaces a smaller portion of the dye from its complex with PAMAM, so in these solutions the dye is found on average in a state intermediate between bound and free, and the dicarboxylate anion clusters end up positioned closer to the bound-dye reference cluster.

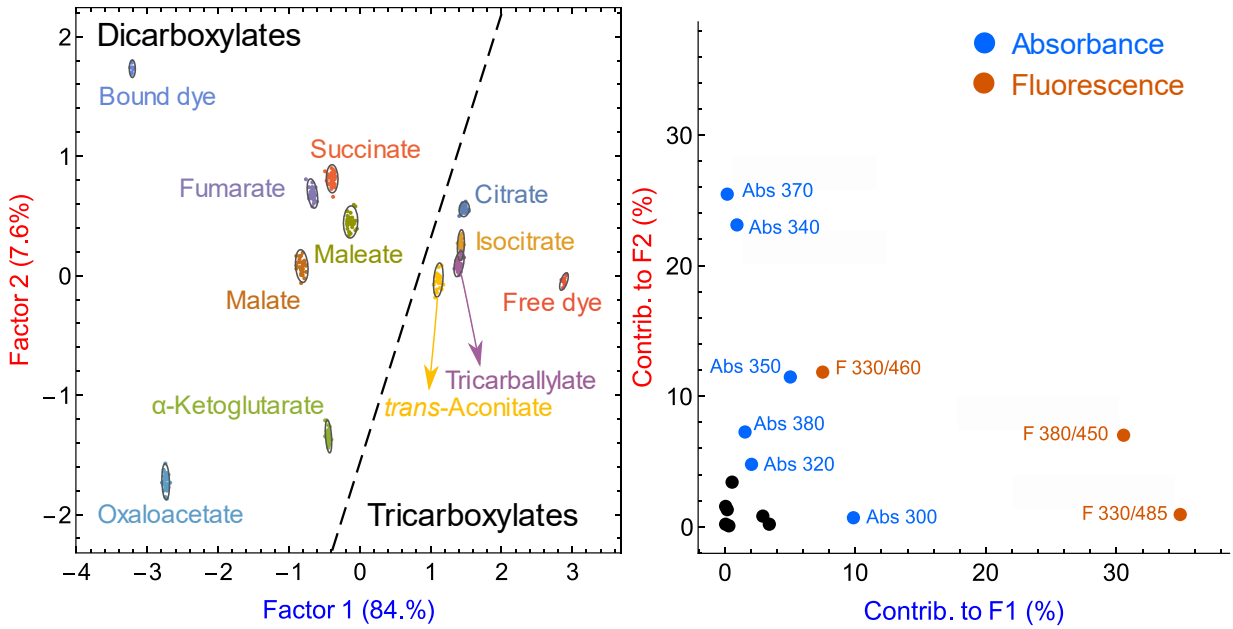

Figure 3-5 LDA results of ten carboxylates for qualitative discrimination using [calcein blue•PAMAM] sensor. Left: scores plot; right: loadings plot (Abs: absorbance, F: fluorescence emission $\lambda_{ex}/\lambda_{em}$). [calcein blue] = 10.2 μM, [PAMAM G5] = 12.7 μM, [carboxylates] = 1.28 mM. Performed in 50 mM aqueous HEPES buffer at pH 7.4, T = 25 °C.

Although acceptable, the differentiation was still imperfect. On the one hand, factor 1 carried a disproportionate weight (84%) when compared to factor 2 (7.6%): this seems to indicate the possibility that a simpler, unidimensional data reduction might be possible, probably on the simple basis of relative affinities. Secondary interactions that would help discrimination are either absent in the underlying chemical system, or not captured in the raw data set. As a consequence, the isocitrate cluster overlaps with the tricarballylate cluster so the two anions cannot be properly differentiated. Thus, we moved on to using other sensors for carboxylate differentiation.

Table 3-1 Loadings for instrumental measurements used for the qualitative discrimination of carboxylates using [calcein blue•PAMAM] sensor. F*n*% (columns) is the percent of the information explained by Factor *n* that is provided by each raw measurement (rows).The numbers correspond to Figure 3-5.

Variable type	Wavelength (nm)	F1%	F2%	F3%
Absorbance	300	10	1	70
Absorbance	310	0	0	7
Absorbance	320	2	5	11
Absorbance	330	3	1	1
Absorbance	340	1	23	0
Absorbance	350	5	11	2
Absorbance	360	3	0	0
Absorbance	370	0	25	1
Absorbance	380	2	7	0
Absorbance	390	0	1	1
Fluorescence emission	330/450	0	2	5
Fluorescence emission	330/460	8	12	1
Fluorescence emission	330/485	35	1	0
Fluorescence emission	380/450	31	7	0
Fluorescence emission	380/460	0	0	0
Fluorescence emission	380/485	1	3	0

3.2.3 Qualitative discrimination of carboxylates using [pyranine•PAMAM G5] sensor

The most appropriate concentration of carboxylate to use for discrimination with this sensor was determined by comparing the binding titrations obtained with different carboxylates, as we did before. From previous experiences, dicarboxylates and tricarboxylates had a very obvious difference, therefore here, titrations using a dicarboxylate (α-ketoglutarate) and a tricarboxylate (citrate) were carried out to determine the best working concentration. In this case, the optimal concentration was found at 2.04 mM carboxylate, as shown in Figure 3-6.

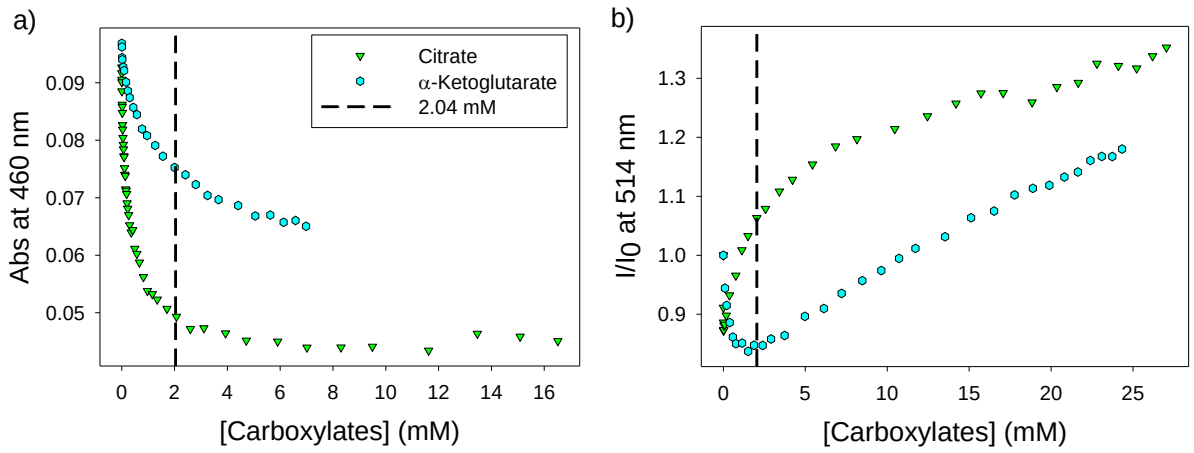

Figure 3-6 Binding of carboxylates to PAMAM G5 using pyranine as indicator (the same set as shown in Figure 2-13). Titration profiles of citrate and α-ketoglutarate into [pyranine•PAMAM G5] complex: a) absorbance; b) fluorescence emission; c) fluorescence anisotropy; dashed line: at 2.04 mM, the maximum pair-wise difference. Excitation: 420 nm, emission: 514 nm. [pyranine] = 6.04 μM, [PAMAM G5] = 0.213 μM. Performed in 50 mM aqueous HEPES buffer at pH 7.4, T = 25 °C.

Data acquisition and processing proceeded as explained above for calcein. A subset of instrumental measurements was retained for PCA and LDA studies, as shown in Table 3-2. The results of PCA analysis on this 38-dimentional dataset are shown in Figure 3-7. Unfortunately, discrimination by [pyranine•PAMAM G5] sensor using PCA algorithm in this dataset was still incomplete. However, we could distinguish a tricarboxylate supercluster (marked in yellow, and closer to the free pyranine dye) from a dicarboxylate supercluster (marked in green, and closer to the bound pyranine dye). Oxaloacetate, a dicarboxylate, does not conform to this behavior: we suspect that this was due to its uniquely high intrinsic UV absorbance.

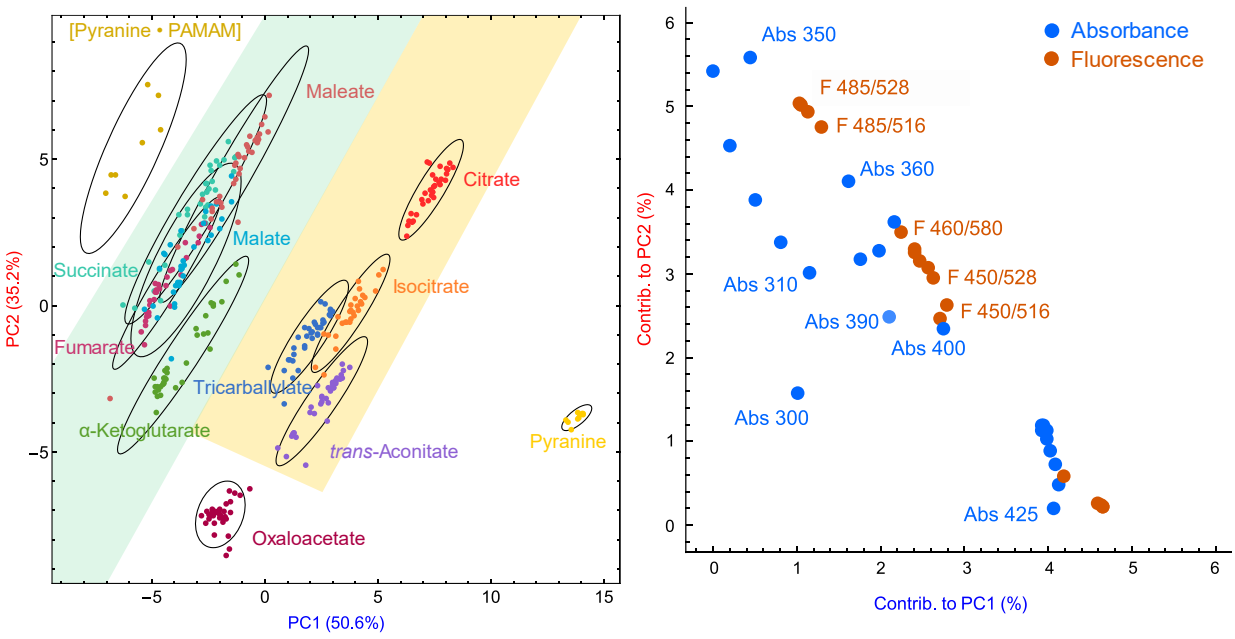

Figure 3-7 PCA results for qualitative discrimination of ten carboxylates using [pyranine•PAMAM] sensor. Left: scores plot; right: loadings plot (Abs: absorbance, F: fluorescence emission $\lambda_{ex}/\lambda_{em}$, A: fluorescence anisotropy $\lambda_{ex}/\lambda_{em}$). [pyranine] = 6.04 μM, [PAMAM G5] = 0.213 μM, [carboxylates] = 2.04 mM. Performed in 50 mM aqueous HEPES buffer at pH 7.4, T = 25 °C.

LDA scores plot and loadings plot are shown in Figure 3-8. Together, factor 1 (54.8% of total information) and factor 2 (another 30.9%) summarized 85.7 of the original information, with good balance of contribution of each factor. The differentiation of carboxylates by pyranine alone is not very good; for instance, one can easily identify superclusters that contains multiple carboxylates with similar structures that cannot be differentiated. Two large groupings ("superclusters") can be identified in the scores plot, one for citrate, isocitrate, and tricarballylate, and the other for malate and succinate. The anions in each of these superclusters are structurally very similar to each other, with the only difference being the presence of hydroxy groups in some of these structures. This behavior therefore seems to indicate that the [pyranine•PAMAM] complex is not sensitive to the presence of hydroxyl group in the carboxylate structure. Tentatively, we ascribed this behavior to a possible "blocking effect"

exercised by un-displaced pyranine dye on the bound anions. In fact, pyranine is significantly more hydrophobic than calcein, so it is likely to be bound deeper within the PAMAM structure, where it is more effectively shielded from the aqueous solvent. The leftover bound pyranine in the core of the dendrimer establishes effective hydrogen bonding with the carbonyl moieties of the internal amide groups, the most effective hydrogen bond acceptors in the dendrimer's structure, so that H bond donating hydroxianions cannot establish any further interaction with the dendrimer. In other words, the presence of the pyranine makes the dendrimer insensitive to the presence or absence of H bonding donor motifs.

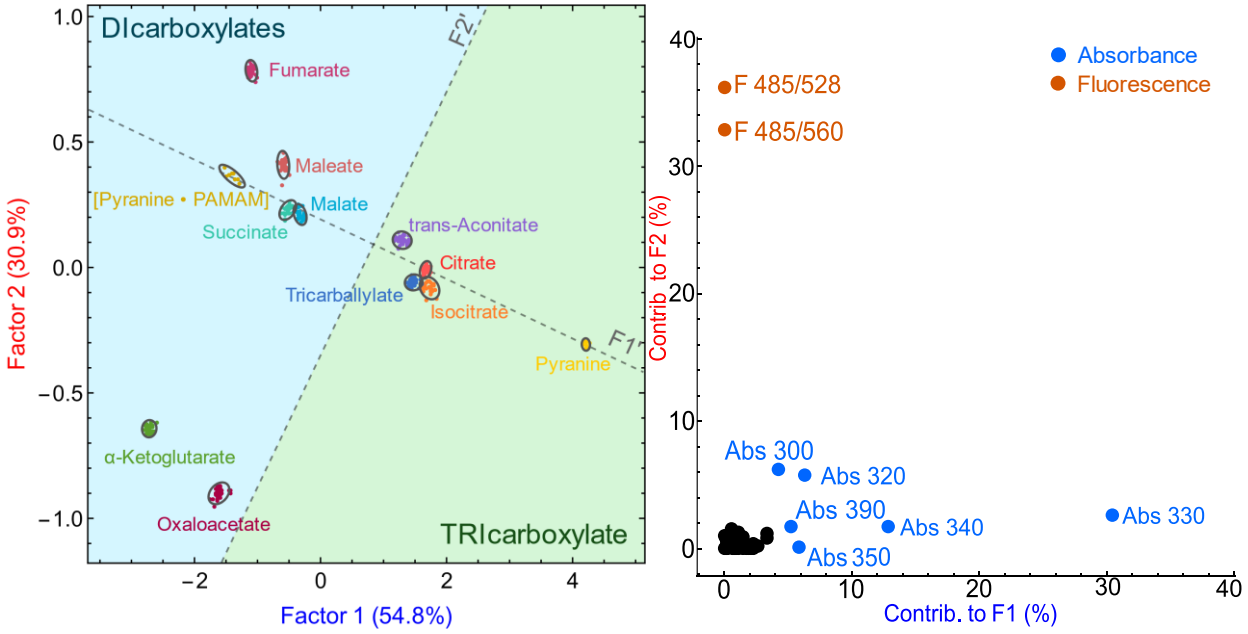

Figure 3-8 LDA results for qualitative discrimination of ten carboxylates using [pyranine•PAMAM] sensor. Left: scores plot; right: loadings plot (Abs: absorbance, F: fluorescence emission $\lambda_{ex}/\lambda_{em}$). [pyranine] = 6.04 μM, [PAMAM G5] = 0.213 μM, [carboxylates] = 2.04 mM. Performed in 50 mM aqueous HEPES buffer at pH 7.4, T = 25 °C.

Table 3-2 Loadings for instrumental measurements used for the qualitative discrimination of carboxylates using [pyranine•PAMAM] sensor. F*n*% (columns) is the percent of the information explained by Factor *n* that is provided by each raw measurement (rows). The numbers correspond to Figure 3-8.

Variable type	Wavelength (nm)	F1%	F2%	F3%
Absorbance	300	4	6	20
Absorbance	310	1	0	10
Absorbance	320	6	6	1
Absorbance	330	30	3	0
Absorbance	340	15	2	1
Absorbance	350	6	0	0
Absorbance	360	0	0	0
Absorbance	370	1	1	1
Absorbance	380	3	1	0
Absorbance	390	5	2	0
Absorbance	400	3	1	0
Absorbance	405	2	0	0
Absorbance	425	1	0	0
Absorbance	430	1	0	0
Absorbance	435	1	0	0
Absorbance	440	2	0	0
Absorbance	445	0	0	0
Absorbance	450	1	2	0
Absorbance	455	0	0	0
Absorbance	460	2	0	0
Absorbance	465	1	0	0
Absorbance	470	1	1	0
Fluorescence emission	380/516	3	0	0
Fluorescence emission	380/528	2	0	1
Fluorescence emission	380/560	0	1	4
Fluorescence emission	380/580	0	1	3
Fluorescence emission	450/516	1	0	0
Fluorescence emission	450/528	1	0	0
Fluorescence emission	450/560	0	0	0
Fluorescence emission	450/580	1	0	0
Fluorescence emission	460/516	0	1	0
Fluorescence emission	460/528	2	1	1
Fluorescence emission	460/560	2	0	0
Fluorescence emission	460/580	0	0	1
Fluorescence emission	460/516	1	1	1
Fluorescence emission	460/528	0	36	36
Fluorescence emission	460/560	0	33	19
Fluorescence emission	460/580	0	1	0

Further insight can be gathered by the relative position of the clusters in the LDA scores plot. For instance, assume the presence of a new axis, F1', defined by connecting the free dye and the bound dye clusters in the scores plot. It was found that the position of the projection of all clusters onto this axis (i.e. the "score" along this new axis) is related to the structure and resulting affinity to the PAMAM receptor of these anions. It is interesting to note that there is a correlation with the expected affinity of these carboxylates for the positively charged G5 dendrimers, and the position of the corresponding clusters in the LDA score plot with respect to the free and bound dye clusters. As being discussed in the LDA scores plot of [calcein blue•PAMAM] sensors in Figure 3-5, all carboxylates are in between the imaginary line between free dye (pyranine) and bound dye ([pyranine•PAMAM] complex), with tricarboxylates being closer to free dye and dicarboxylates being closer to the bound dye.

If a second ancillary axis was then added, perpendicular to F1', called F2', it was found that the score along F2' for these clusters correlates with the strength of the corresponding anion's intrinsic absorbance in the UV range. Oxaloacetate and α-ketoglutarate, which contain a carbonyl group and have the highest UV absorption (especially around 300 nm to 350 nm region, refer to Figure 2-10), also have the largest absolute F2' value, followed by fumarate, maleate and *trans*-aconitate, all of which contain a carbon-carbon double bond, a weak chromophore. The anions whose clusters lie on F1' (i.e. citrate, malate, and succinate) do not have intrinsic UV absorption at all. This makes sense because looking at the corresponding loadings plot, absorbance at 300 nm is a main contributor to this differentiation. Those carboxylates who have no UV absorption (citrate, malate, and succinate) had a zero "score" on the F2' axis, so they lay directly on the F1' axis.

To improve the differentiation, a system that captures more differences among carboxylates during their binding with PAMAM dendrimer is needed, rather than concentrating on the UV absorbance of carboxylates to avoid spurious responses such as those from oxaloacetate and α-ketoglutarate.

3.2.4 Qualitative discrimination of carboxylates using [calcein•PAMAM G5] sensor

The most appropriate concentration of carboxylate to use for discrimination with this sensor was determined by comparing the binding titrations obtained with different carboxylates, as we did before. In this case, the optional concentration was found at 2.30 mM carboxylate, as shown in Figure 3-9. We were pleased to see that the differentiation already provided a good result, as shown in Figure 3-10, even when using the less aggressive unsupervised (i.e., label free) PCA clustering technique. In this case, 29 of the 42 original measurements were retained for further analysis. The 29 instrumental measurements that were retained for PCA and LDA studies are shown in Table 3-3. PC1 contained contributions from a combination of absorbance, fluorescence emission and anisotropy measurements, and PC2 from the absorbance typical of the calcein dye (490 nm to 500 nm). The absorbance of carboxylates in the UV region was not as overwhelming as in the previous cases.

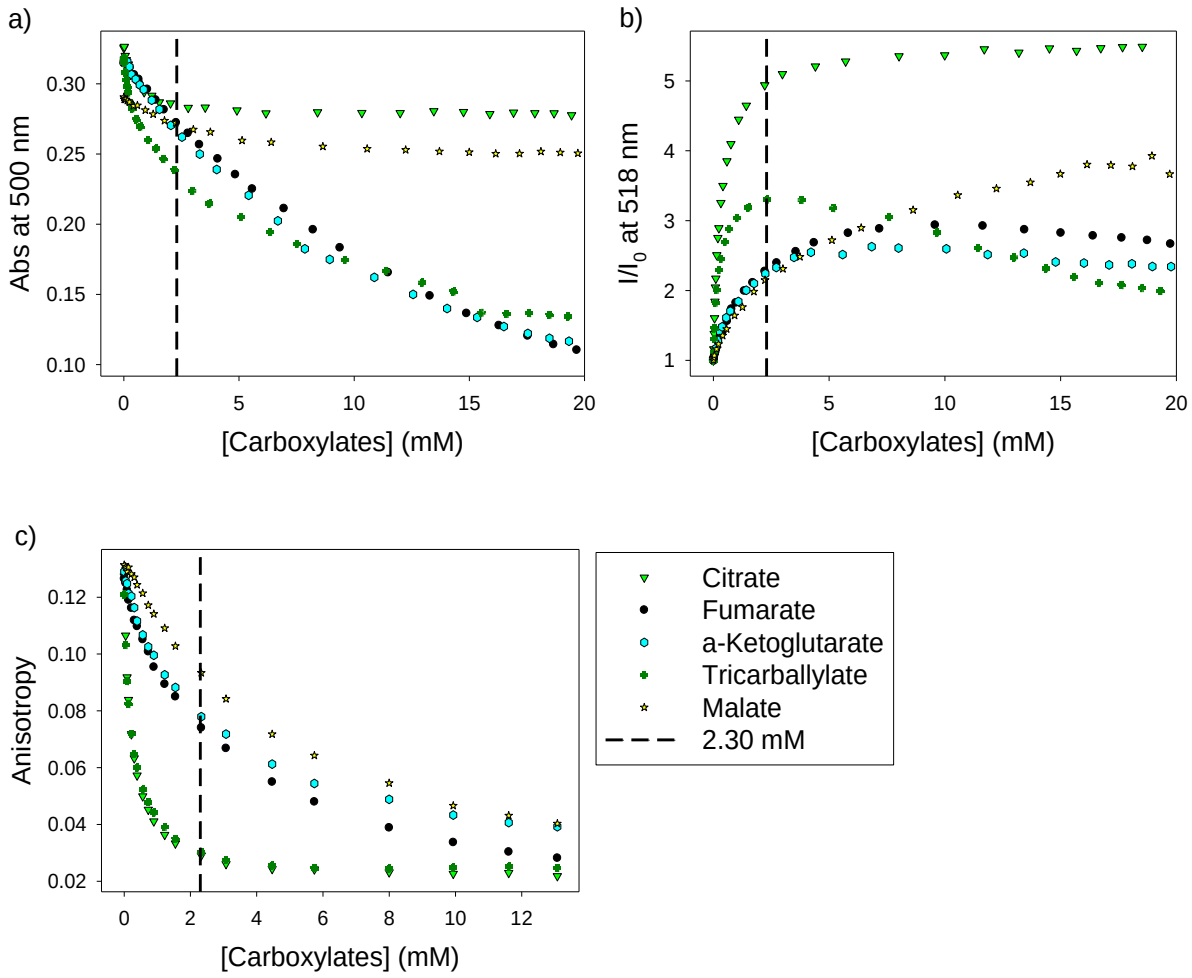

Figure 3-9 Binding of carboxylates to PAMAM G5 using calcein as indicator (the same set as shown in Figure 2-15). Titration profiles of all carboxylates of interests into [calcein•PAMAM G5] complex: a) absorbance; b) fluorescence emission; c) fluorescence anisotropy; dashed line: at 2.30 mM, the maximum pair-wise difference. Excitation: isosbestic point from absorbance spectra of each carboxylate in Figure 2-14, emission: 518 nm. [calcein] = 6.36 μM, [PAMAM G5] = 2.13 μM. Performed in 50 mM aqueous HEPES buffer at pH 7.4, T = 25 °C.

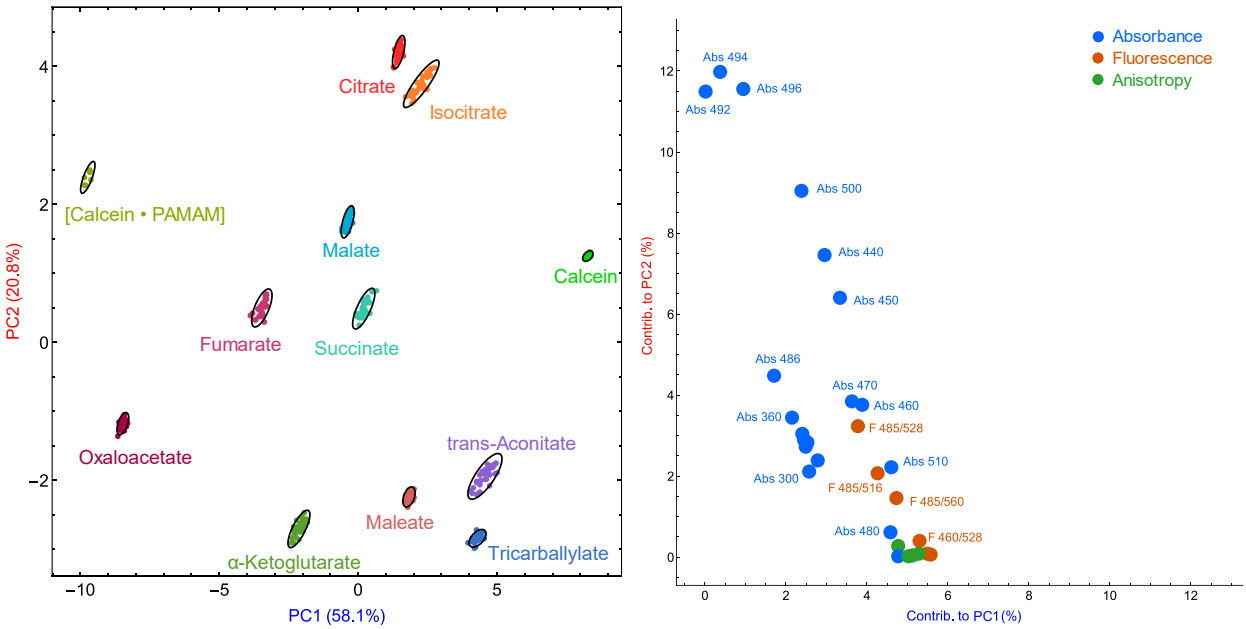

Figure 3-10 PCA results for qualitative discrimination of ten carboxylates using [calcein•PAMAM] sensor. Left: scores plot; right: loadings plot (Abs: absorbance, F: fluorescence emission $\lambda_{ex}/\lambda_{em}$, A: fluorescence anisotropy $\lambda_{ex}/\lambda_{em}$). [calcein] = 6.36 μM, [PAMAM G5] = 2.13 μM, [carboxylates] = 2.30 mM. Performed in 50 mM aqueous HEPES buffer at pH 7.4, T = 25 °C.

LDA results for the same dataset, shown in Figure 3-11, indicate that all carboxylates were well differentiated, including the "supercluster" carboxylates that could not be differentiated by the previous sensors. Each cluster, with 36 replicates, was very tight and well differentiated from each other, indicating strong reproducibility and excellent discriminatory power of this sensor, providing a high tolerance against outliers.

Here again, tricarboxylates are closer to the free calcein dye, and dicarboxylates are found closer to the bound dye complex. However, the number of negative charges on the analytic was not the dominant driver of superclusters; oxaloacetate and α-ketoglutarate clusters are also not as far apart from the rest of the clusters, indicating that their own absorbance is no longer such a heavy contributor. This is also supported by analysis of the loadings plot (Figure 3-11b). Instead, other chemical properties of these anions were well captured by the system. In

particular, if the free dye and bound dye clusters are connected, the scores plot is divided in the gray and yellow regions shown in Figure 3-11a. In most cases, the projection of tricarboxylates on this construction line are closer to the free dye cluster than the projections of the dicarboxylates clusters, which indicates a stronger affinity for the tricarboxylates (they displace the dye more completely, therefore their clusters "look like" free dye), and confirms previous results in the group shown in this work above, as well as previously reported by our group.[152]

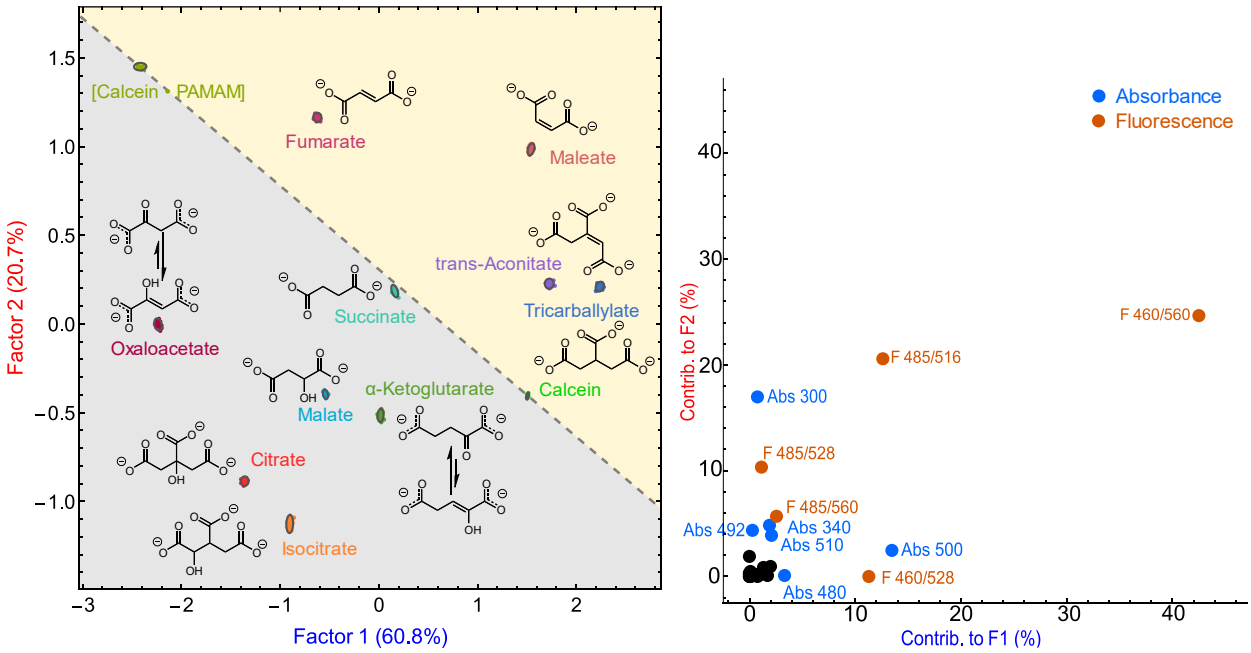

Figure 3-11 LDA results for qualitative discrimination of ten carboxylates using [calcein•PAMAM] sensor. Left: scores plot; right: loadings plot (Abs: absorbance, F: fluorescence emission $\lambda_{ex}/\lambda_{em}$). [calcein] = 6.36 μM, [PAMAM G5] = 2.13 μM, [carboxylates] = 2.30 mM. Performed in 50 mM aqueous HEPES buffer at pH 7.4, T = 25 °C

Table 3-3 Loadings for instrumental measurements used for the qualitative discrimination of carboxylates using [calcein•PAMAM] sensor. F*n*% (columns) is the percent of the information explained by Factor *n* that is provided by each raw measurement (rows). The numbers correspond to Figure 3-11.

Variable type	Wavelength (nm)	F1%	F2%	F3%
Absorbance	300	1	17	32
Absorbance	310	1	1	0
Absorbance	320	2	0	1

Absorbance	330	0	2	7
Absorbance	340	0	5	5
Absorbance	350	0	0	0
Absorbance	360	0	0	4
Absorbance	440	0	0	1
Absorbance	450	0	0	0
Absorbance	460	1	0	0
Absorbance	470	1	0	0
Absorbance	480	3	0	0
Absorbance	486	0	0	0
Absorbance	492	0	4	1
Absorbance	494	1	0	0
Absorbance	496	2	1	0
Absorbance	500	13	2	0
Absorbance	510	2	4	3
Absorbance	520	0	0	0
Fluorescence emission	460/516	0	0	8
Fluorescence emission	460/528	11	0	0
Fluorescence emission	460/560	42	25	15
Fluorescence emission	485/516	13	21	7
Fluorescence emission	485/528	1	10	5
Fluorescence emission	485/560	3	6	9
Fluorescence anisotropy	460/528	0	0	0
Fluorescence anisotropy	460/560	0	0	0
Fluorescence anisotropy	485/528	0	0	0
Fluorescence anisotropy	485/560	0	0	0

Looking at the two regions in the scores plot, carboxylates that contain hydroxyl functional groups are found in the gray region, whereas carboxylates with other features are found in the yellow region, and “featureless” carboxylate, such as succinate, are found closer to the “free dye – bound dye” construction line. Specifically, in the gray region citrate, isocitrate, and malate all have a hydroxyl group. Oxaloacetate and α-ketoglutarate behave as hydroxy acids as well because they both form an enol when dissolved in water as shown in Figure 3-11a. In particularly, the enol form of oxaloacetate is more prevalent than its keto form due to the six membered hydrogen bonded ring that stabilizes the hydroxyl group, so this anion is found further

away from the line than α-ketoglutarate. The yellow region contains carboxylates that do not have a hydroxyl group but that have other features: fumarate, maleate, and *trans*-aconitate contain a carbon-carbon double bound, while maleate, trans aconitate, and tricarballylate all have relatively closely spaced and interacting carboxylate groups, but without any hydroxyl groups. This pattern of separation based on the hydroxy feature agrees with the group's previous results, that PAMAM dendrimers act as hydrogen bond acceptors, so they are more sensitive to the presence of hydrogen bond donor groups in the guest.[152] Finally the cluster for succinate, an anions whose carboxylate moieties are the only chemical features of note, was found along the "bound-free dye" line.

The measurement of data from this plate took about 2.5 hours, so reducing the number of instrumental measurements to be acquired would result in speeding up the reading process. By inspection of the loadings plot, we selected for retention only those measurements whose contribution was at least 2.5%, and removed all others contributing less to either of the first two factors. Only 9 of the original 29 measurements were retained as shown in Table 3-4, for a total of 86.7% of the information in the complete dataset. The system still showed good discriminatory ability as shown in Figure 3-12. Compare with the previous LDA scores plot for the complete set (Figure 3-11a), LDA scores plot of the simplified dataset had slightly larger cluster size and shorter intercluster distances, which indicated a small decrease in selectivity. The reading time for the plate was reduced to about less than half of the original. Reducing the plate reading time is very helpful for fast or large-batch scans.

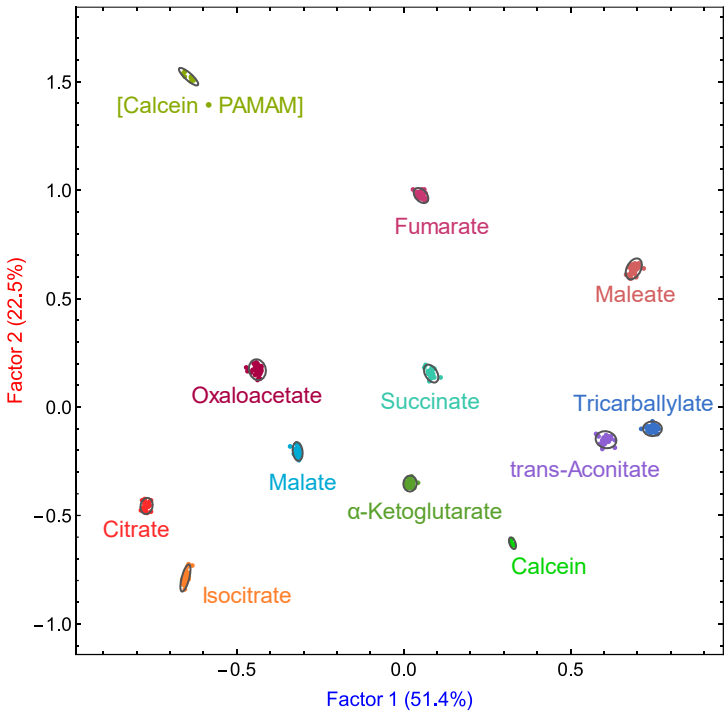

Figure 3-12 LDA scores plot for qualitative discrimination of ten carboxylates using [calcein•PAMAM] sensor with reduced measurements. [calcein] = 6.36 μM, [PAMAM G5] = 2.13 μM, [carboxylates] = 2.30 mM. Performed in 50 mM aqueous HEPES buffer at pH 7.4, T = 25 °C.

Table 3-4 Loadings for instrumental measurements used for the qualitative discrimination of carboxylates using [calcein•PAMAM] sensor. F*n*% (columns) is the percent of the information explained by Factor *n* that is provided by each raw measurement (rows). The numbers correspond toto Figure 3-12.

Variable type	Wavelength (nm)	F1%	F2%	F3%
Absorbance	300	1	4	32
Absorbance	340	0	10	5
Absorbance	500	0	12	0
Absorbance	510	2	35	3
Fluorescence emission	460/528	2	3	0
Fluorescence emission	460/560	59	3	15
Fluorescence emission	485/516	12	19	7
Fluorescence emission	485/528	20	7	5
Fluorescence emission	485/560	4	6	9

The limit of differentiation for this system was estimated by measuring a series of samples with varying carboxylates concentrations. Figure 3-13 showed that at a concentration of 250 μM (Figure 3-13a) i.e., about ten times lower than the working concentration discussed above, the carboxylates were still separated, whereas at a concentration of 100 μM (Figure 3-13b), the fumarate and succinate clusters started to lose definition. The limit of differentiation of our system could therefore be estimated to be between 100 μM and 250 μM, and probably closer to 100 μM. This would be more than enough for many relevant applications, such as prostate cancer screening.

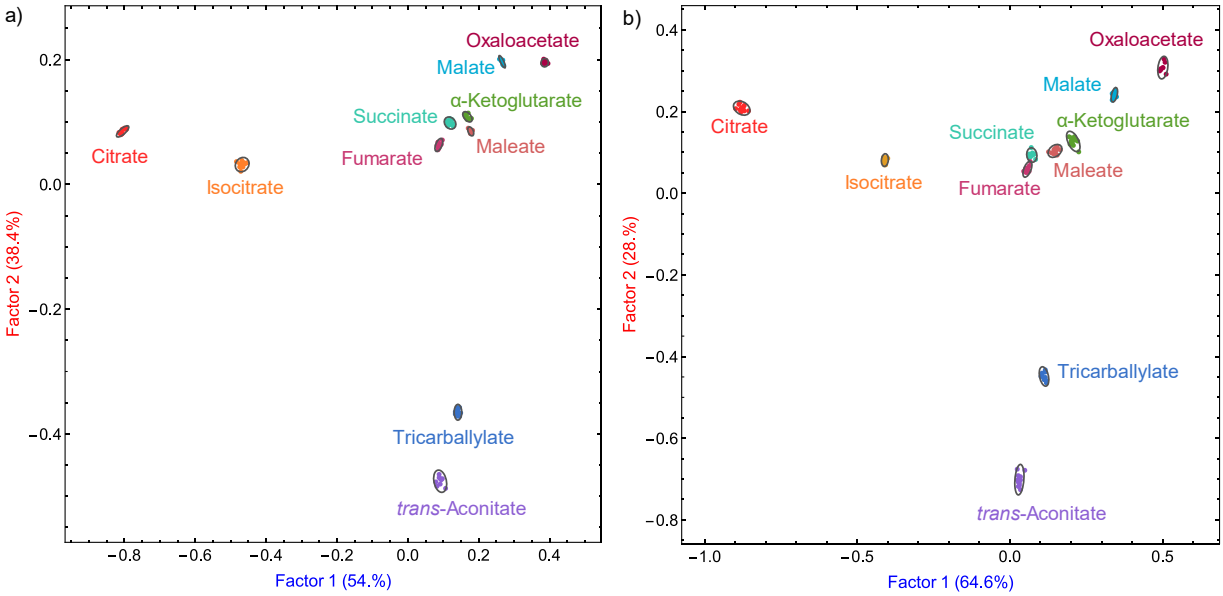

Figure 3-13 LDA scores plots for qualitative discrimination of ten carboxylates using [calcein•PAMAM] sensor as a function of anion concentration. Left: [carboxylates] = 250 μM; right: [carboxylates] = 100 μM. [calcein] = 6.36 μM, [PAMAM G5] = 2.13 μM. Performed in 50 mM aqueous HEPES buffer at pH 7.4, T = 25 °C.

3.2.5 Qualitative discrimination of carboxylates using three [dye•PAMAM] sensors

Putting all the data from the three dyes together, as shown in Figure 3-14 left, the separation is even better with an even smaller cluster size when compared with any of the

[dye•PAMAM] sensors (Figure 3-5, Figure 3-8, and Figure 3-11). However, the arrangements of the analyte clusters is very similar to the differentiation obtained using [calcein•PAMAM] sensor (Figure 3-11). After analysis (shown in Figure 3-14 right), measurements that contributed more than 5% along Factor 1 or/and Factor 2 were labeled. Six measurements using [calcein•PAMAM] sensor had significant contribution to differentiation, however, only one measurement using [calcein blue•PAMAM] complex and one using [pyranine•PAMAM] sensor contributed slightly more than 5% along Factor 1. This indicated that [calcein•PAMAM] sensor is the main contributor to this differentiation. Even though the differentiation is slightly better using all three dyes, considering the time and cost for differentiation we decided to use [calcein•PAMAM]sensor alone for future unknown analysis studies.

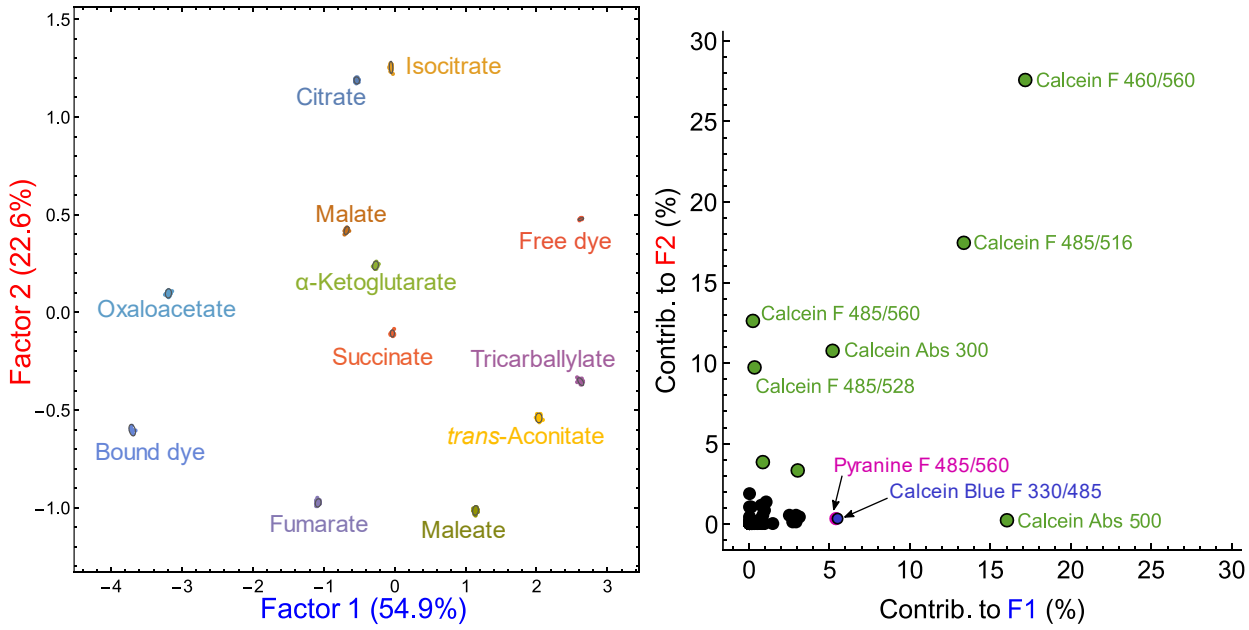

Figure 3-14 LDA results for qualitative discrimination of ten carboxylates using all 3 [dye•PAMAM] sensors, combining data from Figure 3-5, Figure 3-8, and Figure 3-11. Left: scores plot; right: loadings plot (Abs: absorbance, F: fluorescence emission $\lambda_{ex}/\lambda_{em}$). Performed in 50 mM aqueous HEPES buffer at pH 7.4, T = 25 °C.

3.3 Simultaneous determination of unknown identity and concentration

With ten carboxylates of interest being discriminated successfully using [calcein•PAMAM] complex as a sensor, and low enough limit of differentiation, we wanted to expand our scope to be able to identify and quantify unknown carboxylates because, in practice, an unknown analyte always has unknown concentration as well. First, carboxylates with different concentration were tested, to see the tolerance of this system to small concentration variations: it is desired that the system can still recognize and identify unknown carboxylate even when their concentration is close to the nominal one used in training above. Then, we wanted to develop a sensor only sensitive to the concentration of carboxylate groups, and not their identity, to be able to quantify the unknown's concentration, then perform qualitative discrimination.

3.3.1 LDA scores plot with different carboxylates concentration

Figure 3-15 contains the results of the discrimination of carboxylates using [calcein•PAMAM] complex as a sensor under a series of increasing concentration. This experiment was performed to see the tolerance of this system towards concentration variations. From 0.5 mM to 6 mM [carboxylate], the discriminatory power was retained, and the orientations of clusters remained similar as well. This proves that the discrimination of carboxylates was dominated by their structure; small changes in concentration would not change the nature of the response.

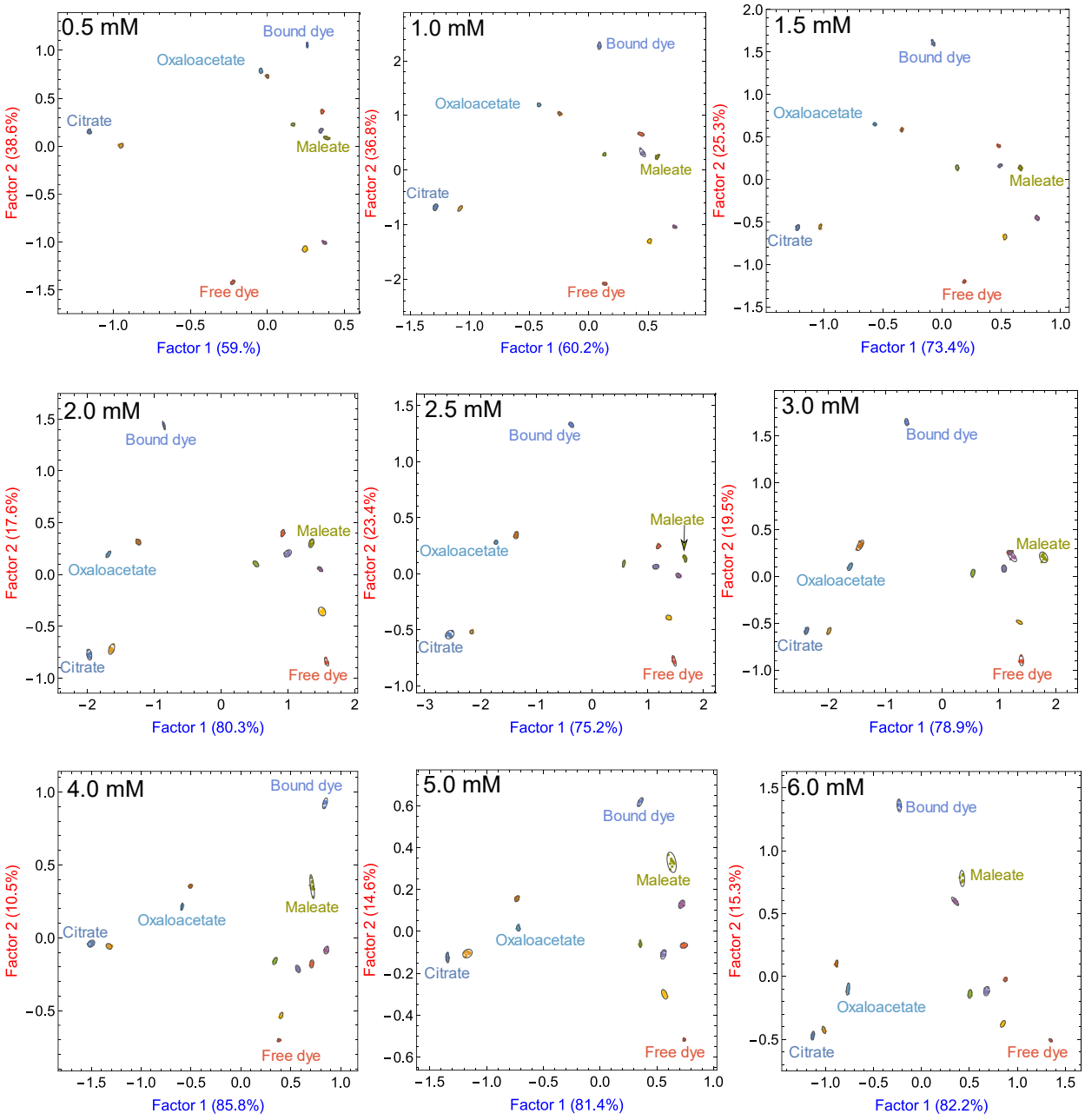

Figure 3-15 LDA scores plots of ten carboxylates for qualitative discrimination using [calcein•PAMAM]sensor. Carboxylates concentration from left to right, top to bottom: 0.5 mM, 1.0 mM, 1.5 mM, 2.0 mM, 2.5 mM, 3.0 mM, 4.0 mM, 5.0 mM, and 6.0 mM, respectively. [calcein] = 6.36 μM, [PAMAM G5] = 2.13 μM. Performed in 50 mM aqueous HEPES buffer at pH 7.4, T = 25 °C.

However, a concern about using LDA is that LDA is a supervised clustering technique, in which the identity of the analytes within a sample is provided to the algorithm. The algorithm will attempt to separate samples with different labels, which makes it an excellent choice for training, but possibly a poor one for unknown identification. In fact, the algorithm may end up overemphasizing adventitious differences in order to achieve differentiation, even among two identical samples, if they are labeled differently (e.g. reference and unknown samples) Thus, an unsupervised technique is needed for unknown analysis: PCA was used for this portion of our work.

3.3.2PCA scores plot with different carboxylates concentration

Being an unsupervised clustering technique, PCA does not try to separate two identical clusters. To study the effect of small change in concentration, a qualitative discrimination experiment using [calcein•PAMAM] sensor was performed with ten carboxylates at concentration of 2.5 mM, as well as 5 of the carboxylates at a concentration of 2.0 mM and 3.0 mM. As shown in Figure 3-16, clusters of the same carboxylate were overlapped or very close to each other, even though their concentration were slightly different. For each carboxylate that had different concentration, the samples with the lowest concentration (2.0 mM) was always closest to the bound dye reference, whereas the sample with the highest concentration (3.0 mM) was always closest to the free dye reference. This is consistent with the previous experiment, that is, with more carboxylate anions, more dye was being displaced, therefore the solution behaved like free dye. Overall, the separation of different carboxylates was dominated by their structure if the difference in concentration was small (e.g., 25% in this experiment). Carboxylate concentration of 2.5 mM was used as a target concentration in the further unknown analyte studies.

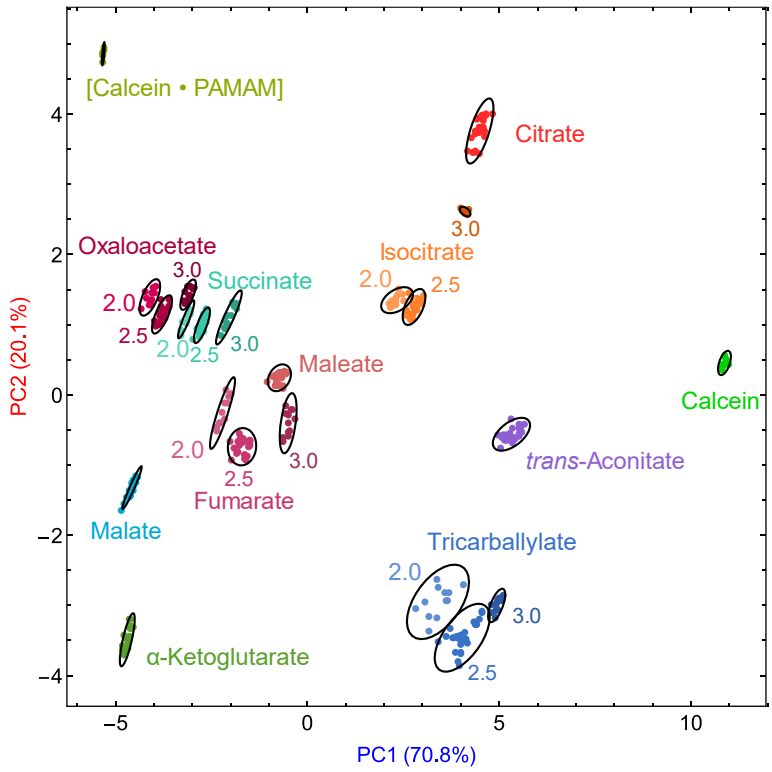

Figure 3-16 PCA scores plot from the investigation of the effect of a small variation in concentration in the qualitative discrimination of the ten carboxylate analyte targets using the [calcein•PAMAM] sensor. The following carboxylates appear over a range of concentrations (2.0 mM, 2.5 mM, 3.0 mM): oxaloacetate, succinate, isocitrate, fumarate, and tricarballylate; other carboxylates only had one concentration of 2.5 mM. Performed on a 384-well plate in 50 mM aqueous HEPES buffer at pH 7.4, T = 25 °C. [calcein] = 6.36 μM, [G5] = 2.13 μM.

3.3.3 Standard curve for quantitative analysis

Although fluorescence anisotropy was a great direct reporter of dye-PAMAM binding, its contribution to carboxylates differentiation was always poor, indicating that it was insensitive to the structure of the carboxylate. This property of the fluorescence anisotropy response made it less useful when trying to tell the carboxylates apart. On the other hand, however, it became very useful in the present context, where we seek a response that is only sensitive to total carboxylate concentration, and not to the identity of the carboxylate involved. Using anisotropy, the concentration of the unknown carboxylate could be determined first, then the sample could be

diluted appropriately to be qualitatively discriminated. It was also known that tricarboxylates had a better affinity to PAMAM G5 than the dicarboxylates, thus, two fluorescence anisotropy standard curve were prepared for concentration determination. In Figure 3-17, a "tricarboxylate standard" curve was generated by averaging the 4 tricarboxylates anisotropy titration profiles. Similarly, a "dicarboxylate standard" curve was generated by averaging the 6 dicarboxylate anisotropy titration profiles.

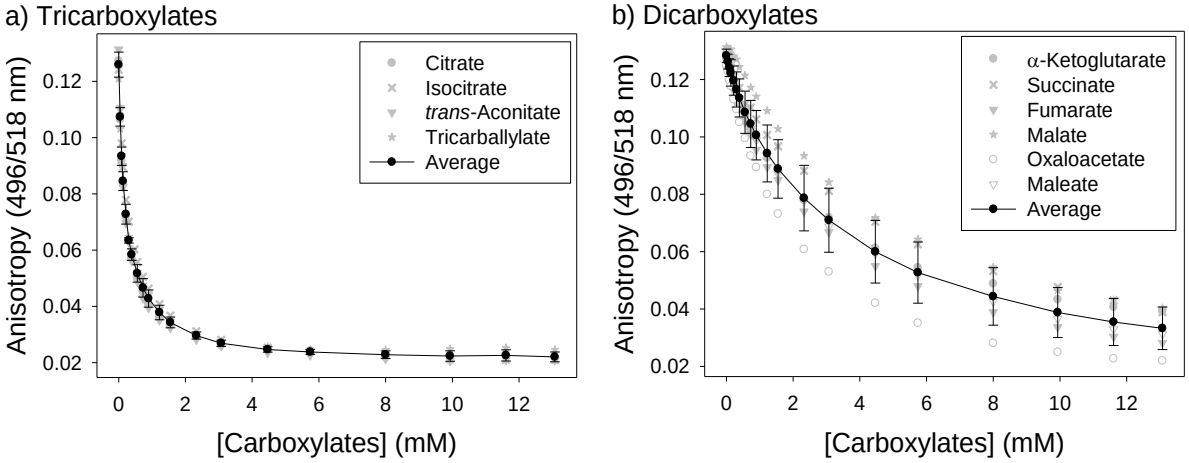

Figure 3-17 Fluorescence anisotropy emission as standard curve for carboxylate concentration determination using [calcein•PAMAM] sensor. a) tricarboxylates; b) dicarboxylates. Excitation: 496 nm, emission: 518 nm. [calcein] = 6.36 μM, [PAMAM G5] = 2.13 μM. Performed in 50 mM aqueous HEPES buffer at pH 7.4, T = 25 °C.

3.3.4 Unknown carboxylate analysis – quantitation

Four unknown samples were prepared by a co-worker, Dr. Xiaoli Liang. Each sample was dissolved in 50 mM HEPES buffer with [calcein•PAMAM] sensor and adjusted pH to 7.4. Each sample was then used as a titrant and added into [calcein•PAMAM] complex to generate a titration profile of fluorescence anisotropy as a function of the volume of diluted unknown. The profile for each unknown was then fit to the two separate standard curves discribed above (i.e. dicarboxylates and tricaboxylates), generating two hypothezed concentrations, as shown in

Figure 3-18. For example, the anisotropy profile for Unknown **C** was fitted to both standard curves, and the concentration was estimated to be 34.4 mM as a tricarboxylate (Figure 3-18e), or 436 mM as a dicarboxylate (Figure 3-18f). Then, Unknown **C** was split into two solutions, and each was diluted to the 2.5 mM working concentration for identification; in particular, half of Unknown **C** was diluted 13.76 fold (34.4 mM to 2.5 mM) and marked as **C tri**; the other half was diluted 174.4 fold (436 mM to 2.5 mM) and marked as **C di**. In this case, the anisotropy profile of this unknown fits better on the tricarboxylate curve, but both hypotheses were taken into consideration nonetheless.

Similarly, the concentration of Unknown **A** was determined to be 54.3 mM as a tricarboxylate (leading to a 21.2 fold dilution to make sample **A tri**), or 666 mM as a dicarboxylate (266.4 fold dilution to make sample **A di**); Unknown **B** was determined to be 1.86 mM as a tricarboxylate (considered as-is to be sample **B tri**), or 23.1 mM as a dicarboxylate (9.24 fold dilution to make sample **B di**); and Unknown **D** was determined to be 2.27 mM as a tricarboxylate (used as-is as sample **D tri**), or 29.1 mM as a dicarboxylate (11.64 fold dilution to make sample **D di**). The true values for the concentrations of the unknown samples are listed in Table 3-5.

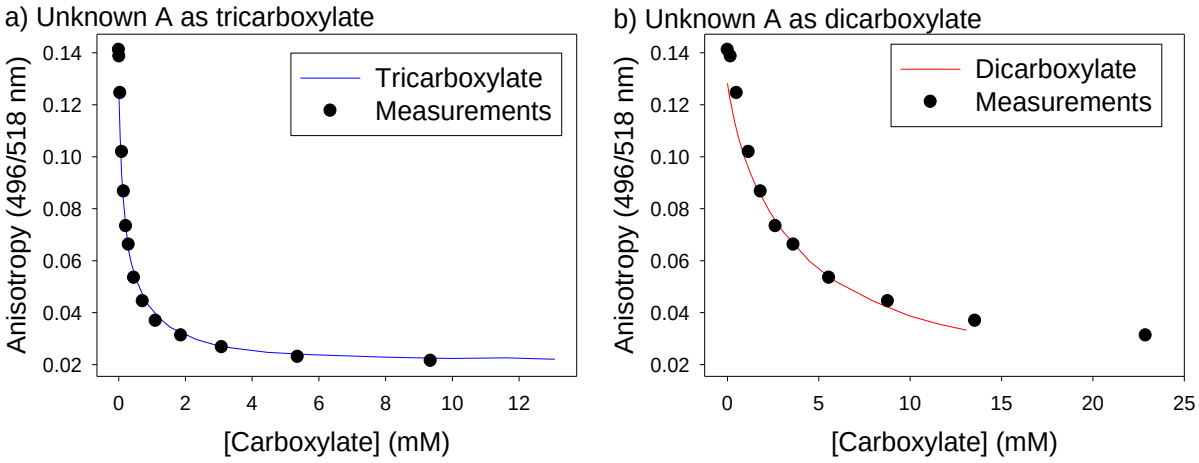

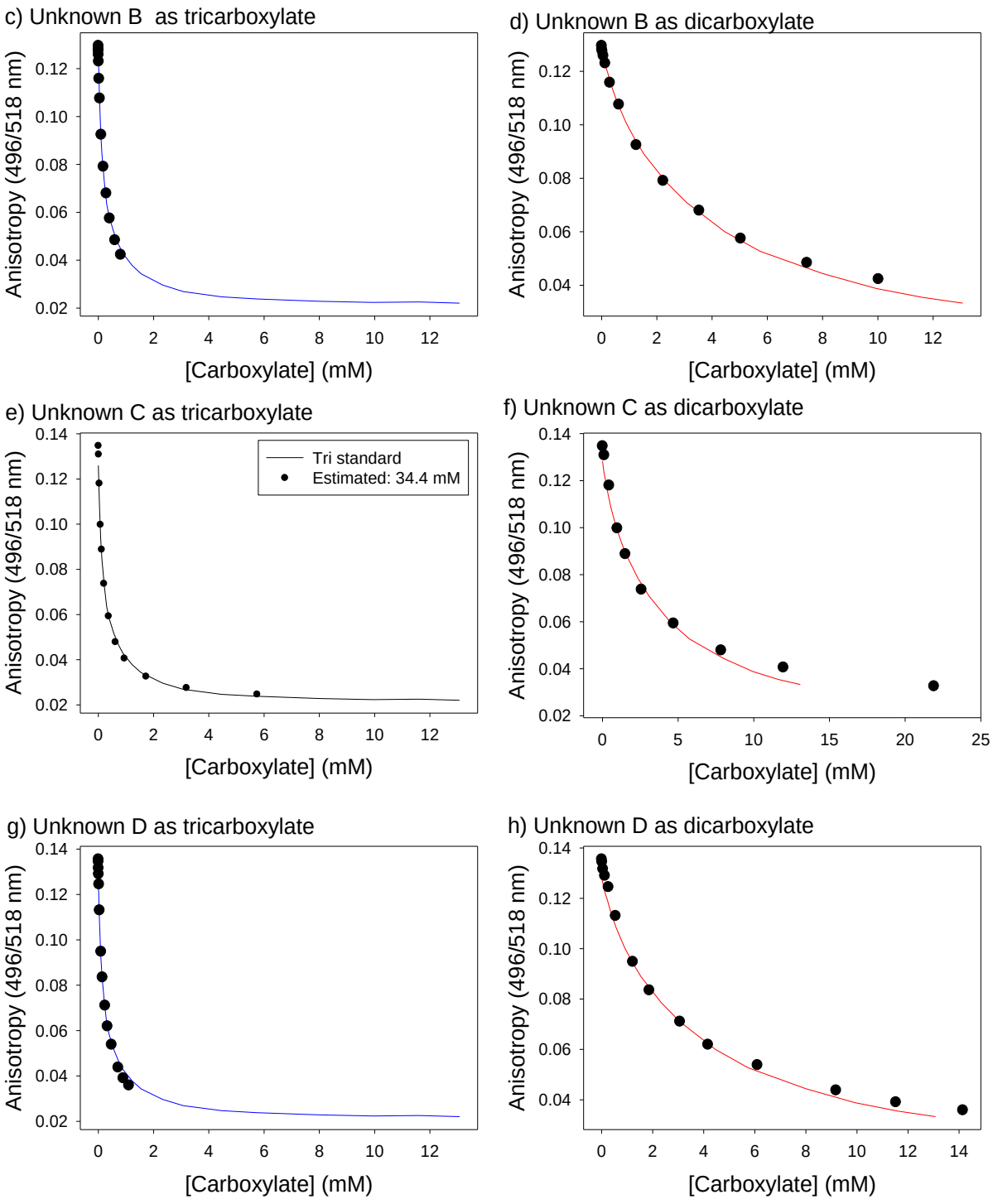

Figure 3-18 Fluorescence anisotropy of unknown A (a, b), unknown B (c, d), unknown C (e, f), and unknown D (g, h) fitted to the two standard curves shown in Figure 3-17. Left: anisotropy readings fitted to tricarboxylate standard curve; right: the same anisotropy readings fitted to dicarboxylate standard curve. Excitation: 496 nm, emission: 518 nm. [calcein] = 6.36 μM, [PAMAM G5] = 2.13 μM. Performed in 50 mM aqueous HEPES buffer at pH 7.4, T = 25 °C.

3.3.5 Unknown carboxylate analysis – identification

Four unknowns (8 samples in total, where considering the dicarboxylate vs. tricarboxylate option) were measured in a discrimination experiment using [calcein•PAMAM] complex as a sensor, together with ten carboxylate references. Initial PCA results are shown in Figure 3-19a, in which carboxylate reference clusters are shown in gray and unknown sample clusters are shown in color. Continuing to use Unknown **C** as an example, the "**C tri**" cluster was found overlapping with the citrate reference in the scores plot, while the"**C di**" cluster was not overlapping or even nearby any of the reference clusters. Therefore, Unknown **C** was assigned to be citrate, a tricarboxylate. On this basis we could also assign it a concentration of 34.4 mM , as determined by comparison to the "tricarboxylate" standard curve, as described above. Similarly, the "**A tri**" cluster was found overlapping with the *trans*-aconitate reference cluster while the "**A di**" cluster was isolated, so Unknown **A** was determined to be a 36.9 mM sample of *trans*-aconitate; the "**B di**" cluster was close to α-ketoglutarate reference cluster, while the very isolated "**B tri**" cluster could be eliminated, leaving Unknown **B** to be 25.4 mM α-ketoglutarate; and the "**D tri**" cluster was found overlapping with the tricarballylate reference cluster, while the "**D di**" cluster was isolated, so Unknown **D** was determined to be a 3.05 mM sample of tricarballylate. With these results, a new PCA scores plot was generated and shown in Figure 3-19b, for clarity.

All results were summarized in Table 3-5 where they are also compared with their actual identities and concentrations: all unknown samples were correctly identified, and quantified with relatively low error.

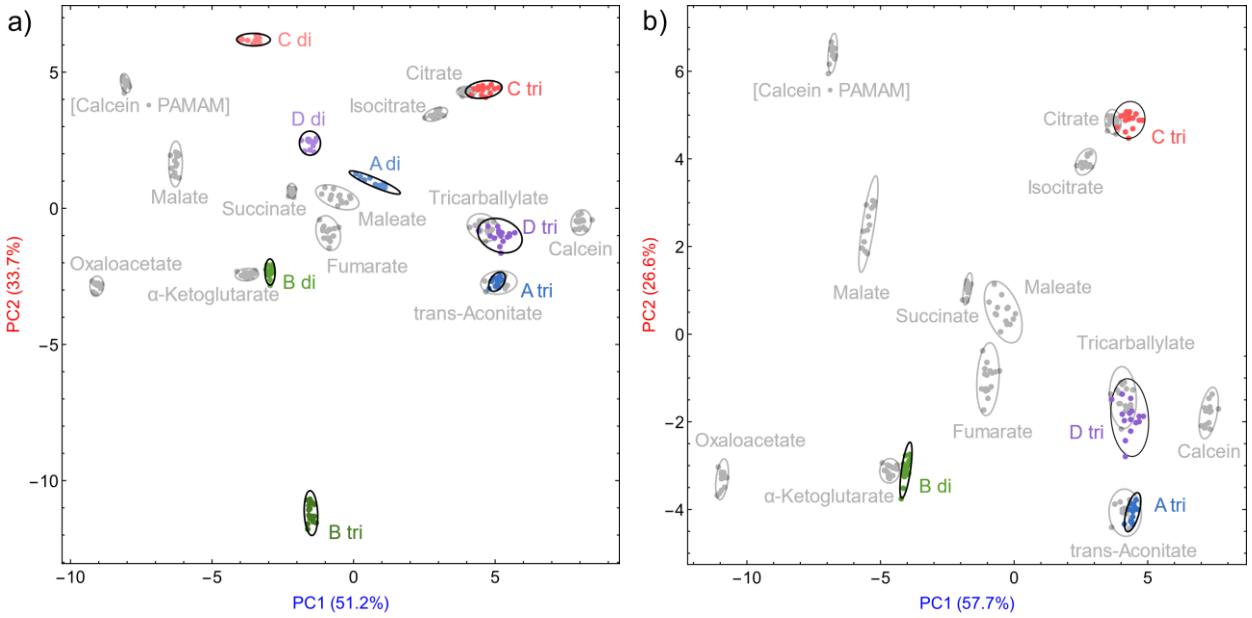

Figure 3-19 PCA scores plots for the determination of identity and concentration of 4 unknown carboxylate samples using the [calcein•PAMAM] sensor. Left: all unknown samples; right: only the best estimates for each sample were retained. In color: intermediate samples for each unknown; in gray: pure carboxylate reference samples. [calcein] = 6.36 μM, [PAMAM G5] = 2.13 μM, [carboxylates] = 2.50 mM. Performed in 50 mM aqueous HEPES buffer at pH 7.4, T = 25 °C.

Table 3-5 Experimentally determined vs. actual concentrations of unknown samples.

Unknown #	Actual identity	Actual conc. (mM)	Exp. conc. (mM)	Percent error (%)
A	*trans*-Aconitate	54.3	36.9	47.2
B	α-Ketoglutarate	23.1	25.4	9.06
C	Citrate	34.4	38.5	10.6
D	Tricarballylate	2.27	3.05	25.6

3.4 Conclusions

A supramolecular pattern recognition sensing system for carboxylate anions building upon non-covalent interaction was developed. Commercially available organic fluorophores (calcein blue, pyranine, and calcein) and supramolecular host PAMAM dendrimer were used as the sensing probe that functioned in neutral aqueous solution. Ten carboxylate analytes of interest were successfully differentiated through absorbance, fluorescence emission and

anisotropy measurements. PCA and LDA were used as pattern recognition algorithms for data processing. Of all three [dye•PAMAM] sensors, [calcein•PAMAM] complex proved to be the most selective towards carboxylate analytes, with a limit of discrimination close to 100 μM.

Unknown carboxylate samples were also screened by this sensing system using [calcein•PAMAM] complex as a sensor. A fluorescence anisotropy titration was first carried out to determine a tentative concentration; this was followed by discrimination of the unknown carboxylates, and by comparison with carboxylate references samples. We proved the accuracy of unknown detection, with 100% correct identification and with 50% maximum error of quantification. Although the percent error for one analyte (*trans*-aconitate) was quite high, on the other hand all other analytes had much lower errors of quantitation. More in general, considering that pattern-based recognition systems are normally very poor at quantitative analysis, this was an exciting result nonetheless. Overall, this method provided easy, fast, and sensitive access to recognition, discrimination, and quantitation of common carboxylates in aqueous media.

3.5 Experimental details

3.5.1 Materials

Fifth-generation, amine-terminated poly(amidoamine) (PAMAM) dendrimer with a 1,2-diaminoethane core was manufactured by Dendritech, Inc., and purchased as a solution in methanol with exact concentration of 1.419 mM. The final solution used for all experiment was obtained by dilution with buffer and contained negligible amount of methanol (< 0.8%). Dye solutions were prepared from calcein disodium salt and calcein blue, purchased from Sigma Aldrich; and pyranine, purchased from Alfa Aesar. Carboxylate solutions were prepared from DL-isocitric acid trisodium salt hydrate purchased from Acros; fumaric acid, α-ketoglutaric acid,

trans-aconitic acid, succinic acid, DL-malic acid, and oxaloacetic acid purchased from Sigma Aldrich; tricarballylic acid and maleic acid purchased from Alfa Aesar; anhydrous citric acid purchased from EMD Millipore. 50 mM 4-(2-hydroxyethyl) piperazine-1-ethanesulfonic acid (HEPES) buffer was prepared from HEPES purchased from IBI Scientific. All prepared solutions were adjusted to pH 7.4 using solutions of NaOH, prepared from NaOH purchased from Fisher Scientific, and HCl, prepared from HCl purchased from BDH Aristar. Nunc 384-well polystyrene black-wall plates were purchased from Thermo Scientific. All materials were used as received.

3.5.2 Instrumentation

Fluorescence anisotropy titrations were carried out on an ISS PC1 spectrofluorometer, with a broad-spectrum high-pressure xenon lamp (CERMAX, 300W) as an excitation light source; manual calibrated slits; excitation correction by a rhodamine B quantum counter with a dedicated detector; emission light detector was a Hamamatsu red-sensitive PMT operating in photon-counting mode. High aperture Glan Thompson calcite polarizers were used for fluorescence anisotropy measurement. For all titration experiments, an external circulating water bath was used to control the cuvette temperature as 25 °C.

Microwell plate-based discrimination studies were carried out on a Biotek Synergy II multimode plate reader, with a tungsten lamp light source. A monochromator was used for absorbance measurements; different bandpass filters were used for fluorescence emission; and plastic sheet polarizers were used for fluorescence anisotropy measurements. A “top-detected” mode was used for all fluorescence measurements: a dichroic mirror was automatically positioned between the emission source and sample wells to block excitation light from reaching to the detector.

3.5.3 Discrimination experiment conditions

Concentration for qualitative discrimination experiments were: [calcein blue] = 10.2 μM with [G5] = 12.7 μM, and [carboxylates] = 1.28 mM; [pyranine] = 6.04 μM with [G5] = 0.213 μM, and [carboxylates] = 2.4 mM; or [calcein] = 6.36 μM with [G5] = 2.13 μM, and [carboxylates] = 2.30 mM. Concentration of carboxylate analytes for quantitative analysis experiments were varied as described previously for each experiment.

3.5.4 384-microwell plate experiments

For qualitative discrimination experiments, each carboxylate sample was prepared in 36 replicates; while for unknown experiments, each reference carboxylate and unknown sample had 16 replicates. Solutions were prepared in 50 mM HEPES buffer, and 100 μL of each sample was deposited onto the plates by hand using Eppendorf Research multichannel pipettors. Absorbance, fluorescence emission and anisotropy were measured through a plate reader, and data process was carried out by Principal Component Analysis (PCA) and Linear Discriminant Analysis (LDA) algorithms.

3.5.5 Simultaneous determination of unknown identity and concentration

Two standard curves, one for tricarboxylates and a second one for dicarboxylates, were prepared by averaging the measurements of fluorescence anisotropy displacement titrations. Unknown samples were prepared by co-worker Dr. Xiaoli Liang, and then displacement titrations were run as described previously. Titration profiles for each unknown were fitted onto both standard curves, to estimate the unknown concentration under the hypothesis of it being either a tricarboxylate or a dicarboxylate. The fitting resulted in two estimated concentrations; therefore each unknown sample was split into two parts, and diluted to 2.5 mM according to the estimated concentrations.

Unknown samples were deposited onto a plate, together with reference carboxylate samples. PCA was used for data processing. For the two parts of each unknown, only one cluster was found matching with one of the reference carboxylates clusters, while the other one corresponded to none of the clusters in the training set. Therefore, the identity and concentration of the unknown could be determined.

CHAPTER 4
BETA-LACTAM ANTIBIOTICS DISCRIMINATION IN NEUTRAL AQUEOUS SOLUTION USING A [CALCEIN•PAMAM] SENSOR

4.1 Introduction

4.1.1 Importance of β-lactam antibiotics

Antibiotics are used for treatment of human and animal diseases. They are also added to animal feed to improve growth rates and feed efficiency.[157-159] However, the increasing use of antibiotics gave a rising number of multi-resistant bacteria, and the residues in food cause serious allergic problems.[160] Research showed that penicillins and cephalosporins, members of the β-lactam antibiotic family, comprised about 65% of the world market for antibiotics.[161] Thus, there is a need for the detection of these antibiotics appearing in foods and environmental samples.

We will discuss work leading to the discrimination of five cephalosporins and two penicillins whose structures are shown in Scheme 4-1, where the structure in red is the β-lactam ring, while green and blue stands for the core structure of cephalosporins and penicillins, respectively. For easier representation of the analytes, here we used P for penicillins, and C for cephalosporins (numbers stand for the cephalosporin generation number). Monoanions and dianions were marked as “mono” and “di”, respectively. We also introduced an organic dicarboxylate and a monocarboxylate, terephthalate and benzoate, as controls in the study (structures shown in Scheme 4-2). Several applications can benefit from a system that can recognize the identity of common β-lactam antibiotics easy and fast: testing antibiotic residues in food (for example, milk) to prevent food allergies; measuring the type and amount of antibiotics

in sewer water, to get an overall picture of the drug consumption of an area; comparing the downstream and upstream antibiotics content of a pasture to test if there is abusive administration of antibiotics to domestic animals.

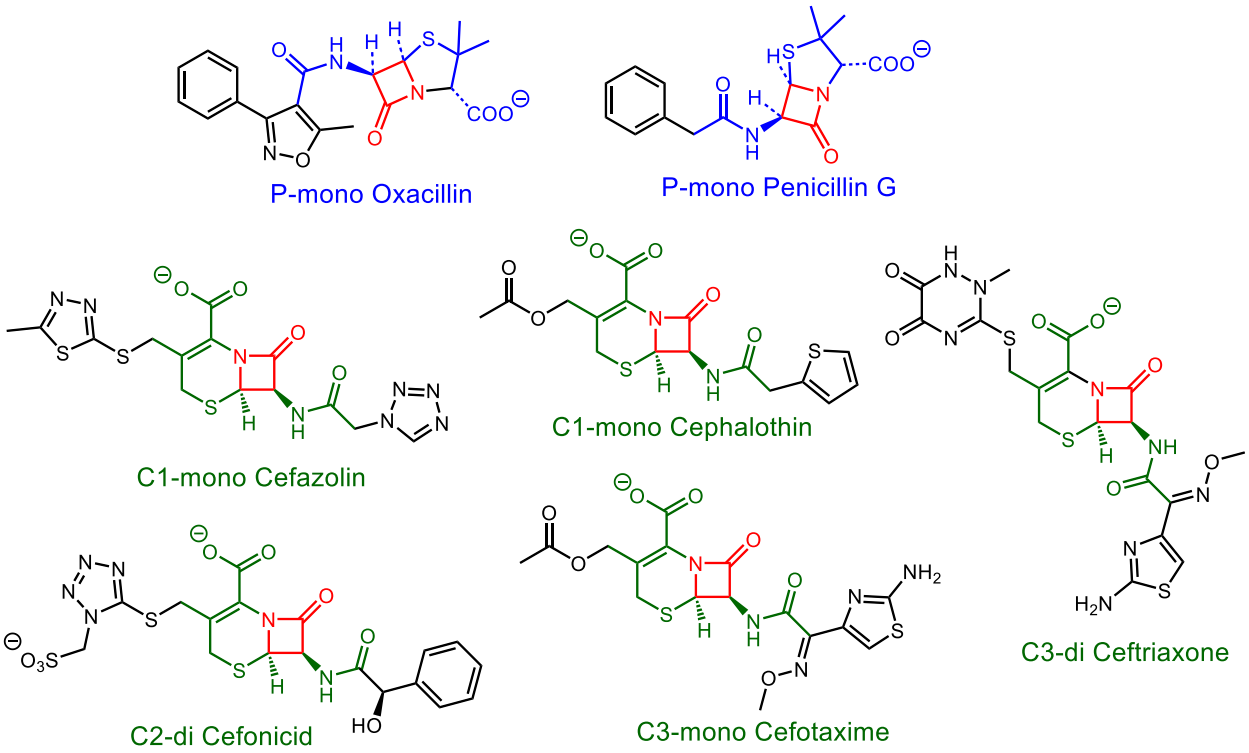

Scheme 4-1 Structures of the penicillins and cephalosporins of interest (red: β-lactam ring, blue: penicillin core structure, green: cephalosporin core structure), shown in their most likely protonation state in water at pH 7.4. P: penicillin, C: cephalosporin generation number; mono: monoanion, di: dianion.

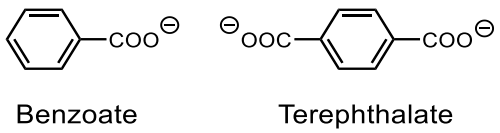

Scheme 4-2 Structures of benzoate and terephthalate shown in their most likely protonation state in water at pH 7.4.

Common detection methods for β-lactam antibiotics include the European Union Four-Plate Test (EU4pt),[162-163] the *Bacillus stearothermophilus* Disc Assay (BsDA),[164-165] the Nouws

Antibiotic Test (NAT),[166-167] and the PremiTest.[168-169] Counterfeiting of antibiotics is also a global health issue. Structures reported to be counterfeited include cefazolin, cefotaxime, and ceftriaxone (included as analytes in our study).[170] Common problems with counterfeit antibiotics include reduced concentration of the active principle, reduced stability, altered chemical ingredient, and introduction of impurities.[171] The currently available tests mentioned above require relatively complex multi-step procedures and typically required more technical expertise than optical spectroscopy. Therefore, we propose here to use a sensing complex (a host molecule and a fluorophore) based on simpler techniques and detection systems for the detection and discrimination of β-lactam antibiotics.

4.1.2 Sensing of carboxylate-containing molecules

Previously in chapters 2 and 3, we proved that PAMAM G5 (Scheme 4-3) could interact with calcein dye (Scheme 4-4) through hydrogen bonding and electrostatic interactions in aqueous solution at pH 7.4. Upon addition of PAMAM G5 into calcein solution, a [calcein•PAMAM] is complex formed (Figure 4-1), as discussed in Section 2.2.4. Then, addition of a carboxylate to this complex caused it to bind to PAMAM dendrimer, and displaced the calcein dye from its complex and to its free (Section 2.3.3). By monitoring the optical behavior of calcein dye (absorbance, fluorescence emission intensity and anisotropy), this sensing complex was able to successfully differentiate 10 structurally similar carboxylates from the citric acid cycle, based on their different affinities to PAMAM dendrimer (Chapter 3.2.4).

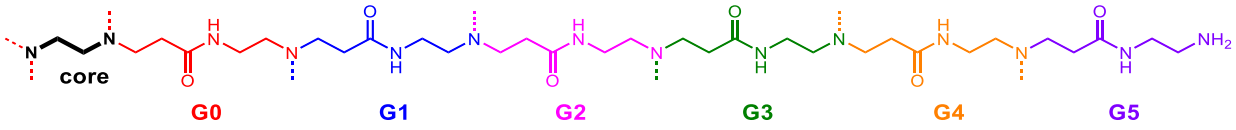

Scheme 4-3 One branch of an amine-terminated fifth generation poly(amidoamine) (PAMAM G5) dendrimer with ethylene diamine core. Each generation ends with an amine group, and

branches out twice: one branch is shown in the scheme, and the other branch is represented by the dashed line.

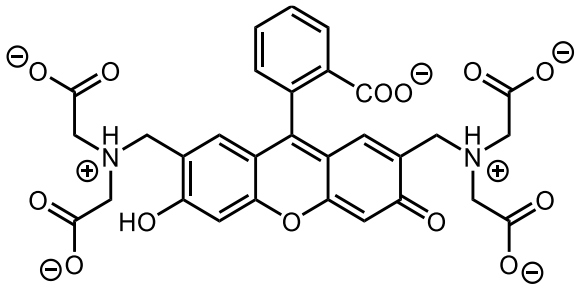

Scheme 4-4 Structures of calcein in its most likely protonation state in water at pH 7.4.

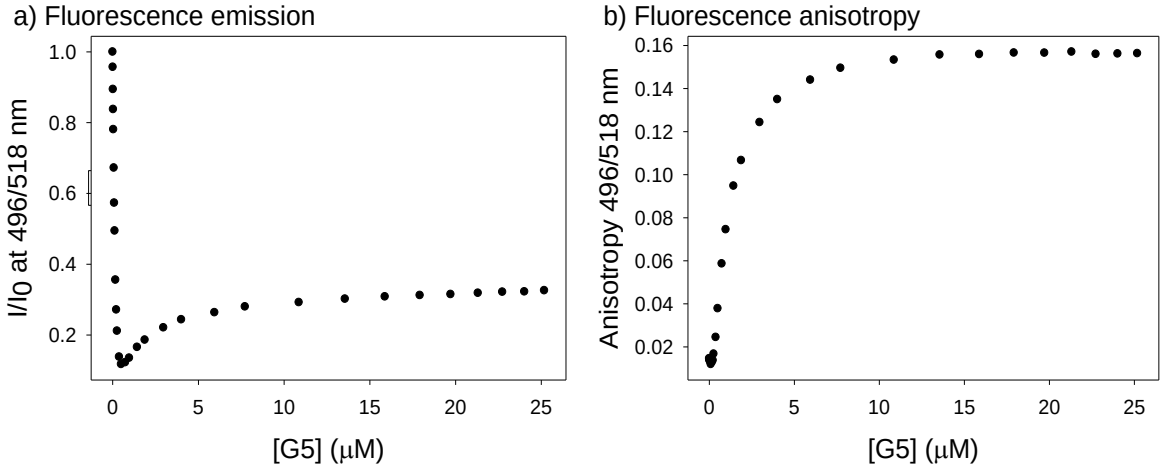

Figure 4-1 Titration of G5 into calcein to form [calcein•PAMAM] complex in solution. a) fluorescence emission intensity (same as Figure 2-9b); b) fluorescence anisotropy (same as Figure 2-10b). [calcein] = 6.36 μM, [PAMAM G5] = 2.13 μM. Performed in 50 mM aqueous HEPES buffer at pH 7.4, T = 25 °C, excitation: 496 nm, emission: 518 nm.

The β-lactam antibiotics all contain one carboxylate group in their core structure, which can be a point of interaction with the PAMAM-calcein sensor. Therefore in this study, we decided to repurpose the same sensing complex we used previously for carboxylate analytes towards antibiotic sensing, under the same conditions we used previously: [calcein] = 6.36 μM and [PAMAM G5] = 2.13 μM in 50 mM aqueous HEPES buffer at pH 7.4. Benchtop titrations

were carried out for determining the ability of antibiotics binding with PAMAM dendrimer, and the working concentration for discrimination studies. Discrimination studies were carried out using 384-multiwell plates and a plate reader, and linear discrimination analysis (LDA) was used for data processing.

4.2 Antibiotics binding to [calcein•PAMAM] sensor

We first tested the affinity of the antibiotic analytes for PAMAM G5 by introducing them into the [calcein•PAMAM] sensor complex, to see if they could displace the calcein dye from its complex. The fluorescence emission titration spectra are shown in Figure 4-2; while their profiles and profiles of fluorescence anisotropy are shown in Figure 4-3. Fluorescence emission increased as more antibiotics were introduced, and at the end of titration, the emission spectra looked very similar to the free dye spectra. Based on the fact that both PAMAM and analytes were not fluorescent, this indicated that the dye was in its free form at the end of the titration. Fluorescence anisotropy decreased during titration. Fluorescence anisotropy correlates with the binding between a small fluorophore and a larger host molecule: anisotropy reading is high when the small fluorophore is bound with the host molecule, and low when free in solution. The observed decrease in anisotropy suggested that the calcein dye was being released from its complex to the free form. Overall, both fluorescence emission and anisotropy showed that the antibiotics were able to displace the calcein dye from its complex and made a spectroscopic difference.

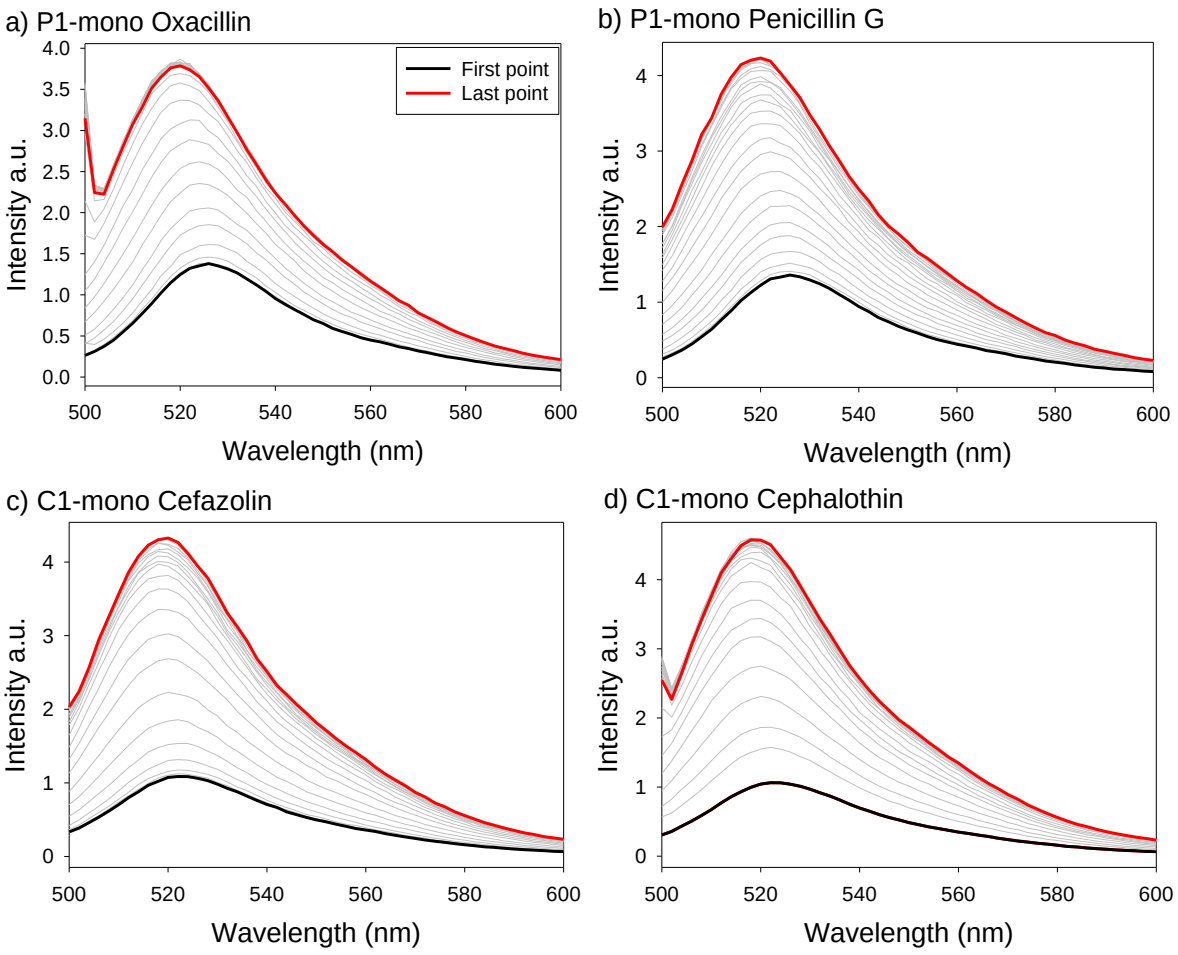

Continued on the next page.

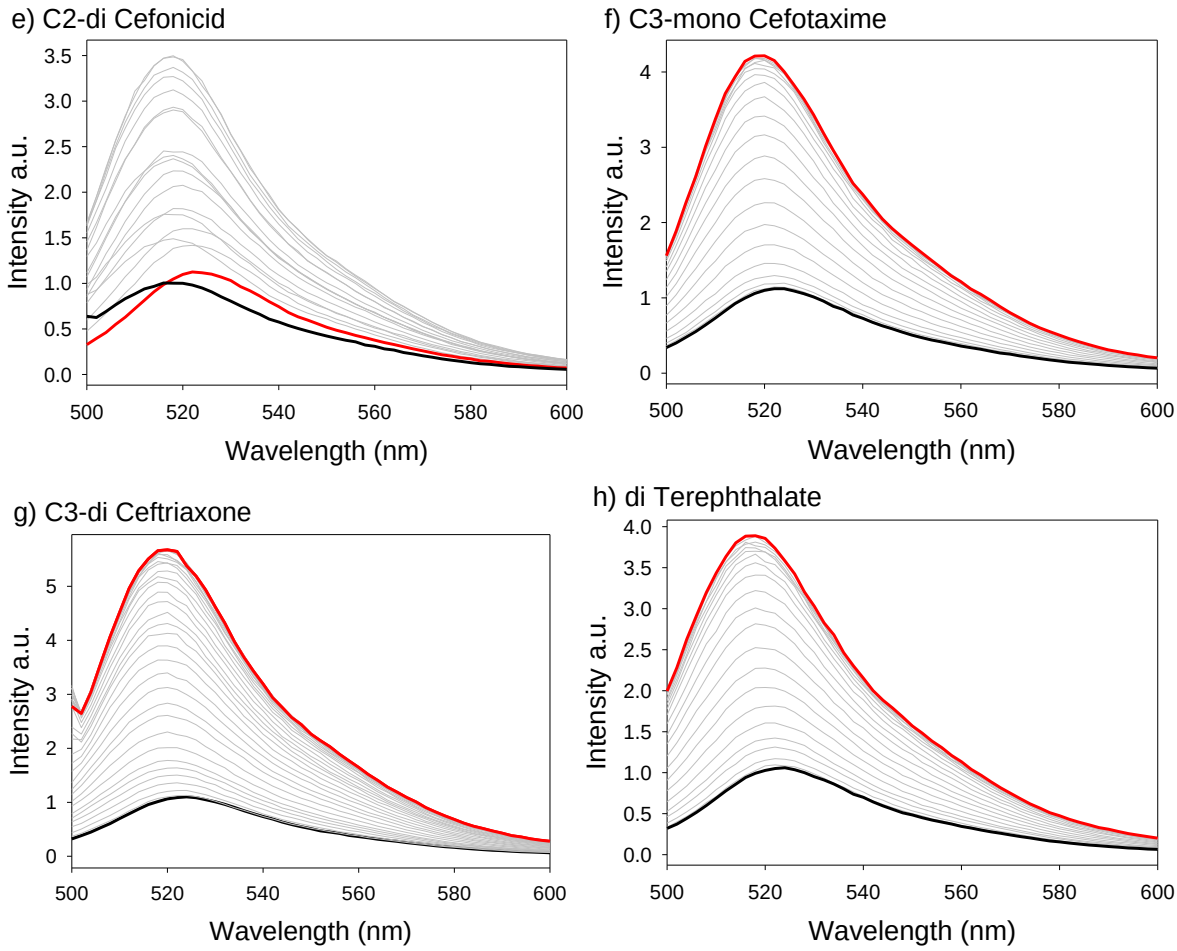

Figure 4-2 Fluorescence emission spectra from titrating analytes into [calcein•PAMAM] complex in solution. a) oxacillin, b) penicillin G, c) cefazolin, d) cephalothin, e) cefonicid, f) cefotaxime, g) ceftriaxone, h) terephthalate. Spectrum in black: first titration point; spectrum in red: the last titration point; spectra in gray: titration points in between. [calcein] = 6.36 μM, [PAMAM G5] = 2.13 μM, excitation: 494 nm. Performed in 50 mM aqueous HEPES buffer at pH 7.4, T = 25 °C.

However, we observed that high concentration of antibiotics would result in precipitation when added into the sensing complex. The precipitation skewed the absorbance measurements; therefore, absorbance titration measurements could not be used in these conditions. Fluorescence emission had a higher tolerance for precipitation in this case. Cefonicid (Figure 4-2e) was an exception: with the addition of cefonicid to the sensing complex, emission intensity increased

and then decreased due to formation of precipitate. The precipitation always happened after a plateau had been reached, and fortunately the working concentration for discrimination was always lower than the concentration that would cause precipitation, so precipitation did not affect the discrimination results. On the other hand, titration of benzoate was not possible because its solubility was too low, so we could not prepare a titrant solution of sufficiently high concentration, given its relatively low affinity as a monoanion.

From the profiles shown in Figure 4-3, almost all analytes were showing similar trends during titration: fluorescence emission increased until saturation; and fluorescence anisotropy decreased to a minimum. The slopes of the profiles were different, and often related to the analytes' affinities. As mentioned in Chapter 2, tri-anions had a higher affinity for PAMAM dendrimers than dianions, therefore they had a steeper slope than dianions during displacement titration experiments. This was more obvious in fluorescence anisotropy profiles because it is directly related to the state of the dye molecule. A similar behavior was observed with this set of di and monoanions: dianion cephalosporins had the highest affinity for PAMAM dendrimers, followed by monoanion cephalosporins, then monoanion penicillins. Since hydrophobic interactions favor the binding of these anions to PAMAM, and since penicillins are more water-soluble than cephalosporins, therefore they had weaker hydrophobic interactions with PAMAM dendrimers, leading to a lower affinity, as shown by a less steep binding profile.

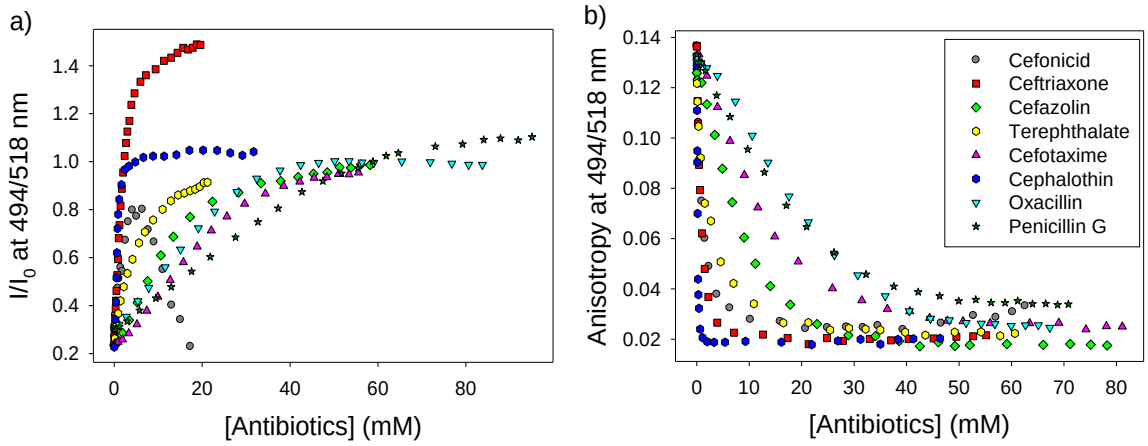

Figure 4-3 Binding of antibiotics and terephthalate to PAMAM G5 using calcein as an indicator. Titration profiles of analytes of interest into [calcein•PAMAM] complex. a) fluorescence emission intensity; b) fluorescence anisotropy. [calcein] = 6.36 μM, [PAMAM G5] = 2.13 μM, excitation: 494 nm. Performed in 50 mM aqueous HEPES buffer at pH 7.4, T = 25 °C.

Notice that cephalothin is a monoanion but still had a high affinity, as high as the dianions: this was because we had to hydrolyze the β-lactam ring to make it soluble at the working concentration. Hydrolysis was carried out by dissolving cephalothin at a basic pH (12.0) and then the solution's pH was adjusted to the working pH (7.4). The hydrolysis process created one extra carboxylate group (see Scheme 4-5) and made cephalothin a dianion, so it was not surprising that it behaved like one.

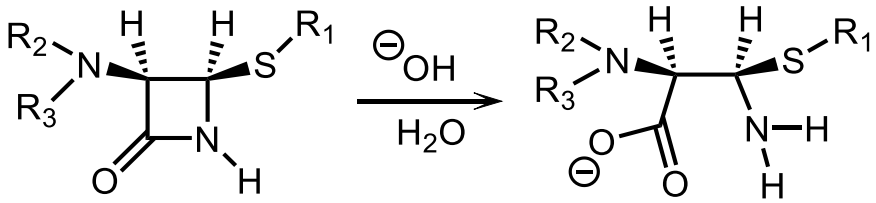

Scheme 4-5 Hydrolysis of β-lactam ring under basic condition.

As discussed in Chapter 3, the most appropriate concentration of antibiotic to use for discrimination with the [calcein•PAMAM] sensor complex was determined by comparing the

binding titrations obtained with different antibiotics, to determine the concentration at which they displayed maximum pair-wise differences. In this case, the optimal concentration was found to be 5.0 mM antibiotics. At this concentration there was no precipitation, so we could measure absorbance as well.

4.3 Antibiotics discrimination at pH 7.4

On a 384-polystyrene black-wall multiwell plate, 32 replicates of each analyte (100 μL, 5.0 mM), as well as free dye and bound dye references, and HEPES buffer as blanks, were deposited. For each sample, 54 instrumental measurements (Table 4-1) were taken by a plate reader including 30 absorbance wavelengths, 12 fluorescence emission measurements and 12 fluorescence anisotropy measurements (with different excitation and emission wavelengths combinations) in a 3-hour period. Multiple optical measurements collected for each sample generated a multidimensional dataset. In order to pinpoint the most useful information among these measurements for antibiotic discrimination, LDA was used for further data processing.

Table 4-1 Loadings for instrumental measurements used for the qualitative discrimination of antibiotics using [calcein•PAMAM] sensor. F*n*% (columns) is the percent of the information explained by Factor *n* that is provided by each raw measurement (rows). The numbers correspond to to Figure 4-4.

Variable type	Wavelength (nm)	F1%	F2%	F3%
Absorbance	350	41	44	8
Absorbance	360	0	10	2
Absorbance	370	0	12	2
Absorbance	380	0	3	1
Absorbance	390	0	0	0
Absorbance	400	0	0	0
Absorbance	410	0	0	0
Absorbance	420	0	0	0
Absorbance	430	0	0	0
Absorbance	440	0	0	0
Absorbance	450	0	0	0
Absorbance	460	0	0	0
Absorbance	470	0	0	0

Absorbance	480	0	0	0
Absorbance	486	0	0	0
Absorbance	492	0	0	0
Absorbance	494	0	0	3
Absorbance	496	0	0	0
Absorbance	500	0	0	1
Absorbance	510	0	0	7
Absorbance	520	0	0	0
Fluorescence emission	450/516	1	1	0
Fluorescence emission	450/528	9	3	4
Fluorescence emission	450/560	8	2	0
Fluorescence emission	450/580	0	2	0
Fluorescence emission	460/516	0	6	46
Fluorescence emission	460/528	12	3	2
Fluorescence emission	460/560	1	1	1
Fluorescence emission	460/580	0	4	1
Fluorescence emission	485/516	1	0	2
Fluorescence emission	485/528	3	1	10
Fluorescence emission	485/560	8	5	7
Fluorescence emission	485/580	13	1	0
Fluorescence anisotropy	450/528	0	0	0
Fluorescence anisotropy	450/560	0	0	0
Fluorescence anisotropy	450/580	0	0	0
Fluorescence anisotropy	460/528	0	0	0
Fluorescence anisotropy	460/560	0	0	0
Fluorescence anisotropy	460/580	0	0	0
Fluorescence anisotropy	485/528	0	0	0
Fluorescence anisotropy	485/560	0	0	0
Fluorescence anisotropy	485/580	0	0	0

As discussed in Chapter 3, the average value of the corresponding blank readings was subtracted from all optical measurements. Then each measurement channel was evaluated individually to eliminate those for which the response was similar across all analytes. After, 32 replicates of each sample were subjected to principal component analysis (PCA) to remove any outliers. The remaining dataset was subjected to LDA algorithms, transforming the original dataset into a new matrix with the same dimensions as the original, containing the same information. Therefore, by retaining the first two factors, we were able to reduce the

multidimensional dataset to a 2D “scores plot” retaining most of the original information and providing maximum discrimination. The relative contribution of each original measurement to the new factors in each scores plot are represented graphically in a corresponding “loadings plot”.

A good LDA scores plot requires a balanced factor 1 and factor 2; the most desirable result is each factor containing nearly 50% of the original information because this reproduces an ideal portion of the original instrumental measurements, as well as provides excellent multivariate differentiation. Also, the intracluster distance should be small: tight clusters suggesting good repeatability of each analyte; and intercluster distance should be large: clusters distanced from each other suggest clear difference among different analytes and high tolerance for small variations of any unknown samples, if needed.

The LDA scores plot of this dataset is shown in Figure 4-4: a scores plot of the full analyte set is shown on the left, and on the right is an enlargement of the gray rectangular area of the plot on the left, for clearer interpretation. Factor 1 contained 68.8% of the original information, while factor 2 contained 16.6% of the original information; the balance between the two factors was not ideal but still acceptable. For any samples with 32 replicates, the clusters were very tight, and all the cephalosporin clusters were well separated, indicating that this system worked well for cephalosporin discrimination. However, even though the two penicillin clusters were separated, the intercluster distance was very small. A similar situation was found for benzoate and terephthalate. Considering that the clusters were all very close to the bound dye reference, this could be caused by their low affinity for PAMAM dendrimer. Therefore, at the concentration of 5.0 mM, these analytes could only displace a small amount of dye from its complex with PAMAM. With a majority of the calcein dye being bound to PAMAM dendrimer,

the analyte solutions would “looked like” bound dye spectroscopically and could not be discriminated from each other.

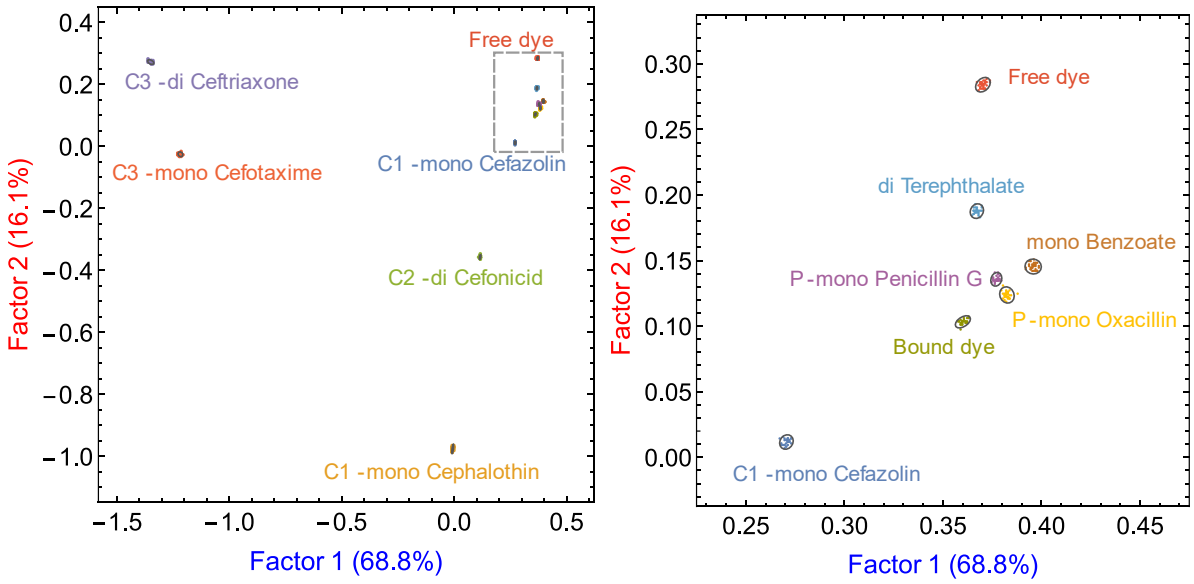

Figure 4-4 LDA scores plot for qualitative discrimination of 9 analytes (two penicillins, five cephalosporins and 2 reference carboxylates) using [calcein•PAMAM] sensor. a) full scale of the scores plot, b) an enlargement of the rectangular area in a. [calcein] = 6.36 μM, [PAMAM G5] = 2.13 μM, [analytes] = 5.0 mM. Performed in 50 mM aqueous HEPES buffer at pH 7.4, T = 25 °C.

The loadings plot corresponding to the scores plot from Figure 4-4 is shown in Figure 4-5. The absorbance at 350 nm was the main contributor to both factor 1 and factor 2. This was the reason that ceftriaxone and cefotaxime were very clearly separated from the rest of the clusters along factor 1: they had very high intrinsic absorption in the UV range, especially aroung 350 nm; and cephalothin was far away from the rest of the analytes along factor 2 because it also had instrinsic absorption in the UV range, only not as high as the other two. Although fluorescence measurements did contribute to both factors, at least to to some extent, they were still insignificant compared with absorbance at 350 nm. An ideal loadings plot would have different instrumental measurements contributing along each factor; the current situation did not

capture much of the differential information in the system, instead primarily responding to a single-variate stimulus, i.e. the absorbance in the UV region. However, the differentiation was not improved even after removing the absorbance measurements in the UV range, so we needed to further improve this differentiation method.

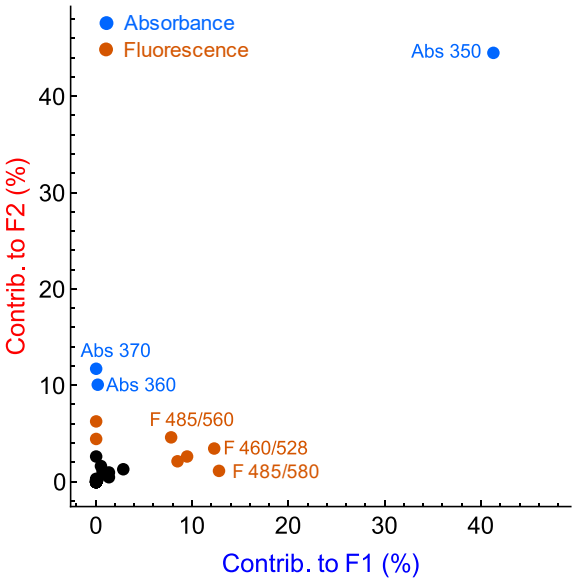

Figure 4-5. LDA loadings plot for qualitative discrimination of 9 analytes (two penicillins, five cephalosporins and 2 reference carboxylates) using [calcein•PAMAM] sensor (same dataset as the scores plot shown in Figure 4-4). Abs: absorbance, F: fluorescence emission $\lambda_{ex}/\lambda_{em}$. [calcein] = 6.36 μM, [PAMAM G5] = 2.13 μM, [analytes] = 5.0 mM. Performed in 50 mM aqueous HEPES buffer at pH 7.4, T = 25 °C.

Overall, the discrimination was successful for most of the analytes, but not enough for the full analyte set. For further improvement, we decide to hydrolyze the β-lactam ring to increase the number of carboxylate groups, and therefore increase the affinity for PAMAM dendrimers. This was promising considering the successful attempt we had made with cephalothin (see above).

4.4 Increasing affinity by analyte hydrolysis

To be able to determine the best working pH for β-lactam ring hydrolysis, we performed displacement titration with analytes dissolved at pH 10 and brought back to pH 7.4 (marked as "pH 10-7.4"), as well as analytes dissolved at pH 12 and brought back to pH 7.4 (marked as "pH 12-7.4"). Three analytes were studied: penicillin G, cefazolin, and ceftriaxone; a monoanion penicillin, a monoanion cephalosporin, and a dianion ceftriaxone, respectively.

Binding titrations conducted with the hydrolyzed samples (in Figure 4-6) produced results similar to those previously obtained with non-hydrolyzed samples (Figure 4-2), proving that, even after hydrolysis, analytes could still bind to PAMAM dendrimers as indicated by the displacement of the calcein dye from its complex with the dendrimer. By plotting the fluorescence emission and anisotropy profile obtained from samples hydrolyzed at pH 10 or 12, or not hydrolyzed (Figure 4-7), we could capture the differences among different working conditions. For penicillin G (monoanion), the sample hydrolyzed at pH 12 had a clearly higher affinity for PAMAM dendrimers, while the sample hydrolyzed at pH 10, and the non-hydrolyzed one were very similar. For cefazolin (monoanion), we noticed that the observed affinity increased with the working pH. For ceftriaxone (dianion), all three profiles were very similar. This proved that hydrolysis could increase the affinity of some analytes for PAMAM dendrimers. The variation in behavior among analytes could add more difference to the system to improve the discrimination.

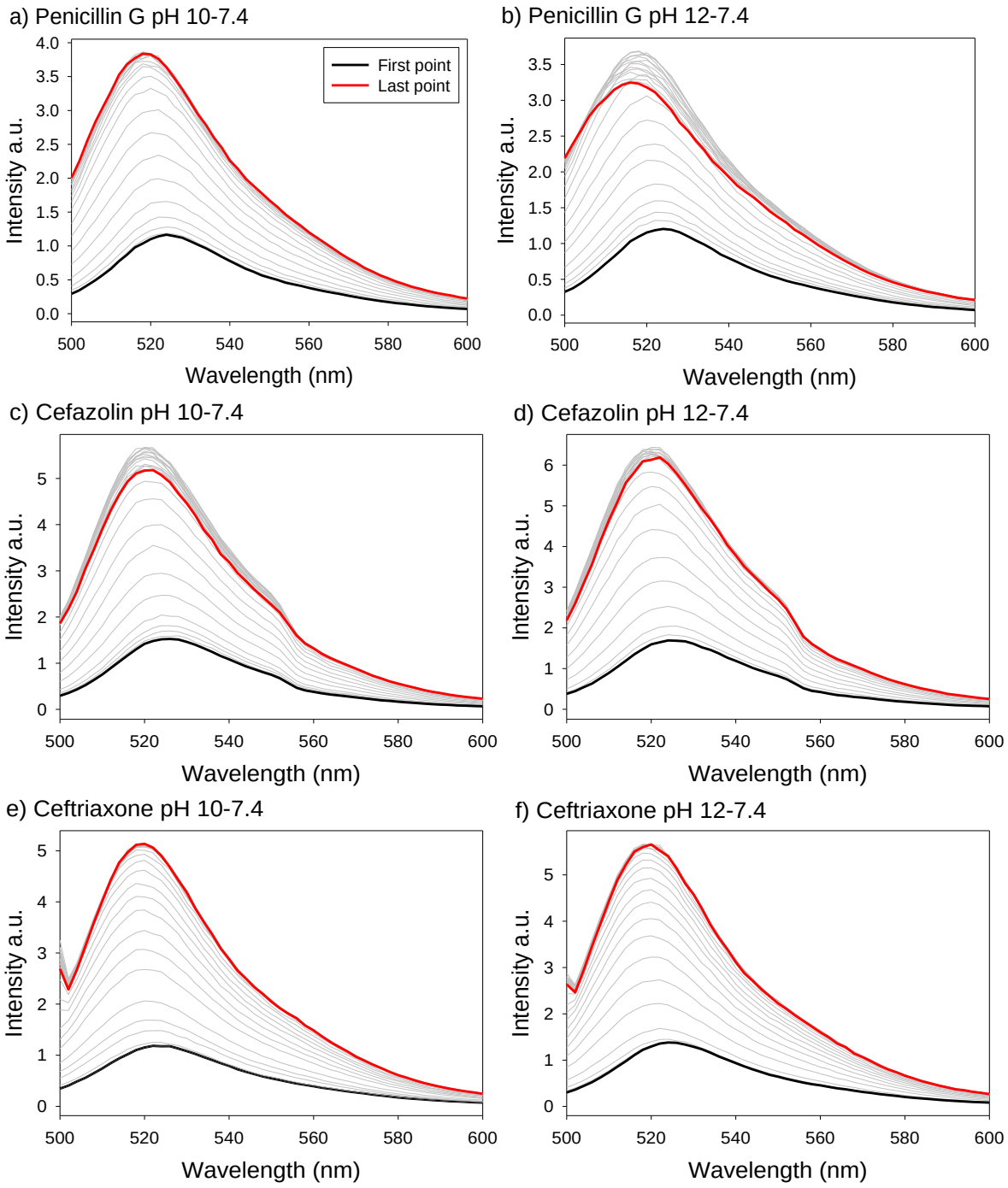

Figure 4-6 Fluorescence emission spectra of titrating penicillin G (a, b), cefazolin (c, d) and ceftriaxone (e, f) into [calcein•PAMAM] complex in solution. Left: solutions prepared at pH 10 and brought back to 7.4; right: solutions prepared at pH 12 and brought back to 7.4. Spectrum in black: first titration point; spectrum in red: the last titration point; spectra in gray: titration points in between. [calcein] = 6.36 μM, [PAMAM G5] = 2.13 μM, excitation: 494 nm. Performed in 50 mM aqueous HEPES buffer at pH 7.4, T = 25 °C.

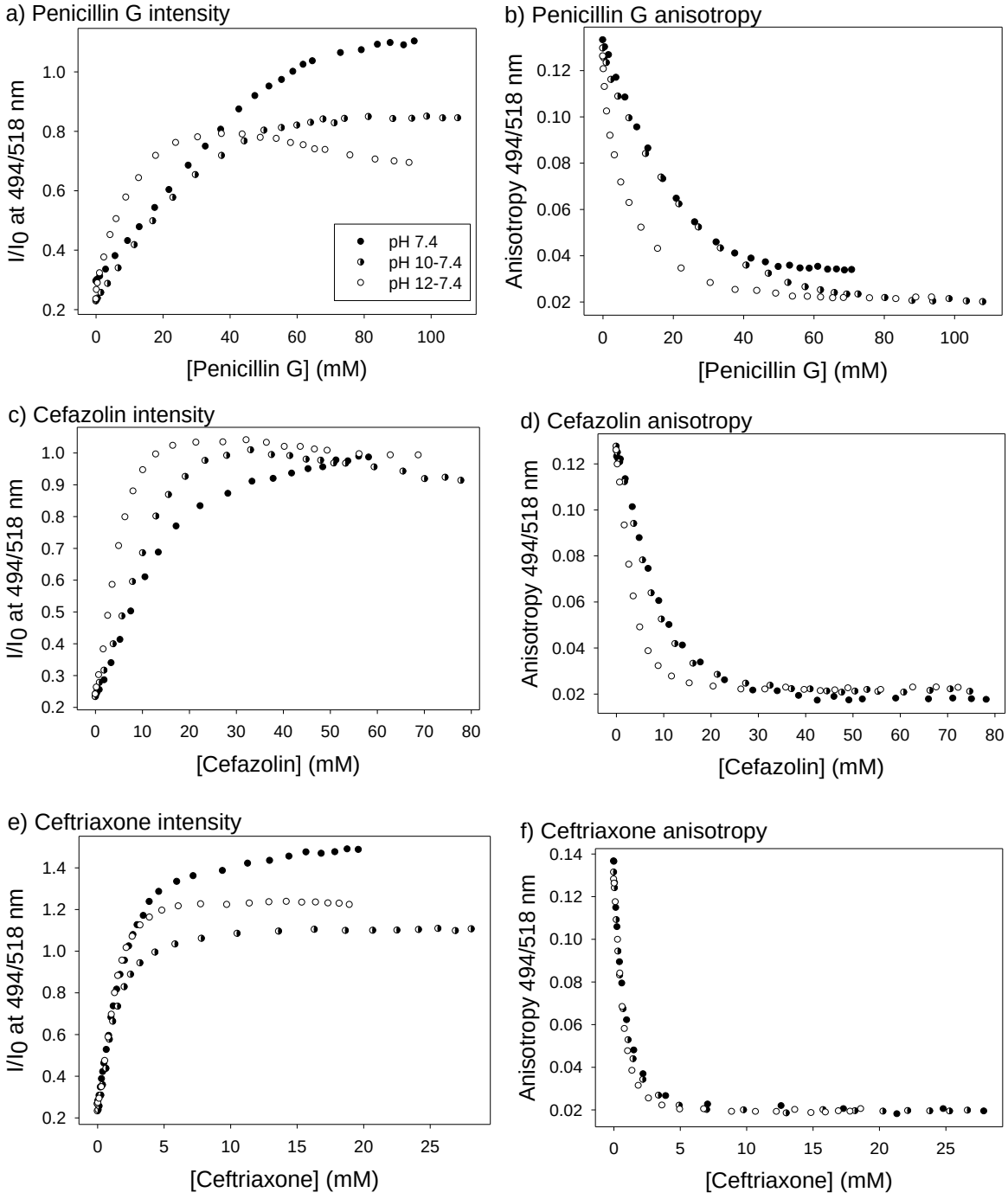

Figure 4-7 Fluorescence emission profiles of titrating penicillin G (a, b), cefazolin (c, d) and ceftriaxone (e, f) into [calcein•PAMAM] complex in solution that prepared at different pH (7.4, 10, and 12) and brought back to pH 7.4 for different level of β-lactam ring hydrolysis. Left: fluorescence emission; right: fluorescence anisotropy. [calcein] = 6.36 μM, [PAMAM G5] = 2.13 μM, excitation: 494 nm, emission: 518 nm. Performed in 50 mM aqueous HEPES buffer at pH 7.4, T = 25 °C.

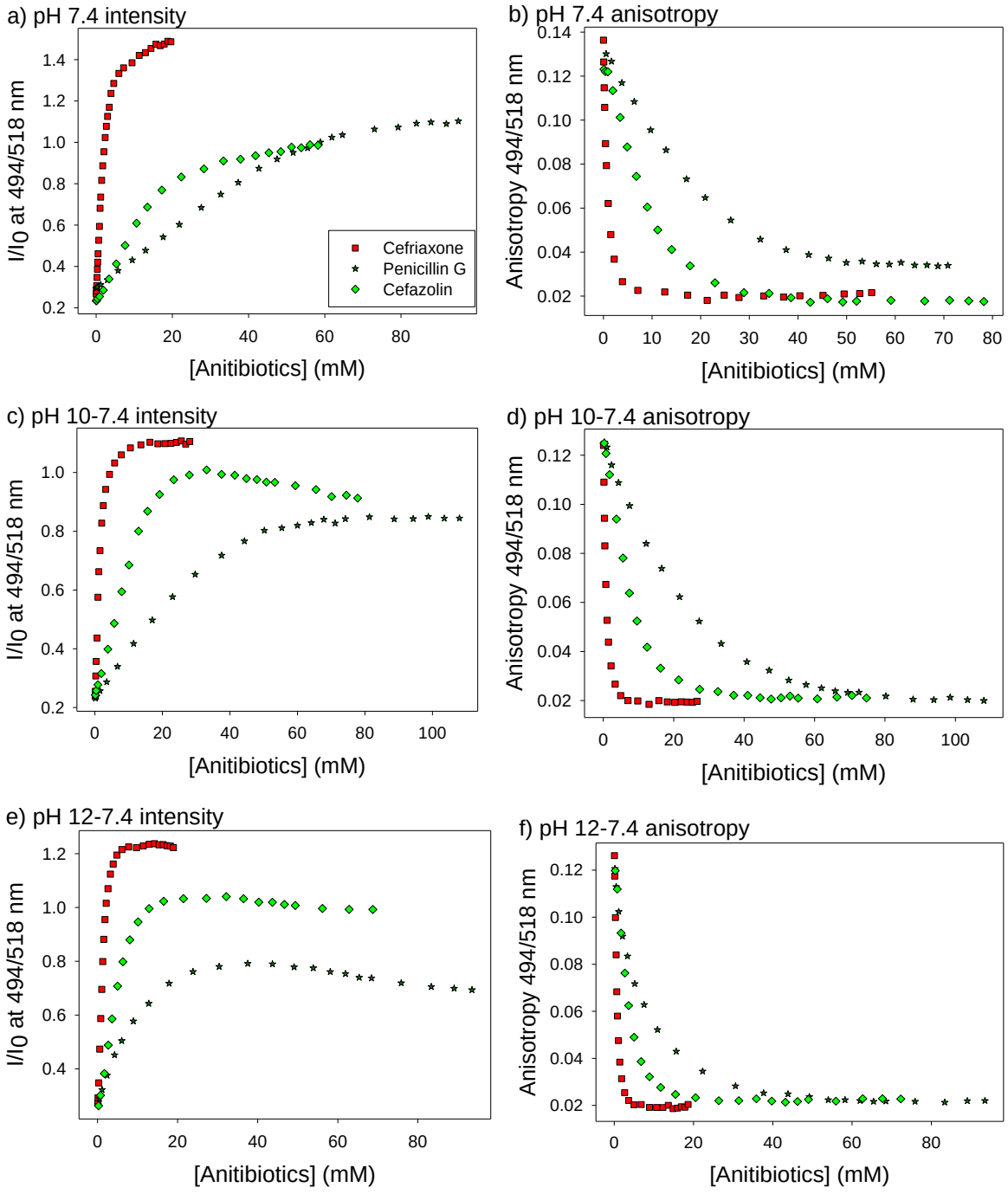

Figure 4-8 Fluorescence emission profiles of titrating penicillin G, ceftriaxone and cefazolin into [calcein•PAMAM] complex in solution. a, b) solutions prepared at pH 7.4; c, d) solutions prepared at pH 10 and brought back to 7.4; e, f) solutions prepared at pH 12 and brought back to 7.4. Left: fluorescence emission; right: fluorescence anisotropy. [calcein] = 6.36 μM, [PAMAM G5] = 2.13 μM, excitation: 494 nm, emission: 518 nm. Performed in 50 mM aqueous HEPES buffer at pH 7.4, T = 25 °C.

Plotting these three analytes prepared at different working pH showing (Figure 4-8), at 5.0 mM of analyte, solutions prepared at pH 10 and brought back to pH 7.4 showed the best pair-wise separation. Therefore, we decided to use “pH 10-7.4” as the working condition to perform further discrimination experiments.

4.5 Antibiotics discrimination on partially hydrolyzed samples

A new discrimination experiment was performed under the same condition as described for Figure 4-4, except analyte solutions were prepared at pH 10 and brought back to pH 7.4 for discrimination analysis. The same 54 instrumental measurements were taken, followed by data reduction, outlier rejection, as well as dataset transformation and retaining the first two factors.

The resulting LDA scores plot is shown in Figure 4-10, with factor 1 vs factor 2 being 66.8%: 20.1% that was slightly better than Figure 4-10. But we were very excited to see that this time, all the analyte clusters were separated, with larger intercluster distances (clusters were further from each other) compared with previous and small intracluster distances (tight clusters). Analytes that had been too close to each other for effective separation, and also very close to the bound dye reference cluster, were now more spread-out, and further away to the reference cluster. This proved that the hydrolysis process did increase the analytes’ affinity for PAMAM dendrimers, leading to better differentiation.

Looking at the loadings plot shown in Figure 4-10 right, this time fluorescence measurements started to contribute more to both factors. High contribution of absorbance measured at 350 nm was still the reason of the great separation between ceftriaxon and cefotaxime and the rest of the sample clusters along factor 1. However, it was still an improvement compared with Figure 4-5: instrumental measurements reporting on properties of the sensing complex started to contribute more compared than the absorption of the analyte in

the UV range, proving the ability of the sensing complex in differentiation of antibiotics analytes; also, there were more instrumental measurements contributing to each factor, indicating a more properly multivariate approach and capture of more information. Overall the differentiation of partially hydrolyzed analytes was much more successful than our previous attempt.

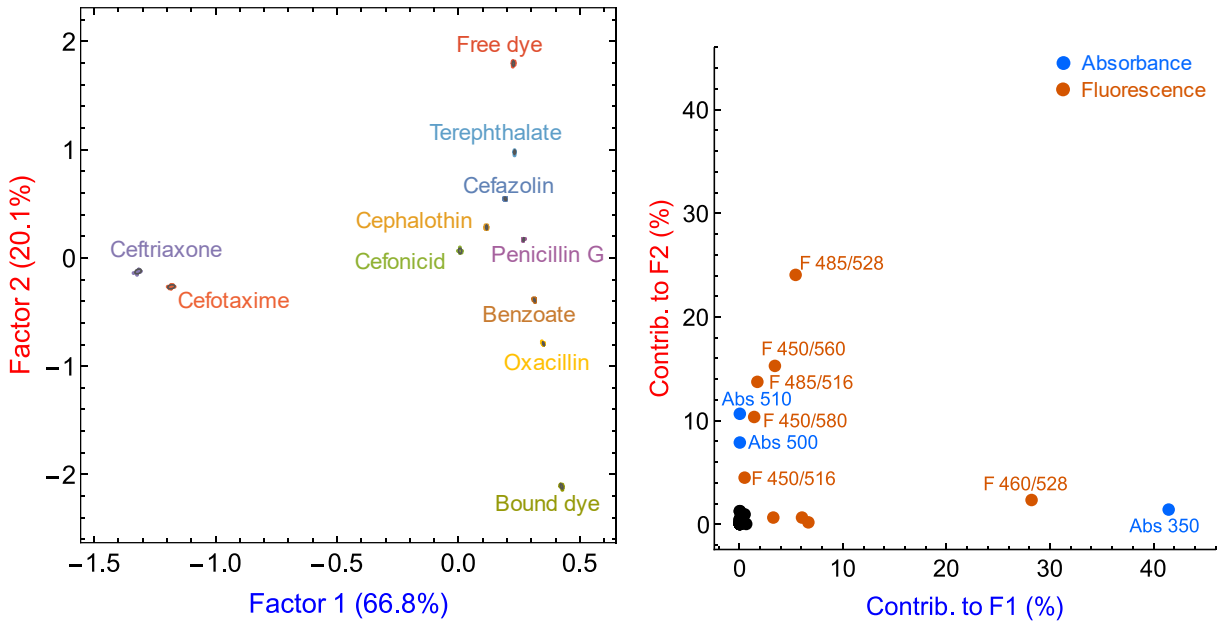

Figure 4-9 LDA results for qualitative discrimination of 9 analytes (two penicillins, five cephalosporins and 2 reference carboxylates) using [calcein•PAMAM] sensor. Left: scores plot; right: loadings plot (Abs: absorbance, F: fluorescence emission $\lambda_{ex}/\lambda_{em}$). Analyte solutions were prepared at pH 10 and then brought back to pH 7.4 for β-lactam ring hydrolysis. [calcein] = 6.36 μM, [PAMAM G5] = 2.13 μM, [analytes] = 5.0 mM. Performed in 50 mM aqueous HEPES buffer, T = 25 °C.

In the LDA scores plot, ceftriaxone and cefotaxime clusters are positioned on the left side of the scores plot, compressing the rest of the clusters toward the right area of the plot. Since these two cephalosporins had very high intrinsic absorption in the UV range, the huge differences in the UV absorbance reading between these two analytes and the rest overwhelmed other measurements. In order to amplify the differences of the analytes' interaction with

PAMAM dendrimers, we removed the UV absorbance measurements from the dataset, as well as the reference clusters. After re-processing the dataset, LDA scores plot is shown in Figure 4-10. The balance between the first two factors was better than before. Even though the intracluster distances were enlarged, the clusters were still tight, and the intercluster distances were larger than previous. Commonly, more blank space on the LDA scores plot indicates less effective discrimination. By removing some measurements and the reference clusters, the analyte clusters were more spread-out and the space of the scores plot was more occupied. This was a much better result compared with previous LDA scores plot. According to the loadings plot in Figure 4-10 right, all absorbance measurements and many fluorescence measurements did not contribute to the differentiation. Therefore, we could further reduce the instrumental measurements.

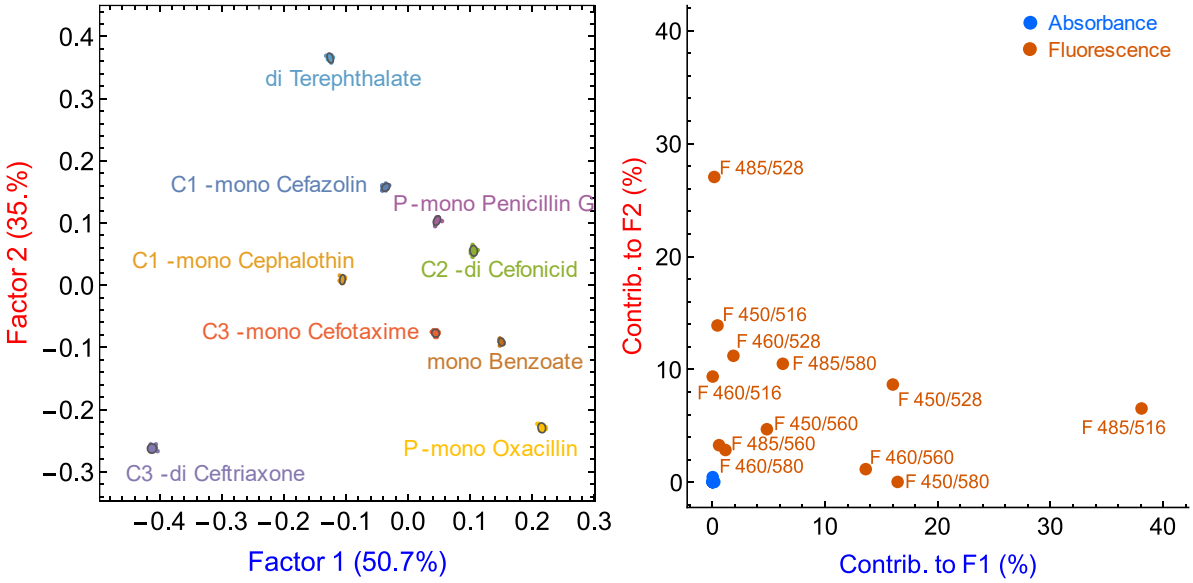

Figure 4-10 LDA results for qualitative discrimination of 9 analytes (two penicillins, five cephalosporins and 2 reference carboxylates) using [calcein•PAMAM] sensor. Left: scores plot; right: loadings plot (Abs: absorbance, F: fluorescence emission $\lambda_{ex}/\lambda_{em}$). Analyte solutions were prepared at pH 10 and then brought back to pH 7.4 for β-lactam ring hydrolysis. The same set of raw measurements was used as in Figure 4-9, but measurements of absorbance in the UV range, and dye clusters, were removed to improve analyte separation. [calcein] = 6.36 μM, [PAMAM G5] = 2.13 μM, [analytes] = 5.0 mM. Performed in 50 mM aqueous HEPES buffer, T = 25 °C.

On the same dataset, we also attempted to retain as few instrumental measurements as possible, in order to save data acquisition time. Based on the previous LDA loadings plot (Figure 4-10right), we tried different combinations of fluorescence measurements: in each successive we removed the least contributing measurement according to the loadings plot, until we impaired the differentiation. Ultimately, the instrumental measurements were reduced to 7, all of which were fluorescence emission with different excitation and emission wavelength combinations (shown in Figure 4-11Right). The resulting LDA scores plot is shown in Figure 4-11: this showed balance between the factor contributions, and good discrimination among analytes. By retaining 7 fluorescence emission measurements, the acquisition time for the construction of these training sets could be reduced from the original 2 hours to around 1 hour.

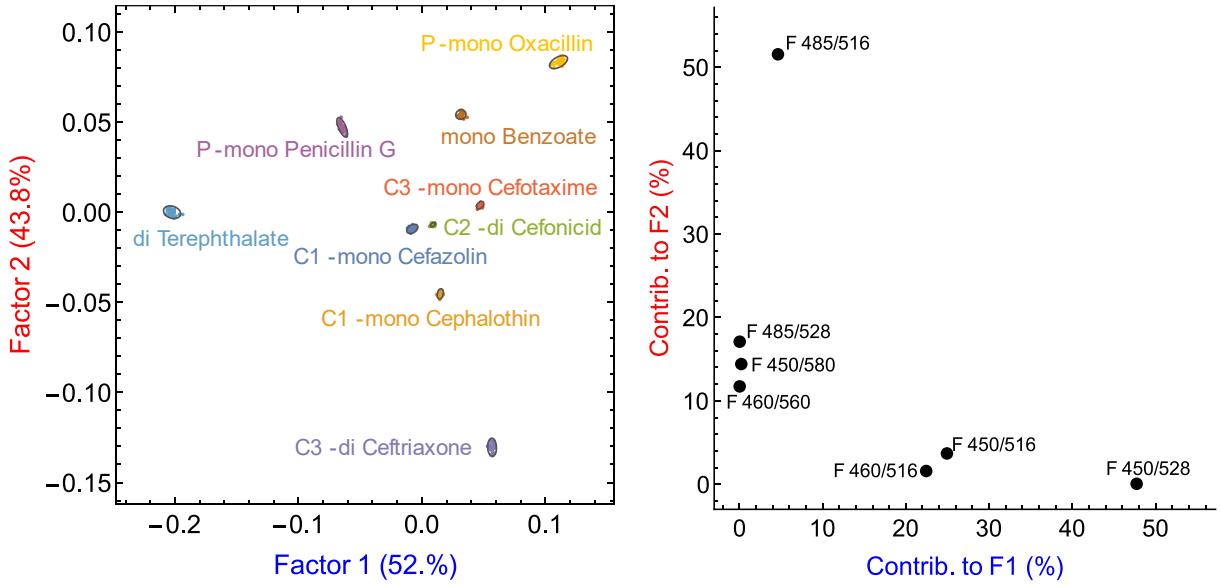

Figure 4-11 LDA results for qualitative discrimination of 9 analytes (two penicillins, five cephalosporins and 2 reference carboxylates) using [calcein•PAMAM]sensor. Left: scores plot; right: loadings plot (F: fluorescence emission $\lambda_{ex}/\lambda_{em}$). Analyte solutions were prepared at pH 10 and then brought back to pH 7.4 for β-lactam ring hydrolysis. The same set of raw measurements was used as in Figure 4-9, but only the most important 7 measurements were retained, and dye clusters were removed clarity. [calcein] = 6.36 μM, [PAMAM G5] = 2.13 μM, [analytes] = 5.0 mM. Performed in 50 mM aqueous HEPES buffer, T = 25 °C.

Although the process of construction of the training sets described here would not be repeated each time an unknown sample is measured, nevertheless such calibrations would still have to be repeated periodically in practical use (e.g. daily, weekly), so it was still important to minimize the repetitive effort required; besides, acquiring low-information-content measurements would increase the noise in the system while contributing little to the useful discriminatory power.

4.6 Limit of discrimination

Finally, an experiment was performed to determine the limit of discrimination by reducing the analyte concentration to 1.0 mM, while the rest of experimental conditions and data processing procedures remained the same as the results prepared above in Figure 4-10. The LDA scores plot shown in Figure 4-12 had resulted from a dataset in which UV absorbance were removed. Dye clusters were also removed for clarity. Although the analyte clusters were all separated, the intercluster distance became very small, and the information of factor 1 and 2 was starting to get unbalanced. There was a great chance that lowering the analyte concentration further would impair the discriminatory power. Therefore, the limit of discrimination of this sensing system for antibiotics can be estimated as not lower than 1.0 mM.

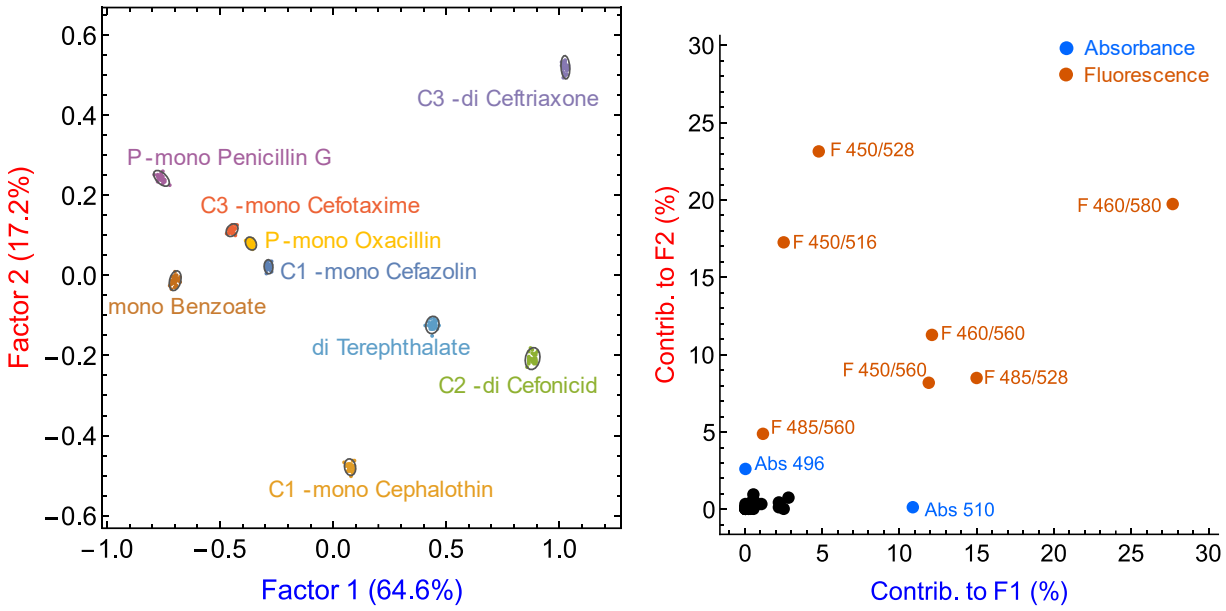

Figure 4-12 LDA results to estimate the limit of discrimination of 9 analytes (two penicillins, five cephalosporins and 2 reference carboxylates) using [calcein•PAMAM] sensor. Left: scores plot; right: loadings plot (Abs: absorbance, F: fluorescence emission $\lambda_{ex}/\lambda_{em}$). Analyte solutions were prepared at pH 10 and then brought back to pH 7.4 for β-lactam ring hydrolysis. Measurements of absorbance at UV range and dye clusters were removed for better separation of analyte clusters. [calcein] = 6.36 μM, [PAMAM G5] = 2.13 μM, [analytes] = 1.0 mM. Performed in 50 mM aqueous HEPES buffer, T = 25 °C.

4.7 Conclusions

Taking advantage of the discriminatory power of [calcein•PAMAM] supramolecular sensor complex towards carboxylate-containing compounds in neutral aqueous solution, we expanded its analytical scope to penicillins and cephalosporins, which are β-lactam antibiotics that contains at least one carboxylate group. In this case, we also developed a method for sample pre-treatment in aqueous base that partially hydrolyzes the lactam ring, revealing an additional carboxylate and increasing the observed binding affinities. Both calcein dye and PAMAM dendrimer host are commercially available. Using this method, two penicillin analytes, five cephalosporin analytes, and two reference analytes of interest were successfully differentiated through absorbance, fluorescence emission and anisotropy measurements after β-lactam ring

hydrolysis. LDA was used as pattern recognition algorithm for data processing. The limit of discrimination of the system for these antibiotics was estimated to be not lower than 1.0 mM.

4.8 Experimental details

4.8.1 Materials

Fifth-generation, amine-terminated poly(amidoamine) (PAMAM) dendrimer with a 1,2-diaminoethane core was manufactured by Dendritech, Inc., and purchased as a solution in methanol with exact concentration of 1.419 mM. The final solution used for all experiment was obtained by dilution with buffer and contained negligible amount of methanol (< 0.8%). Dye solution was prepared from calcein disodium salt purchased from Sigma Aldrich. Analyte solutions were prepared from terephthalic acid, benzoic acid and ceftriaxone sodium salt hemiheptahydrate purchased from Acros; cefazolin sodium and cefonicid sodium purchased from CHEM-IMPEX; penicillin G sodium salt purchased from Alfa Aesar; cephalothin, oxacillin sodium salt monohydrate and cefotaxime sodium salt purchased from TCI. 50 mM 4-(2-hydroxyethyl) piperazine-1-ethanesulfonic acid (HEPES) buffer was prepared from HEPES purchased from IBI Scientific. All prepared solutions were adjusted to pH 7.4 using solutions of NaOH, purchased from Fisher Scientific, and HCl, purchased from BDH Aristar. Nunc 384-well polystyrene black-wall plates were purchased from Thermo Scientific. All materials were used as received.

4.8.2 Instrumentation

Absorbance titrations were carried out on a HP 8452A diode array spectrophotometer, measuring from 230 nm to 800 nm with a 2 nm wavelength resolution. Fluorescence emission and fluorescence anisotropy titration were carried out on an ISS PC1 spectrofluorometer, with a broad-spectrum high-pressure xenon lamp (CERMAX, 300W) as an excitation light source;

manual calibrated slits; excitation correction by a rhodamine B quantum counter with a dedicated detector; and emission light detector was a Hamamatsu red-sensitive PMT operating in photon-counting mode. High aperture Glan Thompson calcite polarizers were used for fluorescence anisotropy measurement. For all titration experiments, an external circulating water bath was used to control the cuvette temperature as 25 °C.

Microwell plate-based discrimination studies were carried out on a Biotek Synergy II multimode plate reader, with a tungsten lamp light source. A monochromator was used for absorbance measurements; different bandpass filters were used for fluorescence emission; and plastic sheet polarizers were used for fluorescence anisotropy measurements. A "top-detected" mode was used for all fluorescence measurements: a dichroic mirror was automatically positioned between the emission source and sample wells to block excitation light from reaching to the detector.

4.8.3 Experiment conditions

All experiments were performed in 50 mM HEPES buffer at pH 7.4. pH was adjusted by NaOH or HCl solutions. Concentrations for anion binding titrations: [calcein] = 6.36 μM with [G5] = 2.13 μM. For hydrolysis of antibiotics, around 0.1 M of analytes were dissolved at pH 10 or pH 12 for two minutes with shaking, and then adjusted to pH 7.4. Concentration for qualitative discrimination experiments were: [calcein] = 6.36 μM with [G5] = 2.13 μM, and [analytes] = 5.0 mM. Concentration for limit of discrimination experiments were: [calcein] = 6.36 μM with [G5] = 2.13 μM, and [analytes] = 1.0 mM.

4.8.4 Titration experiments

Anion binding experiments were studied by adding a "titrant" solution containing one analyte and [calcein•PAMAM] complex (concentration listed above), into2 mL of a "cuvette"

solution containing the same concentration of [calcein•PAMAM] complex. Therefore, concentration of the calcein dye and PAMAM dendrimer were maintained constant during titration. All titrations were performed in a 1 cm quartz cuvette.

4.8.5 384-microwell plate experiments

For qualitative discrimination experiments, each analyte sample was prepared in 32 replicates. Solutions were prepared in 50 mM HEPES buffer, and 100 μL of each sample was deposited into the wells by hand using Eppendorf Research multichannel pipettors. Absorbance, fluorescence emission and anisotropy were measured through a plate reader, and data process was carried out by Linear Discriminant Analysis (LDA) algorithms developed in house using Wolfram Mathematica.

CHAPTER 5
DISPOSABLE PAPER STRIPS FOR CARBOXYLATE SENSING USING [CALCEIN•PAMAM G5] SENSOR

5.1 Introduction

Solid-supported sensors have gained increasing attention due to their portability and convenience. Some such sensors were developed from solution-based systems.[172] Among all solid-based sensors, sensor-soaked paper[173-176] and paper-based devices[177-180] are most interesting: paper has several advantages as a promising solid support for sensing material because it is low in cost; its long shelf life and light weight leading to easy storage and transportation; its excellent liquid absorption ability makes it a good candidate for transitions existing solution sensors to solid support, and its relative chemical inertness suggests it being a all-purpose solid support.[181-183] With the success in the sensing of carboxylate anions discussed previously using a [calcein•PAMAM] sensor, we became interested in transitioning these sensors onto different solid materials for *in situ* analysis purposes. The sensing complex could only function for less than a week in aqueous media. By transition on to solid materials, we could elongate the shelf life of the sensor.

5.2 Experimental design

To prove the principle, we selected 9 carboxylates with different characteristics (i.e. number of carboxylate groups, presence of double bonds and hydroxyl groups), whose structures are shown in Scheme 5-1. Conceptually, a solution containing calcein (Scheme 5-2) and PAMAM G5 (Scheme 5-3) in conditions chosen to form the [calcein•PAMAM] sensor was

deposited on various solid supports and let dry. Then, carboxylate analytes could be deposited onto those sensor spots, causing the displacement of calcein dye from its PAMAM complex. This would show a difference in the dye's florescence behavior, which would lead to the differentiation of carboxylate analytes. In this case, absorbance measurements were not taken into consideration because, at the experimental concentration of calcein dye, the short optical path length of the solid supported system would not provide readable absorbance measurements; besides, most of the solid support materials we considered were opaque.

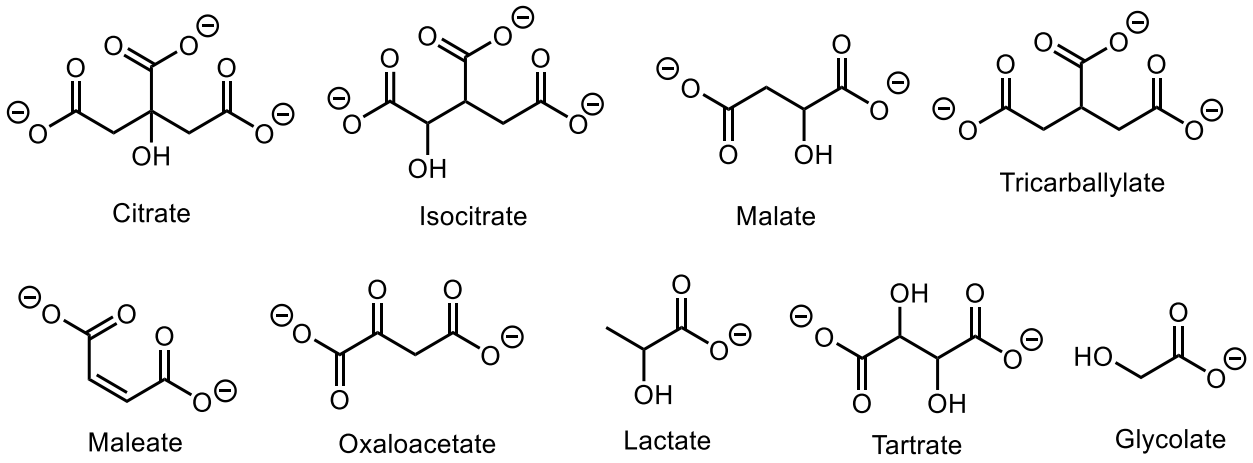

Scheme 5-1 Carboxylate anions considered in this study, shown in their most likely protonated state at pH 7.4.

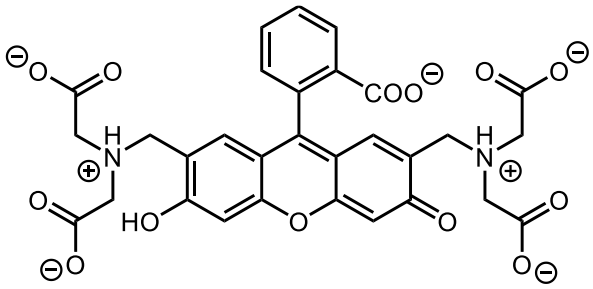

Scheme 5-2 Calcein dye structure at pH 7.4.

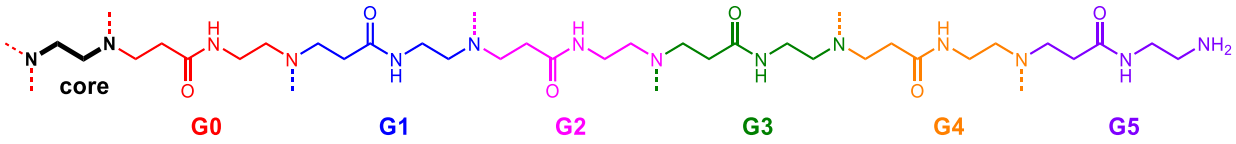

Scheme 5-3 One branch of an amine terminated fifth generation poly(amidoamine) (PAMAM G5) dendrimer with ethylene diamine core. Each generation ends with an amine group, and branches out twice: one branch is shown in the scheme, and the other branch is represented by the dashed line.

In this study, cellulose acetate overhead transparencies, silica gel on aluminum-backed thin layer chromatography (TLC) sheets, printer paper, filter paper, and chromatography paper were considered as promising support candidates for the transition of our carboxylate sensing system to solid support. Each material was tested for their volume loading capacity, and the ability of retaining the differentiation power of [calcein•PAMAM] complex for carboxylate analytes. Here, loading capacity stands for the maximum volume of deposited sample that could remain within the spot range and not interfere with neighboring spots on each solid support. More specifically, support surfaces that were more hydrophobic (e.g. transparencies and printer paper) were found to have a higher loading capacity, because the sample solution was not absorbed and did not spread, compared with those with high liquid absorption capacity (TLC plates, filter paper and chromatography paper). With our extensive experience using multiwell plates, and the ubiquity and simplicity of plate reading instrumentation in analytical and biological labs, we decided to take advantage of the 96-well plate format and plate reader. Finally, in the differentiation experiments linear discriminant analysis (LDA) was used for data processing.

Using printer paper as an example, as shown in Figure 5-1, the layout format of a 96-well plate was printed on regular printer paper using an office laser printer, and cut to the size of a standard multiwell plate, according to the ANSI/SLAS dimensional specifications (ANSI/SLAS

1-2004 (R2012)).[184] The printed black rings were simply an aid to help spot the assays in the correct positions for measurement on a plate reader. Due to the flexible and thin nature of paper materials, printer paper, filter paper, and chromatography paper were all taped to a rigid polystyrene microplate to reduce crinkle and warping during the evaporation of solvent. Figure 5-1 (left) shows the results obtained when sample droplets were deposited immediately, and Figure 5-1 (right) is the same plate after the solvent was allowed to dry for 2 hours. Samples were deposited in every other well to prevent droplets from bleeding into each other, and to avoid cross-talk among the fluorescent droplets. In this example, columns 1-5 (counting from left) contained calcein dye in its free form (yellow); columns 6-10 contained the [calcein•PAMAM] sensor (orange); and columns 11-12 contained HEPES buffer as blank. For printer paper plates, measurements could be taken with both wet and dry samples. However, for filter paper, and chromatography paper which had lower loading capacity, the solutions dried very fast (within the plate reading duration): therefore, reliable measurements could only be obtained after the samples had dried completely.

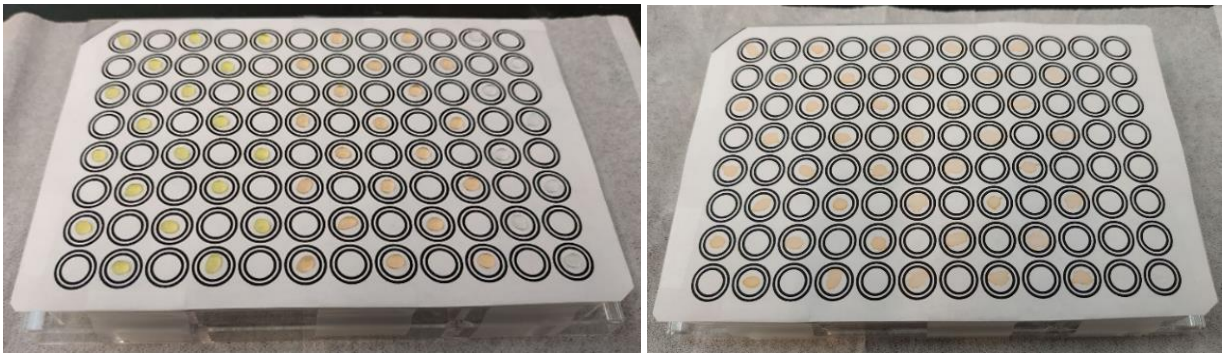

Figure 5-1 A representation of experimental set up of a printer paper plate, on which each sample was deposited on every other position. Left: wet sample droplets right after deposit; right: samples were allowed to dry for 2 hours. Columns 1-5: calcein dye (yellow when wet, and orange when dried); columns 6-10: [calcein•PAMAM] sensor (orange both wet and dry); columns 11-12: HEPES buffer as blank (clear).

5.3 Chromatography paper as a solid support

As discussed in the previous chapters, calcein binds to PAMAM G5 in solution and forms [calcein•PAMAM] complex (shown in Figure 5-2a). With the introduction of carboxylate analytes into the complex solution, carboxylates bind to PAMAM G5 and displace calcein from its complex, releasing it to its free form (shown in Figure 5-2b). This sensing system was effective in the discrimination of carboxylates in solution, as discussed in Chapter 3. To test if the same system could retain its discrimination power when deposited on solid support, we first needed to regenerate the same dye binding and displacement behavior these on solid supports. In-solution differentiation required a sample volume of 100 μL using polystyrene 384-well plates. For solid supports, the sample volume was reduced to 1-10 μL, so we increased the working concentration of the deposited solutions 10-fold to retain high fluorescence emission. That is: solution containing 63.6 μM of calcein, 21.3 μM of PAMAM G5, and 23.0 mM of carboxylate analytes, were used in the deposition steps.

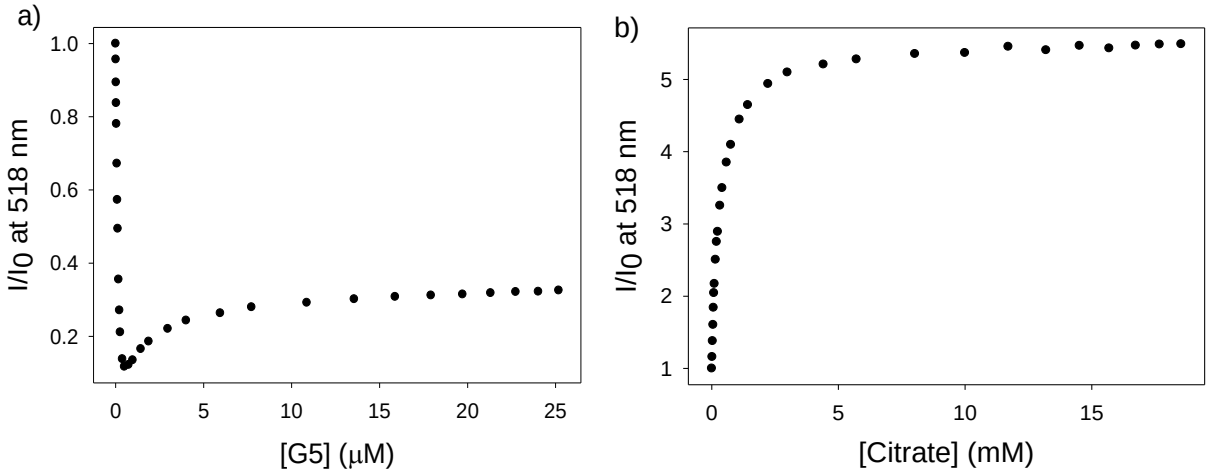

Figure 5-2 a) titration of G5 into calcein to form [calcein•PAMAM] complex in solution (same as Figure 2-9b), [calcein] = 6.36 μM; b) titration of citrate into [calcein•PAMAM] complex in solution (same as Figure 2-16b, profile of citrate), [calcein] = 6.36 μM, [PAMAM G5] = 2.13 μM. Performed in 50 mM aqueous HEPES buffer at pH 7.4, T = 25 °C, excitation: 496 nm.

Chromatography paper was first considered as a possible solid support. On a chromatography paper plate, prepared to mimic the dimension and layout of a standard microwell plate as described above, we first tested the ability of calcein binding to PAMAM G5. 1 μL of a 63.6 μM (63.6 pmol) of calcein solution was first deposited on the chromatography paper plate, then the solvent was allowed to evaporate (10 min). Then solutions containing PAMAM G5 were deposited on the dried calcein spot, with increasing amount in each column. Fluorescence emission measurements ($\lambda_{ex}/\lambda_{em}$: 485/516 nm) showed a decrease in the emission of calcein dye upon the addition of PAMAM G5 to reach a plateau (Figure 5-3a). The overall trend is similar to the complex forming in solution (Figure 5-2a), only without the sharp turn at the beginning of the in-solution titration. This might be because in solution when small amount of PAMAM G5 was introduced, multiple calcein bound to one PAMAM G5 and quenched each other, then with more PAMAM added, calcein dye in solution could freely move and rearrange to bind with free PAMAM dendrimer, therefore reducing the dye-to-dye quenching. However, on solid support the rearrangement of calcein dye to different PAMAM dendrimers could not occur, so fluorescence revival upon addition of further dendrimer was prevented, leading to a simpler titration profile.

[Calcein•PAMAM] complex in solution had a ratio of 3 eq. of calcein to 1 eq. of PAMAM G5. This ratio also applied to binding on a solid support: a plateau was reached upon addition of 21.3 pmol of PAMAM G5 to 63.6 pmol of dye, i.e., a roughly 3:1 dye:PAMAM ratio.

In this case, the same dye-to-dendrimer ratio was used for further studies. On another chromatography paper plate, 1 μL of [calcein•PAMAM] complex solution (63.6 pmol of calcein and 21.3 pmol of PAMAM G5) was deposited and let dry first. Then, increasing amounts of citrate anion were deposited on each of the dried complex spot. Fluorescence intensity of calcein

dye in Figure 5-3b showed a reverse trend of the binding profile, and was very similar to the profile of the same titration in solution (Figure 5-2b). The great success in replicating the solution-based dye binding and displacement experiment proved that the [calcein•PAMAM] complex could function on solid support. Therefore, we could move on to testing each solid support material to see if they could retain the discriminatory power of the sensor complex.

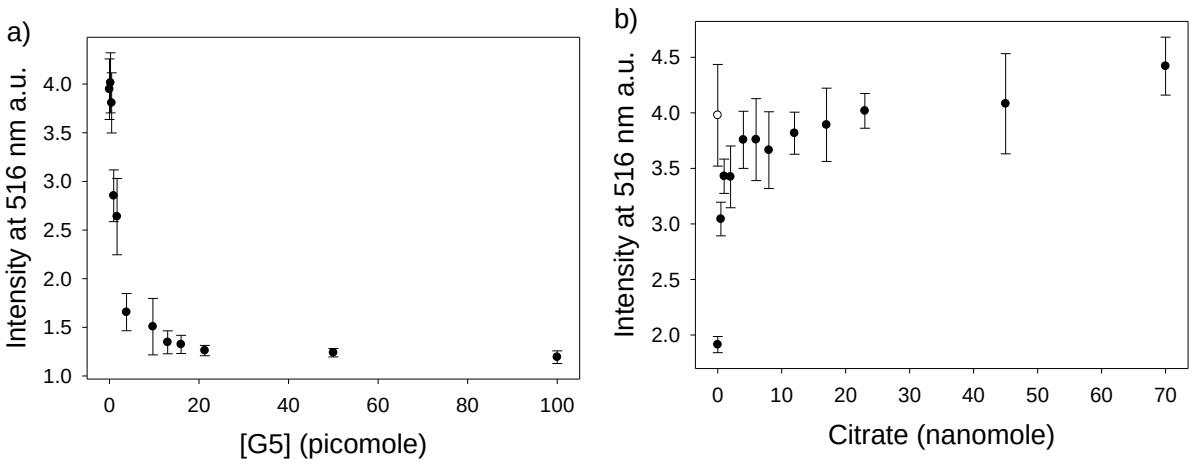

Figure 5-3 Fluorescence emission response on chromatography paper from the calcein dye upon: a) binding with PAMAM G5 to form [calcein•PAMAM] complex (calcein = 63.6 pmol); and b) displacing from its [calcein•PAMAM] complex form by citrate (calcein = 63.6 pmol, PAMAM G5 = 21.3 pmol). The hollow dot indicates the emission of the free dye, and the bar stands for standard deviation of 7 replicates. Excitation: 485 nm, emission: 516 nm.

5.4 Transparencies and TLC plates

For more rigid solid support materials, such as transparencies and TLC plates, a 3D printed plate holder was used (Figure 5-4). This was more convenient than taping the material down to an actual plate. The two rectangular holes in the holder had been designed to use with transparent glass microscope slides, to measure absorbance; however, this was not pursued further.

Figure 5-4 A 3D-printed plate adapter for solid supports. This adapter's extension dimensions are the same as standard microwell plates. This was used for transparencies and TLC plates. Other paper-based supports were taped directly on a plastic 96-well plate with transparent wells and bottom.

5.4.1 Transparencies as solid supports

Transparency films (3M brand, for plain paper copiers, cellulose acetate) were first tested as a promising candidate due to their inertness and transparent nature. The films were used as received, and gloves were always worn when handling them, to avoid contamination. A loading capacity experiment was done when first using each of the materials as supports. Using transparencies as an example, the plate layout for testing the loading capacity is shown in Table 5-1. Each cell in the table stands for a loading spot on the solid plate; 132 μM calcein solution (marked as "C"), 50 mM HEPES buffer (marked as "B"), and 214 μM pyranine solution (marked as "P") were deposited with different volumes (numbers in μL). Sample droplets were deposited in every other spot to prevent cross-talk. Buffer droplets that were the same volume were deposited beside each other to test the maximum volume that would still avoid the droplets bleeding into each other. After several tests with different volume sets, transparencies were

found to have a maximum loading capacity of 40 μL per spot, which was the highest among all materials.

Table 5-1 A plate layout for testing transparencies support capacity. Each cell in the table stands for a spot on the plate. C stands for calcein (132 μM), B stands for HEPES buffer (50 mM), and P stands for pyranine (214 μM). The number after each letter stands for volume in μL. Each plate material was tested several times using the same layout with, but different volumes, to determine the maximum volume capacity.

	1	2	3	4	5	6	7	8	9	10	11	12
A												
B			C5		C10		C20		C30		C40	
C												
D			B5		B10		B20		B30		B40	
E			B5		B10		B20		B30		B40	
F												
G			P5		P10		P20		P30		P40	
H												

After sample deposition, the plate was read immediately, while the sample droplets were still wet (shown in Table 5-2), and read again after the sample droplets were allowed to dry completely (shown in Table 5-3), which took around 2 hours. Looking at row B (calcein) and row G (pyranine) in Table 5-2, there was a definite trend of increasing fluorescence emission as the volume of dye increased. However, when sample droplets were dried, in Table 5-3, the fluorescence emission of the dye was completely overwhelmed by the high reflected light scattering from the transparency plate. Columns that were positioned in a portion of the holder with an opaque bottom (referring to Figure 5-4) had a much stronger reflection than those sitting on one of the holes in the holder.

Table 5-2 Raw fluorescence intensity measurements of a transparency plate immediately after sample droplets were deposited and still wet, sample deposition shown in Table 5-1 at $\lambda_{ex}/\lambda_{em}$: 450/516 nm.

	1	2	3	4	5	6	7	8	9	10	11	12
A	1962	1949	1175	1132	1170	1924	1923	1142	1113	1156	1941	1993
B	1918	1914	9631	1131	18524	1914	60986	1151	53654	1174	73287	1914
C	1874	1912	1178	1145	1174	1973	1949	1156	1134	1174	1909	1919
D	1934	1857	1121	1148	1195	1918	2035	1154	1367	1158	2033	1887
E	1916	1910	1114	1141	1187	1932	2063	1158	1374	1155	2054	1877
F	1907	1942	1152	1132	1149	1955	1939	1142	1118	1144	1866	1838
G	1920	1956	3698	1127	7049	1926	26615	1134	20882	1147	27977	1887
H	1894	1964	1164	1133	1157	1897	1915	1146	1120	1165	1886	1954

Table 5-3 Raw fluorescence intensity measurements of *the same plate* as Table 5-2 after sample droplets were let dry completely (~2 hours). Number in each excel cell stands for the raw reading of fluorescence intensity at $\lambda_{ex}/\lambda_{em}$: 450/516 nm.

	1	2	3	4	5	6	7	8	9	10	11	12
A	77904	76745	47171	45181	46035	74611	74866	44367	43182	44770	75137	77303
B	76152	75323	49621	44883	49737	74654	82607	44851	45553	45500	77901	74751
C	74680	75198	46888	45217	46111	77443	76404	45118	44300	45758	74572	75022
D	75966	73163	46720	45177	46610	75447	74276	45403	44165	45273	74231	74192
E	75316	75027	46219	44957	47030	75974	76274	45600	44508	45215	74926	73910
F	74877	76288	45376	44386	45355	76660	76252	44846	43968	45041	73531	72799
G	75308	76774	46123	44420	46040	75877	76667	44782	43947	45105	75113	74431
H	74701	77257	45926	44718	45643	74770	75361	45306	44205	45935	74462	77508

The highly reflective nature of transparencies unfortunately overwhelmed the useful information that could be obtained from the sensing system and made it inappropriate for fluorescence measurements, so this support was not considered further in this study. On the other hand, the 3D plate holder was very convenient for more rigid supports materials compared with taping paper-based plates onto an actual polystyrene plate. It would be a great tool to ensure correct spot positioning on different solid supports.

5.4.2 TLC plates as solid supports

Figure 5-5 is a reminder of the previously obtained LDA scores plot of the differentiation of ten carboxylate analytes using [calcein•PAMAM] complex as a sensor in solution. A full analysis of this dataset was presented in Chapter 3 (Figure 3-11). Here, however, we repeated the

analysis, using only the fluorescence measurements from that dataset, to best approximate the conditions on the solid support, where absorbance measurements are not available. Data processing was similar to the previous study. At first, instrumental measurements that provided a low signal to noise ratio were eliminated to reduce noise. Then, using Principal Component Analysis, replicates in each analyte sample set that fell out the 95% confidence intervals were considered as outliers and removed from the dataset. Instrumental measurements were transformed to factors using Linear Discriminant Analysis (the dimensions of the data matrix remained the same), arranged in the order of decreasing amount of information that could help differentiation. Finally, only the first two factors were retained to generate a 2D LDA scores plot.

Figure 5-5 provides an example of a good scores plot for analytical differentiation: each sample cluster is small and well separated from the others , and the information distribution of two factors is somewhat balanced (the ideal distribution would be factor 1 50% vs. factor 2 50%). Because we could deposit only 48 samples on each solid support, we restricted our first study to only 4 carboxylates, to be able to retain a high enough number of replicates for each sample. Citrate, maleate, and oxaloacetate were selected from a practical standpoint, because they are structurally very different and were always well differentiated in the previous studies; isocitrate was selected as a particularly challenging example, because its structure is very similar to citrate's, and very hard to differentiate. Thus, we hypothesized that any promising solid support would retain the discriminatory power among citrate, maleate, and oxaloacetate; furthermore, great support material would also retain the discriminatory power to differentiate isocitrate from citrate.

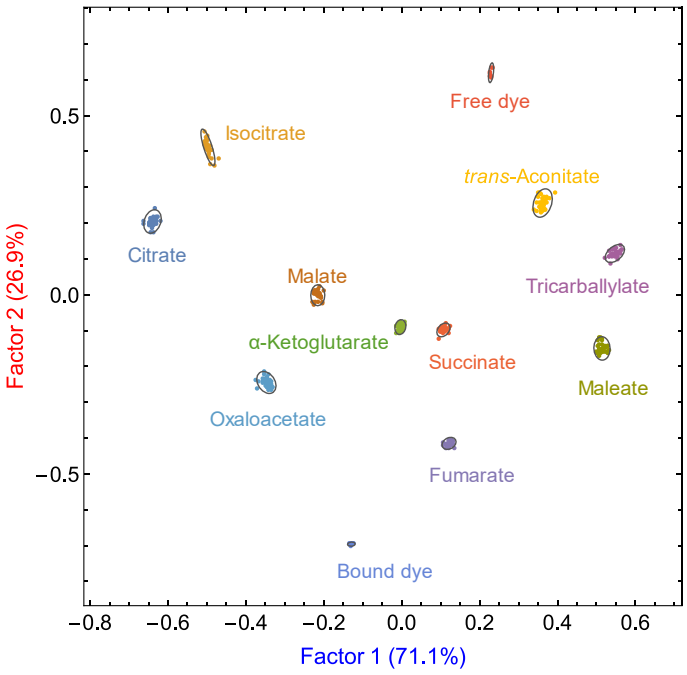

Figure 5-5 LDA scores plot for the discrimination of ten carboxylates in solution, using [calcein•PAMAM] sensor in a polystyrene 384-microwell plate. The same dataset that generated Figure 3-11 was used here, but only fluorescence measurements were considered. [calcein] = 6.36 μM, [PAMAM G5] = 2.13 μM, [carboxylates] = 2.30 mM. Performed in 50 mM aqueous HEPES buffer at pH 7.4, T = 25 °C.

TLC sheets (Merck aluminum-backed silica gel 60 plates, containing a 254 nm fluorescent indicator) were then tested with the 4 chosen carboxylates. Due to its great capacity to absorb liquids, the deposited liquid would expand horizontally on the support, and a small volume of liquid was able to fill up the full spot, so TLC plates only had a loading capacity of 3 μL, much lower than the more hydrophobic samples used before, and the deposited samples took only a very short time to dry. The sensing complex was deposited first and let dry completely for 10 minutes, and then the analytes were deposited on top of the dried sensing complex spots. Sample droplets were deposited by a single channel pipettor: considering that the samples were deposited in positions corresponding to every other well on a standard microwell

plate, a single channel pipettor was more convenient here than a multichannel one, from which we would have had to remove every other channel for use here.

Each carboxylate was deposited on the plate as 12 replicate samples, and 12 fluorescence intensity measurements (different combinations of excitation and emission wavelengths as shown in Table 5-4) were taken. After selecting the most useful emission wavelengths, and rejecting outlying replicates, LDA was used to interpret the 12-dimensional data, and the resulting scores plot is shown in Figure 5-6. Unfortunately, the clusters were large and overlapped with each other, indicating that SiO_2 TLC plate failed to retain the discriminatory power that the same system possessed in solution. Therefore, this support was not used further in this study.

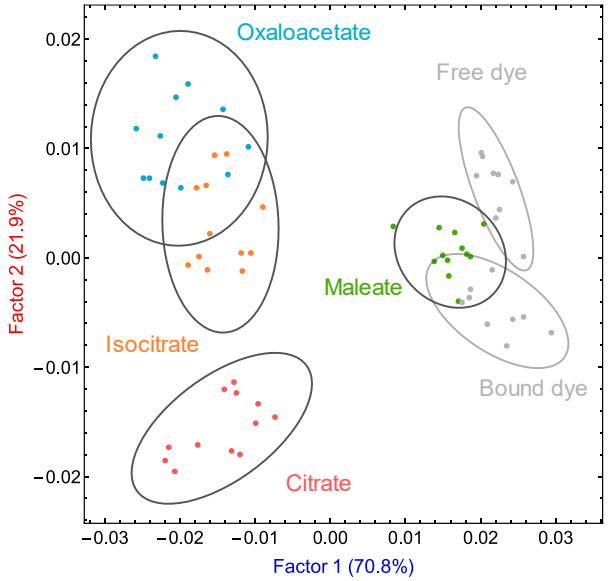

Figure 5-6 LDA scores plot for the differentiation of citrate, isocitrate, oxaloacetate, and maleate using [calcein•PAMAM] on SiO_2 TLC plate. Calcein = 190.8 pmol, PAMAM G5 = 63.9 pmol, carboxylates = 69 nmol.

Table 5-4 Loadings for instrumental measurements used for the qualitative discrimination of carboxylates using [calcein•PAMAM] sensor on all solid support materials. F*n*% (columns) is the percent of the information explained by Factor *n* that is provided by each raw measurement ((rows). The numbers correspond to to Figure 5-12.

Variable type	Wavelength (nm)	F1%	F2%	F3%
Fluorescence emission	450/516	0	0	0
Fluorescence emission	450/528	3	10	1
Fluorescence emission	450/560	14	17	1
Fluorescence emission	450/580	9	0	5
Fluorescence emission	460/516	2	17	9
Fluorescence emission	460/528	21	0	2
Fluorescence emission	460/560	15	17	17
Fluorescence emission	460/580	0	1	0
Fluorescence emission	485/516	1	17	5
Fluorescence emission	485/528	20	21	2
Fluorescence emission	485/560	15	1	46
Fluorescence emission	485/580	0	0	12

5.5 Printer paper as solid support

Pinter paper (USA 11 xerographic copy paper, “92 bright”, 75 g/m^2) was then tested. It was the most widely available, cheapest supports materials among the five materials tested. Common treatment of general-purpose office printer paper includes hydrophobic surface treatment that prevent ink bleed, and the addition of optical brighteners.[185] Brighteners are fluorophores that absorb in the near UV region, and fluoresce around 450 nm; these would not interfere with our measurements. Thanks to the hydrophobic surface treatment, printer paper had the largest loading capacity (10 μL) among the three paper support materials. In this case 9 replicates were deposited for each of the 4 carboxylate analyte, and 12 fluorescence emission measurements were taken. The reduction in the number of replicates stems from the behavior of the droplets during drying. In fact, on TLC plates droplets did not expand during drying process, and sample deposition was every other cell, so the dye reference samples and blank samples could be deposited on the blank cells between sample cells (normally the very last row of the

plate). Therefore, we were able to have 12 replicates for each analyte. However, for printer paper plate here, the sample droplets often expanded irregularly during drying, so every droplet had to be well separated from the others, taking up more space on the support; so each analyte had to be limited to only 9 replicates. The larger loading capacity of printer paper compared to the SiO_2 TLC plate, and its more hydrophobic surface, allowed us to take measurements both while the samples were still wet, as well as after the samples had dried completely.

5.5.1 Single-deposition procedures

We first started by adding aliquots of the 4 chosen carboxylates (citrate, isocitrate, maleate, and oxaloacetate) into solutions that already contained [calcein•PAMAM] sensor. Then, these solutions, already containing the analyte and sensor, were deposited on the support. In this case, the carboxylates had already bound with PAMAM dendrimers and displaced the calcein dye from its complex, to different extent, therefore the solutions were optically different among analytes. A more practical design of this experiment would be depositing the [calcein•PAMAM] sensing complex on printer paper first and let it dry, followed by separate deposition of the analyte solutions. However, this experiment could fail in two anticipated ways: first, the analytes deposited after the sensing complex had dried may no longer be able to displace the calcein dye from its complex and therefore could not induce any spectroscopic changes; secondly,the analytes deposited later could actually displace the calcein dye, but the difference among analytes may not be captured after solvent removal. It would be very hard to pinpoint the failure mode.

By making every analyte and the sensor together in one solution, the deposited solution would already be different, so we could at least rule out the first failure mode mentioned above, i.e. the possibility that, on the solid support, the carboxylate analyte would no longer be able to

bind to PAMAM dendrimer and displace the calcein dye from its complex with the dendrimer. Sample droplets were deposited on the printer paper, then measurements were taken both immediately after sample deposition, and after 2 hours, after the droplets had completely dried. The printer paper support was taped on an plastic 96-well plate to prevent warping during solvent evaporation.

LDA scores plots obtained after the usual data pro are shown in Figure 5-7. The "wet plate" dataset (Figure 5-7a) showed very poor differentiation. That might stem from limitations in sample deposition by hand. In which each droplet was likely to be at a slightly different position with respect to the printed ring-area, and a different shape, which may have influenced the light scattering and emission direction. The "dry plate" (Figure 5-7b) showed much better differentiation, although there was significant overlap among some clusters.

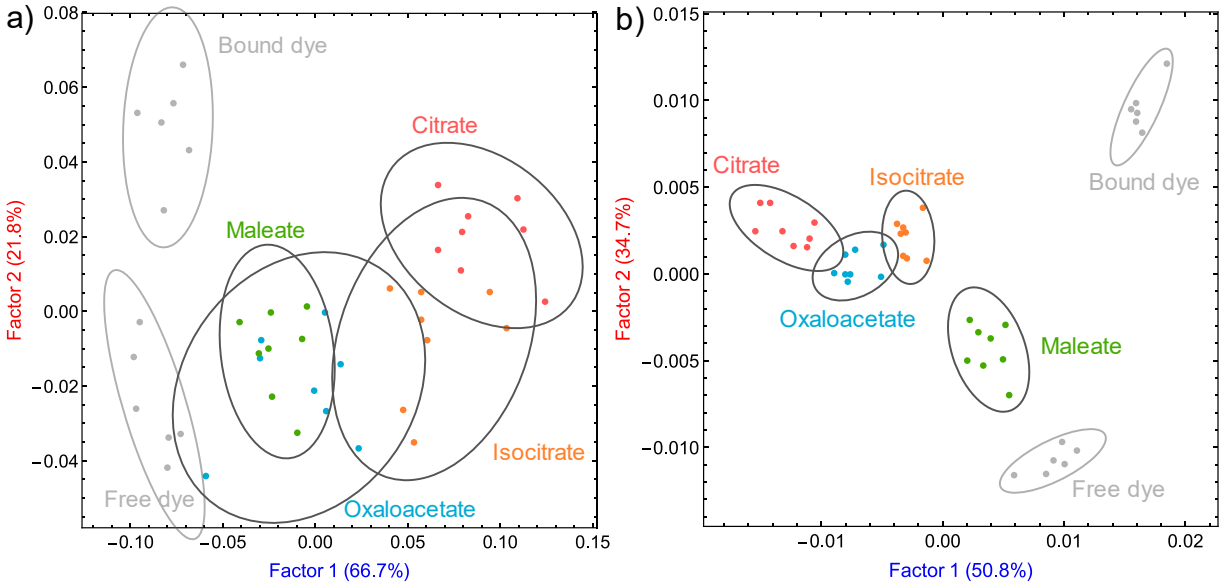

Figure 5-7 LDA scores plot for the differentiation of citrate, isocitrate, oxaloacetate, and maleate using [calcein•PAMAM] on printer paper plate. a) plate was measured immediately after sample droplets were deposited and still wet; b) *the same plate* that was allowed to dry completely (~2 hours). Calcein = 636 pmol, PAMAM G5 = 213 pmol, carboxylates = 230 nmol.

Surprisingly, when the two datasets ("wet plate" and "dry plate") were combined, we were able to differentiate the four carboxylates successfully: the resulting LDA scores plot is shown in Figure 5-8. Factor 1 contained 60.3% of the original information, and factor 2 contained 27.2%; together, 87.5% of the original information was retained. Clusters of samples (9 replicates each) were much tighter and more separated compared to previous results, indicating good differentiation; even citrate and isocitrate were well discriminated. Overall, this was a good differentiation result: good information distribution on the two factors, and tight, well-separated clusters. This indicated that the [calcein•PAMAM] system, when deposited on printer paper as solid support, retained a discriminatory power similar to what it had in solution. As the first successful result, this was very promising.

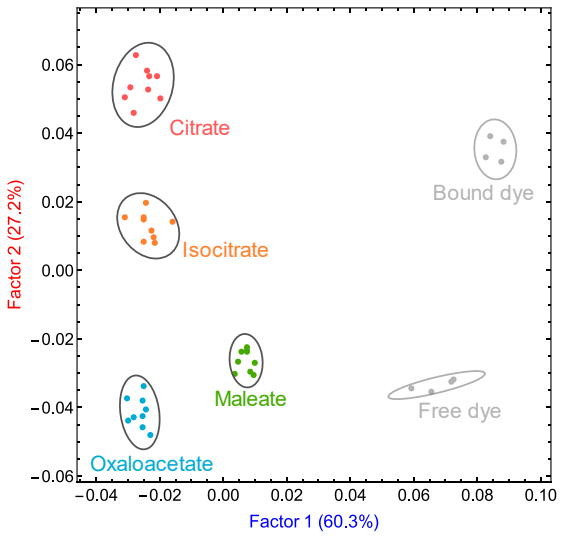

Figure 5-8 LDA scores plot for the differentiation of citrate, isocitrate, oxaloacetate, and maleate using [calcein•PAMAM] on printer paper plate. In this case, datasets from Figure 5-7a and Figure 5-7b were combined and processed together generating one LDA scores plot. Calcein = 636 pmol, PAMAM G5 = 213 pmol, carboxylates = 230 nmol.

This was an encouraging first result with successful differentiation. In practice, however, this result would be of limited practical use because of the way the sample was deposited

together with the sensor solution in one single deposition. Much more preferable would be for samples to be deposited on a pre-treated support that already contains the [calcein•PAMAM] sensor, similar to a test strip for carboxylates. Furthermore, the plate had to be measured twice (wet and dry), and neither of the two dataset worked as well as the combined dataset. What's more, in Figure 5-8, half of the LDA scores plot area was occupied by the free dye and bound dye clusters, indicating ineffective discrimination. Therefore, we moved to a new procedure, first loading the sensor onto the solid support; the analytes were then loaded on the dry complex spots, to see whether carboxylates can still be detected.

5.5.2 Separate deposition procedure

In this next experiment using printer paper as a solid support, the sensor was deposited first and left to dry completely, then the carboxylate analyte solutions were deposited on these dried sensor spots. Measurements were still taken for both wet and dry analyte spots. An LDA scores plot was generated by combining both wet and dry measurements (Figure 5-9). Differentiation of the four carboxylates was successful. This was exciting to see because it proved that the dry sensor could still respond to carboxylate analytes. However, like the previous experiment, discrimination was still shown to be ineffective. For example, in Figure 5-9, one third of Factor 1 (26% of original information) and half of Factor 2 (8% of original information) was used to differentiate reference clusters from analyte clusters, which was not useful. However, removing the reference clusters would not enhance the differentiation of analyte clusters. The long waiting time for solvent to evaporate, first from the sensor, and then from the sample spots, made the procedure very time-consuming. Another problem that needed to be solved was the fact that the plate-to-plate difference was significant: when combining datasets from two separate printer paper plates, the separation was not successful. This was likely caused

by location variations in the droplet depositions, and by warping during the drying phase. We decided to move to a sturdier solid support to prevent those problems.

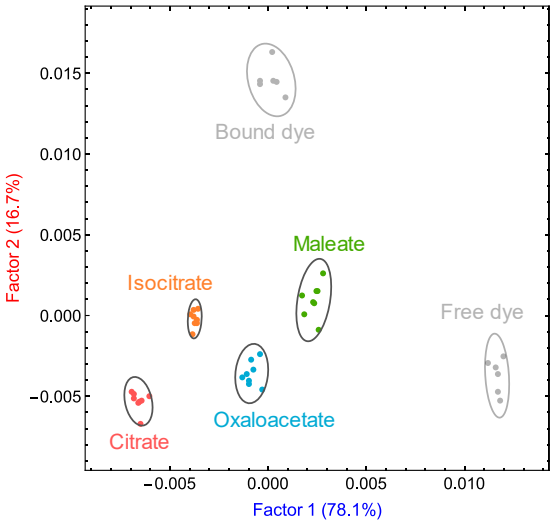

Figure 5-9 LDA scores plot for the differentiation of citrate, isocitrate, oxaloacetate, and maleate using [calcein•PAMAM] on printer paper. In this case, [calcein•PAMAM] complex was deposited first, let dry completely (~2 hours), then carboxylate analytes were added on top of the dried sensor spot. Measurements were taken both immediately after analytes were deposited, and after solvent had evaporated completely. Calcein = 636 pmol, PAMAM G5 = 213 pmol, carboxylates = 230 nmol.

5.6 Filter paper as solid support

We moved on to consider filter paper (Whatman 597, diameter 150 mm filter paper circles). For this candidate support, the higher absorbing capacity and lack of hydrophobic treatment often generated wide and poorly defined sample spots compared to printer paper. To prevent sample crosstalk, the spot loading was reduced to 1 μL. An experiment was performed to differentiate all ten carboxylates of interest in chapter 2 and 3, with 4 replicates for each carboxylate. Even though 4 replicates were much lower than our typical plate studies, this was still a good test run to demonstrate the ability of filter paper to retain the discriminatory power that the [calcein•PAMAM] sensor displayed in solution.

A [calcein•PAMAM] solution was first deposited onto the filter paper, and took less than 10 minutes to dry. Then carboxylate solutions were deposited onto each dried sensor spot. Because in this case we found that the solvent evaporation time was shorter than the plate reading time, reliable measurements could only be taken after the samples had dried. The LDA scores plot obtained from this plate is shown in Figure 5-10. Clearly, using filter paper as a solid support did not lead to complete differentiation of all ten carboxylates. Nevertheless, compared to any previous experiment that used dataset from only one measurement (Figure 5-6, Figure 5-7a and b), filter paper showed a significant improvement in intercluster and intracluster distances, indicating a higher discriminatory power overall.

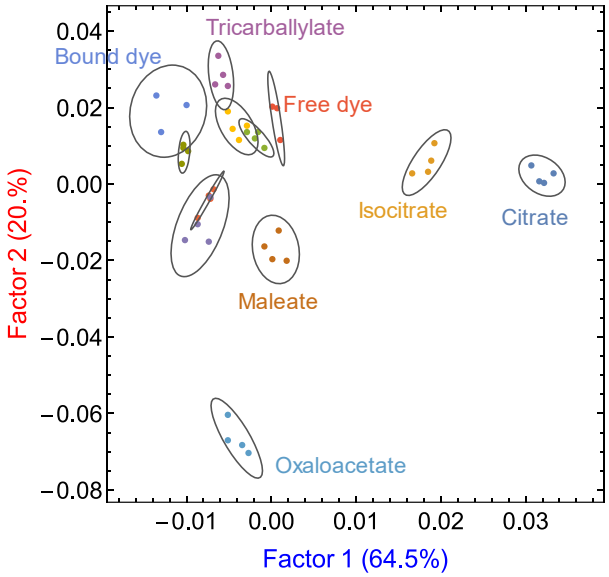

Figure 5-10 LDA scores plot for the differentiation of the complete set of carboxylate analytes(Figure 5-5) using [calcein•PAMAM] on filter paper. Calcein = 63.6 pmol, PAMAM G5 = 21.3 pmol, carboxylates = 23 nmol.

Among all carboxylates, citrate, isocitrate, oxaloacetate, maleate, and tricarballylate appeared to be best differentiated, therefore a new differentiation study was performed using these 5 carboxylates. Also, with a smaller number of analytes, each analyte could have more

replicates. We had previously found that on printer paper the sample spot would expand and spread during solvent evaporation, so sample deposition could only be done at every other position to prevent sample crosstalk. However, this was not a problem with filter paper and chromatography paper, so we could use every spot for sample deposition, allowing us to deposit more replicates for each sample. Therefore, we were able to use all 96 spots on the plate layout, and each carboxylate had 16 replicates.

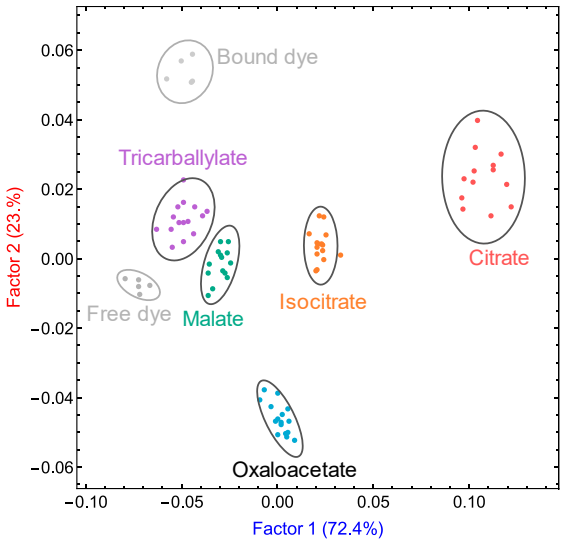

Figure 5-11 LDA scores plot for the differentiation of citrate, isocitrate, oxaloacetate, malate, and tricarballylate using [calcein•PAMAM] on filter paper. Calcein = 63.6 pmol, PAMAM G5 = 21.3 pmol, carboxylates = 23 nmol.

The corresponding LDA scores plot is shown in Figure 5-11: all five analytes were differentiated with one measurement, better results than we had obtained using printer paper. Filter paper also had a much lower prep time: solvents took less than 20 minutes in total to evaporate, while for printer paper the total evaporation time for separate deposition was 4 hours. Cluster arrangements on the scores plot were also improved: the free dye and bound dye reference clusters were found to take less space on the plot relative to the more informative analyte clusters. However, the cluster sizes were still relatively large, and repeatability still a

challenge. Although it provided some significant improvements over previously considered candidates for solid supports, filter paper still had some shortcomings that forced us to consider further opportunities.

5.7 Chromatography paper as solid support

5.7.1 Discrimination and repeatability experiments

Chromatography paper (Whatman Chromatography paper, 1CHR) was very similar to filter paper, only thicker, so its spot loading capacity was found to be higher (2.5 μL). The same five carboxylate analytes were tested in the manner described above. Results are shown in Figure 5-12a: carboxylates were successfully differentiated, with smaller and tighter clusters, indicating that chromatography paper was better at retaining the discriminatory power that the [calcein•PAMAM] sensing complex displays in solution. The balance of contributions between factor 1 and factor 2 was more even, suggesting that multiple independent measurements were contributing to the separation. Chromatography paper had all the advantages of filter paper, plus, when combining data from two replicate plates prepared separately, the results were not degraded (see Figure 5-12b). This excellent repeatability was a very exciting result.

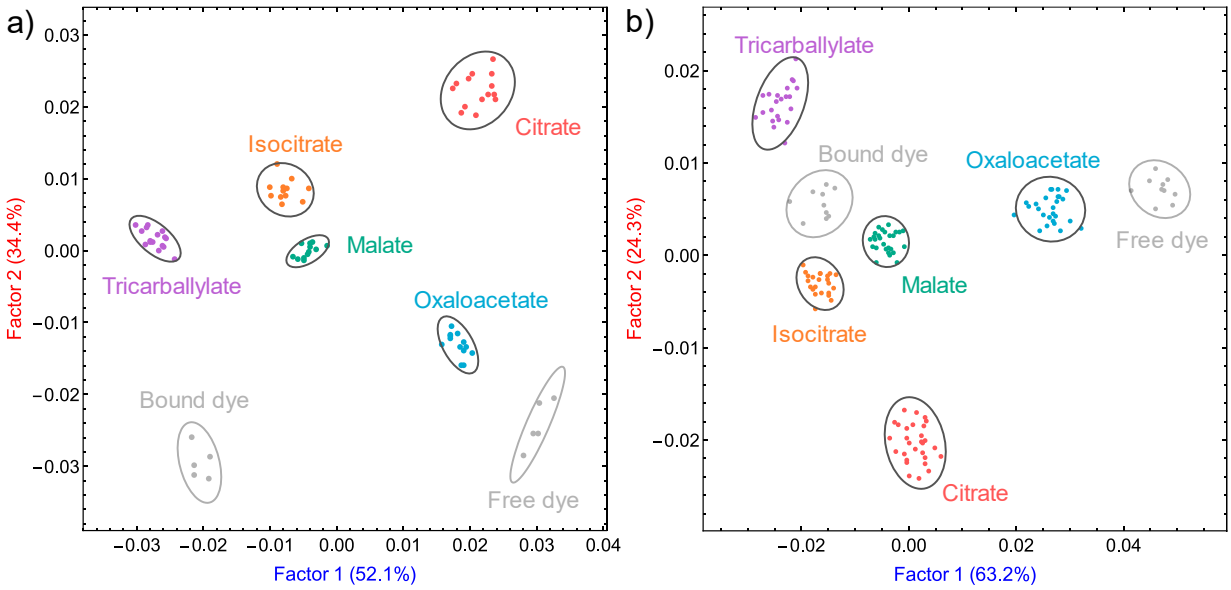

Figure 5-12 LDA scores plot for the differentiation of citrate, isocitrate, oxaloacetate, malate, and tricarballylate using [calcein•PAMAM] on chromatography paper. a) Scores plot from a single plate; b) Scores plot from the measurement of two identically prepared plates, to test for repeatability. Calcein = 159 pmol, PAMAM G5 = 53.25 pmol, carboxylates = 57.5 nmol.

Compared to printer paper, chromatography paper (shown in Figure 5-13) also had better differentiation on the same set of carboxylates (referring to Figure 5-7). Not only were the clusters from chromatography paper tighter (smaller intracluster distances) and more separated (larger intercluster distances), but the sample clusters were also more spread out on the scores plot, suggesting more efficient differentiation. In Figure 5-7 using printer paper, factor 1 almost did not differentiate among carboxylates, only separating the analyte clusters from the references. Here, using chromatography paper, both factors were contributing to the differentiation of analytes.

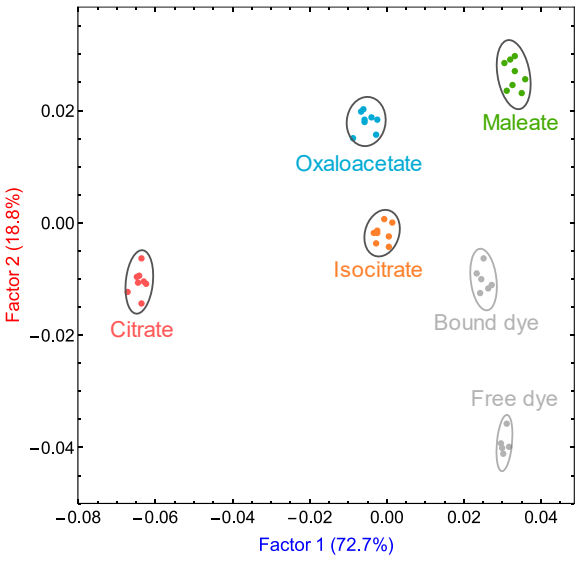

Figure 5-13 LDA scores plot for the differentiation of citrate, isocitrate, oxaloacetate, and maleate using [calcein•PAMAM] on chromatography paper. Calcein = 159 pmol, PAMAM G5 = 53.25 pmol, carboxylates = 57.5 nmol.

5.7.2 Hydroxy-carboxylates analysis

In our group's previous work, PAMAM dendrimers were counterintuitively found to behave primarily as hydrogen bond acceptors.[152] Further experiments have shown that they are often more sensitive to guest molecules who contains hydroxy groups.[58] It was interesting to investigate whether this effect would still be active on solid support, so we selected 7 common carboxylates (citrate, isocitrate, oxaloacetate, malate, tartrate, glycolate and lactate) that contained hydroxy groups, and ran the same differentiation experiments on our best solid support candidate so far, i.e. chromatography paper. Figure 5-14 showed the resulting LDA scores plot, with most of the carboxylates differentiated.

The orientation of carboxylate clusters on the scores plot was very interesting. Monocarboxylates glycolate and lactate were found very close to the bound dye cluster, while dicarboxylates malate, tartrate, and oxaloacetate were found close to the free dye cluster. Due to stronger electrostatic interactions, dicarboxylates had higher affinity for PAMAM dendrimers,

thus they could displace more calcein from its complex. Therefore, the dicarboxylate samples would contain calcein mostly in its free state and spectroscopically look more like the free dye reference. Consequently, the weaker-binding monocarboxylate would contain dye mostly in its bound form, so their samples would look more like the bound dye reference. Tricarboxylates citrate and isocitrate, however, had clearly different spectroscopic behaviors, which might be caused by the formation a three-body complex ([tricarboxylate•calcein•PAMAM] complex). This different behavior was also found in the solution titrations previously described in Chapter 2.

Lactate contained a secondary hydroxy group while glycolate contained a primary hydroxy group: overlapping of the two clusters indicated that the system was not selective for the position of the hydroxy group. Also, tartrate had one more hydroxy group than malate, but their clusters were still very close: this suggested that the system was not sensitive to the number of hydroxy groups. These two superclusters suggested that the cellulose in the paper solid support may interfere with PAMAM dendrimer and saturate its ability to accept hydrogen bonds. Overall, the number or positions of hydroxyl groups of structurally similar monocarboxylates and dicarboxylates was not recognized and differentiated by this system.

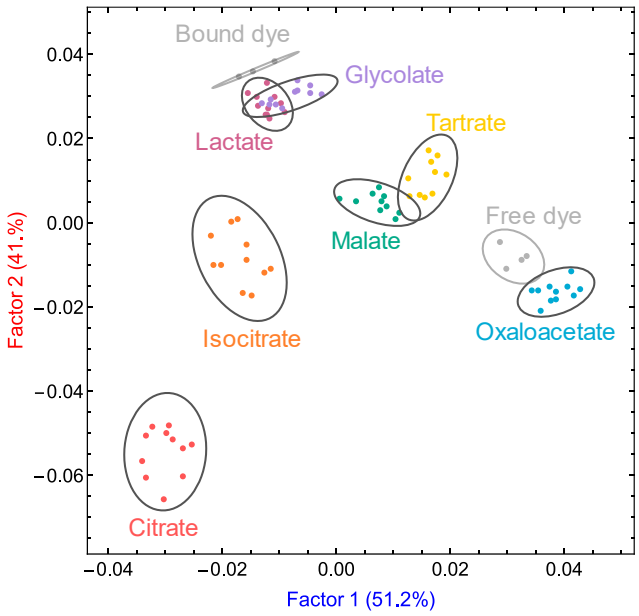

Figure 5-14 LDA scores plot for the differentiation of citrate, isocitrate, oxaloacetate, malate, tartrate, glycolate and lactate using [calcein•PAMAM] on chromatography paper. Calcein = 159 pmol, PAMAM G5 = 53.25 pmol, carboxylates = 57.5 nmol.

As shown in Figure 5-15a, the dye reference clusters were removed to focus on the analyte clusters. Compared to the original LDA scores plot (Figure 5-14), the dye clusters retained a similar orientation. It was also very exciting to see that the analyte clusters took up most of the space on the scores plots, in contrast to previous results (for instance, on printer paper, see Figure 5-8 and Figure 5-9), where the reference clusters took up a significant portion on the scores plots, reducing the feature space available for discrimination of the analyte clusters. This suggested a less informative data set: with a large portion of the original information being used to differentiate between the reference dye and analytes, less information was contributing to differentiate among analytes. In the previous cases, however, removing the reference dye clusters caused very poor differentiation of the analytes. Here instead, removing the reference dye clusters was very effective, as shown in Figure 5-15: all analytes were successfully differentiated, with 94.2% of the original information contributing to the differentiation. This

result proved that this solid support was able to retain the discriminatory power the system had in solution to carry out effective differentiation.

Furthermore, the LDA scores plot in Figure 5-15b was obtained by combining the datasets from three identical plates. We were pleased to see that the clusters remained in the same orientation, even though with slightly increased cluster sizes, proving that this system had excellent repeatability.

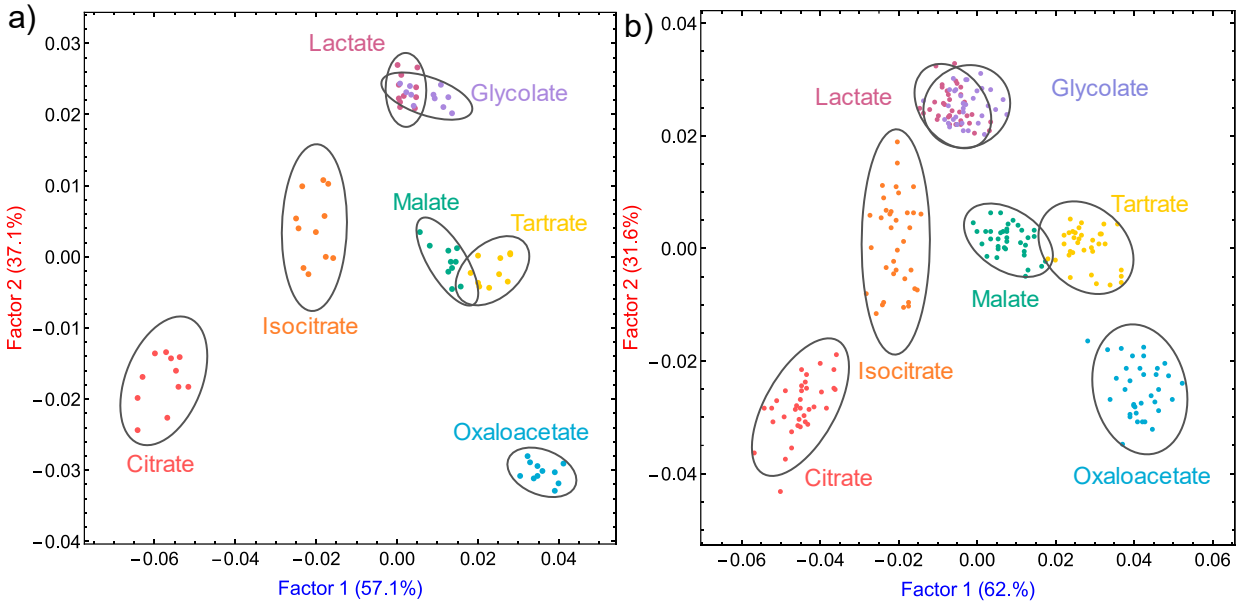

Figure 5-15 LDA scores plot for the differentiation of citrate, isocitrate, oxaloacetate, malate, tartrate, glycolate and lactate using [calcein•PAMAM] complex as sensor on chromatography paper plate. a) scores plot from a single plate; b) scores plot from combining data from three separate plates with identical sample deposition. Calcein = 159 pmol, PAMAM G5 = 53.25 pmol, carboxylates = 57.5 nmol.

5.8 Shelf life of pre-deposited sensing system

As mentioned previously in the introduction, the [calcein•PAMAM] complex in HEPES buffer at pH 7.4 was only stable for less than a week. Indeed, even PAMAM G5 dendrimers are most stable in methanol and must be stored at low temperature. We were interested in the stability of the deposited sensing complex on chromatography paper, the most promising solid

support we tested. The ideal application would involve pre-loading the sensor on the support and storing it indefinitely after drying. When ready to use, the solid support would work as a “test strip”.

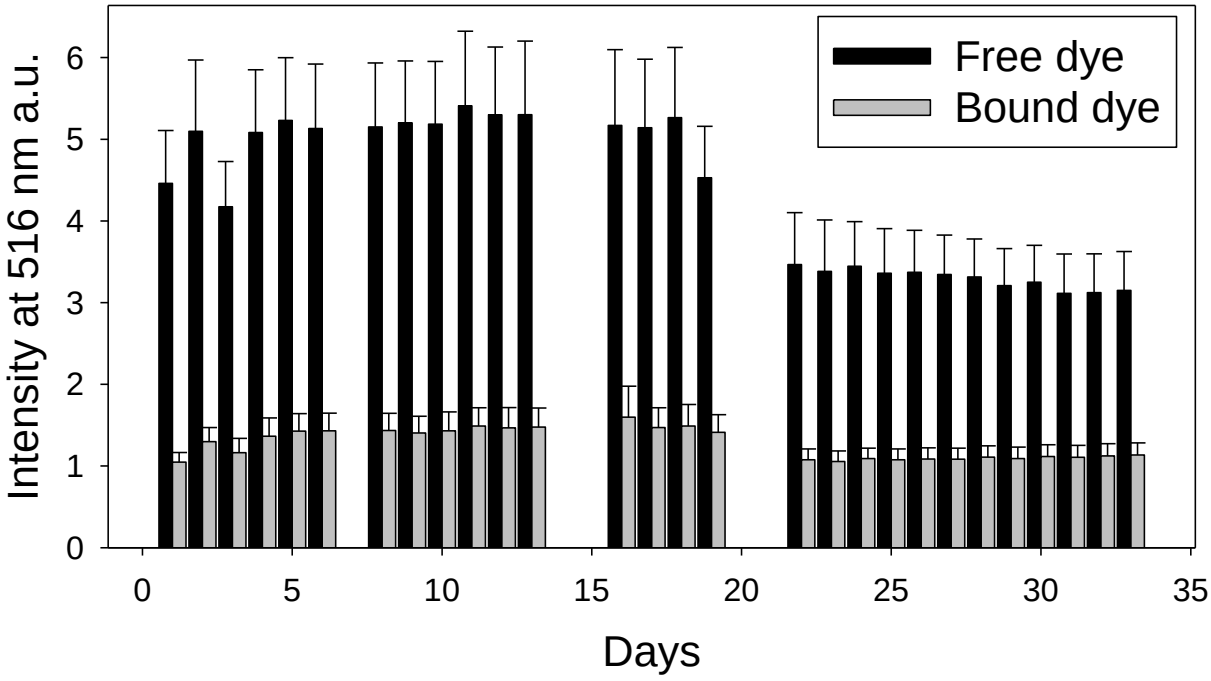

Figure 5-16 Fluorescence emission of free dye (calcein) and bound dye ([calcein•PAMAM] complex) on chromatography paper during a 33-day period, to test for stability on solid support. Calcein = 63.6 pmol, PAMAM G5 = 21.3 pmol,

To test the shelf-life of the method (long-term stability), 20 replicates of free calcein dye sample and 20 replicates of [calcein•PAMAM] complex sample were deposited on each of three chromatography paper plates at the same time under the same condition. Paper plates were stored in sealed polyethylene bags in the dark, and fluorescence intensity was measured over a 33-day period. Shown in Figure 5-16 is the emission intensity over each day, with each bar being the average of 60 replicates from three plates, with the corresponding confidence interval. Fluorescence intensity remained constant for the first 18 days, then starting from day 19 the

intensity started to decrease. Compared with the sensing complex in aqueous solution, the stability of the complex on the solid support was at least twofold, and probably even better. In practice, this would reduce the cost, and ease the storage and transportation of the sensing complex.

5.9 Cost analysis

A cost analysis was generated based on screening 96 samples on various materials (shown in Table 5-5), including commercial 96-well polystyrene microwell plate with black walls (commonly used for fluorescence measurements), and the three paper-based supports that were most promising in this study (printer paper, filter paper, and chromatography paper). Both sensor complex cost and the support material cost were taken into consideration. Overall, although PAMAM G5 had the highest unit cost, the amount of PAMAM dendrimers used in any sensing method was so small that it did not add significantly to the cost. In most cases the support was the main contributor to total cost. Comparing with the 96-well black wall plate that cost $3.5 each, filter paper and chromatography paper led to a more than tenfold cost reduction, and printer paper cost even less. In this case, a cost reduction would also go hand in hand with a lower consumption of plastic disposables, thereby making to paper-supported methods more green and environmentally friendly.

Table 5-5 Cost analysis of regular plate and paper-based plates

material	support ($)	calcein (g)	PAMAM G5 (g)	HEPES (g)	total cost ($)
Unit cost ($)		$7.325/g	$346/g	$0.313/g	
96-well plate (black wall)	$3.573	122 μg	41 μg	960 μg	$3.588
Printer paper	$0.004	41 μg	14 μg	32 μg	$0.009
Filter paper	$0.247	4 μg	1.4 μg	3.2 μg	$0.248
Chromatography paper	$0.323	10 μg	3.4 μg	8 μg	$0.324

5.10 Conclusions

This study showed that the transition of [calcein•PAMAM] to differentiate carboxylate analytes from solution to a variety of solid support materials was successful. The discriminatory power was retained and could be monitored through fluorescence emission intensity alone, forgoing absorbance measurements and allowing the use of opaque supports as well. Different support media were studied including cellulose acetate transparencies, silica TLC aluminum plates, printing paper, filter paper, and chromatography paper. They all appeared to be cheaper and needed less analyte than solution-based measurements conducted in common black-wall polystyrene 96-well plates. Among all materials, paper-based solid supports showed the most promising results. Printing paper was found to be the cheapest and most widely available, but it showed low discrimination ability. Filter paper afforded better differentiation than printing paper, and it needed less materials.

Overall, chromatography paper performed the best, with excellent differentiation that showed large intercluster distance and tight clusters on LDA scores plot. We also found it to be conducive to excellent repeatability and an improvement on the shelf-life of the sensing system compared to the same system in aqueous media. Overall, this low-cost and easy to use solid support gave us further insights in transitioning sensors that function in solution media to a “test strip” and *in situ* detection.

5.11 Experimental details

5.11.1 Materials

Fifth generation, amine terminated poly(amidoamine) (PAMAM) dendrimers with a 1,2-diaminoethane core were manufactured by Dendritech, Inc., and purchased as a solution in methanol with exact concentration of 1.419 mM. The final solution used for all experiment was

obtained by dilution with buffer and contained a negligible amount of methanol (< 0.8%). Calcein dye was purchased from Sigma Aldrich and was used as received. Carboxylate solutions were prepared from DL-isocitric acid trisodium salt hydrate and sodium glycolate purchased from Acros; DL-malic acid and oxaloacetic acid purchased from Sigma Aldrich; maleic acid, tricarballylic acid, and sodium L-lactate purchased from Alfa Aesar; potassium sodium -(+)-tartrate tetrahydrate purchased from TCI; anhydrous citric acid purchased from EMD Millipore. 50 mM 4-(2-hydroxyethyl)-piperazine-1-ethanesulfonic acid (HEPES) buffer was prepared from HEPES purchased from IBI Scientific. All prepared solutions were adjusted to pH 7.4 using solutions of NaOH, prepared from NaOH purchased from Fisher Scientific, and HCl, prepared from HCl purchased from BDH Aristar. All materials were used as received. Nunc 96-well polystyrene plates were purchased from Thermo Scientific. Silica gel 60 aluminum-backed TLC sheets were purchased from EMD Millipore. Filter paper (150 mm diameter circles) and chromatography paper (1 CHR) were purchased from Whatman. Office xerographic printer paper (US Letter size, 92 brightness, 75 g/m^2) was obtained from Staples.

5.11.2 Instrumentation

Sample spots were printed (transparencies and printer paper plates) or hand drawn (TLC plates, filter paper, and chromatography paper plates) on solid supports. Sample deposition was carried out by an Eppendorf Research pipettor. A Biotek Synergy II multimode microwell plate reader was used for the measurement of fluorescence intensity: 12 combinations of excitation and emission wavelengths ($\lambda_{ex}/\lambda_{em}$ in nm: 450/516, 450/528, 450/560, 450/580, 460/516, 460/528, 460/560, 460/580, 485/516, 485/528, 485/560, 485/580) were measured for each sample. A “top detected” mode was used for all fluorescence measurements: a dichroic mirror

was placed between emission channel and sample wells to block excitation light from reaching the detector.

5.11.3 Experimental conditions

All solution prepared for solid support had concentration of 63.6 μM of calcein, 21.3 μM of PAMAM G5, and 23.0 mM of carboxylate. Calcein binding with PAMAM G5 experiment on chromatography paper: 1 μL per spot; 63.6 pmol of calcein per spot; 7 replicates each. Citrate binding with PAMAM G5 on chromatography paper: 1 μL per spot; 63.6 pmol of calcein, 21.3 pmol of PAMAM G5 per spot; 7 replicates each. SiO_2 on aluminum TLC plates as support: 3 μL per spot; 190.8 pmol of calcein, 63.9 pmol of PAMAM G5, and 69 nmol of carboxylate per spot; 12 replicates each. Printer paper: 10 μL per spot; 636 pmol of calcein, 213 pmol of PAMAM G5, 230 nmol of carboxylate per spot; 9 replicates each. Filter paper: 1 μL per spot; 63.6 pmol of calcein, 21.3 pmol of PAMAM G5, and 23.0 nmol of carboxylate per spot; 4 replicates each for 10 analytes, and 16 replicates each for 5 analytes. Chromatography paper: 2.5 μL per spot; 159 pmol of calcein, 53.25 pmol of PAMAM G5, and 57.5 nmol of carboxylate per spot; 16 replicates each for 5 analytes, and 12 replicates each for 7 analytes.

5.11.4 Solid support plate experiments

Each material was tested for their maximum loading capacity first, to determine the maximum sample amount that would avoid sample crosstalk between neighboring samples. For binding and displacement "titration" experiments on chromatography paper, a "cuvette" solution (i.e. calcein in the dye binding experiment, and [calcein•PAMAM] complex in the anion binding / dye displacement experiment) was first deposited on the solid support and let dry. Then, a "titrant" solution (i.e. PAMAM G5 in the dye binding experiment, and citrate in the anion binding / dye displacement experiment) was deposited on the dried "cuvette" solution spots and

let dry. For initial screening on printer paper, analyte and sensor were mixed in a single solution and deposited together on the paper support. For the rest of the experiment, the sensor complex was deposited first on the solid support and let dry, then the analyte solution was deposited in a second step. Fluorescence emission intensity was measured on each spot for each solid support.

CHAPTER 6
CHLOROFORM DETECTION USING A FLUORESCENCE-ENHANCED FUJIWARA TEST

6.1 Introduction

Volatile organic compounds (VOCs) can be found in household chemicals, ground water and tap water, and architectural coatings; and they can cause serious damage to human health as well as to the environment.[186-187] Therefore, developing methods for the detection of those chemicals is very urgent. Chloroform is considered one of the most interesting analytes among all VOCs because of its common appearance in daily water as a by-product of water chlorination; but it can cause liver and kidney damage, anesthesia, and even death.[188-189]

Common detection methods for chloroform including electrochemical sensors,[190-191] mass spectrometry,[192] and chromogenic assays. Chromogenic sensors are advantageous because the color change can be captured by the naked eye. The most widely used $CHCl_3$ assay is the Fujiwara test: pyridine and NaOH react with chloroform upon heating to produce a red product.[193-194] Recently, other chromophore or fluorophore sensors were also developed, using synthetic dyes or polymers.[195-198] Here, we will discuss a method to detect chloroform by enhancing the sensitivity of the Fujiwara test through fluorescence detection.

In 1916, the Fujiwara reaction for the detection of chloroform using spectroscopic methods was first reported.[199] This two-phase system included an organic layer (pyridine), and an aqueous layer (aqueous NaOH); under heat, chloroform reacted with pyridine and produced an opened ring product. As shown in Scheme 6-1a, the strong base first removed the acidic

proton in chloroform to form a tri-chlorinated anion intermediate which expelled a chloride to form dichlorocarbene. Then the dichlorocarbene reacted with pyridine and yielded a colored product. This product had an intense red color and therefore allowed the detection and quantitation of chloroform. A study in 1981 used benzotrichloride (i.e. phenylchloroform) to further investigate the structure of the product of the Fujiwara reaction and proved that this reaction has at least two possible products, deriving by the reaction of the trichlorinated reagent with one or two pyridine molecules.[200] In analogy to the results of that study, the predicted product structures deriving from chloroform are shown in Scheme 6-1b, in which the carbon and hydrogen atoms shown in red are from a chloroform molecule; while the atoms in black are from pyridine. The Fujiwara test was further improved over the years to achieve lower detection limit, higher sensitivity, detection for chloroform vapor, one-phase reaction, and to introduce other reagents less toxic than pyridine.[193-194,201-204]

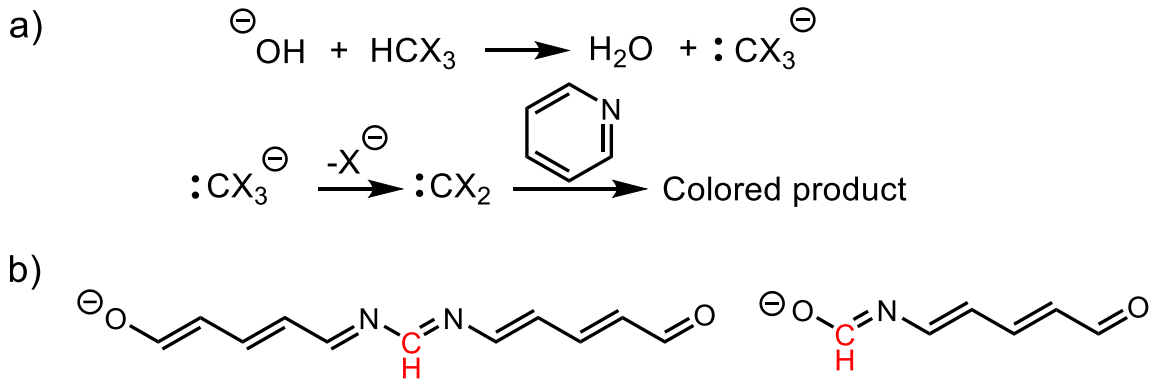

Scheme 6-1 a) Fujiwara reaction process; b) possible structures of the "colored product" from the Fujiwara test with chloroform. The atoms in red are from chloroform; the ones in black are from pyridine.

In this ongoing study, we propose a system to increase the sensitivity of the Fujiwara test by coupling it with a fluorescence measurement, typically a more sensitive detection technique. This approach takes advantage of the colored product of the Fujiwara test. By placing the

Fujiwara product between the excitation source and a fluorophore that has the same absorption as the Fujiwara product, the latter can absorb the incoming excitation light and cause a modulation of the fluorescence signal. The Fujiwara test product has a peak at 370 nm, therefore we chose three coumarin dyes who had absorption at 370 nm as good candidates for this experiment (Scheme 6-2).

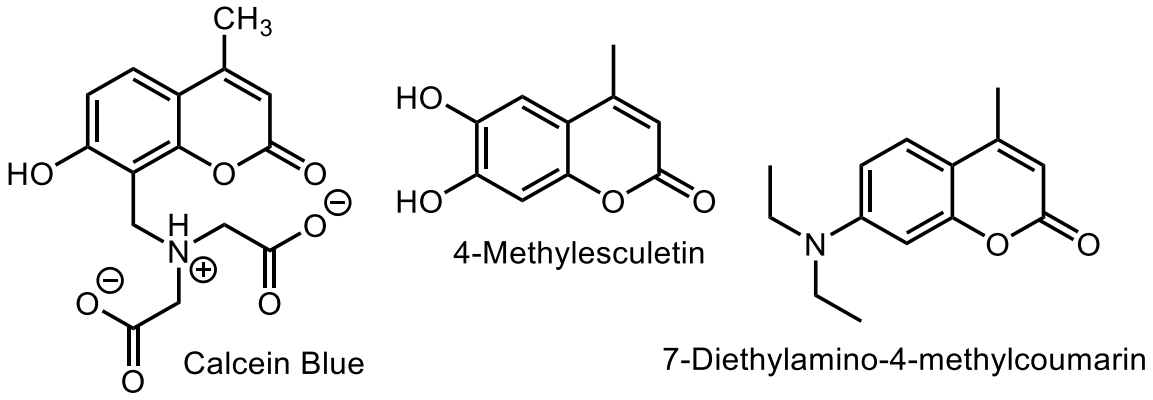

Scheme 6-2 Dyes used in this study.

6.2 Experiment design

6.2.1 Determination of optimal fluorophore concentration

Three dyes, calcein blue, 7-diethylamino-4-methylcoumarin and 4-methylesculetin, were tested to determine an optimal working concentration. The most desired concentration is the highest concentration at which the dye's emission is still linear with concentration. The higher the concentration of the dye is, the higher the dynamic range is when determining the presence of chloroform, and the linearity can help to do quantitative analysis.

Linearity titrations for each dye were performed with fluorescence spectra shown in Figure 6-1, and the corresponding fluorescence profiles shown in Figure 6-2. Among all dyes, 7-diethylamino-4-methylcoumarin was only soluble in protic solvent, therefore it was dissolved in methanol, and the working concentration was determined to be 0.9 μM. Calcein blue was

dissolved in 50 mM HEPES buffer at pH 7.4,and the working concentration was determined to be 0.6 μM. 4-methylesculetin was dissolved in minimum amount of methanol first, then diluted using 50 mM HEPES aqueous buffer. From the group's previous experience, 4-methylesculetin worked well at both neutral pH and basic pH,[55] therefore titrations were performed at both pH 7.4 and pH 10, and the best working concentration was determined to be 3.0 μM in both conditions. The concentrations remained the same throughout this experiment.

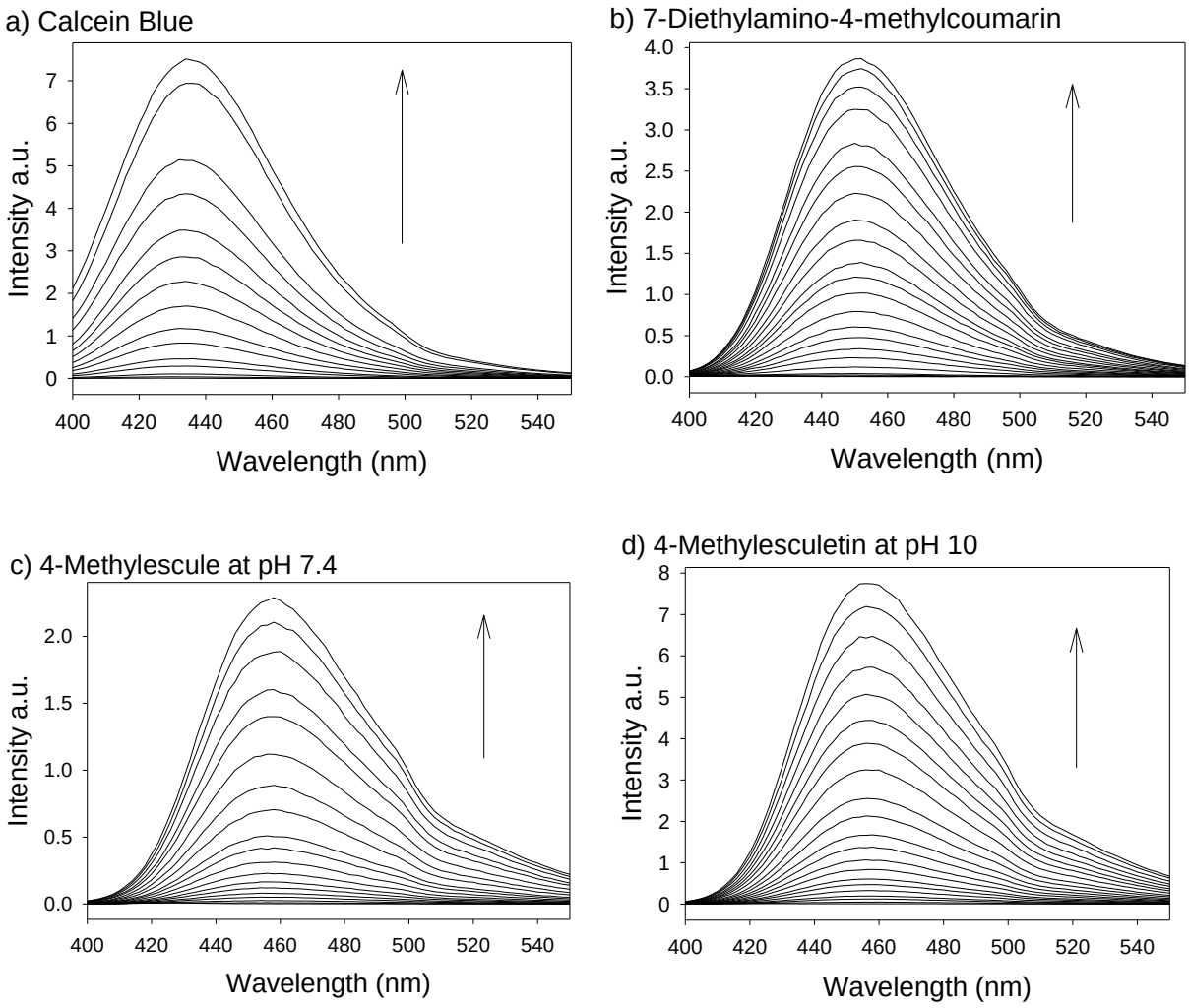

Figure 6-1 Fluorescence emission spectra to determine the linear response range for a) calcein blue, b) 7-diethylamino-4-methylcoumarin, c) and d) 4-methylesculetin. a) and c) were performed in 50 mM aqueous HEPES buffer at pH 7.4; b) was performed in methanol; and d) was performed in 50 mM aqueous HEPES buffer at pH 10.

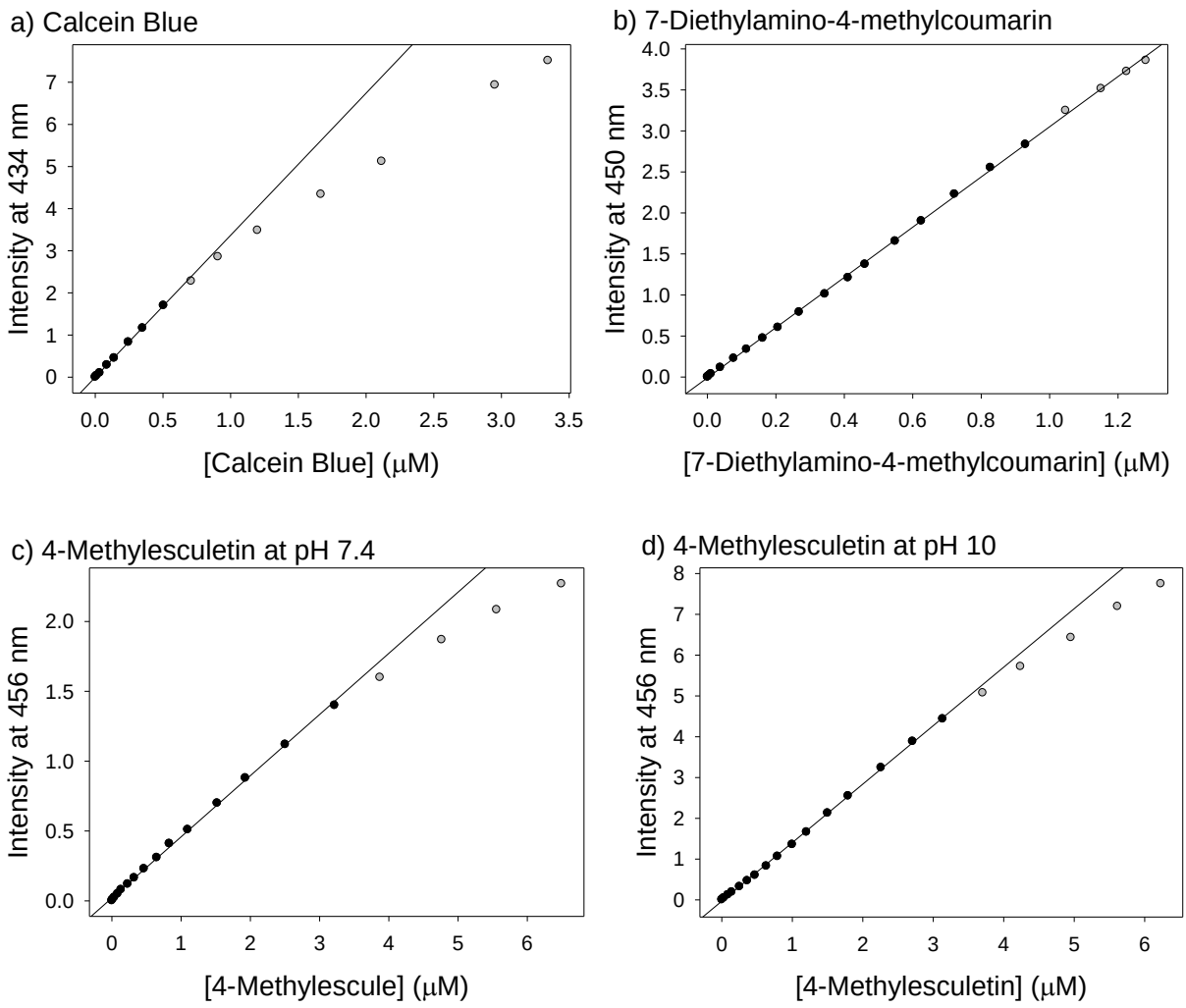

Figure 6-2 Fluorescence profiles from linearity tests at maximum emission wavelength of a) calcein blue, b) 7-diethylamino-4-methylcoumarin, c) and d) 4-methylesculetin. a) and c) were performed in 50 mM aqueous HEPES buffer at pH 7.4; b) was performed in methanol; and d) was performed in 50 mM aqueous HEPES buffer at pH 10. Excitation: 370 nm.

6.2.2 Fujiwara test conditions

We started to test the best condition to perform the Fujiwara test. The procedure was inspired by a paper published by the Gupta group in 1999.[204] To establish a background, 5 M of NaOH and pyridine were mixed in a 1:1 volume ratio. The two-phase reagents were then heated in a boiling water bath for 2 minutes, cooling down to room temperature and then put in ice bath for 15 minutes. The top pyridine layer was then taken for centrifugation to remove any of the

aqueous suspensions. Finally, the absorbance of the reacted pyridine layer was measured for absorbance. However, as shown in Figure 6-3, this process formed a precipitate, even without addition of chloroform, which quenched the fluorescence emission of the dyes. We tried different combination of NaOH volume and concentration (see Figure 6-3): with the same concentration (5 M) but lower volume, precipitation still appeared; on the other hand, with the same volume (4 mL) but a lower concentration, there was less to no precipitation.

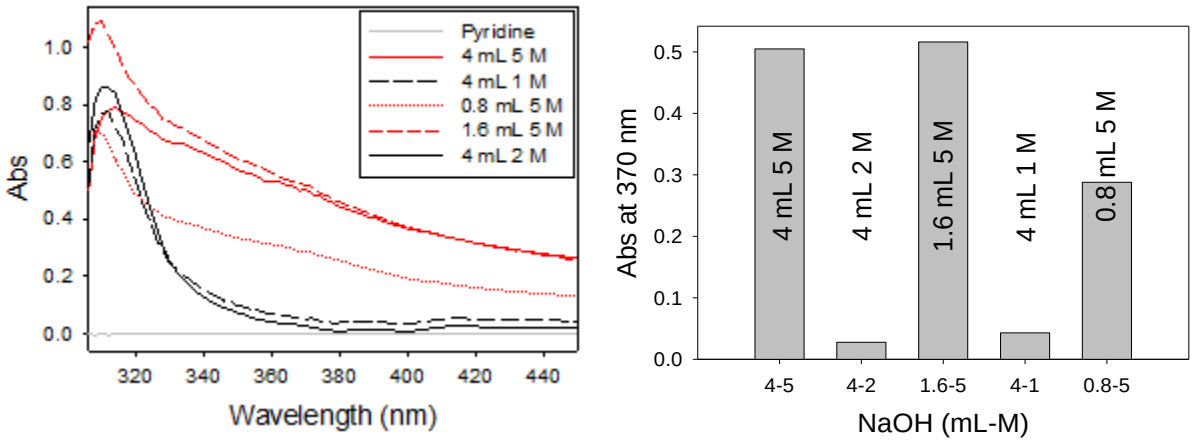

Figure 6-3 Absorbance measurements of precipitation test of the result of heating 4 mL of pyridine and various amount and concentration of NaOH (shown in legend). a) absorbance spectra, b) absorbance profile at 370 nm.

After absorption measurements, each product was positioned between the excitation source and the dye sample in the fluorometer. Fluorescence emission spectra for each dye are shown in Figure 6-4, and the corresponding profiles are shown in Figure 6-5. In this case, the precipitate would scatter the excitation light and cause reduction of the fluorescence of the dye, which was undesired for chloroform sensing. On the other hand, reaction product with less to no precipitation barely absorbed at 370 nm (Fujiwara test product peak), therefore any quenching of the dye could only be caused by the presence of chloroform. Based on our result, both 1 M and

2 M NaOH with a 1:1 volume ratio to pyridine were good candidate for the experiment. So, we moved on to titration with different chloroform concentration.

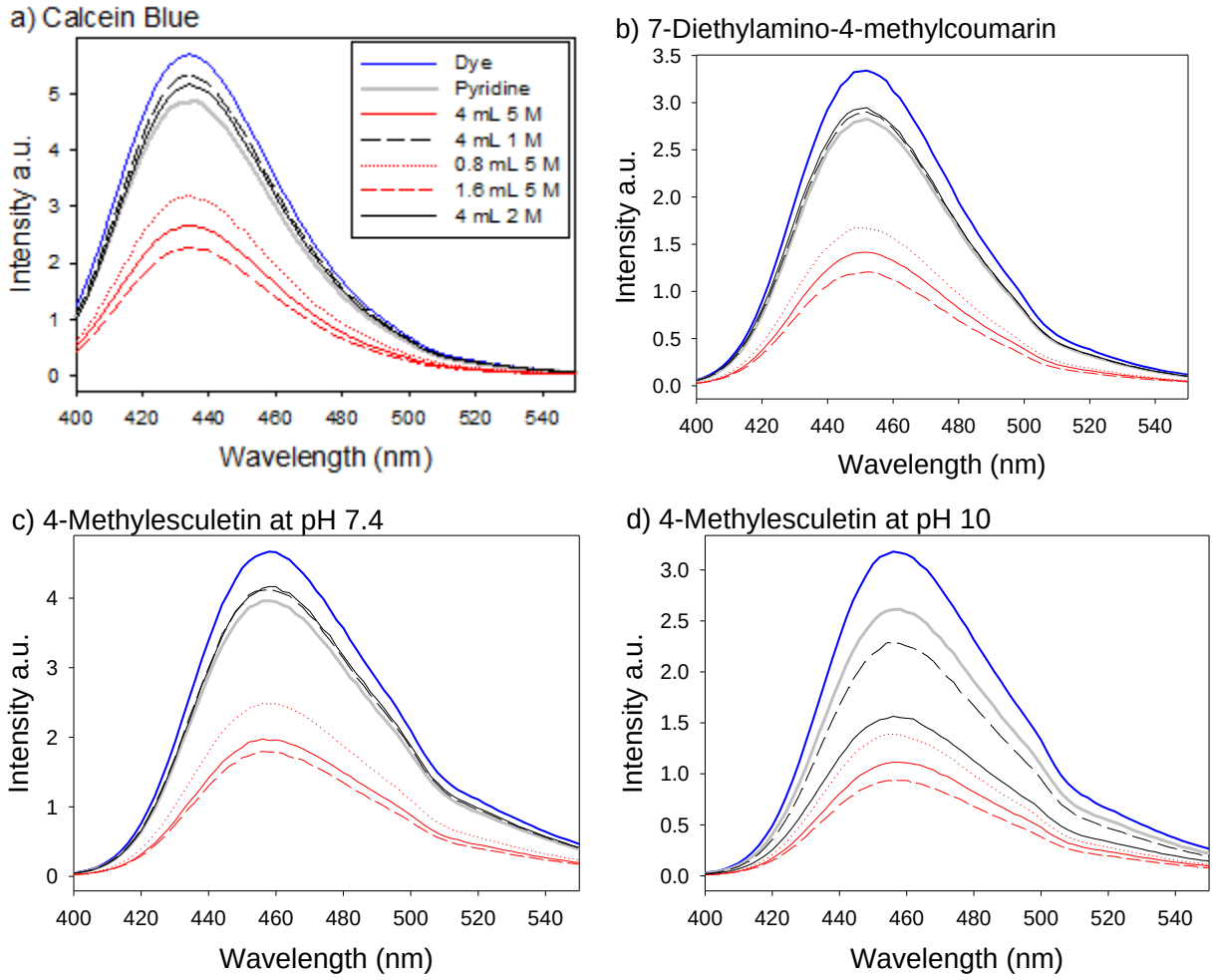

Figure 6-4 Fluorescence spectra of precipitation tests obtained by placing the product of heating 4 mL of pyridine and various amounts and concentrations of aqueous NaOH (shown in legend) between excitation source and fluorephore: a) calcein blue, b) 7-diethylamino-4-methylcoumarin, c) and d) 4-methylesculetin. Dye solutions were the same throughout: a) and c) were in 50 mM aqueous HEPES buffer at pH 7.4; b) was in methanol; and d) was in 50 mM aqueous HEPES buffer at pH 10.

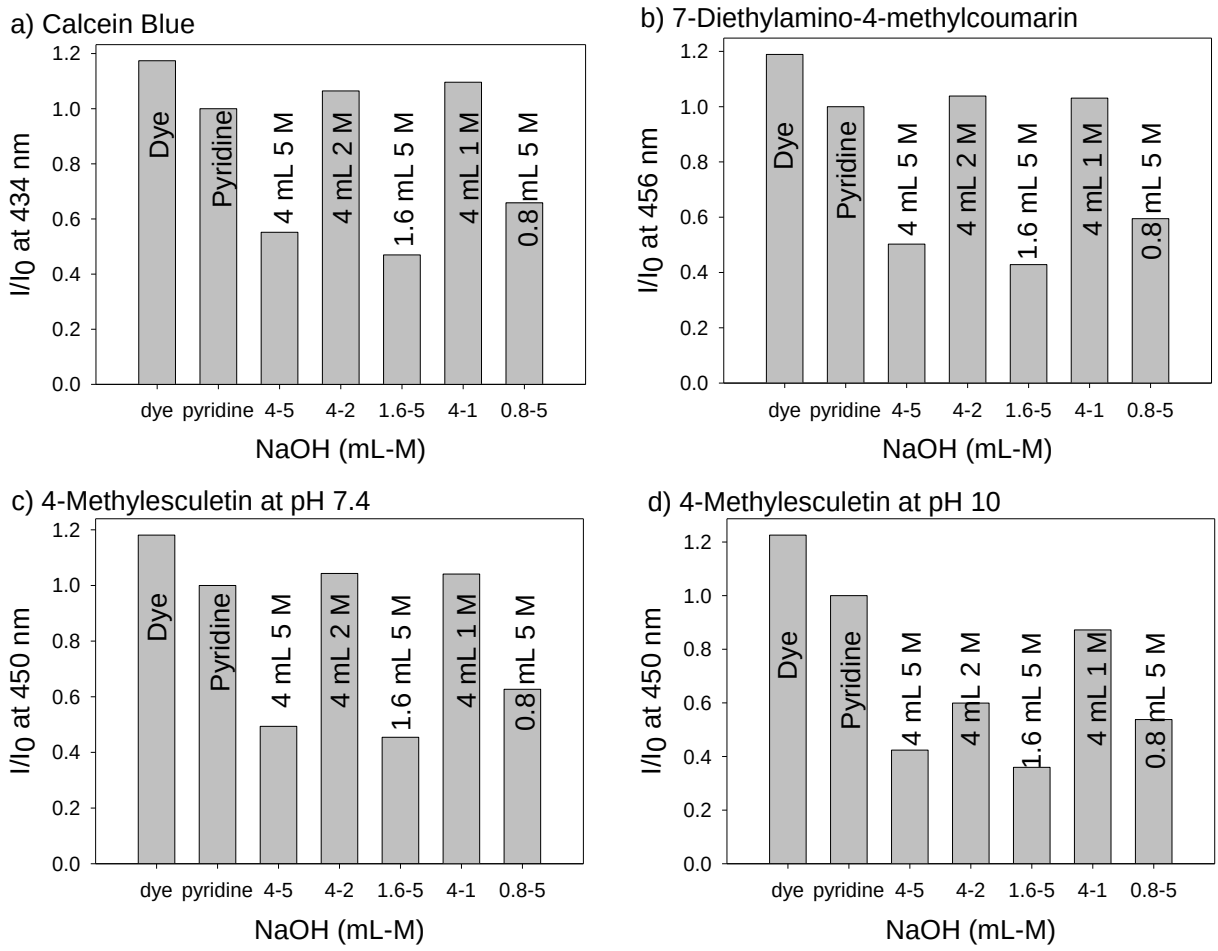

Figure 6-5 Fluorescence of precipitation test by placing the product of heating 4 mL of pyridine and various amount and concentration of NaOH between excitation source and fluorophore at their maximum emission wavelength: a) calcein blue, b) 7-diethylamino-4-methylcoumarin, c) and d) 4-methylesculetin. The numbers on x-axis refer to the volume (mL) and the concentration (M) of aqueous NaOH. Dye solutions were the same throughout the experiment: a) and c) were in 50 mM aqueous HEPES buffer at pH 7.4; b) was in methanol; and d) was in 50 mM aqueous HEPES buffer at pH 10. Excitation: 370 nm.

6.3Chloroform sensing titrations with 1.0 M NaOH and 2.0 M NaOH

Titration was performed using different concentrations of chloroform reacting with the two-phase reagent discussed before. The same experimental procedure described before was used. 1 M NaOH in H_2O was first tried, and the titration absorbance spectra and profile are shown in Figure 6-6: each titration point stands for a single experiment. The profile showed a

linear relationship between the chloroform concentration and absorbance measurements, which was a successful result.

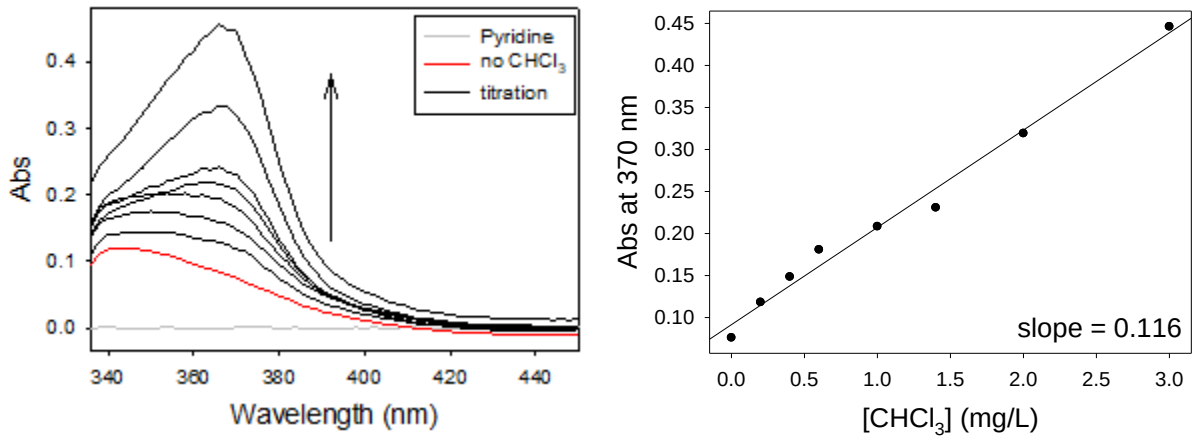

Figure 6-6 Absorbance measurements of Fujiwara test results with different concentration of chloroform. a) absorbance spectra, b) absorbance profile with linear regression line at 370 nm. Each spectra represent one reaction. Pyridine: 4 mL, 1.0 M NaOH: 4 mL.

The product for each experiment was then positioned between the excitation source and dye sample for fluorescence measurements. Shown in Figure 6-7 are the fluorescence spectra of different dyes corresponding with each of the absorbance measurement. The same experiment was performed two more times on separate days. Absorbance and fluorescence profiles for each dye are presented in Figure 6-8 Left for comparison. Then, the same experiment using 2 M NaOH was performed in triplicate, and profiles are shown in Figure 6-8 Right. Comparing the three repeat experiments using 1 M NaOH with experiments using 2 M NaOH, the latter showed better linearity and reproducibility; the larger slope (absolute value) indicated that the detection was also more sensitive to the presence of chloroform. Therefore, we decided to use 2 M NaOH in the following chloroform quantitation experiment.

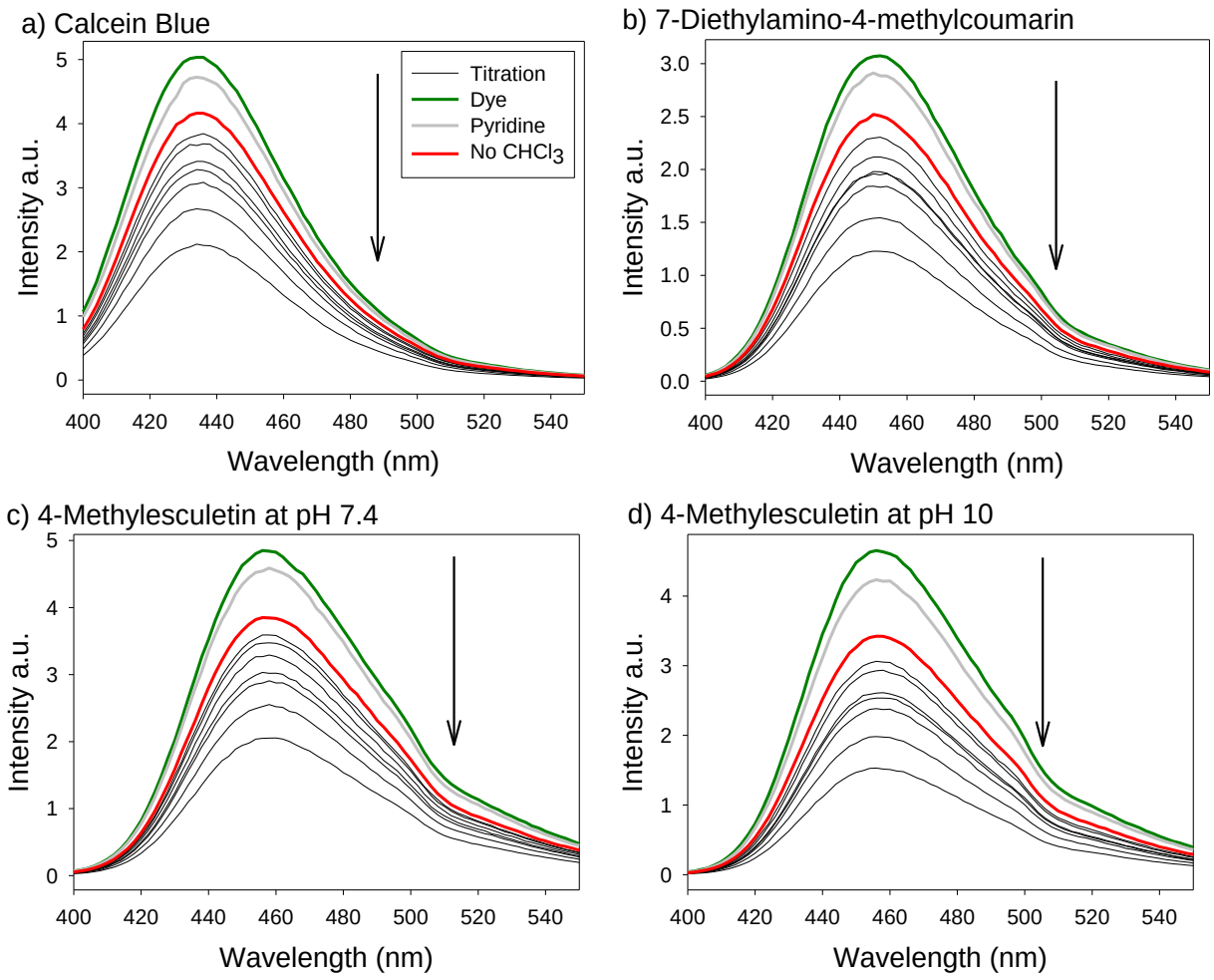

Figure 6-7 Fluorescence spectra obtained by placing the product of Fujiwara test with various concentrations of chloroform between the excitation source and fluorephore: a) calcein blue, b) 7-diethylamino-4-methylcoumarin, c) and d) 4-methylesculetin. Dye solutions were the same during experiment, and each spectrum represents one reaction. a) and c) were in 50 mM aqueous HEPES buffer at pH 7.4; b) was in methanol; and d) was in 50 mM aqueous HEPES buffer at pH 10.

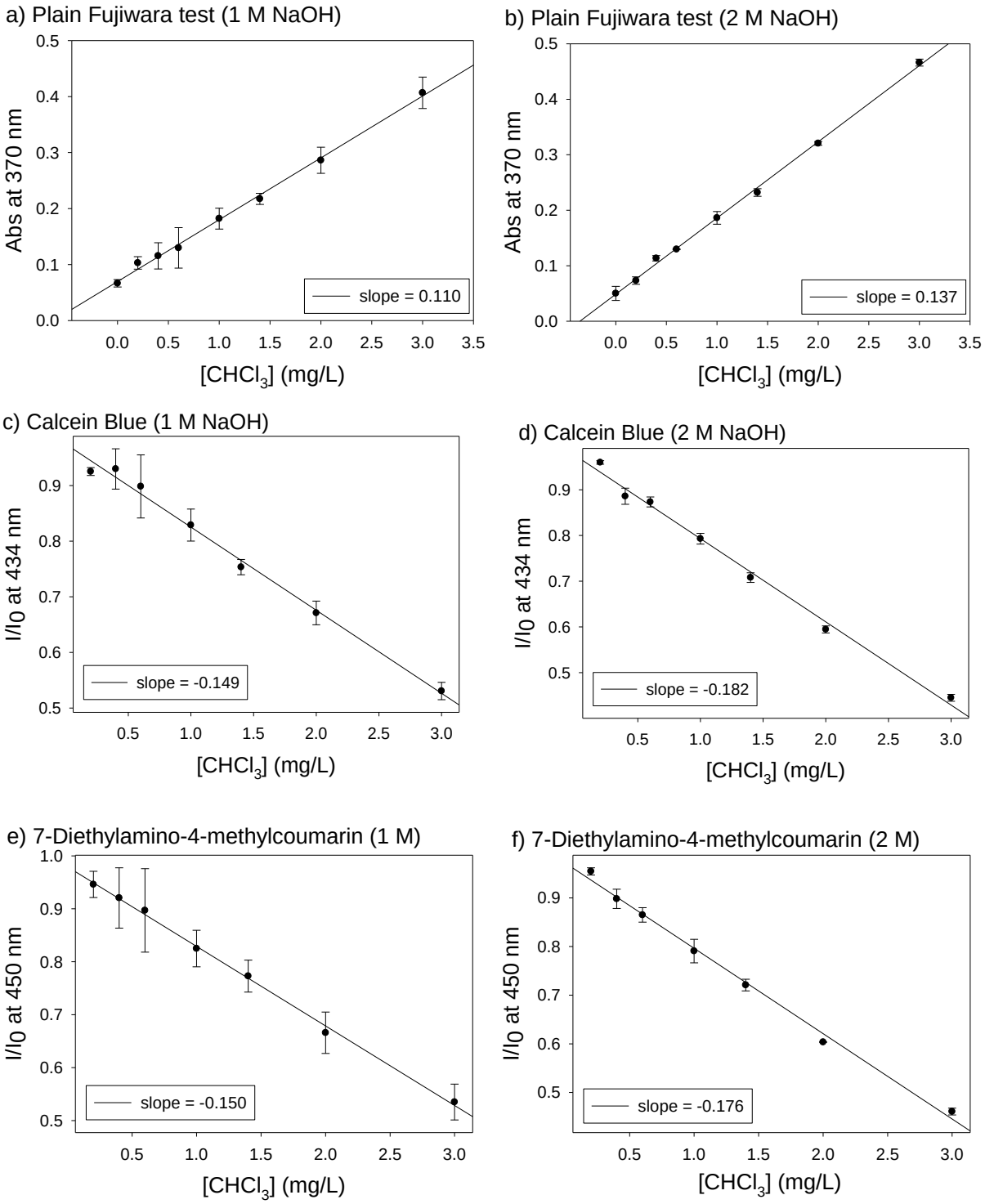

Continued on the next page.

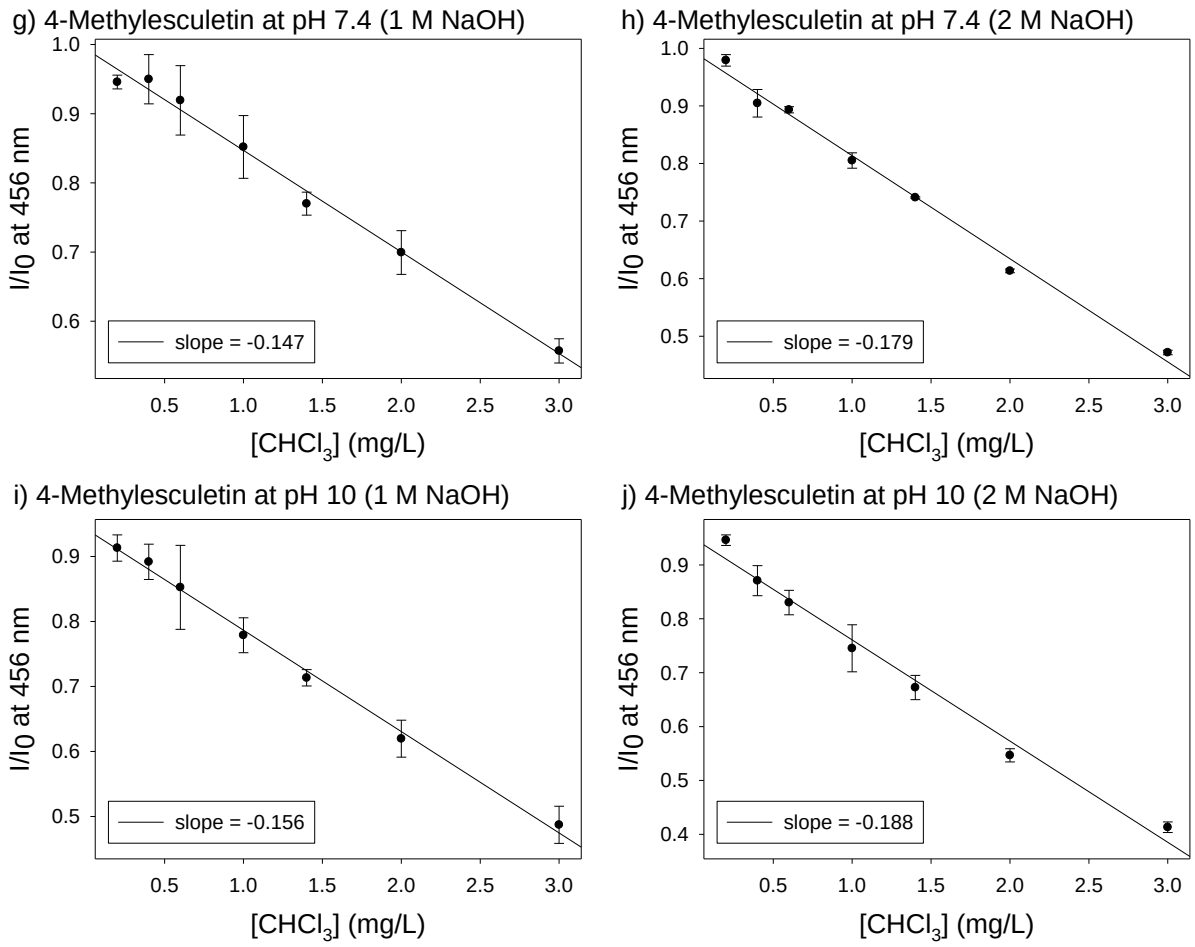

Figure 6-8 Absorbance profiles of product of Fujiwara test with various concentration of chloroform: a) and b). Fluorescence profile of placing the product of Fujiwara test between excitation light and fluorophore: c-d) calcein blue, e-f) 7-diethylamino-4-methylcoumarin, h-j) 4-methylesculetin. Left: reaction using 4 mL of aqueous 1 M NaOH; right: reaction using 4 mL of aqueous 1 M NaOH. Dye solutions were the same during experiment, and each point represents the average of three experiments with error bars. c-d) and g-h) were in 50 mM aqueous HEPES buffer at pH 7.4; e-f) were in methanol; and i-j) was in 50 mM aqueous HEPES buffer at pH 10.

6.4 Chloroform concentration determination

Once we proved that this method could provide standard curves, it was necessary to test the ability to quantitatively detect chloroform. For each unknown analysis experiment, a titration with a different chloroform concentration was first carried out to generate a standard curve, to

expand the detection range. Using absorbance measurements as an example, as shown in Figure 6-9, a standard curve was generated and the corresponding equation was y = 0.111x + 0.047. Then, four unknown samples were made by a co-worker. The same experiment was performed on these, with the results shown in Figure 6-10. Each unknown sample was measured twice, and both readings were fit to the standard curve using the same equation. The estimated concentration was marked black in Figure 6-10Right, then the actual concentration was plotted in red for comparison. In this experiment, the three unknowns with lower chloroform concentration had a better estimation of concentration, whereas the estimated [$CHCl_3$] significantly over that the actual value for sample with higher true [$CHCl_3$]. We were glad to see this result as a first success, particularly since the performance was better at lower concentration of analyte. The next step was moving to fluorescence measurements and testing their ability for concentration estimation.

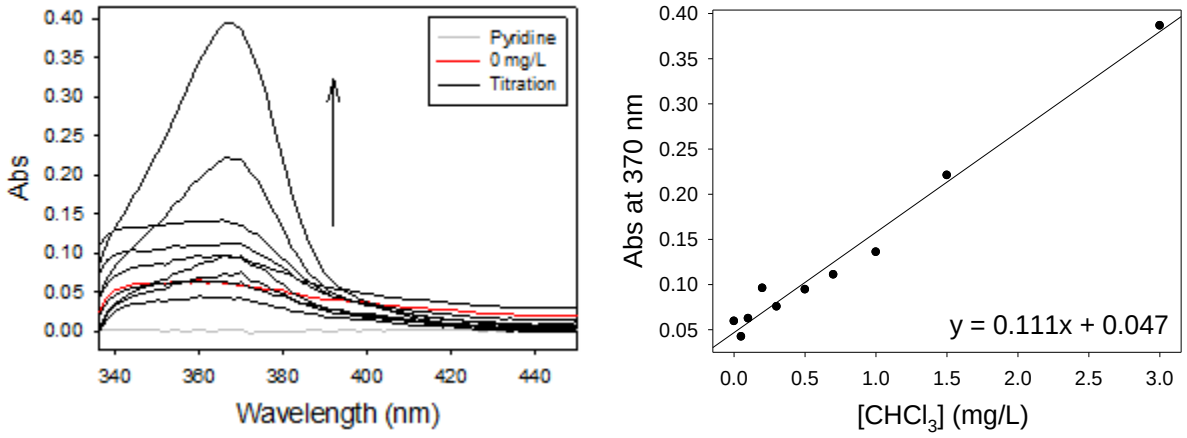

Figure 6-9 Absorbance measurements of Fujiwara test results with different concentration of chloroform. a) absorbance spectra, b) absorbance profile with linear regression line at 370 nm. Each spectra represent one reaction. Pyridine: 4 mL, 2.0 M NaOH: 4 mL.

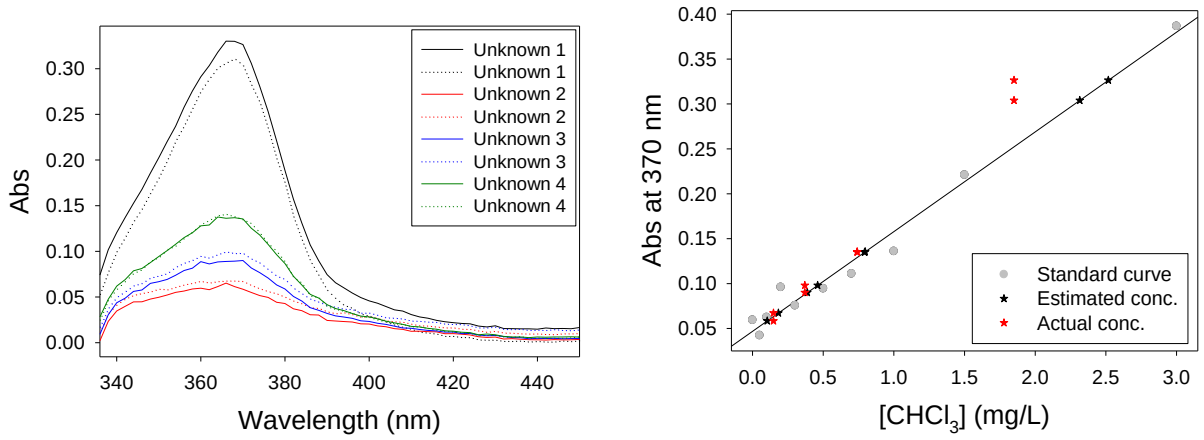

Figure 6-10 Absorbance measurements of Fujiwara test results for different unknown chloroform samples. a) absorbance spectra, b) fitting of absorbance at 370 nm to the linear regression line in Figure 6-9. Gray points: samples to generate standard curve; black points: extimated concentration using the linear regression equation; red points: actual concentration of unknown samples. Each spectrum represents one reaction. Pyridine: 4 mL, 2.0 M NaOH: 4 mL.

The absorbance and fluorescence profiles are shown in Figure 6-11Left. Figure 6-11a is the same figure as Figure 6-10b, for comparison purposes. Fluorescence spectra are not shown here for conciseness. Looking at the estimated concentration from fluorescence emission profiles for calcein blue, 7-diethylamino-4-methylcoumarin and 4-methylesculetin at pH 7.4, the first three unkown estimations seemed to be close to the actual concentration, which was exciting to see. However, measurements using 4-methylesculetin at pH 10 fluorescence emission as indicator had poor results, probably due to reduced dye stability during the experiment.

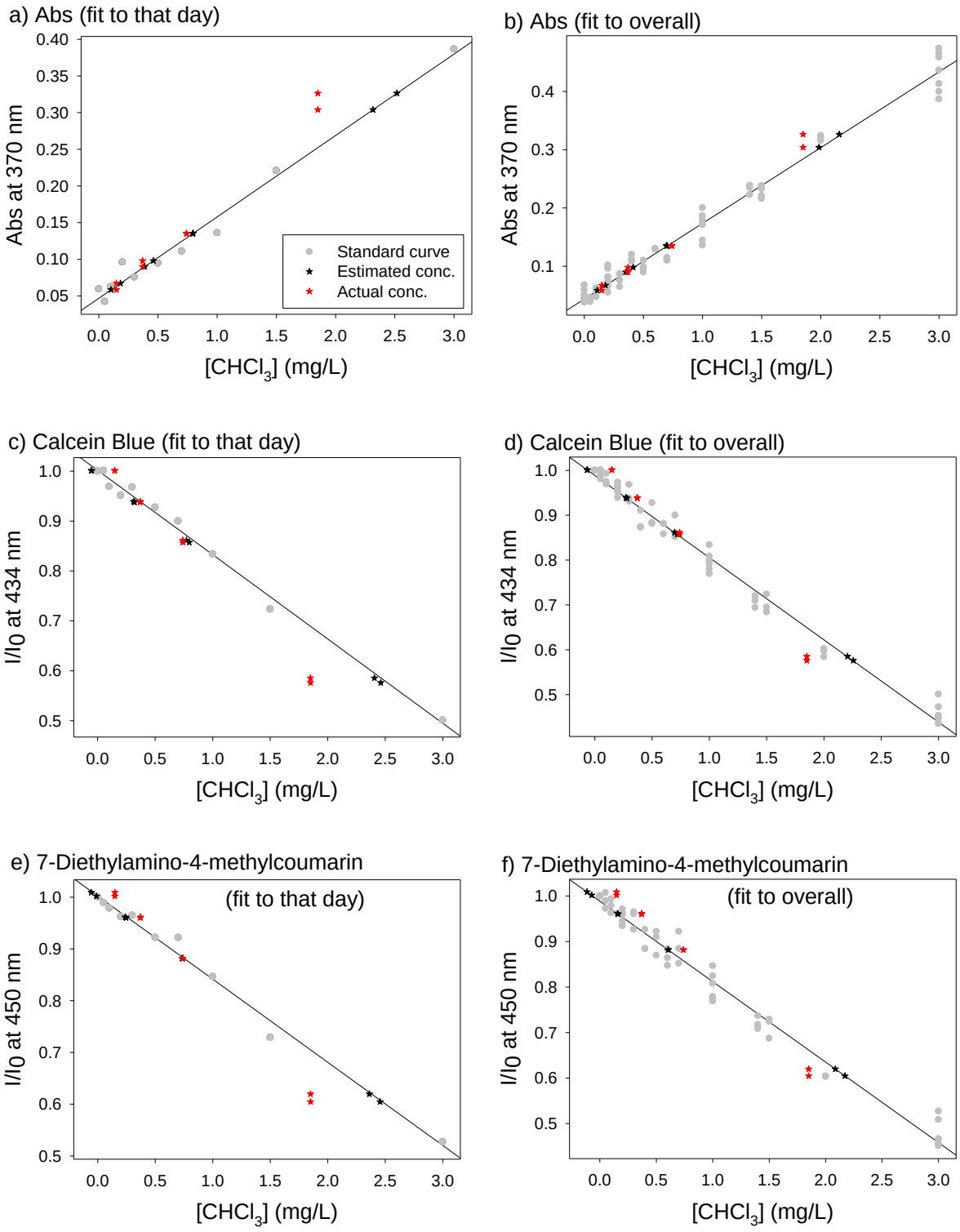

Continued on the next page.

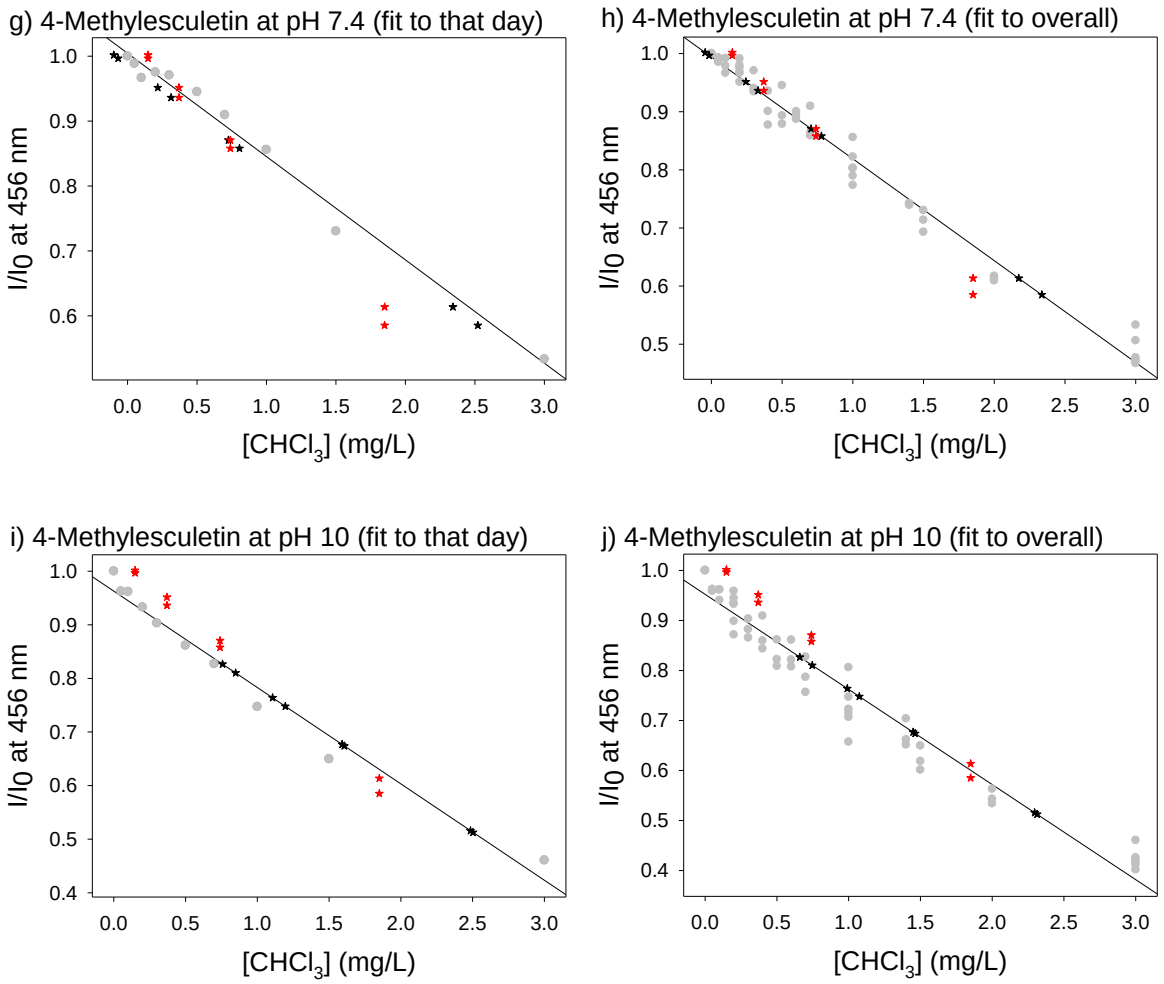

Figure 6-11 Absorbance profile of product of Fujiwara test for different unknown chloroform samples: a) and b). Fluorescence profile from placing the product of Fujiwara test between excitation light and fluorophore: c-d) calcein blue, e-f) 7-diethylamino-4-methylcoumarin, h-j) 4-methylesculetin. Left: concentration estimated by the same day's calibration curve; right: concentration estimated by the linear regression of 5 different titrations on separate day's calibration curve. Gray points: samples to generate standard curve; black points: estimated concentration using the linear regression equation; red points: actual concentration of unknown samples. Dye solutions were the same during experiment, and each point represents one reaction. c-d) and g-h) were in 50 mM aqueous HEPES buffer at pH 7.4; e-f) were in methanol; and i-j) was in 50 mM aqueous HEPES buffer at pH 10.

The experiment was repeated several times with different unknown samples: a standard curve was first generated, to which the unknown measurements were fitted. Five titrations were made and combined as an overall standard curve for each absorbance or dye fluorescence

emission. Then, each unknown was fitted to the overall standard curve, to compare with results obtained just with that day's experiment. The estimated concentration of one of the unknown samples with the highest concentration, whose estimate was far off the mark when determined using the standard curve generated on the same day, was re-estimated using the overall curve. This provided a much closer estimation. But it was very hard to compare in detail by just looking at the profiles. Therefore, two tables with the unknown samples from all experiments and the percent errors were made for direct comparison.

The comparison of estimated and actual concentration of unknown chloroform samples is shown in Table 6-1 and Table 6-2. Table 6-1 shows the estimated concentration and percent error from the standard curve generated on the same day of the sample analysis, while Table 6-2 shows the estimated concentration and percent error when fitting to the standard curve generated from all calibration data over separate dates. Percent error analysis is color-coded for clarity: cells in green stand for smaller percent error, while cells in red stand for large percent error.

Overall, the two ways of fitting did not show a significant difference. Analysis based on the absorbance measurements was unfortunately still the most accurate: fluorescence measurements of calcein blue, 7-diethylamino-4-methylcoumarin and 4-methylesculetin at pH 7.4 were acceptably accurate, but not as good as absorbance measurements; on the other hand, fluorescence measurements obtained with 4-methylesculetin at pH 10 were not accurate at all because of dye degredation during measurements, as discussed previously. Our purpose was to take the advantage of the more sensitive nature of fluorescence compared to absorbance measurements, and to get a better chloroform sensing method (higher sensitivity and lower detection limit) than just Fujiwara test. Although at this point we were able to detect and

quantitatively analyze chloroform samples, it unfortunately did not fulfill our original expectations.

Table 6-1 Comparison of the actual and estimated concentration of unknown chloroform samples with different methods: absorbance of Fujiwara test, and fluorescence. Concentrations were estimated through a calibration curve determined on the same day of the sample measurement. Red stands for large percent error; green stands for small percent error. CB = calcein blue; 4ML = 4-methylesculetin; 4MC = 7-diethylamino-4-methylcoumarin; Ave = average.

	Standard curve that day											
Actual	Abs	% error	CB	% error	4ML pH7.4	% error	4ML pH10	% error	4MC	% error	Ave	% error
0.148	0.143	3.21%	-0.054	136.45%	-0.083	156.22%	0.803	442.80%	-0.034	123.11%	-0.007	104.75%
0.259	0.279	7.61%	0.160	38.28%	0.218	15.83%	0.679	162.16%	0.219	15.58%	0.219	15.52%
0.296	0.321	8.55%	0.213	27.94%	0.292	1.47%	0.994	235.93%	0.274	7.35%	0.275	7.05%
0.37	0.424	14.57%	0.316	14.58%	0.265	28.28%	1.151	211.01%	0.242	34.49%	0.312	15.70%
0.666	0.720	8.06%	0.785	17.89%	0.834	25.23%	1.453	118.19%	0.737	10.65%	0.769	15.45%
0.74	0.866	17.07%	0.903	22.05%	0.940	27.07%	1.300	75.72%	0.886	19.78%	0.899	21.49%
0.74	0.795	7.44%	0.784	5.95%	0.766	3.48%	1.598	115.94%	0.734	0.87%	0.770	4.00%
0.962	0.941	2.15%	0.935	2.86%	1.022	6.20%	1.791	86.22%	1.033	7.34%	0.983	2.13%
1.295	1.486	14.78%	1.572	21.37%	1.614	24.63%	1.943	50.04%	1.592	22.94%	1.566	20.93%
1.85	2.416	30.61%	2.434	31.54%	2.432	31.44%	2.494	34.80%	2.408	30.19%	2.422	30.94%
2.368	1.416	40.19%	1.535	35.16%	1.534	35.23%	2.183	7.81%	1.473	37.81%	1.490	37.10%

Table 6-2 Comparison of the actual and estimated concentration of unknown chloroform samples with different methods: absorbance of Fujiwara test, and fluorescence. Concentrations were estimated through a calibration curve determined on all experiment titrations. Red stands for large percent error; green stands for small percent error. CB = calcein blue; 4ML = 4-methylesculetin; 4MC = 7-diethylamino-4-methylcoumarin; Ave = average.

	Standard curve overall											
Actual	Abs	% error	CB	% error	4ML pH7.4	% error	4ML pH10	% error	4MC	% error	Ave	% error
0.148	0.144	2.50%	-0.066	144.86%	-0.030	120.27%	0.703	375.10%	-0.093	163.01%	-0.011	107.66%
0.259	0.313	20.69%	0.199	23.20%	0.269	3.69%	0.713	175.15%	0.300	15.83%	0.270	4.25%
0.296	0.200	32.43%	0.193	34.66%	0.309	4.26%	1.121	278.56%	0.201	31.94%	0.226	23.70%
0.37	0.382	3.26%	0.275	25.57%	0.287	22.47%	1.032	179.01%	0.158	57.24%	0.276	25.51%
0.666	0.571	14.26%	0.756	13.51%	0.829	24.53%	1.577	136.76%	0.646	3.04%	0.701	5.19%
0.74	0.891	20.43%	0.946	27.90%	1.008	36.18%	1.340	81.12%	0.975	31.82%	0.955	29.08%
0.74	0.697	5.86%	0.708	4.37%	0.741	0.19%	1.456	96.76%	0.605	18.23%	0.688	7.07%
0.962	0.778	19.18%	0.903	6.16%	1.009	4.93%	1.913	98.90%	0.930	3.36%	0.905	5.94%
1.295	1.502	15.98%	1.619	25.01%	1.697	31.01%	1.990	53.67%	1.689	30.42%	1.627	25.61%
1.85	2.070	11.90%	2.231	20.59%	2.255	21.90%	2.304	24.56%	2.129	15.06%	2.171	17.36%
2.368	1.220	48.49%	1.494	36.92%	1.501	36.62%	2.303	2.74%	1.352	42.89%	1.392	41.23%

6.5 Conclusion and future works

In this ongoing project, we developed a method to determine the concentration of chloroform in water samples by excitation-modulated fluorescence. Chloroform reacts with the Fujiwara test reagents (pyridine and a strong base NaOH) and produces a colored product with

maximum absorption at 370 nm. This product was used as an optical filter to modulate the emission of appropriately chosen standard fluorophores with excitation around 370 nm, therefore being able to quantify unknown chloroform samples. Because fluorescence measurements are typically more sensitive than absorbance measurement, we hoped to achieve an amplification of the analytical signal and a lower detection limit using this method than with the traditional Fujiwara test. So far, we were able to determine the concentration of $CHCl_3$ in unknown samples using three dyes: calcein blue, 7-diethylamino-4-methylcoumarin and 4-methylesculetin. However, we have not yet been able to improve on the sensitivity of the absorbance-based Fujiwara test.

6.6 Experimental details

6.6.1 Materials

Pyridine purchased from Sigma Aldrich was used as received; pyridine purchased from Beantown Chemical had to be distilled before use. Dye solutions were prepared from calcein blue purchased from Sigma Aldrich; and 6,7-Dihydroxy-4-methylcoumarin and 7-diethylamino-4-methylcoumarin from Alfa Aesar. 50 mM 4-(2-hydroxyethyl) piperazine-1-ethanesulfonic acid (HEPES) buffer was prepared from HEPES purchased from IBI Scientific. Its pH was adjusted using aqueous solutions of NaOH and HCl. NaOH was purchased from Fisher Scientific, and HCl was purchased from BDH Aristar. Chloroform and methanol were purchased from BDH. Materials were used as received unless mentioned specifically.

6.6.2 Instrumentation

Absorbance measurements were carried out on an HP 8452A diode array spectrophotometer, with the measuring range from 230 nm to 800 nm and a 2 nm wavelength resolution. Fluorescence emission measurements were carried out on an ISS PC1

spectrofluorometer, with an excitation light source as a broad-spectrum high-pressure xenon lamp (CERMAX, 300W); manual calibrated slits; excitation correction by a rhodamine B quantum counter with a dedicated detector; and emission light detector was a Hamamatsu red-sensitive PMT operating in photon-counting mode. For all spectroscopic experiments, an external circulating water bath was used to control the cuvette temperature as 25 °C.

6.6.3 Dye solution conditions

0.6 µM of calcein blue solution was prepared in 50 mM HEPES buffer at pH 7.4. 0.9 µM of 7-diethylamino-4-methylcoumarin solution was prepared in methanol. 3.0 µM of 4-methylesculetin solution was prepared by first dissolving the dye in a minimum amount of methanol and then diluting with 50 mM HEPES buffer at pH 7.4, another sample was then being adjusted to pNaOH solutions were prepared in DL water.

6.6.4 Procedures

Fujiwara test was carried out by adding chloroform to the pyridine layer of Fujiwara reagent (pyridine and NaOH in a 1:1 volume ratio). The mixture was heated in a boiling water bath for 2 minutes, cooled down to room temperature and then put in an ice water bath for 15 minutes. The top pyridine layer was then taken for centrifugation to remove any of the aqueous suspensions. Finally, the reacted pyridine layer was measured for absorbance in a 1 cm quartz cuvette. Fluorescence measurements were carried out by positioning a cuvette containing the Fujiwara product between the excitation light source and the measurement cuvette containing the fluorescent dye.

CHAPTER 7
SUMMARY AND PERSPECTIVE

We have established the use of PAMAM dendrimers as receptors for the sensing and discrimination of carboxylate analytes, including citric acid cycle intermediates and β-lactam antibiotics, in neutral aqueous media. Through an indicator displacement assay based on common commercially-available organic dyes, we were able to monitor the interaction between the spectroscopically silent poly(amidoamine) (PAMAM) dendrimer host molecules and analyte guest molecules through optical methods (UV-vis absorption, fluorescence emission and anisotropy intensity). We focused on optical spectroscopy methods particularly because of their low-cost, accessibility, and ubiquitous presence in any analytical laboratory; additionally, this instrumentation lends itself easily to miniaturization and field deployment using solid-state components such as LED light sources and photodiode array detectors, so its use enables our methods to be considered for portable device development and point-of-use measurement. The resulting datasets were processed through well-known pattern-based recognition algorithms, such as principal component analysis (PCA) and linear discriminant analysis (LDA), to generate unique response patterns for each analyte, and therefore achieve the discrimination. These well-established algorithms, based on optimized matrix algebra routines and available in most high-level programming languages, are fast and have very low computational demands, so they are well compatible with low-power portable devices.

A notable improvement introduced here is a general method to determine the concentration of samples whose identity has been established through pattern-based recognition

systems. Normally, these systems perform very well in qualitative differentiation of analytes (i.e. identity determination); however, they often do not easily provide quantitative information. In this work, we showed that one of the detection methods available to us, fluorescence anisotropy, was almost completely insensitive to the *identity* of the carboxylate species under study, but sensitive to the total *concentration* of carboxylates. Thus, combining the quantitative information, obtained through fluorescence anisotropy measurements after appropriate calibration, with the qualitative (identity) information obtained from the pattern-based recognition approach, we were able to use the [calcein•PAMAM] sensor to determine identity and concentration of unknown samples containing carboxylate analytes. When confronted with unidentified samples, the system performed with 100% correct identification rate and with 50% maximum error of quantification. This was particularly noteworthy because previously reported systems struggled to accomplish the simultaneous determination of the concentration and the identity of a sample through pattern-based recognition.

We also successfully transferred the carboxylate sensing system from solution, where it was originally developed, to a solid support. Among the solid supports tested, chromatography paper performed the best, with excellent differentiation and repeatability, and an improvement on the shelf-life of the sensing system compared to the same system in aqueous media.

The dye-PAMAM sensor showed a promising result for the discrimination of carboxylate anions. In the future, it will be interesting to expand the dye sensor panel and analyte pool, to be able to discriminate even more structurally similar analyte. More solid support candidates could also be investigated, such as cloth, fabrics, and structurally more robust cardboard.

Another interesting avenue of future research is in the simplification and streamlining of data acquisition, with an eye towards using portable instrumentation. Ultimately, it would be

interesting to explore the use of cellphone cameras, now ubiquitous and typically high quality, instead of a laboratory-based microwell plate reader for data assumption. If cell phone cameras can be used, the processing power available on modern portable devices is more than enough to carry out the necessary data processing once the method has been optimized in lab conditions.

Finally, our work on improving the sensitivity of the colorimetric Fujiwara test for detecting the concentration of chloroform samples using excitation-modulated fluorescence showed some preliminary advances, but more work is needed to improve on experimental conditions. In particular, future work will focus on replacing the harsh conditions currently required to carry out the assay; an attempt will also be made to reduce the use of pyridine (which is highly flammable and has deleterious health implications), to transition the assay to a single phase from the current biphasic conditions, and ultimately to improve the sensitivity of the assay as well as lower the error of determination.

REFERENCES

(1) Schneider, H.-J. Binding mechanisms in supramolecular complexes. *Angew. Chem., Int. Ed.* 2009, *48*, 3924-3977.

(2) Lehn, J. M. Perspectives in supramolecular chemistry: from molecular recognition to molecular information processing and self organization. *Angew. Chem.* 1990, *102*, 1347-1362.

(3) Linclau, B.; Arda, A.; Reichardt, N.-C.; Sollogoub, M.; Unione, L.; Vincent, S. P.; Jimenez-Barbero, J. Fluorinated carbohydrates as chemical probes for molecular recognition studies. Current status and perspectives. *Chem. Soc. Rev.* 2020, *49*, 3863-3888.

(4) Gimeno, A.; Reichardt, N.-C.; Canada, F. J.; Perkams, L.; Unverzagt, C.; Jimenez-Barbero, J.; Arda, A. NMR and molecular recognition of N-glycans: remote modifications of the saccharide chain modulate binding features. *ACS Chem. Biol.* 2017, *12*, 1104-1112.

(5) Jeon, H. B.; Park, S.; Ryu, K. R.; Ghosh, S. K.; Jung, J.; Park, K. M.; Ha, J. W. In situ reversible tuning of chemical interface damping in single gold nanorod-based recyclable platforms through manipulation of supramolecular host-guest interactions. *Chem. Sci.* 2021, *12*, 7115-7124.

(6) Clarke, D. E.; Wu, G.; Wu, C.; Scherman, O. A. Host-guest induced peptide folding with sequence-specific structural chirality. *J. Am. Chem. Soc.* 2021, *143*, 6323–6327.

(7) Kurniawan, Y. S.; Sathuluri, R. R.; Ohto, K. *Droplet microfluidic device for rapid and efficient metals separation using host-guest chemistry*; IntechOpen Ltd., 2020.

(8) Banti, C. N.; Raptopoulou, C. P.; Psycharis, V.; Hadjikakou, S. K. Novel silver glycinate conjugate with 3D polymeric intermolecular self-assembly architecture; an antiproliferative agent which induces apoptosis on human breast cancer cells. *J. Inorg. Biochem.* 2021, *216*, 111351.

(9) Shibata, M.; Matsumoto, M.; Hirai, Y.; Takenaka, M.; Sawamoto, M.; Terashima, T. Intramolecular folding or intermolecular self-assembly of amphiphilic random copolymers: on-demand control by pendant design. *Macromolecules* 2018, *51*, 3738-3745.

(10) Paluch, K. J.; Tajber, L.; McCabe, T.; O'Brien, J. E.; Corrigan, O. I.; Healy, A. M. Preparation and solid state characterization of chlorothiazide sodium intermolecular self-assembly suprastructure. *Eur. J. Pharm. Sci.* 2010, *41*, 603-611.

(11) Chakraborty, G.; Chowdhury, M. P.; Saha, S. K. Solvent-induced molecular folding and self-assembled nanostructures of tyrosine and tryptophan analogues in aqueous solution: Fascinating morphology of high order. *Langmuir* 2017, *33*, 6581-6594.

(12) Katoono, R.; Tanaka, Y.; Fujiwara, K.; Suzuki, T. A foldable cyclic oligomer: chiroptical modulation through molecular folding upon complexation and a change in temperature. *J. Org. Chem.* 2014, *79*, 10218-10225.

(13) Zhao, W.; Wang, R.; Mosey, N. J.; Petitjean, A. Alkoxyamine-derived formamidines: configurational control and molecular folding. *Org. Lett.* 2011, *13*, 5160-5163.

(14) Wanasinghe, S. V.; Schreiber, E. M.; Thompson, A. M.; Sparks, J. L.; Konkolewicz, D. Dynamic covalent chemistry for architecture changing interpenetrated and single networks. *Polym. Chem.* 2021, *12*, 1975-1982.

(15) Liu, F.; Niko, Y.; Bouchaala, R.; Mercier, L.; Lefebvre, O.; Andreiuk, B.; Vandamme, T.; Goetz, J. G.; Anton, N.; Klymchenko, A. Drug-sponge lipid nanocarrier for in situ cargo loading and release using dynamic covalent chemistry. *Angew. Chem., Int. Ed.* 2021, *60*, 6573-6580.

(16) Behera, P. K.; Raut, S. K.; Mondal, P.; Sarkar, S.; Singha, N. K. Self-healable polyurethane elastomer based on dual dynamic covalent chemistry using Diels-Alder "click" and disulfide metathesis reactions. *ACS Appl. Polym. Mater.* 2021, *3*, 847-856.

(17) You, L.; Zha, D.; Anslyn, E. V. Recent advances in supramolecular analytical chemistry using optical sensing. *Chem. Rev.* 2015, *115*, 7840-7892.

(18) Stephan, H.; Kubeil, M.; Gloe, K.; Gloe, K. Extraction methods for supramolecular analytical chemistry. In *Analytical Methods in Supramolecular Chemistry, 2nd*; Wiley-VCH Verlag GmbH & Co. KGaA: 2012; Vol. 1, p 105-127.

(19) Mutihac, R.-C.; Bunaciu, A. A.; Buschmann, H.-J.; Mutihac, L. A brief overview on supramolecular analytical chemistry of cucurbit[n]urils and hemicucurbit[n]urils. *J. Inclusion Phenom. Macrocyclic Chem.* 2020, *98*, 137-148.

(20) Anslyn, E. V., and Dennis A. Dougherty *Modern Physical Organic Chemistry*; Univ. Science Books: Sausalito, Calif., 2005.

(21) Hillyer, M. B.; Gibb, B. C. Molecular shape and the hydrophobic effect. *Annu. Rev. Phys. Chem.* 2016, *67*, 307-329.

(22) Ben-Amotz, D. Water-mediated hydrophobic interactions. *Annu. Rev. Phys. Chem.* 2016, *67*, 617-638.

(23) Mahadevi, A. S.; Sastry, G. N. Cation-π interaction: its role and relevance in chemistry, biology, and material science. *Chem. Rev.* 2013, *113*, 2100-2138.

(24) Riley, K. E.; Hobza, P. On the importance and origin of aromatic interactions in chemistry and biodisciplines. *Acc. Chem. Res.* 2013, *46*, 927-936.

(25) Prasanna de Silva, A.; McCaughan, B.; McKinney, B. O. F.; Querol, M. Newer optical-based molecular devices from older coordination chemistry. *Dalton Trans.* 2003, 1902-1913.

(26) Ni, W.; Kaur, G.; Springsteen, G.; Wang, B.; Franzen, S. Regulating the fluorescence intensity of an anthracene boronic acid system: a B-N bond or a hydrolysis mechanism? *Bioorg. Chem.* 2004, *32*, 571-581.

(27) Zhu, L.; Shabbir, S. H.; Gray, M.; Lynch, V. M.; Sorey, S.; Anslyn, E. V. A Structural Investigation of the N-B Interaction in an o-(N,N-Dialkylaminomethyl)arylboronate System. *J. Am. Chem. Soc.* 2006, *128*, 1222-1232.

(28) Wright, A. T.; Zhong, Z.; Anslyn, E. V. A functional assay for heparin in serum using a designed synthetic receptor. *Angew. Chem., Int. Ed.* 2005, *44*, 5679-5682.

(29) Loudet, A.; Burgess, K. BODIPY dyes and their derivatives: Syntheses and spectroscopic properties. *Chem. Rev.* 2007, *107*, 4891–4932.

(30) Melendez, R. E.; Carr, A. J.; Linton, B. R.; Hamilton, A. D. Controlling hydrogen bonding: from molecular recognition to organogelation. *Struct. Bonding* 2000, *96*, 31-61.

(31) Sedgwick, A. C.; Brewster, J. T., II; Wu, T.; Feng, X.; Bull, S. D.; Qian, X.; Sessler, J. L.; James, T. D.; Anslyn, E. V.; Sun, X. Indicator displacement assays (IDAs): the past, present and future. *Chem. Soc. Rev.* 2021, *50*, 9-38.

(32) Sasaki, Y.; Lyu, X.; Zhou, Q.; Minami, T. Indicator displacement assay-based chemosensor arrays for saccharides using off-the-shelf materials toward simultaneous on-site detection on paper. *Chem. Lett.* 2021, *50*, 987-995.

(33) Hu, C.; Grimm, L.; Prabodh, A.; Baksi, A.; Siennicka, A.; Levkin, P. A.; Kappes, M. M.; Biedermann, F. Covalent cucurbit[7]uril-dye conjugates for sensing in aqueous saline media and biofluids. *Chem. Sci.* 2020, *11*, 11142-11153.

(34) Tobey, S. L.; Anslyn, E. V. Energetics of phosphate binding to ammonium and guanidinium containing metallo-receptors in water. *J. Am. Chem. Soc.* 2003, *125*, 14807-14815.

(35) Zwicker, V. E.; Sergeant, G. E.; New, E. J.; Jolliffe, K. A. A colorimetric sensor array for the classification of biologically relevant tri-, di- and mono-phosphates. *Org. Biomol. Chem.* 2021, *19*, 1017-1021.

(36) Yang, Y.; Chen, P.; Liu, Y.; Cai, Z.; Wang, X.; Me, Y.; Ding, X.; Lin, L.; Jiang, H.; Zhang, Z.; Ju, Y. A colorimetric indicator-displacement assay based on stable Cu^{2+} selective carbon dots for fluorescence turn-on detection of pyrophosphate anions in urine. *Spectrochim. Acta, Part A* 2021, *251*, 119479.

(37) Razavi, F.; Khajehsharifi, H. A colorimetric paper-based sensor with nanoporous SBA-15 for simultaneous determination of histidine and cysteine in urine samples. *Chem. Pap.* 2021, *75*, 3401–3410.

(38) Fukushima, Y.; Aikawa, S. Colorimetric detection of homocysteine by a pyridylazo dye-based Cu^{2+} complex via indicator displacement mechanism. *Anal. Biochem.* 2021, *621*, 114185.

(39) Vance, D. H.; Czarnik, A. W. Real-time assay of inorganic pyrophosphatase using a high-affinity chelation-enhanced fluorescence chemosensor. *J. Am. Chem. Soc.* 1994, *116*, 9397-9398.

(40) Prasanna de Silva, A.; Gunaratne, H. Q. N.; Gunnlaugsson, T.; Nieuwenhuizen, M. Fluorescent switches with high selectivity towards sodium ions: correlation of ion-induced conformation switching with fluorescence function. *Chem. Commun.* 1996, 1967-1968.

(41) Phillips, M. D.; James, T. D. Boronic acid based modular fluorescent sensors for glucose. *J. Fluoresc.* 2004, *14*, 549-559.

(42) Ihde, M. H.; Pridmore, C. F.; Bonizzoni, M. Pattern-based recognition systems: overcoming the problem of mixtures. *Anal. Chem.* 2020, *92*, 16213-16220.

(43) Buryak, A.; Severin, K. A Chemosensor Array for the Colorimetric Identification of 20 Natural Amino Acids. *J. Am. Chem. Soc.* 2005, *127*, 3700-3701.

(44) Sasaki, Y.; Lyu, X.; Kubota, R.; Takizawa, S.-y.; Minami, T. Easy-to-Prepare Mini-Chemosensor Array for Simultaneous Detection of Cysteine and Glutathione Derivatives. *ACS Appl. Bio Mater.* 2021, *4*, 2113-2119.

(45) Wang, B.; Han, J.; Bojanowski, N. M.; Bender, M.; Ma, C.; Seehafer, K.; Herrmann, A.; Bunz, U. H. F. An optimized sensor array identifies all natural amino acids. *ACS Sens.* 2018, *3*, 1562-1568.

(46) Sun, W.; Lu, Y.; Mao, J.; Chang, N.; Yang, J.; Liu, Y. Multidimensional sensor for pattern recognition of proteins based on DNA-gold nanoparticles conjugates. *Anal. Chem.* 2015, *87*, 3354-3359.

(47) Pode, Z.; Peri-Naor, R.; Georgeson, J. M.; Ilani, T.; Kiss, V.; Unger, T.; Markus, B.; Barr, H. M.; Motiei, L.; Margulies, D. Protein recognition by a pattern-generating fluorescent molecular probe. *Nat. Nanotechnol.* 2017, *12*, 1161-1168.

(48) Xu, S.; Lu, X.; Yao, C.; Huang, F.; Jiang, H.; Hua, W.; Na, N.; Liu, H.; Ouyang, J. A visual sensor array for pattern recognition analysis of proteins using novel blue-emitting fluorescent gold nanoclusters. *Anal. Chem.* 2014, *86*, 11634-11639.

(49) Bicker, K. L.; Sun, J.; Harrell, M.; Zhang, Y.; Pena, M. M.; Thompson, P. R.; Lavigne, J. J. Synthetic lectin arrays for the detection and discrimination of cancer associated glycans and cell lines. *Chem. Sci.* 2012, *3*, 1147-1156.

(50) Silva, M. L. S. Lectin biosensors in cancer glycan biomarker detection. *Adv. Clin. Chem.* 2019, *93*, 1-61.

(51) Phillips, R. L.; Miranda, O. R.; You, C.-C.; Rotello, V. M.; Bunz, U. H. F. Rapid and efficient identification of bacteria using gold-nanoparticle-poly(para-phenyleneethynylene) constructs. *Angew. Chem., Int. Ed.* 2008, *47*, 2590-2594.

(52) Ngernpimai, S.; Geng, Y.; Makabenta, J. M.; Landis, R. F.; Keshri, P.; Gupta, A.; Li, C.-H.; Chompoosor, A.; Rotello, V. M. Rapid identification of biofilms using a robust multichannel polymer sensor array. *ACS Appl. Mater. Interfaces* 2019, *11*, 11202-11208.

(53) Tan, S. S.; Kim, S.-J.; Kool, E. T. Differentiating between fluorescence-quenching metal Ions with polyfluorophore sensors built on a DNA backbone. *J. Am. Chem. Soc.* 2011, *133*, 2664-2671.

(54) Mallet, A. M.; Davis, A. B.; Davis, D. R.; Panella, J.; Wallace, K. J.; Bonizzoni, M. A cross reactive sensor array to probe divalent metal ions. *Chem. Commun.* 2015, *51*, 16948-16951.

(55) Liang, X.; Bonizzoni, M. Boronic acid-modified poly(amidoamine) dendrimers as sugar-sensing materials in water. *J. Mater. Chem. B* 2016, *4*, 3094-3103.

(56) Liang, X.; Trentle, M.; Kozlovskaya, V.; Kharlampieva, E.; Bonizzoni, M. Carbohydrate sensing using water-soluble poly(methacrylic acid)-co-3-(acrylamido)phenylboronic acid copolymer. *ACS Appl. Polym. Mater.* 2019, *1*, 1341-1349.

(57) Liu, Y.; Bonizzoni, M. A supramolecular sensing array for qualitative and quantitative analysis of organophosphates in water. *J. Am. Chem. Soc.* 2014, *136*, 14223-14229.

(58) Mallet, A. M.; Liu, Y.; Bonizzoni, M. An off-the-shelf sensing system for physiological phosphates. *Chem. Commun.* 2014, *50*, 5003-5006.

(59) Zhang, C.; Suslick, K. S. A colorimetric sensor array for organics in water. *J. Am. Chem. Soc.* 2005, *127*, 11548-11549.

(60) Huang, W.; Bender, M.; Seehafer, K.; Wacker, I.; Schroeder, R. R.; Bunz, U. H. F. A tetraphenylethene-based polymer array discriminates nitroarenes. *Macromolecules* 2018, *51*, 1345-1350.

(61) Pushina, M.; Farshbaf, S.; Shcherbakova, E. G.; Anzenbacher, P. A dual chromophore sensor for the detection of amines, diols, hydroxy acids, and amino alcohols. *Chem. Commun.* 2019, *55*, 4495-4498.

(62) Askim, J. R.; Li, Z.; La Gasse, M. K.; Rankin, J. M.; Suslick, K. S. An optoelectronic nose for identification of explosives. *Chem. Sci.* 2016, *7*, 199-206.

(63) Eaidkong, T.; Mungkarndee, R.; Phollookin, C.; Tumcharern, G.; Sukwattanasinitt, M.; Wacharasindhu, S. Polydiacetylene paper-based colorimetric sensor array for vapor phase detection and identification of volatile organic compounds. *J. Mater. Chem.* 2012, *22*, 5970-5977.

(64) Lin, H.; Jang, M.; Suslick, K. S. Preoxidation for colorimetric sensor array detection of VOCs. *J. Am. Chem. Soc.* 2011, *133*, 16786-16789.

(65) Li, Z.; Suslick, K. S. Colorimetric sensor array for monitoring CO and ethylene. *Anal. Chem.* 2019, *91*, 797-802.

(66) Rakow, N. A.; Suslick, K. S. A colorimetric sensor array for odor visualization. *Nature* 2000, *406*, 710-713.

(67) Takeuchi, T.; Montenegro, J.; Hennig, A.; Matile, S. Pattern generation with synthetic sensing systems in lipid bilayer membranes. *Chem. Sci.* 2011, *2*, 303-307.

(68) Umali, A. P.; LeBoeuf, S. E.; Newberry, R. W.; Kim, S.; Tran, L.; Rome, W. A.; Tian, T.; Taing, D.; Hong, J.; Kwan, M.; Heymann, H.; Anslyn, E. V. Discrimination of flavonoids and red wine varietals by arrays of differential peptidic sensors. *Chem. Sci.* 2011, *2*, 439-445.

(69) Jikei, M.; Kakimoto, M.-a. Hyperbranched polymers: a promising new class of materials. *Prog. Polym. Sci.* 2001, *26*, 1233-1285.

(70) Bhat, S. I.; Ahmadi, Y.; Ahmad, S. Recent advances in structural modifications of hyperbranched polymers and their applications. *Ind. Eng. Chem. Res.* 2018, *57*, 10754-10785.

(71) Bonizzoni, M.; Long, S. R.; Rainwater, C.; Anslyn, E. V. PAMAM dendrimer-induced aggregation of 5(6)-carboxyfluorescein. *J. Org. Chem.* 2012, *77*, 1258-1266.

(72) Ihde, M. H.; Steelman, A. M.; Bonizzoni, M. Fluorescent Probes for the Supramolecular Interactions responsible for Binding of Polycyclic Aromatic Hydrocarbons to Hyperbranched Polyelectrolytes in Aqueous Media. *Israel Journal of Chemistry* 2021, *61*, 261-272.

(73) Tang, M.; Redemann, C. T.; Szoka, F. C., Jr. In vitro gene delivery by degraded polyamidoamine dendrimers. *Bioconjugate Chem.* 1996, *7*, 703-714.

(74) Tomalia, D. A.; Baker, H.; Dewald, J.; Hall, M.; Kallos, G.; Martin, S.; Roeck, J.; Ryder, J.; Smith, P. A new class of polymers: Starburst-dendritic macromolecules. *Polym. J.* 2002, *34*, 132-147.

(75) Esfand, R.; Tomalia, D. A. Poly(amidoamine) (PAMAM) dendrimers: from biomimicry to drug delivery and biomedical applications. *Drug Discovery Today* 2001, *6*, 427-436.

(76) http://www.dendritech.com/index.html accessed 06.07.2021

(77) Gogulapati, N.; Manalan, B. V.; Nadendla, R. R. Poly (propylene imine) dendrimer: synthesis, characterization and applications in various drug delivery. *Asian J. Pharm. Pharmacol.* 2020, *6*, 190-203.

(78) Duncan, R. The dawning era of polymer therapeutics. *Nat. Rev. Drug Discovery* 2003, *2*, 347-360.

(79) Wang, J.; Cooper, R. C.; Yang, H. Polyamidoamine dendrimer grafted with an acid-responsive charge-reversal layer for improved gene delivery. *Biomacromolecules* 2020, *21*, 4008-4016.

(80) Smith, P. E. S.; Brender, J. R.; Durr, U. H. N.; Xu, J.; Mullen, D. G.; Banaszak Holl, M. M.; Ramamoorthy, A. Solid-state NMR reveals the hydrophobic-core location of poly(amidoamine) dendrimers in biomembranes. *J. Am. Chem. Soc.* 2010, *132*, 8087-8097.

(81) Willerich, I.; Li, Y.; Grohn, F. Influencing particle size and stability of ionic dendrimer-dye assemblies. *J. Phys. Chem. B* 2010, *114*, 15466-15476.

(82) Kaewtong, C.; Jiang, G.; Ponnapati, R.; Pulpoka, B.; Advincula, R. Redox nanoreactor dendrimer boxes: in situ hybrid gold nanoparticles via terthiophene and carbazole peripheral dendrimer oxidation. *Soft Matter* 2010, *6*, 5316-5319.

(83) Niu, Y.; Sun, L.; Crooks, R. M. Determination of the intrinsic proton binding constants for poly(amidoamine) dendrimers via potentiometric pH titration. *Macromolecules* 2003, *36*, 5725-5731.

(84) Jolly, A. M.; Bonizzoni, M. PAMAM dendrimers as supramolecular hosts through non-covalent interactions. *Supramol. Chem.* 2015, *27*, 151-160.

(85) Viltres, H.; Lopez, Y. C.; Leyva, C.; Gupta, N. K.; Naranjo, A. G.; Acevedo-Pena, P.; Sanchez-Diaz, A.; Bae, J.; Kim, K. S. Polyamidoamine dendrimer-based materials for environmental applications: A review. *J. Mol. Liq.* 2021, *334*, 116017.

(86) Omar, N. A. S.; Fen, Y. W.; Ramli, I.; Sadrolhosseini, A. R.; Abdullah, J.; Yusof, N. A.; Kamil, Y. M.; Mahdi, M. A. An optical sensor for dengue envelope proteins using polyamidoamine dendrimer biopolymer-based nanocomposite thin film: enhanced sensitivity, selectivity, and recovery studies. *Polymers* 2021, *13*, 762.

(87) Nguyen, N. H.; Dang, L. H.; Doan, P.; Huynh, C. K.; Nguyen, C. K.; Nguyen, B. T.; Nguyen, N. T.; Tran, N. Q. Polyacrylic-conjugated polyamidoamine G4.0 dendrimer as a potential nanocarrier for effective delivery of cisplatin. *Bull. Mater. Sci.* 2021, *44*, 87.

(88) Ban, J.; Li, S.; Zhan, Q.; Li, X.; Xing, H.; Chen, N.; Long, L.; Hou, X.; Zhao, J.; Yuan, X. PMPC modified PAMAM dendrimer enhances brain tumor-targeted drug delivery. *Macromol. Biosci.* 2021, *21*, 2000392.

(89) Wu, S.-Y.; Chou, H.-Y.; Tsai, H.-C.; Anbazhagan, R.; Yuh, C.-H.; Yang, J. M.; Chang, Y.-H. Amino acid-modified PAMAM dendritic nanocarriers as effective chemotherapeutic drug vehicles in cancer treatment: a study using zebrafish as a cancer model. *RSC Adv.* 2020, *10*, 20682-20690.

(90) Jolly, A. M.; Bonizzoni, M. Intermolecular forces driving encapsulation of small molecules by PAMAM dendrimers in water. *Macromolecules* 2014, *47*, 6281-6288.

(91) Stewart, S.; Adams Ivy, M.; Anslyn, E. V. The use of principal component analysis and discriminant analysis in differential sensing routines. *Chem. Soc. Rev.* 2014, *43*, 70-84.

(92) Lavigne, J. J.; Savoy, S.; Clevenger, M. B.; Ritchie, J. E.; McDoniel, B.; Yoo, S.-J.; Anslyn, E. V.; McDevitt, J. T.; Shear, J. B.; Neikirk, D. Solution-based analysis of multiple analytes by a sensor array: toward the development of an "electronic tongue". *J. Am. Chem. Soc.* 1998, *120*, 6429-6430.

(93) Collins, B. E.; Anslyn, E. V. Pattern-based peptide recognition. *Chem. - Eur. J.* 2007, *13*, 4700-4708.

(94) Moita Neto, J. M.; Moita, G. C. Introduction to exploratory multivariate data analysis. *Quim. Nova* 1998, *21*, 467-469.

(95) Xie, R.; Yang, P.; Liu, J.; Zou, X.; Tan, Y.; Wang, X.; Tao, J.; Zhao, P. Lanthanide-functionalized metal-organic frameworks based ratiometric fluorescent sensor array for identification and determination of antibiotics. *Talanta* 2021, *231*, 122366.

(96) Yin, K.; Wu, S.; Zheng, H.; Gao, L.; Liu, J.; Yang, C.; Qi, L.-W.; Peng, J. Lanthanide metal-organic framework-based fluorescent sensor arrays to discriminate and quantify ingredients of natural medicine. *Langmuir* 2021, *37*, 5321–5328.

(97) Zhang, B.; Dong, X.; Zhou, Q.; Lu, S.; Zhang, X.; Liao, Y.; Yang, Y.; Wang, H. Carboxymethyl chitosan-promoted luminescence of lanthanide metallogel and its application in assay of multiple metal ions. *Carbohydr. Polym.* 2021, *263*, 117986.

(98) Palacios, M. A.; Wang, Z.; Montes, V. A.; Zyryanov, G. V.; Anzenbacher, P., Jr. Rational design of a minimal size sensor array for metal ion detection. *J. Am. Chem. Soc.* 2008, *130*, 10307-10314.

(99) Zhou, H.; Baldini, L.; Hong, J.; Wilson, A. J.; Hamilton, A. D. Pattern recognition of proteins based on an array of functionalized porphyrins. *J. Am. Chem. Soc.* 2006, *128*, 2421-2425.

(100) Rodriguez-Aguilar, M.; Diaz de Leon-Martinez, L.; Gorocica-Rosete, P.; Perez-Padilla, R.; Dominguez-Reyes, C. A.; Tenorio-Torres, J. A.; Ornelas-Rebolledo, O.; Mehta, G.; Zamora-Mendoza, B. N.; Flores-Ramirez, R. Application of chemoresistive gas sensors and chemometric analysis to differentiate the fingerprints of global volatile organic compounds from diseases. Preliminary results of COPD, lung cancer and breast cancer. *Clin. Chim. Acta* 2021, *518*, 83-92.

(101) Roggo, Y.; Duponchel, L.; Huvenne, J. P. Comparison of supervised pattern recognition methods with McNemar's statistical test. Application to qualitative analysis of sugar beet by near-infrared spectroscopy. *Anal. Chim. Acta* 2003, *477*, 187-200.

(102) Bocklitz, T. Richard G. Brereton: Chemometrics: data driven extraction for science, 2nd ed. *Anal. Bioanal. Chem.* 2019, *411*, 2995-2996.

(103) Yang, J.-Y.; Jia, X.-D.; Gao, R.-X.; Chen, M.-L.; Yang, T.; Wang, J.-H. Discrimination of pathogenic bacteria with boronic acid modified protonated g-C_3N_4 nanosheets at various pHs. *Sens. Actuators, B* 2021, *340*, 129951.

(104) Zhou, W.; Hou, J.; Li, Y.; Zhou, H.; Huang, H.; Zhang, L.; Hayat Nawaz, M. A.; Yu, C. Protein discrimination based on DNA induced perylene probe self-assembly. *Talanta* 2021, *224*, 121897.

(105) Geana, E.-I.; Ciucure, C. T.; Apetrei, C. Electrochemical sensors coupled with multivariate statistical analysis as screening tools for wine authentication issues: a review. *Chemosensors* 2020, *8*, 59.

(106) Carneiro, S. V.; Holanda, M. H. B.; Cunha, H. O.; Oliveira, J. J. P.; Pontes, S. M. A.; Cruz, A. A. C.; Fechine, L. M. U. D.; Moura, T. A.; Paschoal, A. R.; Zambelli, R. A.; Freire, R. M.; Fechine, P. B. A. Highly sensitive sensing of food additives based on fluorescent carbon quantum dots. *J. Photochem. Photobiol., A* 2021, *411*, 113198.

(107) Mitchell, L.; Shen, C.; Timmins, H. C.; Park, S. B.; New, E. J. A versatile fluorescent sensor array for platinum anticancer drug detection in biological fluids. *ACS Sens.* 2021, *6*, 1261-1269.

(108) Owen, O. E.; Kalhan, S. C.; Hanson, R. W. The key role of anaplerosis and cataplerosis for citric acid cycle function. *J. Biol. Chem.* 2002, *277*, 30409-30412.

(109) Krebs, H. A. History of the tricarboxylic acid cycle. *Perspect. Biol. Med.* 1970, *14*, 154-170.

(110) Wolfe, R. R.; Jahoor, F. Recovery of labeled CO_2 during the infusion of C-1- vs C-2-labeled acetate: implications for tracer studies of substrate oxidation. *Am. J. Clin. Nutr.* 1990, *51*, 248-252.

(111) Akram, M. Citric acid cycle and role of its intermediates in metabolism. *Cell Biochem. Biophys.* 2014, *68*, 475-478.

(112) Tatke, G.; Kumari, H.; Silva-Herzog, E.; Ramirez, L.; Mathee, K. Pseudomonas aeruginosa MifS-MifR two-component system is specific for α-ketoglutarate utilization. *PLoS One* 2015, *10*, e0129629/0129621-e0129629/0129631.

(113) Ninfa, A. J.; Jiang, P. PII signal transduction proteins: Sensors of α-ketoglutarate that regulate nitrogen metabolism. *Curr. Opin. Microbiol.* 2005, *8*, 168-173.

(114) He, W.; Miao, F. J. P.; Lin, D. C. H.; Schwandner, R. T.; Wang, Z.; Gao, J.; Chen, J.-L.; Tian, H.; Ling, L. Citric acid cycle intermediates as ligands for orphan G-protein-coupled receptors. *Nature* 2004, *429*, 188-193.

(115) Bourrellier, A. B. F.; Valot, B.; Guillot, A.; Ambard-Bretteville, F.; Vidal, J.; Hodges, M. Chloroplast acetyl-CoA carboxylase activity is 2-oxoglutarate-regulated by interaction of PII with the biotin carboxyl carrier subunit. *Proc. Natl. Acad. Sci. U. S. A.* 2010, *107*, 502-507, S502/501-S502/502.

(116) Eng, C.; Kiuru, M.; Fernandez, M. J.; Aaltonen, L. A. A role for mitochondrial enzymes in inherited neoplasia and beyond. *Nat. Rev. Cancer* 2003, *3*, 193-202.

(117) Selnaes, K. M.; Gribbestad, I. S.; Bertilsson, H.; Wright, A.; Angelsen, A.; Heerschap, A.; Tessem, M.-B. Spatially matched in vivo and ex vivo MR metabolic profiles of prostate cancer - investigation of a correlation with Gleason score. *NMR Biomed.* 2013, *26*, 600-606.

(118) Costello, L. C.; Franklin, R. B. Prostatic fluid electrolyte composition for the screening of prostate cancer: a potential solution to a major problem. *Prostate Cancer Prostatic Dis.* 2009, *12*, 17-24.

(119) Pourreza, N.; Sharifi, H.; Golmohammadi, H. Curcumin nanoparticles combined with cloud point extraction for citrate determination in food and drug samples. *Microchem. J.* 2016, *129*, 213-218.

(120) Gao, Y.; Huang, G.; Ou, Z.; Wang, Z.; Ju, B.; Li, Y.; Wang, X.; Yin, S. Selective sensing of citrate by a supramolecular ensemble formed by a phenazine copper(I) complex and a perylene diimide derivative. *New J. Chem.* 2015, *39*, 8948-8955.

(121) Ghosh, K.; Ranjan Sarkar, A. Pyridinium-based symmetrical diamides as chemosensors in visual sensing of citrate through indicator displacement assay (IDA) and gel formation. *Org. Biomol. Chem.* 2011, *9*, 6551-6558.

(122) Olin, J. W. Atherosclerotic renal artery disease. *Cardiol Clin* 2002, *20*, 547-562, vi.

(123) Jandeleit-Dahm, K.; Cooper, M. E. Hypertension and diabetes. *Current Opinion in Nephrology and Hypertension* 2002, *11*, 221-228.

(124) Stepinski, J.; Pawlowska, D.; Angielski, S. Effect of lithium on renal gluconeogenesis. *Acta Biochim. Pol.* 1984, *31*, 229-240.

(125) Eiam-Ong, S.; Spohn, M.; Kurtzman, N. A.; Sabatini, S. Insights into the biochemical mechanism of maleic acid-induced Fanconi syndrome. *Kidney Int.* 1995, *48*, 1542-1548.

(126) Ghosh, K.; Saha, I.; Frohlich, R.; Patra, A. Selective sensing of fumarate over maleate by benzimidazolium - based fluororeceptors. *Mini-Rev. Org. Chem.* 2011, *8*, 31-37.

(127) Costero, A. M.; Colera, M.; Gavina, P.; Gil, S. Fluorescent sensing of maleate versus fumarate by a neutral cyclohexane based thiourea receptor. *Chem. Commun.* 2006, 761-763.

(128) Compton, K. K.; Hildreth, S. B.; Helm, R. F.; Scharf, B. E. Sinorhizobium meliloti chemoreceptor McpV senses short-chain carboxylates via direct binding. *J. Bacteriol.* 2018, *200*, e00519-00518/00511-e00519-00518/00516.

(129) Brewster, J. L.; McKellar, J. L. O.; Finn, T. J.; Newman, J.; Peat, T. S.; Gerth, M. L. Structural basis for ligand recognition by a Cache chemosensory domain that mediates carboxylate sensing in Pseudomonas syringae. *Sci. Rep.* 2016, *6*, 35198.

(130) Davey, E. A.; Zucchero, A. J.; Trapp, O.; Bunz, U. H. F. Discrimination of organic acids using a three molecule array based upon cruciform fluorophores. *J. Am. Chem. Soc.* 2011, *133*, 7716-7718.

(131) Bang, J. H.; Lim, S. H.; Park, E.; Suslick, K. S. Chemically responsive nanoporous pigments: colorimetric sensor arrays and the identification of aliphatic amines. *Langmuir* 2008, *24*, 13168-13172.

(132) McGrier, P. L.; Solntsev, K. M.; Miao, S.; Tolbert, L. M.; Miranda, O. R.; Rotello, V. M.; Bunz, U. H. F. Hydroxycruciforms: amine-responsive fluorophores. *Chem. - Eur. J.* 2008, *14*, 4503-4510.

(133) Goodman, M. S.; Hamilton, A. D.; Weiss, J. Self-assembling, chromogenic receptors for the recognition of dicarboxylic acids. *J. Am. Chem. Soc.* 1995, *117*, 8447-8455.

(134) Linton, B. R.; Goodman, M. S.; Fan, E.; Van Arman, S. A.; Hamilton, A. D. Thermodynamic aspects of dicarboxylate recognition by simple artificial receptors. *J. Org. Chem.* 2001, *66*, 7313-7319.

(135) Hall, A. J.; Achilli, L.; Manesiotis, P.; Quaglia, M.; De Lorenzi, E.; Sellergren, B. A substructure approach toward polymeric receptors targeting dihydrofolate reductase

inhibitors. 2. Mmolecularly imprinted polymers against Z-L-glutamic acid showing affinity for larger molecules. *J. Org. Chem.* 2003, *68*, 9132-9135.

(136) Liu, S. Y.; Fang, L.; He, Y. B.; Chan, W. H.; Yeung, K. T.; Cheng, Y. K.; Yang, R. H. Cholic-acid-based fluorescent sensor for dicarboxylates and acidic amino acids in aqueous solutions. *Org Lett* 2005, *7*, 5825-5828.

(137) Mishra, A.; Lee, S.; Kim, H.; Cook, T. R.; Stang, P. J.; Chi, K.-W. Selective detection of multicarboxylate anions based on "turn on" electron transfer by self-assembled molecular rectangles. *Chem. - Asian J.* 2012, *7*, 2592-2599.

(138) Kim, D.-S.; Ahn, K. H. Fluorescence "turn-on" sensing of carboxylate anions with oligothiophene-based o-(carboxamido)trifluoroacetophenones. *J. Org. Chem.* 2008, *73*, 6831-6834.

(139) Goswami, S.; Hazra, A.; Chakrabarty, R.; Fun, H.-K. Recognition of carboxylate anions and carboxylic acids by selenium-based new chromogenic fluorescent sensor: a remarkable fluorescence enhancement of hindered carboxylates. *Org. Lett.* 2009, *11*, 4350-4353.

(140) Haynes, W. M. *CRC handbook of chemistry and physics, 91st ddition*; Taylor & Francis Group, 2010.

(141) Abdel-Sattar, S. H. E. The chemistry of tricarballylic acid (TCA). *Curr. Org. Chem.* 2004, *8*, 1405-1423.

(142) Juranic, I.; Vitnik, Z.; Society of Physical Chemists of Serbia: 2006; Vol. 2, p 769-776.

(143) Chen, H.; Laurent, S.; Bédu, S.; Ziarelli, F.; Chen, H.-l.; Cheng, Y.; Zhang, C.-C.; Peng, L. Studying the signaling role of 2-oxoglutaric acid using analogs that mimic the ketone and ketal forms of 2-oxoglutaric acid. *Chem. Biol.* 2006, *13*, 849-856.

(144) Huitink, G. M. Constant calcein blue: an indicator for fluorometric calcium determination. *Talanta* 1987, *34*, 423-426.

(145) Clement, N. R.; Gould, J. M. Pyranine (8-hydroxy-1,3,6-pyrenetrisulfonate) as a probe of internal aqueous hydrogen ion concentration in phospholipid vesicles. *Biochemistry* 1981, *20*, 1534-1538.

(146) Li, M.; Harbron, R. L.; Weaver, J. V. M.; Binks, B. P.; Mann, S. Electrostatically gated membrane permeability in inorganic protocells. *Nat. Chem.* 2013, *5*, 529-536.

(147) Tomalia, D. A.; Baker, H.; Dewald, J.; Hall, M.; Kallos, G.; Martin, S.; Roeck, J.; Ryder, J.; Smith, P. A New Class of Polymers: Starburst-Dendritic Macromolecules. *Polym. J.* 1985, *17*, 117.

(148) Tang, M. X.; Redemann, C. T.; Szoka, F. C. In vitro gene delivery by degraded polyamidoamine dendrimers. *Bioconjugate Chem.* 1996, *7*, 703-714.

(149) Lakowicz, J. R. *Principles of fluorescence spectroscopy*; Springer US, 2007.

(150) Jablonski, A. Anisotropy of fluorescence of molecules excited by excitation transfer. *Acta Phys. Pol. A* 1970, *38*, 453-458.

(151) Mallet, A. M.; Liu, Y.; Bonizzoni, M. An off-the-shelf sensing system for physiological phosphates. *Chem. Comm.* 2014, *50*, 5003-5006.

(152) Jolly, A. M.; Bonizzoni, M. Intermolecular forces driving encapsulation of small molecules by PAMAM dendrimers in water. *Macromolecules* 2014, *47*, 6281-6288.

(153) Wright, A. T.; Griffin, M. J.; Zhong, Z.; McCleskey, S. C.; Anslyn, E. V.; McDevitt, J. T. Differential receptors create patterns that distinguish various proteins. *Angew. Chem., Int. Ed. Engl.* 2005, *44*, 6375-6378.

(154) Anzenbacher, J. P.; Lubal, P.; Buček, P.; Palacios, M. A.; Kozelkova, M. E. A practical approach to optical cross-reactive sensor arrays. *Chem. Soc. Rev.* 2010, *39*, 3954-3979.

(155) Stich, M. I. J.; Fischer, L. H.; Wolfbeis, O. S. Multiple fluorescent chemical sensing and imaging. *Chem. Soc. Rev.* 2010, *39*, 3102-3114.

(156) Gao, J.; Granzhan, A.; Qian, X.; Severin, K. Pattern-based sensing of short oligodeoxynucleotides with palladium-dye complexes. *Chem. Commun.* 2010, *46*, 5515-5517.

(157) Munteanu, F.-D.; Titoiu, A. M.; Marty, J.-L.; Vasilescu, A. Detection of antibiotics and evaluation of antibacterial activity with screen-printed electrodes. *Sensors* 2018, *18*, 901/901-901/926.

(158) Chafer-Pericas, C.; Maquieira, A.; Puchades, R. Fast screening methods to detect antibiotic residues in food samples. *TrAC, Trends Anal. Chem.* 2010, *29*, 1038-1049.

(159) Rehman, M. S. U.; Rashid, N.; Ashfaq, M.; Saif, A.; Ahmad, N.; Han, J.-I. Global risk of pharmaceutical contamination from highly populated developing countries. *Chemosphere* 2015, *138*, 1045-1055.

(160) Davies, J.; Davies, D. Origins and evolution of antibiotic resistance. *Microbiol. Mol. Biol. Rev.* 2010, *74*, 417-433.

(161) Elander, R. P. Industrial production of β-lactam antibiotics. *Appl. Microbiol. Biotechnol.* 2003, *61*, 385-392.

(162) Okerman, L.; Van Hoof, J.; Debeuckelaere, W. Evaluation of the European four-plate test as a tool for screening antibiotic residues in meat samples from retail outlets. *J. AOAC Int.* 1998, *81*, 51-56.

(163) Oboegbulem, S. I.; Fidelis, A. P. Detection of antimicrobial residues in poultry meat and slaughter cattle in Nigeria. *Meat Sci.* 1996, *43*, 71-74.

(164) Collins-Thompson, D. L.; Wood, D. S.; Thomson, I. Q. Detection of antibiotic residues in consumer milk supplies in north America using the Charm test II procedure. *J. Food Prot.* 1988, *51*, 632-633.

(165) Rajkowski, K. T.; Peeler, J. T.; Messer, J. W. Detectability levels of four beta-lactam antibiotics in eight milk products using the AOAC Bacillus stearothermophilus Disc Assay. *J. Food Prot.* 1986, *49*, 687-690.

(166) Pikkemaat, M. G.; Dijk, S. O.-v.; Schouten, J.; Rapallini, M.; Kortenhoeven, L.; van Egmond, H. J. Nouws antibiotic test: validation of a post-screening method for antibiotic residues in kidney. *Food Control* 2009, *20*, 771-777.

(167) Pikkemaat, M. G.; Rapallini, M. L. B. A.; Dijk, S. O.-v.; Elferink, J. W. A. Comparison of three microbial screening methods for antibiotics using routine monitoring samples. *Anal. Chim. Acta* 2009, *637*, 298-304.

(168) Krisova, M.; Kozarova, I. Detection of residues of antimicrobial compounds in eggs by the rapid screening methods. *Folia Vet.* 2018, *62*, 48-55.

(169) Kozarova, I.; Juscakova, D.; simkova, J.; Milkovicova, M.; Kozar, M. Effective screening of antibiotic and coccidiostat residues in food of animal origin by reliable broadspectrum residue screening tests. *Ital. J. Anim. Sci.* 2020, *19*, 487-501.

(170) Delepierre, A.; Gayot, A.; Carpentier, A. Update on counterfeit antibiotics worldwide; public health risks. *Med. Mal. Infect.* 2012, *42*, 247-255.

(171) Kelesidis, T.; Falagas, M. E. Substandard/counterfeit antimicrobial drugs. *Clin. Microbiol. Rev.* 2015, *28*, 443-464.

(172) Akdeniz, A.; Caglayan, M. G.; Anzenbacher, P. A tri-serine tri-lactone scaffold for the quantification of citrate in urine. *Chem. Commun.* 2016, *52*, 1827-1830.

(173) Das, D. K.; Deka, S.; Guha, A. K. Schiff base derived from 4,4'-methylenedianiline and p-anisaldehyde: colorimetric sensor for Cu^{2+}, paper strip sensor for Al^{3+} and fluorescent sensor for Pb^{2+}. *J. Fluoresc.* 2019, *29*, 1467-1474.

(174) Jaikang, P.; Paengnakorn, P.; Grudpan, K. Simple colorimetric ammonium assay employing well microplate with gas pervaporation and diffusion for natural indicator immobilized paper sensor via smartphone detection. *Microchem. J.* 2020, *152*, 104283.

(175) Jaeger, M.; Schubert, S.; Ochrimenko, S.; Fischer, D.; Schubert, U. S. Branched and linear poly(ethylene imine)-based conjugates: synthetic modification, characterization, and application. *Chem. Soc. Rev.* 2012, *41*, 4755-4767.

(176) Kim, Y.; Jang, G.; Lee, T. S. New fluorescent metal-ion detection using a paper-based sensor strip containing tethered rhodamine carbon nanodots. *ACS Appl. Mater Interfaces* 2015, *7*, 15649-15657.

(177) Ellerbee, A. K.; Phillips, S. T.; Siegel, A. C.; Mirica, K. A.; Martinez, A. W.; Striehl, P.; Jain, N.; Prentiss, M.; Whitesides, G. M. Quantifying colorimetric assays in paper-based microfluidic devices by measuring the transmission of light through paper. *Anal. Chem.* 2009, *81*, 8447-8452.

(178) Bell, J. G.; Mousavi, M. P. S.; Abd El-Rahman, M. K.; Tan, E. K. W.; Homer-Vanniasinkam, S.; Whitesides, G. M. Paper-based potentiometric sensing of free bilirubin in blood serum. *Biosens. Bioelectron.* 2019, *126*, 115-121.

(179) Feng, Q.-M.; Cai, M.; Shi, C.-G.; Bao, N.; Gu, H.-Y. Integrated paper-based electroanalytical devices for determination of dopamine extracted from striatum of rat. *Sens. Actuators, B* 2015, *209*, 870-876.

(180) Wang, Q.; Li, X.; Tang, L.; Fei, Y.; Pan, Y.; Sun, L. Paper-based electroanalytical devices for in situ determination of free 3-indoleacetic acid and salicylic acid in living Pyropia haitanensis thallus under various environmental stresses. *J. Appl. Phycol.* 2020, *32*, 485-497.

(181) Maxwell, E. J.; Mazzeo, A. D.; Whitesides, G. M. Paper-based electroanalytical devices for accessible diagnostic testing. *MRS Bull.* 2013, *38*, 309-314.

(182) Legrini, O.; Oliveros, E.; Braun, A. M. Photochemical processes for water treatment. *Chem. Rev.* 1993, *93*, 671-698.

(183) Walpole, G. S. The use of litmus paper as a quantitative indicator of reaction. *Biochem. J.* 1913, *7*, 260-267.

(184) https://www.slas.org/education/ansi-slas-microplate-standards/ accessed 06.07.2021

(185) Bailey, J. E.; et, a.; Editors *Ullmann's encyclopedia of industrial chemistry, sixth edition, 2000 electronic release, update*; Wiley-VCH, 2000.

(186) Marti, V.; Jubany, I.; Perez, C.; Rubio, X.; De Pablo, J.; Gimenez, J. Human health risk assessment of a landfill based on volatile organic compounds emission, immission and soil gas concentration measurements. *Appl. Geochem.* 2014, *49*, 218-224.

(187) Hunkeler, D.; Laier, T.; Breider, F.; Jacobsen, O. S. Demonstrating a natural origin of chloroform in groundwater using stable carbon isotopes. *Environ. Sci. Technol.* 2012, *46*, 6096-6101.

(188) Reitz, R. H.; Mendrala, A. L.; Corley, R. A.; Quast, J. F.; Gargas, M. L.; Andersen, M. E.; Staats, D. A.; Conolly, R. B. Estimating the risk of liver cancer associated with human exposures to chloroform using physiologically based pharmacokinetic modeling *Toxicol. Appl. Pharmacol.* 1991, *110*, 536.

(189) Mondal, S. P.; Bera, S.; Narender, G.; Ray, S. K. CdSe quantum dots-poly(3-hexylthiophene) nanocomposite sensors for selective chloroform vapor detection at room temperature. *Appl. Phys. Lett.* 2012, *101*, 173108/173101-173108/173104.

(190) Sharma, S.; Nirkhe, C.; Pethkar, S.; Athawale, A. A. Chloroform vapour sensor based on copper/polyaniline nanocomposite. *Sens. Actuators, B* 2002, *85*, 131-136.

(191) Perillo, P. M.; Rodriguez, D. F. A room temperature chloroform sensor using TiO2 nanotubes. *Sens. Actuators, B* 2014, *193*, 263-266.

(192) Toyoda, Y.; Takada, T.; Suzuki, H. Halogenated hydrocarbon solvent-related cholangiocarcinoma risk: biliary excretion of glutathione conjugates of 1,2-dichloropropane evidenced by untargeted metabolomics analysis. *Sci. Rep.* 2016, *6*, 24586.

(193) Rodman, D. L.; Carrington, N. A.; Qiu, H.; Goswami, K.; Xue, Z.-L. Spectroscopic detection of halocarbons using modified Fujiwara reactions. *Anal. Chim. Acta* 2005, *548*, 143-147.

(194) Fong, J. K.; Pena, J. K.; Xue, Z.-L.; Alam, M. M.; Sampathkumaran, U.; Goswami, K. Optical Sensors for the Detection of Trace Chloroform. *Anal. Chem.* 2015, *87*, 1569-1574.

(195) Wu, J.-Y.; Yu, C.-H.; Wen, J.-J.; Chang, C.-L.; Leung, M.-k. Pyrrolo-[3,2-b]pyrroles for photochromic analysis of halocarbons. *Anal. Chem.* 2016, *88*, 1195-1201.

(196) Peng, Z.; Feng, X.; Tong, B.; Chen, D.; Shi, J.; Zhi, J.; Dong, Y. The selective detection of chloroform using an organic molecule with aggregation-induced emission properties in the solid state as a fluorescent sensor. *Sens. Actuators, B* 2016, *232*, 264-268.

(197) Razavi, S. A. A.; Masoomi, M. Y.; Morsali, A. Stimuli-responsive metal-organic framework (MOF) with chemo-switchable properties for colorimetric detection of $CHCl_3$. *Chem. - Eur. J.* 2017, *23*, 12559-12564.

(198) Sheng, K.; Lu, H.; Sun, A.; Wang, Y.; Liu, Y.; Chen, F.; Bian, W.; Li, Y.; Kuang, R.; Sun, D. A naked-eye colorimetric sensor for chloroform. *Chin. Chem. Lett.* 2019, *30*, 895-898.

(199) Fujiwara, K. New reaction for the detection of chloroform. *Sitz. Nat. Ges. Rostock* 1916, *6*, 33-43.

(200) Uno, T.; Okumura, K.; Kuroda, Y. Mechanism of the Fujiwara reaction: structural investigation of reaction products from benzotrichloride. *J. Org. Chem.* 1981, *46*, 3175-3178.

(201) Leibman, K. C.; Hindman, J. D. Modification of the Fujiwara reaction for determination of polyhalogenated organic compounds. *Anal. Chem.* 1964, *36*, 348-351.

(202) Zavar, M. H. A.; Rounaghi, G. H.; Chamsaz, M.; Ashraf, N. Determination of trihalomethanes in tap water by UV-Vis spectrophotometry. *Asian J. Chem.* 2009, *21*, 2903-2910.

(203) Luo, W.; Chen, Z.; Zhu, L.; Chen, F.; Wang, L.; Tang, H. A sensitive spectrophotometric method for determination of carbon tetrachloride with the aid of ultrasonic decolorization of methyl orange. *Anal. Chim. Acta* 2007, *588*, 117-122.

(204) Pillai, A. K.; Rastogi, R.; Gupta, V. K. A sensitive colorimetric method for determination of chloroform. *Indian J. Chem. Technol.* 1999, *6*, 294-296.